Investigation of Liquid-Metal-Embrittlement Crack-path: Role of Grain Boundaries and Responsible Mechanism

by

Mohammad Hadi Razmpoosh

A thesis
presented to the University of Waterloo
in fulfillment of the
thesis requirement for the degree of
Doctor of Philosophy
in
Mechanical and Mechatronics Engineering

Waterloo, Ontario, Canada, 2020

Examining Committee Membership

The following served on the Examining Committee for this thesis. The decision of the Examining Committee is by majority vote.

External Examiner:	Professor Todd Palmer Department of Materials Science and Engineering, PennState University, USA
Supervisor(s):	Professor Norman Y. Zhou and, Professor Elliot Biro Department of Mechanical and Mechatronics Engineering, University of Waterloo, Canada
Internal Member:	Professor Adrian P. Gerlich, Department of Mechanical and Mechatronics Engineering, University of Waterloo, Canada
Internal Member:	Professor Hamid Jahed, Department of Mechanical and Mechatronics Engineering, University of Waterloo, Canada
Other Member(s):	Professor Walter W. Duley, Department of Physics and Astronomy, University of Waterloo, Canada

Author's Declaration

This thesis consists of material all of which the candidate authored or co-authored: see Statement of Contributions included in the thesis. This is a true copy of the thesis, including any required final revisions, as accepted by my examiners.

I understand that my thesis may be made electronically available to the public.

Statement of Contributions

This thesis includes 8 chapters: introduction and literature review (Chapters 1 and 2) which represents a review paper (manuscript submitted for publication in Progress in Materials Science, 2020), and a series of four data chapters starting from Chapter 3 to 6 including published or under-review manuscripts the candidate authored or co-authored. The manuscripts have been modified to fit the style of the thesis. The candidate is the primary author in all manuscripts. It should be noted that the vast majority of the work in the lab (except where noted) including sample preparations, welding of the samples, mechanical testing, characterizations, and writing were done by the candidate. The following co-authors have contributed to the current work as outlined below:

Professor Norman Zhou supervised the research progress, advised the research direction, reviewed and edited the manuscripts. Professor Elliot Biro oversaw research progress, assisted with data analysis, had technical discussions, reviewed and edited the manuscripts.

Dr. Andrew Macwan from ArcelorMittal Dofasco, Hamilton, Canada, and Dr. Frank Goodwin from the international zinc association (IZA), Durham, USA acted as industrial supervisors, provided material, financial support, feedbacks on the research, and assisted with editing the manuscripts.

Chapter 1 and 2

MH Razmpoosh, C DiGiovanni, NY Zhou, E Biro, Review paper: "Pathway to understand Liquid-Metal-Embrittlement: From fundamentals toward applications", submitted to Progress in Materials Science, 2020.

The candidate is the primary author of this review paper, including sections: the LME mechanisms, crack imitation and progression, and the role of grain boundaries (first two-third of the manuscript). Chris DiGiovanni authored the sections describing the role of process parameters on LME, and the effects of LME on mechanical properties, which are entirely excluded from chapter 2. Prof. Zhou and Prof. Biro's role were as described above.

Chapter 3

MH Razmpoosh, A Macwan, E Biro, DL Chen, Y Peng, F Goodwin, Y Zhou, "Liquid Metal Embrittlement in Laser Beam Welding of Zn-Coated 22MnB5 Steel", Materials and Design, 155 (2018) pp. 375-383.

Professor D.L. Chen from Ryerson University supported the scanning electron microscopy, X-Ray diffraction, and energy-dispersive spectroscopy analyses of the LME-cracks and the

coating, which were used in Figures 34 and 36. Mr. Y Peng from Central Iron Steel Research Institute (CISRI), China provided editorial support.

The role of Prof. Zhou, Prof. Biro, Dr. Goodwin, and Dr. Macwan were as described above.

MH Razmpoosh, E Biro, DL Chen, F Goodwin, Y Zhou, Liquid Metal Embrittlement in Laser Lap joining of TWIP and Medium Manganese TRIP Steel: The Role of Grain Boundaries-Materials Characterization, 145 (2018) pp. 627-633.

Professor D.L. Chen from Ryerson University supported the scanning electron microscopy, and energy-dispersive spectroscopy analyses of the LME-cracks, which were used in Figure 44. The role of Prof. Zhou, Prof. Biro, and Dr. Goodwin, and were as described above.

Chapter 4

MH Razmpoosh, A Macwan, F Goodwin, E Biro, N Zhou, "Crystallographic Study of Liquid-Metal-Embrittlement Crack Path", Materials Letters, 2020, 267: 127511. The role of Prof. Zhou, Prof. Biro, Dr. Goodwin, and Dr. Macwan were as described above.

MH Razmpoosh, A Macwan, F Goodwin, E Biro, N Zhou, "Role of random and coincidence site lattice grain boundaries in liquid metal embrittlement of Iron (FCC)-Zn couple", Under-review manuscript in Metallurgical and Materials Transactions A, 2020.

The role of Prof. Zhou, Prof. Biro, Dr. Goodwin, and Dr. Macwan were as described above.

Chapter 5

MH Razmpoosh, B Langelier, E Marzbanrad, HS Zurob, E Biro, N Zhou, Atomic-scale Investigation of Liquid-Metal-Embrittlement Crack-path: Revealing Mechanism and Role of Grain Boundary Chemistry, to be submitted to Acta Materialia, 2020.

The role of role of Prof. Zhou, and Prof. Biro were as described above.

Dr. Brian Langelier from Canadian Centre for Electron Microscopy (CCEM), McMaster University, Hamilton, Canada, operated focused-ion-beam milling of the atom probe tomography needles, ran the atom probe tomography analysis, collected the atom probe tomography data, assisted with the map reconstructions, discussing the results, and editing the manuscript.

Dr. E. Marzbanrad, University of Waterloo, Canada, ran the molecular dynamics models, and assisted in interpretation of the simulation and extracting data. Professor H. Zurob,

McMaster University, Hamilton, Canada, provided financial support for the atom probe tomography analysis, and assisted with reviewing the manuscript.

Chapter 6

MH Razmpoosh, A Macwan, F Goodwin, E Biro, N Zhou, Suppression of Liquid Metal Embrittlement by Twin-based Grain Boundary Engineering Approach, accepted manuscript in Materialia, 2020.

The role of Prof. Zhou, Prof. Biro, Dr. Goodwin, and Dr. Macwan were as described above.

Abstract

Liquid metal embrittlement (LME) has been reported in many structural materials, including steel, aluminum, nickel during hot-working processes e.g. welding, brazing, heat-treatment, leading to abrupt failure. In many of the applications, such as automotive, aerospace, nuclear industries, LME failure is considered as a serious safety concern. Over the last decades, research activities have grown considerably striving to understand the LME phenomenon. However, to date a fundamental understanding of the metallurgical and mechanical micro-events of LME has remained unclear. Moreover, the LME mechanism has been concealed behind the diverse, contradicting propositions without any robust experimental support. Hence, a comprehensive understanding of micro-events of LME calls for in-depth crack-path analysis from macroscopic, microscopic, and atomic viewpoints.

The aim of this research is to explore the role of grain boundary type, and characteristics such as grain boundary misorientation angle, crystallographic plane, and grain boundary microchemistry in LME. Restrained laser beam welding was used to induce LME-cracks in various Zn-coated steels. The crack-path has been characterized to identify types and geometrical characteristics of LME-sensitive grain boundaries. It was found that LME crack-path is a function of misorientation angle and stress component perpendicular to grain boundary plane, where high-angle random (non-ordered) grain boundaries are more LME-sensitive than highly coherent low-Σ coincidence site lattice (CSL) boundaries. At higher misorientation angles, lower tensile stresses trigger grain boundary decohesion. Moreover, liquid metal selectively penetrated the grain boundaries with high-index planes due to their relatively high excess volume. The atomic-scale analysis of LME crack-path provided new insights to the inter-relation between the geometrical configuration and grain boundary chemistry. This validated the grain boundary-based LME mechanism, and revealed the micro-events leading to the embrittler-induced grain boundary decohesion. It was found that grain-boundary-engineering techniques can be employed to manipulate frequency of random and CSL boundaries, which resulted in significantly improved resistance against LME.

Keywords: Advance High Strength Steels; Liquid Metal Embrittlement (LME); Fe-Zn LME Couple; Grain Boundary; Fracture; Microstructure; Welding.

Acknowledgements

Firstly, I would like to express my sincere appreciation to my Supervisors: Prof. Norman Y. Zhou for his great guidance, patience, and giving me all the freedom I would ever need to conduct experiments toward this PhD research. His great knowledge of welding processes and materials science helped me to stay on track throughout my PhD studies; and Prof. Elliot Biro for all fruitful discussions, helpful suggestions, and valuable instructions. He convincingly guided and encouraged me to do the right thing even when the road got tough. Without his persistent help, the goal of this project would not have been realized.

I would also like to thank Dr. Andrew Macwan from ArcelorMittal Global Research, Hamilton, Canada, and Dr. Frank Goodwin from the International Zinc Association (IZA), who sponsored this study, and allowed me to use the resources. My gratitude also goes to the Natural Sciences and Engineering Research Council (NSERC) of Canada for supporting this study. Great thanks are also given to Prof. Hatem Zurob from McMaster University for the financial support with the APT and FIB experiments. I would also like to thank the technical team at the Canadian Centre for Electron Microscopy (CCEM). I am grateful for Dr. Brian Langelier, who operated FIB milling of the APT needles, and ran the APT analyses. I would like to express my gratitude to Dr. Ehsan Marzbanrad for his great help with the molecular dynamics modeling, and helpful discussions. A special thanks to the technical staff of the MME department, who helped me through the experiments, especially Mr. Mark Griffet. This work would not have been possible without all this support. I wish to acknowledge the support and encouragement of my colleagues at the Centre for Advanced Materials Joining (CAMJ) with whom I have a pleasant time during my four-year long PhD journey. I would like to thank all my friends who supported me.

Finally, I would like to mention my family. My warmest thanks to my wife Azar, who inspired me and provided constant encouragement during this journey. Deep thanks for her understanding, patience. and giving me strength day after day. My heartfelt gratitude goes to my parents Mahin and Mohammad, my sisters Leila and Laleh, and my parents-in-law for their endless love and support.

Dedicated to my beloved family; wife, mom, dad, and sisters.

I am very proud to dedicate this work to all of you...

Table of Contents

List of Figures

List of Tables

Chapter 1

Introduction

1.1 Background

Liquid metal embrittlement (LME) was first documented in 1874 [1], where a galvanized iron wire exhibited a sharp break at an elevated temperature. Since then, LME started to be recognized as an abnormal phenomenon in certain solid-liquid metallic couples, where intimate contact of the solid-liquid pairs induced penetration of liquid into the metal, causing abrupt rupture. LME is reported in various liquid/solid metal couples, including the most frequently used engineering metals such as Al, Cu, Ni, and steels [2–14] (Figure 1.1). Since 2000, advanced high strength steels (AHSS) started to be extensively used in automotive industries, however, due to their higher strength and alloying elements, AHSS were seen to be LME-susceptible. Therefore, progress has been made toward understanding the mechanisms controlling LME in Fe-Zn couple [12–20]. The undisputable technological significance of AHSSs, therefore, necessitates study of LME to fundamentally understand: the underlying micro-mechanisms, the role of grain boundaries, and potential metallurgical mitigation methods.

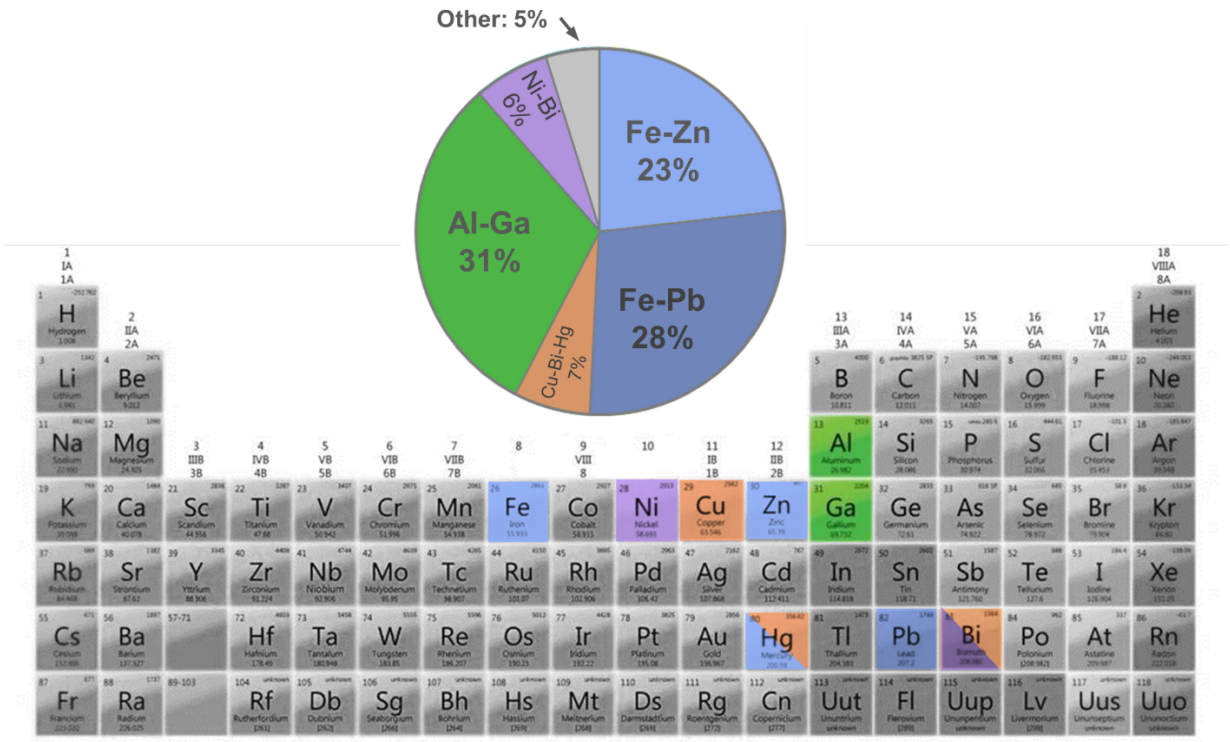

Figure 1.1: The frequency of major reported LME couples in the recent literature including Al-Ga, Cu-Pb. Cu-Bi, Fe-Pb, Fe-Ga, Fe-Zn [2–85].

1.2 Objectives

This study aims to understand LME behavior of Fe-Zn couple and the role of grain boundaries in this phenomenon. The main objectives are:

1. Characterization of Zn-induced LME during laser beam welding (LBW) of different representative AHSS grades: 22MnB5 press-hardening steel (PHS), medium-Mn transformation induced plasticity (MMn-TRIP), and twinning induced plasticity (TWIP),

2. Investigate the effects of applied external loading on LME-cracking, and mechanism

of LME-cracking during the processing.

3. Study the role of grain-boundary geometrical characteristics such as grain boundary type, misorientation angle, and grain boundary crystallographic plane in LME.

4. Investigate atomic-scale mechanism of grain boundary decohesion in LME, and the interrelation between the grain boundary geometrical configuration and its chemistry.

5. Explore the feasibility of grain-boundary-engineering as an approach to manipulate grain boundary character distribution, and suppress LME.

1.3 Thesis outline

This thesis consists of eight chapters. An overview of the research carried out for this thesis is presented in Figure 1.2. The first chapter is an introduction presenting the motivation and the main objectives of this research. Chapter two provides an overview of the present understanding of LME phenomenon, focusing on the systematical summary of the proposed LME mechanisms. The details of the stress-assisted grain boundary diffusion model, as a viable LME mechanism, is reviewed in this chapter. Furthermore, Chapter two discusses the different grain boundary decohesion hypotheses, and reviews the details of the recently proposed electronic effect of embrittler atoms on grain boundary cohesive strength. The majority of chapter one and two content represent the submitted review paper.

Chapter three through chapter six represent the content in the published or under-review research manuscripts. Chapter three discusses Zn-induced LME in LBW of AHSS. This chapter discusses the Zn-induced LME in 3 different AHSS grades: 22MnB5 PHS, medium-Mn TRIP, and TWIP steels. Chapter four describes how grain-boundary geometrical characteristics e.g. type, misorientation angle, and crystallographic plane affects

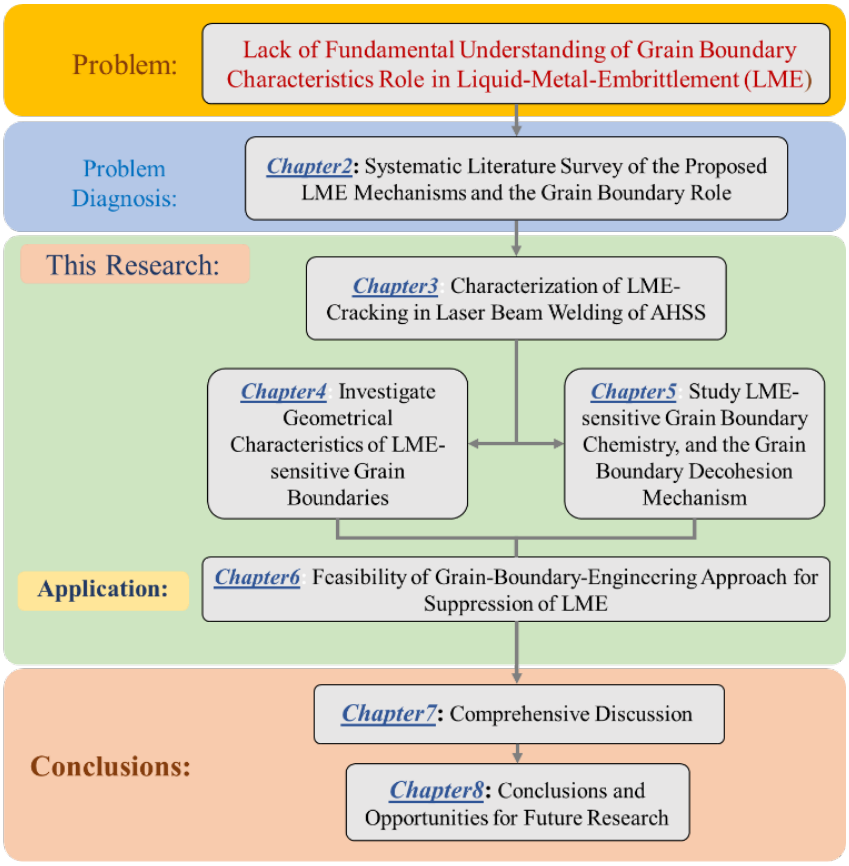

Figure 1.2: Flow chart illustrating the different sections of the present thesis.

LME-sensitivity of a grain boundary. Chapter five presents atomic-scale investigation of LME crack-path. The investigations validate the recently proposed embrittler-induced alteration of electronic configuration as grain boundary decohesion mechanism in LME. Moreover, the interrelation between the grain boundary geometrical configuration and its chemistry are covered. Based on the findings of Chapters four and five regarding high LME-resistivity of special boundaries compared to random grain boundaries, chapter six proposes grain-boundary-engineering as a viable approach to manipulate grain boundary characteristics to suppress LME. The mechanisms of the crack arrest are discussed based

on the random-grain boundary network continuity, and the grain boundary triple junction types and distributions. Chapter seven provides a comprehensive discussion to review Chapters three through six as a whole, and to understand micro-mechanisms leading to LME. Lastly, Chapter eight summarizes the main findings of the present research and proposes the future research opportunities.

Chapter 2

Literature Review[1]

2.1 Overview

LME affects various industrially important materials, including steels, brasses, aluminum, nickel, over a wide range of scenarios [2–14]. These scenarios can be classified as: (a) processing failures: hot-dip galvanizing and hot-stamping [12,13,86]; (b) fabrication failures: soldering, brazing, and welding [87–90]; (c) operation failures: nuclear industries [53,58,69]; and (d) secondary failures, in which LME occurs after initial bolt, bearing, or pressure vessel failures [91–93]. Due to the broad range of failure risks, LME is recognized as a serious safety issue in many applications across aerospace, nuclear, and automotive industries. This phenomenon is characterized by the concurrent action of 3 factors (Figure 2.1): (a) the presence of an aggressive liquid metal (hereafter called embrittler) such as Bi, Ga, Zn; where all the embrittlers have relatively low melting points (room temperature to 419°C), (b) a susceptible polycrystalline material with a grain boundary network into

[1]This chapter consists of a submitted review paper in Progress in Materials Science, MH Razmpoosh, C DiGiovanni, E Biro, Y Zhou, 2020.

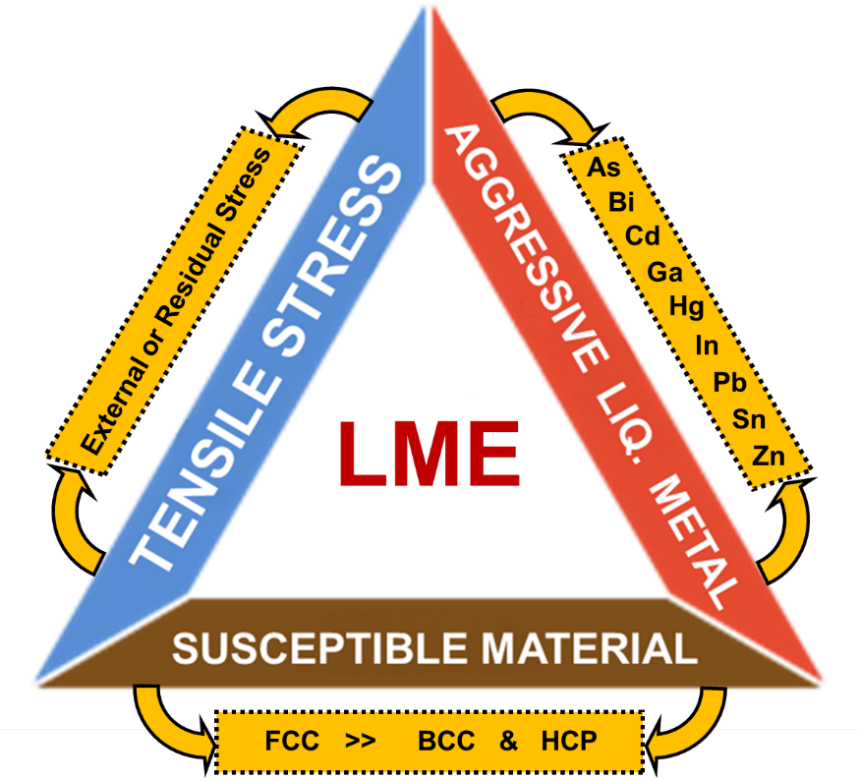

Figure 2.1: The essential factors for liquid metal embrittlement including aggressive liquid metal, a susceptible structure, and tensile stress

which the embrittler may penetrate, and (c) external tensile loading or internal (residual) tensile stress which is normally below the material's yield stress [6,20,82,94–96].

Among the LME couples, Al-Ga system is the most deeply studied system and known as the LME model system due to high LME susceptibility and structural simplicity for atomistic modeling [2,3,6,7,83–85]. Ni-Bi, and Cu-Bi couples are also frequently reported in the literature where ab-intio modeling and high-resolution transmission electron microscopy (TEM) investigation provided understanding about the role of grain boundaries in LME [4,5]. Despite a body of research efforts since 1960, LME is still associated with unexplained results, controversies, and a lack of fundamental understanding. The diverse

and contradicting proposed LME mechanisms in different processing routes and LME couples is puzzling the research communities. In this chapter the present literature is critically reviewed to understand the proposed LME mechanisms, hypotheses of the grain boundary decohesion, and the role of solute atoms segregated to grain boundaries.

2.2 Proposed LME Mechanisms

Thus far, several mechanisms have been proposed to describe micro-events leading to LME-cracking. Despite these efforts, there is still no universal agreement about the LME mechanism. This is due to the general complexity of the phenomenon, lack of experimental/modeling evidence, and differences of the responsible mechanisms for the various couples. Below is a summary of the major LME mechanisms, their breakthrough contribution in better understanding of LME, and the associated shortcomings.

2.2.1 Ductile-Fracture Models

These proposed models all connect dislocations to LME crack formation. The Lynch model [97] is considered as the main model explaining LME by plastic deformation at the crack-tip, where the adsorption of embrittler atoms is accelerated through nucleation and motion of dislocations at the crack-tip (Figure 2.2). Within the deformation zone at the crack-tip, the dislocation source activates on planes intersecting the tip, which contributes to crack progression; however, other dislocation sources contribute in crack blunting and form voids ahead of the crack-tip. The extensive void formation ahead of the crack-tip, in-turn facilitates crack progression (Figure 2.2). Although the Lynch model provided insights in the role of micro-void coalescence through low levels of plastic deformation at the crack-tip, the model fails to explain the failure delay in some LME systems.

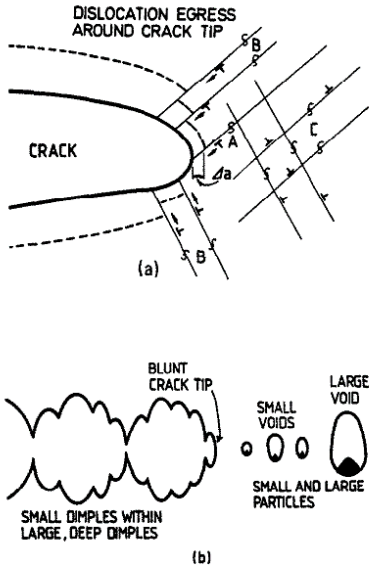

Figure 2.2: Schematic illustration of ductile crack growth as the dislocations nucleate from the crack-tip source where the dislocation of source A (intersecting the tip) contribute in crack progression but the other sources of B and C contribute only in crack-tip [97]

Explanation of LME through crack-tip plasticity was furthered when the early Rostoker's description [98] based on surface energy modification was merged with the Rebinder and Popovich model [99]. This model claims that the plastic deformation ahead of the crack is facilitated due to the surface energy modification, where considerable dislocation activity increases the chance of micro-crack formation (as a result of work-hardening) that can further propagate in a ductile fashion. Here, the liquid metal presence acts as a driving force to the efficient dislocation emission at the tip. In a very similar way, the Hancock-Ives [100] description emphasizes on the essential role of dislocations where the dislocation pile up against grain boundary results in crack-tip localized instability (Figure 2.3). This facilitates solid-state diffusion of the embrittler atom ahead of the crack and resultant decohesion of the bonds. Although the Rebinder and Popovich model [99] ex-

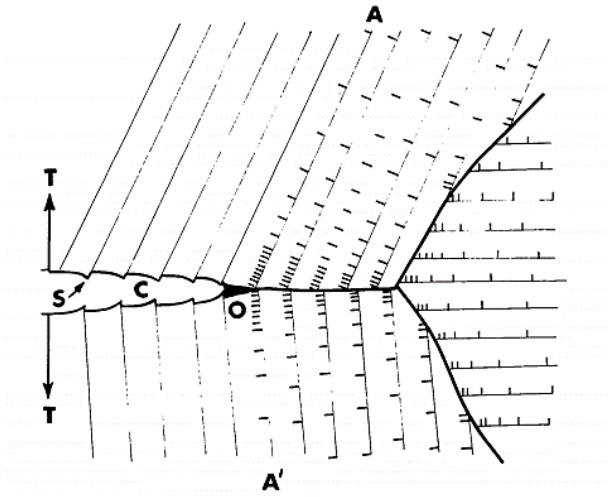

Figure 2.3: Schematic illustration of crack propagation mechanism in between grains A and A' showing the generation of dislocation arrays ahead of crack-tip, as the crack passes the dislocation relax and create the steps on the crack walls [100]

plained the role of diffused embrittler atoms ahead of the crack, the diffusion of embrittler atoms ahead of the propagating crack is not described. This is described by other models discussed below in the grain boundary diffusion-based models.

2.2.2 Brittle-Fracture Mechanisms

In contrast to the models necessitating dislocations and plastic zones ahead of the crack-tip to allow penetration of liquid metal and progress cracking, another major group of the proposed models describe LME-cracking in a brittle-fracture framework.

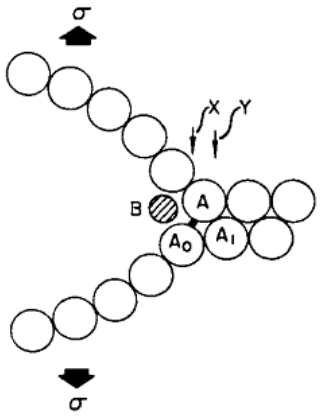

Figure 2.4: Schematic illustration of solid-atoms (A) displacement at the crack-tip where the presence of the embrittler atom (B) from the liquid metal environment weakens the bond A-A_0[102]

Stoloff–Johnson–Westwood–Kamdar (SJWK) Theory

Stoloff–Johnson–Westwood–Kamdar (SJWK) [101,102] theory was developed based on early surface energy modification models proposed by Rostoker and Rehbinder [98,103]. In the SJWK framework, liquid embrittler atoms affect the cohesive strength of grain-to-grain bonds due to the strain-activated chemisorption (Figure 2.4). Hence, in the inter-atomic potential curves there would be a lower barrier energy to break the bond at the crack-tip. Under an applied tensile stress, the weakened bonds break repeatedly, and crack propagates.

DCM-RGM-GALOP Model

The other group of the proposed mechanisms of LME is called 'dissolution condensation mechanism' (DCM) model (aka Robertson-Glickman model-RGM), which was established by Robertson [104] and further developed by Glickman [31,32,94,105]. Robertson described

a stress-assisted dissolution of solid atoms into the embrittler liquid at the propagating crack-tip. At the crack-tip, the chemical potential of solid atoms increases as a result of the applied stress, which accelerates dissolution of solid atoms into the liquid metal. Due to the high diffusion rates in the liquid phase, solid atoms can be transferred from the rapidly propagating tip. Another key factor of this model is the continuous process of initiation and propagation [96,105]. However, this section of the proposed mechanism contradicts the LME observations in the Fe-In system, where distinct initiation and propagation stages were observed [96], so its general validity remains questionable. Glickman [31,32,94,105] further developed this model through a supplementary micro-mechanism known as "condensation"; where the dissolved solid atoms into the liquid (dissolution stage) redeposited on the propagating crack wall (Figure 2.5). In this way, DCM can be considered as a non-electrochemical version of environmentally stress-assisted material degradation, similar to stress-corrosion-cracking. A continuous and rapid mass transfer of solid atoms through the liquid phase is a key-factor in this process [105], which is consistent with the low activation energy of diffusion in liquid phase when compared to diffusion through a solid.

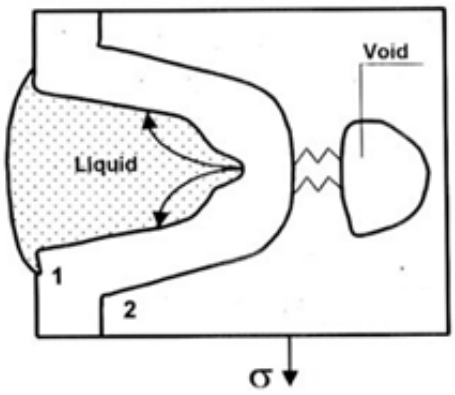

Figure 2.5: A schematic description of the dissolution-condensation model of LME where arrows show the mass diffusion flux of solid atoms in the liquid phase [105]

The DCM was further extended into an associated model, grooving accelerated by local plasticity (GALOP) [32], which is based on the Mullins grain boundary grooving in which small dihedral angles (small liquid-solid interface energy) can concentrate the applied tensile stress at the sharp groove tip. The concentrated stress at the crack-tip will tend to decrease (stress-relieve) by inducing plastic deformation through a localized dislocation activity. This results in significant crack-tip blunting which provides the required sites for redeposition of solid atoms (as described in the condensation micro-mechanism of DCM), but due to crack blunting, the required stress-intensity at the tip decreases. Hence, this model describes a continuous grooving and blunting loop, however, the rate of groove deepening (dislocation activity) should be high enough to overcome the crack blunting. The highlights of the discussed brittle and ductile fracture LME-mechanisms, DCM, and GALOP are presented in Figure 2.6.

2.2.3 Grain Boundary-based Models

The grain boundary-based models emphasize that stress-assisted grain boundary diffusion precedes liquid metal penetration. Importantly, these models assume that the penetration of the embrittler atoms occurs through high diffusion paths into the solid rather than by wetting the grain boundary. However, the Gordon-An [96] model states that mass transfer of liquid phase to the crack-tip still takes place through liquid flow. According to the Gordon-An model [96] and Krishtal [106], grain boundary diffusion is stress-assisted instead of dislocation-aided (as shown in Figure 2.7) [20]. It is stated that first, the embrittler atoms diffuse along grain boundaries that creates obstacles against dislocation slip, and hence, the crack propagates along the grain boundary [18]. However, crack nucleation only occurs after there is a build-up of embrittler atoms. Once the crack nucleates, it

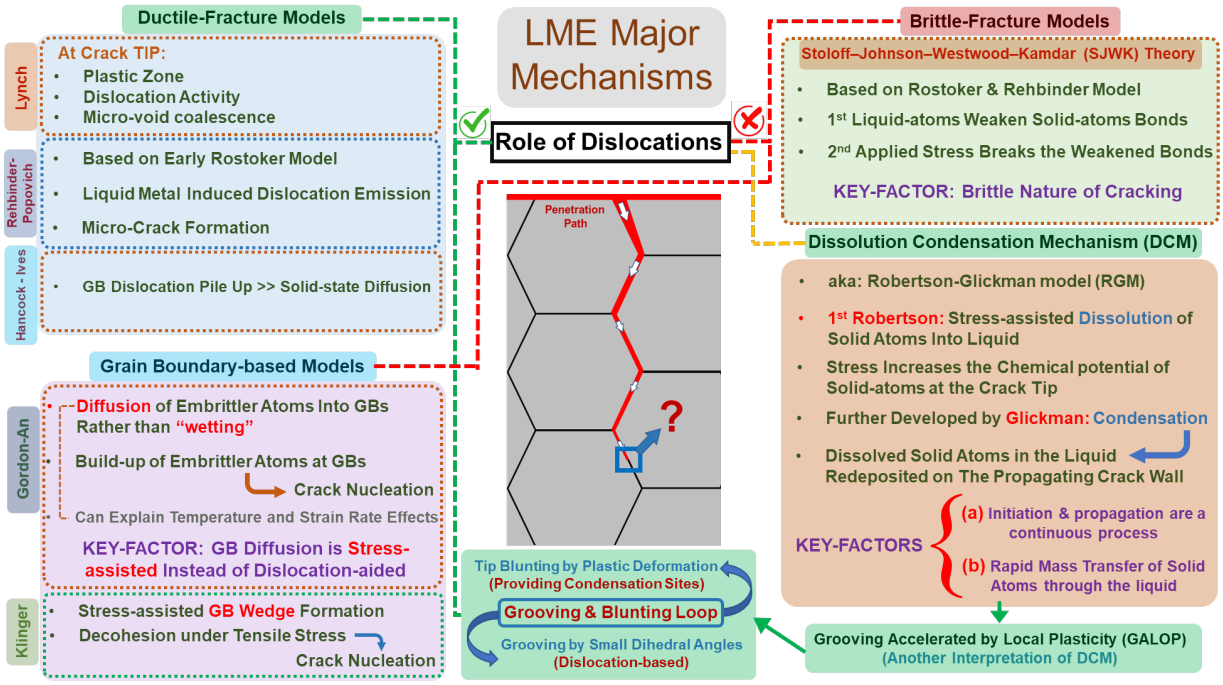

Figure 2.6: Summary of the proposed LME mechanisms emphasizing the major contribution of dislocations at the crack-tip

can grow into the material rapidly. These models describe that grain boundaries show brittle fracture (ductile-to-brittle transition) only in a specific temperature range. Such that, the temperature should be high enough to enable a rapid diffusion path. However, if the temperature is too high, the matrix diffusion of the embrittler atoms away from the grain boundary (into the adjacent solid matrix) becomes competitive and reduces the grain boundary embrittler concentration below that required for decohesion. In other words, there exists two transition temperatures, a lower temperature enabling rapid grain boundary diffusion when a ductile-to-brittle transition occurs, and a higher transition temperature enabling rapid solid-state diffusion when the fracture reverts to a ductile mode again [96].

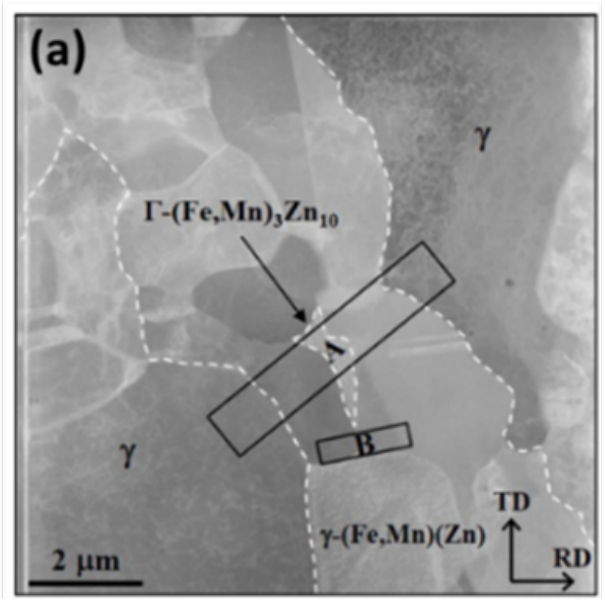

Figure 2.7: TEM micrograph showing the absence of dislocation in the vicinity and crack-tip confirming the minor contribution of dislocation in the Fe-Zn couple LME [18]

The Gordon-An model [96] also describes the effect of strain rate, where higher strain rates increase the brittle-to-ductile transition temperature. This will increase the temperature at which grain boundary to matrix diffusion rate becomes effective. The diffusion-based framework also provides explanation for an incubation time, where it is related to the activation energy required for grain boundary diffusion and is mainly dictated by an Arrhenius-type relation. The Klinger model [107] describes LME mechanism in a similar manner, where after the decohesion occurrence under an applied tensile stress, a crack will nucleate again. The Klinger model requires grain boundary diffusion to precede the cracking. The advancing liquid metal through the opened grain boundary allows more flow of the liquid and hence, a rapid progress of crack into the solid.

2.3 LME Micro-Events: Crack Initiation and Progression

Included in an LME mechanism must be a description for the continuous initiation and propagation of the crack. Within the grain boundary-based model this is described in a multistep process of LME-cracking where a set of "micro-events" leads to the final cracking. Although deconvolution of these micro-events encounters several experimental difficulties due the rapid propagation rate of LME-cracks, the Gordon-An model [96] describes separate stages for crack initiation and propagation, both of which are thermally activated. This includes: (a) a wetting-crack initiation step that is directly triggered by intimate contact of a susceptible solid with an aggressive liquid metal, and (b) rapid progression along the grain boundaries that occurs once the initiated crack is at 10 μm long. However, the Gordon-An model does not account for the necessary re-sharpening mechanism, the model must also include a re-sharpening mechanism to counter-act the blunting at the crack-tip [42,94,96,101,102].

2.3.1 Wetting-Crack Initiation

Before LME cracking initiates, the liquid embrittler must be absorbed into the grain boundary, this is typically described by grooving at the grain boundary. As a susceptible solid is exposed to a liquid metal (with the required wetting characteristics), grooving allows the liquid metal to penetrate deep (a few micrometers) into the solid metal (Figure 2.8), which is governed by the local equilibrium between the energy of the exposed grain boundaries (γ_{GB}) and the solid/liquid interface energy (γ_{SL}) [108,109]. Hence, the dihedral angle (θ) at which the penetration occurs is defined in Eq.2.1 [109]:

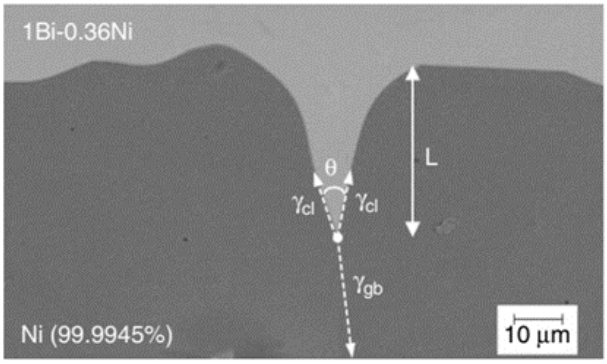

Figure 2.8: Cross-section of a typical grain boundary grooving in Ni-bi couple [109].

$$2\gamma_{SL}\cos\frac{\theta}{2} = \gamma_{GB} \tag{2.1}$$

Due to the isotropy it is assumed that the interface energy for both sides of the liquid grooving are equal. In this regard, the necessary wetting condition is where $\gamma_{GB}>2\gamma_{SL}$. If this necessary condition is not met, the exposed grain boundary remains stable. Although depending on the time exposed to the elevated temperatures, either bulk diffusion or "Mullin's engraving" may take place (Figure 2.9) [108]. Luo et al. [109] investigated the distribution of dihedral angles in various grain boundaries (Figure 2.10) of the Ni-Bi couple in the absence of stress, where the average of the dihedral angles (2) is 40 (after 5hr of annealing at 700°C).

The critical role of temperature in the LME-crack initiation can be defined based on Eq.1. Although grain boundary Gibbs energy shows a linear negative dependence on temperature (Figure 2.11), γ_{SL} decreases at a higher rate due to the solid-material dissolution into the liquid phase [108]. Therefore, there is a transition temperature (T_w) at which the required condition of initial wetting ($\gamma_{GB}>2\gamma_{SL}$) can efficiently be met. This explains the

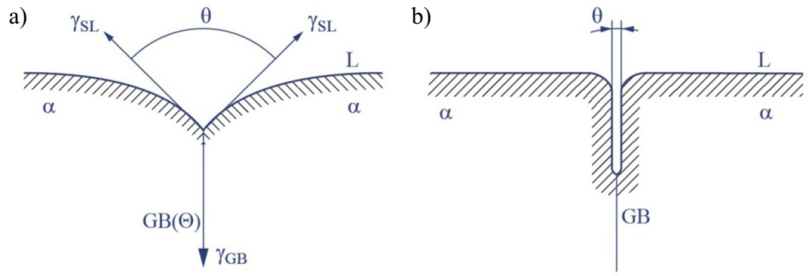

Figure 2.9: The stable grain boundary where (a) the necessary LME wetting condition is not met (Mullins's engraving), and (b) the embrittler liquid film penetrates into the grain boundary and grain boundary rupture takes place [108].

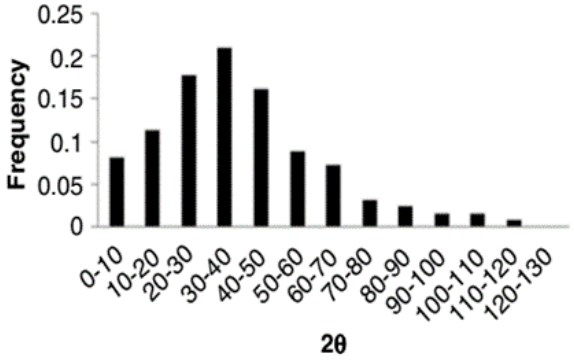

Figure 2.10: The distribution of measured dihedral angles at different grain boundaries in Ni-Bi couple [109].

actual reason that only particular solid-liquid couples are sensitive to LME (Figure 1.1). In the other non-sensitive systems, the energy barrier to produce a groove angle necessary to initiate LME cracking is sufficiently high that the transition temperature (Tw) does not fall within the embrittler's liquid phases-stability range ($T_{Melting}$ - $T_{Boiling}$). However, this theory does not consider the role of the external tensile stress, where external mechanical energy can efficiently reduce the required energy barrier [108].

In the grooving step, having equal interface energies for the two involved grains is

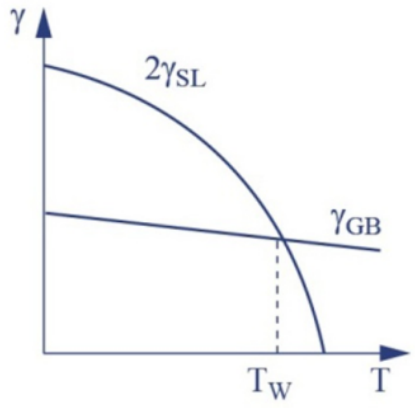

Figure 2.11: Schematic illustration of Gibbs energy of grain boundary and solid-liquid interface, (Tw: transition temperature) [108].

a simplified case, whereas in most of the real-life examples the interface energy is not necessarily equal on both sides of the grain boundary. Unequal interface energies can be attributed to the dependence of the interface energy to grain orientation and grain boundary character e.g. misorientation angle (Figure 2.8) [109]. This partially explains the reason that only a limited fraction of grain boundaries exposed to the liquid embrittler show LME-cracking. In other words, due to an unsatisfactory balance between the surface forces, liquid penetration into the grain boundary is thermodynamically or kinetically unfavorable; it can potentially take place only in a small fraction of the exposed grain boundaries. Additionally, due to the undoubtable role of applied tensile stress on the LME phenomenon, only a few grain boundaries are preferentially orientated to that of the of the applied stress direction [109]. Hence, even by meeting the necessary spontaneous wetting condition, the energy barrier can only be overcame in certain grain boundaries. Therefore, only a small fraction of grain boundaries act as potential crack initiation sites. Apart from the dihedral angle standpoint, the orientation of grains also may affect their solubility into

the liquid metal, which in-turn affects their edge-rounding behavior, where any adsorption and segregation of alloying atoms from the liquid, and solid matrix, respectively, can affect grain boundary energy and, therefore, the wetting behavior.

According to the Gordon-An model [96], LME initiates when the state of the embrittler atoms change from absorbed to dissolved. The dissolution is associated with a localized change of melting point by making bonds with the solid-matrix, and hence, requires an incubation time. The required incubation time (t_n) directly depends on the activation energy of dissolution of embrittler atoms at the surface (ΔG_s), and grain boundary diffusion (ΔG_d) (Eq.2.2) [96]:

$$t_n \sim \exp \frac{\Delta G_s}{RT} \exp \frac{\Delta G_d}{RT} \tag{2.2}$$

According to this model, lowering the solid-liquid interface energy results in lower ΔG_s and therefore, reduced crack-initiation time.

2.3.2 Rapid Crack-Progression

Once the LME-crack nucleates in the wetting stage and passes the critical length (10 μm in the Cu-Bi couple [94]), it rapidly propagates along the grain boundaries. However, a continuous and rapid progression of an LME-crack requires an efficient tip re-sharpening micro-mechanism. As described by the GALOP model [32], several micro-events (smaller cracks) propagate sequentially ending in a final crack length ($L = n\Delta L$),($\Delta L << L$). As stress relaxation blunts the groove tip (by local dislocation activity) (Figure 2.12). After the repetitive grooving-blunting, a macro LME-crack is created. The GALOP model proposes that this repetitive grooving-blunting phenomenon provides the efficient mechanism for

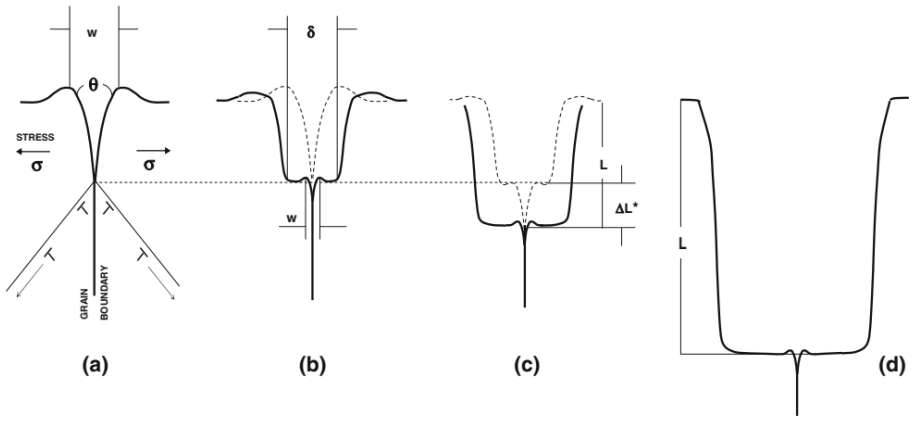

Figure 2.12: Grooving Accelerated by Local Plasticity (GALOP) mechanism (a) LME initiates by grooving into the solid metal grain boundary, (b) under the applied tensile stress (σ), sharp grain boundary groove tip blunts and creates a miniature shelf of the width but grain boundary groove continues to extend, (c) blunting takes place due to plastic deformation, and (d) grooving-blunting micro-events occur repetitively resulting in the final crack length of L [32].

re-sharpening. Although the GALOP best describes the essential re-sharpening (grooving) stage in LME-crack progression, however, as stated earlier the role of dislocations in LME phenomenon remains questionable and still requires support by experimental and modeling results.

Klinger et al. [107] modeled the formation of grain boundary wedge due to grain boundary diffusion of embrittler atoms (Figure 2.13) under applied tensile stress normal to the grain boundary plane. In this study, a semi-infinite bi-crystal of solid material (B) exposed to an infinite supply of liquid metal (A) at the surface. It is assumed that bulk diffusion is negligible compared to that of the grain boundary diffusion, as this is a realistic situation where the grain boundary diffusion and embrittlement takes place at temperatures$>0.4T_m$. The diffusion flux divergence towards the grain boundary results in a narrow and deep diffusion wedge. To comply with the atomic structure of metal B

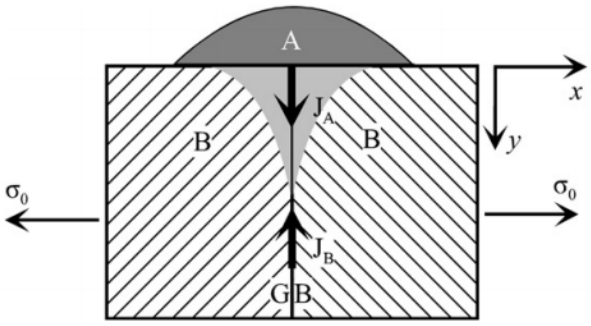

Figure 2.13: Diffusion of liquid metal atoms (A) along the grain boundary in the bicrystal of solid metal (B) under the external stress of 0 (normal to the grain boundary plane) [107].

at the vicinity, the wedge must show high coherency with the surrounding B-atoms [107]. However, once the wedge width increases, the wedge loses its coherency. Due to the atomic structure collapse and high concentration of A-atoms, the wedge melts. After the melting of the wedge, the embrittler flows inward the grain boundaries.

The grain boundary wedge formation hypothesis [107] also sheds light on the critical role of tensile stress in LME. The diffusion wedge width directly correlates to the magnitude of applied tensile loading on the grain boundary plane, where increased tensile stress increases wedge width (Figure 2.14). Nonetheless, the depth of diffusion wedge is independent of the stress magnitude (represented by dimensionless factor of α, Eq.2.3) [107].

$$\alpha = \frac{\sigma_0 \Omega}{kT} \tag{2.3}$$

Where Ω is the atomic volume of the components at grain boundary, σ_0 is the applied stress, k is constant, and T is temperature. The comparison of relative grain boundary concentration and the penetration depth in various dimensionless time intervals in zero-stress

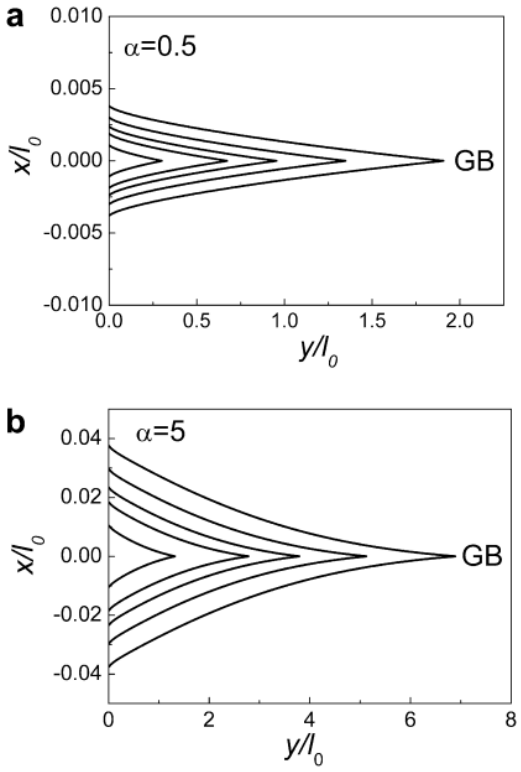

Figure 2.14: The iso-concentration lines in the vicinity of the grain boundary at (a) α=0.5 (low-stress), and (b) α=5 (high stress) conditions [107].

(α=0, dashed lines), low-stress (α=1), and high-stress (α=5) conditions are illustrated in Figure 2.15. It must be noted that in Figure 2.15, in the absence of applied tensile load (the zero-stress condition), the concentration of embrittler at grain boundary is described through the classic error-function [107]. Under the applied tensile stresses, deep and narrow penetration of embrittler atoms along the grain boundary and ahead of the blunted crack-tip acts as crack-tip re-sharpening mechanism after each micro-step of embrittler flow along the opened LME-crack.

The essential role of re-sharpening (grooving) in LME-crack rapid progression is well

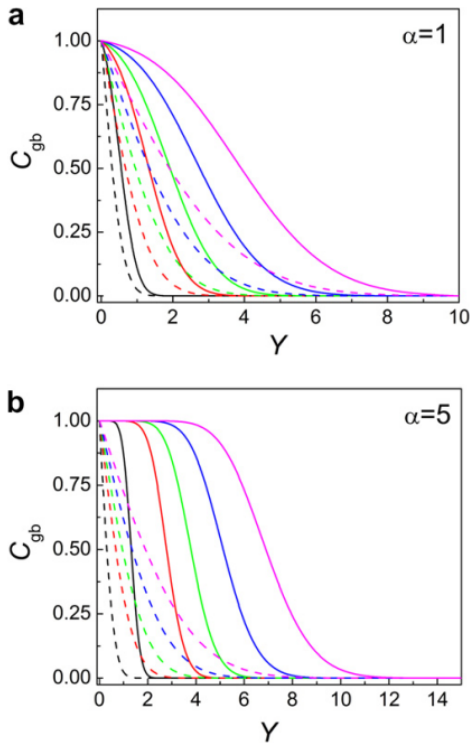

Figure 2.15: The relative grain boundary concentration (C_{gb}) versus the dimensionless penetration depth (Y) in zero-stress (α=0, dashed lines), (a) low-stress (α=1), and (b) high-stress (α=5) conditions [107].

illustrated by Namilae et al. [63]. Atomistic simulation of Al-Ga couple showed that under the applied stress, the presence of liquid-Ga induces a rapid crack progression. In the presence of embrittler atoms (Ga), the diffusion of the embrittler atoms into the grain boundary creates a diffusion wedge similar to the prediction of the Klinger model [107]. In the similar condition and the absence of liquid-Ga at the crack-tip, the applied stress causes crack-tip blunting rather than crack opening. This indicates the minor contribution of dislocations in LME-crack propagation in a direct comparison with the classical crack propagation in metallic materials.

2.4 Grain Boundary Decohesion Mechanism

As stated earlier, the grain boundary-based models (Gordon-An and Klinger [96,107]) require a short-length diffusion of embrittler atoms ahead of the crack-tip. In most of the LME couples, grain boundary decohesion occurs through the formation of sub-monolayer or monolayer [79,109]. Alternatively, in some LME couples (e.g. pure Ni and Cu) a long-range adsorption of atoms and subsequent atom bilayer formation changes the grain boundary atomic bonds from metallic Ni-Ni or Cu-Cu, to Bi-Bi, which has a much lower strength than the original grain boundary [79,109] (Figure 2.16). The penetration of Bi-atoms along the grain boundary of Ni and the formation of Bi-bilayer ahead of the crack-tip is shown in the study by Luo et al. [79] (Figure 2.17). It must be noted that the presence of sub-monolayer or monolayer of Bi along the Ni grain boundaries does not lead to LME as the bonds between Ni and Bi still is not weak enough to break under the applied tensile forces. However, when the absorption of Bi-atoms reaches bi-layer configuration, complete decohesion and LME occurs due to relatively weaker bonds between Bi-Bi at the interface. The observed bilayer formation of embrittler atoms may be restricted to pure Ni or Cu systems with clean grain boundaries, whereas in heavily alloyed metals, potential segregation of impurities into grain boundaries can alter the grain boundary character, and hence, the atomic configurations.

Contrary to the observed bilayer formation, in the other LME couples the presence of sub-monolayer or monolayer is sufficient to induce grain boundary decohesion. It is stated that grain boundary cohesion can be affected through (a) modification of interface energy as suggested by the earlier study of Rice and Wang [110], (b) straining due to atomic size difference of the matrix and embrittler [5], and the recently proposed (c) electronic state modification at grain boundary due to the presence of embrittler atoms [111].

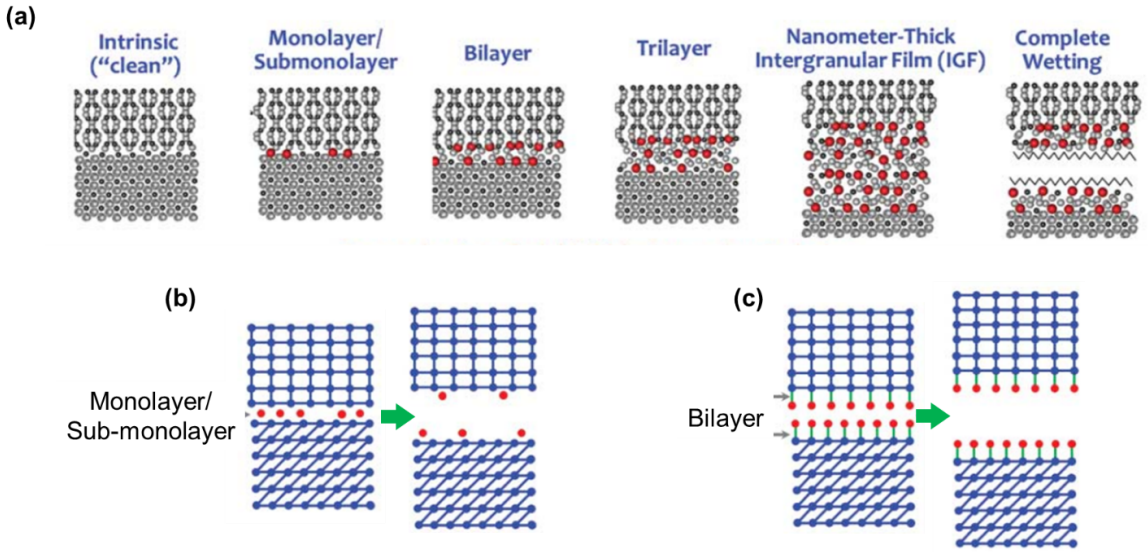

Figure 2.16: (a) Six distinct interfacial configuration of impurity atoms along the parent grain boundary, (b) the most common grain boundary decohesion in embrittler atom adsorption model, and (c) the proposed configuration of the Ni-Bi couple showing the presence of bilayer along the grain boundary [79].

2.4.1 Effect of Atomic Size Difference on Grain Boundary Cohesion

In the earlier study by Dinda [112], tin (Sn) and lead (Pb)-induced embrittlement in steel is investigated. Compared to the Fe-Pb, the Fe-Sn couple is more LME susceptible, which was attributed to the relative atomic size of Pb- and Sn-atoms. While both embrittlers are bigger than Fe, the Sn size-difference is smaller than Pb. Hence, it is concluded that the accommodation of Pb-atoms at available atomic sites of parent grain boundary is more difficult. The first principles quantum mechanical calculations by Schweinfest et al. [5] support the key role of atomic size difference in grain boundary decohesion. This work showed that the over-sized embrittler atoms such as Bi weaken the atomic bonding by increasing the Cu-Cu bond length. These authors claim that the Frenkel

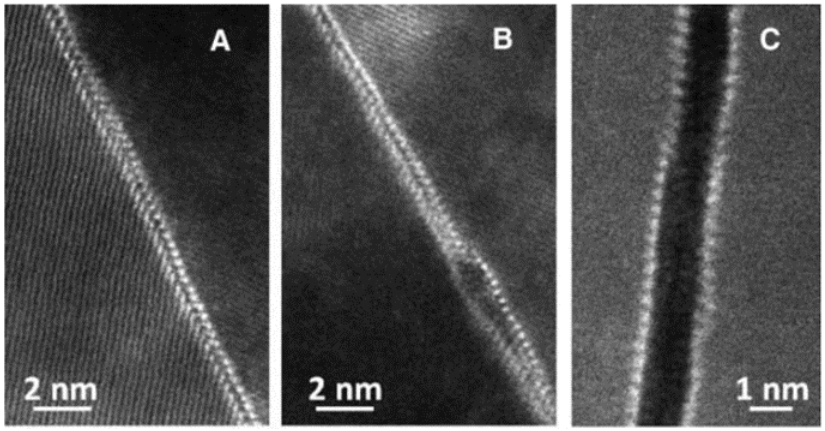

Figure 2.17: STEM-HAADF micrographs showing (a) the formation of Bi bilayers along the grain boundaries of a Ni polycrystal (b) and (c) depicts the decohesion of the weak Bi-Bi bonds [79].

theoretical strength depends only on the atomic volume which is consistent with the minor difference in the embrittlement effects of Bi- and Pb-doping on Cu, and therefore, supports the hypothesis that embrittlement susceptibility is affected by the atomic size difference between the solid metal and the embrittler [5] (Figure 2.18).

The recent study by Peng et al. [113] modeled the effects of embrittler atoms and grain boundary expansion in the Fe-Zn couple in two conditions of: 1-clean, and 2- Zn-doped grain boundaries. As depicted in Figure 2.19, compared to the bond length of the Fe(2)-Fe(-2), Fe(1)-Fe(3), Fe(1)-Fe(2) in the clean grain boundary, the corresponding Fe(2)-Fe(-2), Zn(1)-Fe(3), Zn(1)-Fe(2) in the Zn-doped grain boundary increased by 0.096 Å (∼4.3%), 0.056 Å (∼2.2%), and 0.088 Å (∼3.4%), respectively (Figure 2.19). Zn-doping also caused the Fe(2)-Fe(3) bond length increase about 0.015 Å. The expanded Zn-doped grain boundary can be explained through the higher atomic radius of Zn than Fe (difference: 0.09 Å). The increased bond length directly affects the bond strength, and hence, the grain boundary cohesion [113]; However, as the change in bond length is small, changes in lattice

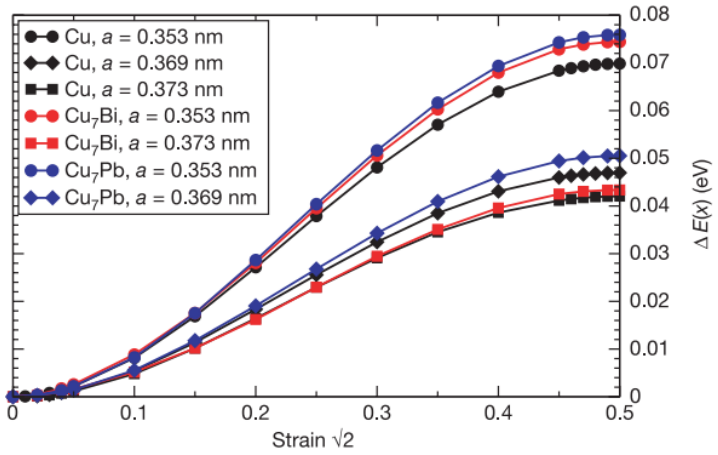

Figure 2.18: Internal energy versus strain in FCC lattice unit cell sheared into itself (111) [112] showing the Frenkel theoretical strength dependence on the atomic volume and the key role of atomic size difference in the bond weakening [5].

strain does not completely explain the decrease in grain boundary cohesive strength.

The tensile strength of the clean and Zn-doped Fe grain boundaries was investigated through first-principles computational tensile test (FPCTT) [113]. In the presence of Zn, the fracture strain of the grain boundary reduces from 32% (in the clean state) to ∼12% (Figure 2.20a). When the simulated atomic movement is seen, the clean grain boundary undergoes a considerable deformation to 34% of strain that the grain boundary symmetrical characteristics is not detectable anymore [113]. As expected, the fracture in the pure Fe grain boundary occurred due to the destruction of the Fe-Fe atomic bonds. In contrast, the Zn-doped grain boundary fractures at 14% of strain; however, the atomic configuration of the grain boundary remained similar to the zero-strain state (Figure 2.20b and c). Interestingly, in the Zn-doped grain boundary, the fracture sequence is as follows: (a) the Fe(2)-Fe(-2) bond due to its parallel direction to that of the applied tensile carries the majority of the strength, (b) the Fe(2)-Fe(-2) bond (the main bond of the grain boundary)

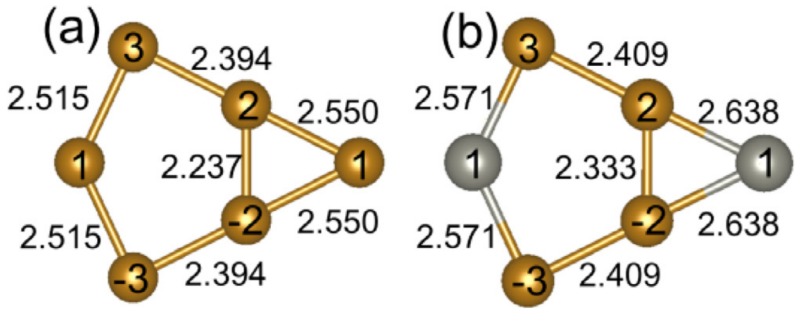

Figure 2.19: The configuration of the Fe–Fe and Fe–Zn bonds in a (a) clean and (b) unclean grain boundary. (Note: The brown and gray atoms represent Fe: brown and Zn: gray atoms, unit: Å) [113].

and the Zn(1)-Fe(3) bond breaks, (c) the Zn(1) bonds with Fe(2) and forms a new Zn(1)-Fe(2) bond, which explains the delay to complete fracture (to 26% strain) [113] (Figure 2.20).

2.4.2 Electronic Effect of Embrittler Atoms on Grain Boundary Cohesion

Although the grain boundary expansion due to the embrittler atoms is considered as one of the grain boundary weakening mechanisms, the role of electronic structure in embrittlement has been reported in an early study by Losch [114]. The majority of strong embrittling elements belong to, but are not limited to, the 3-5 period of groups: IV,V, and VI of periodic table of elements such as Sn, Sb, P, S, Si [115]. This means that there exists a meaningful relationship between their similar electron configuration in outer shells and their embrittlement effects on grain boundaries. The essential role of electronic (sub-atomic) forces in LME was later confirmed by Duscher et al. [116] in the Bi-induced embrittlement of Cu grain boundaries. In this framework, the presence of certain solute elements at grain bound-

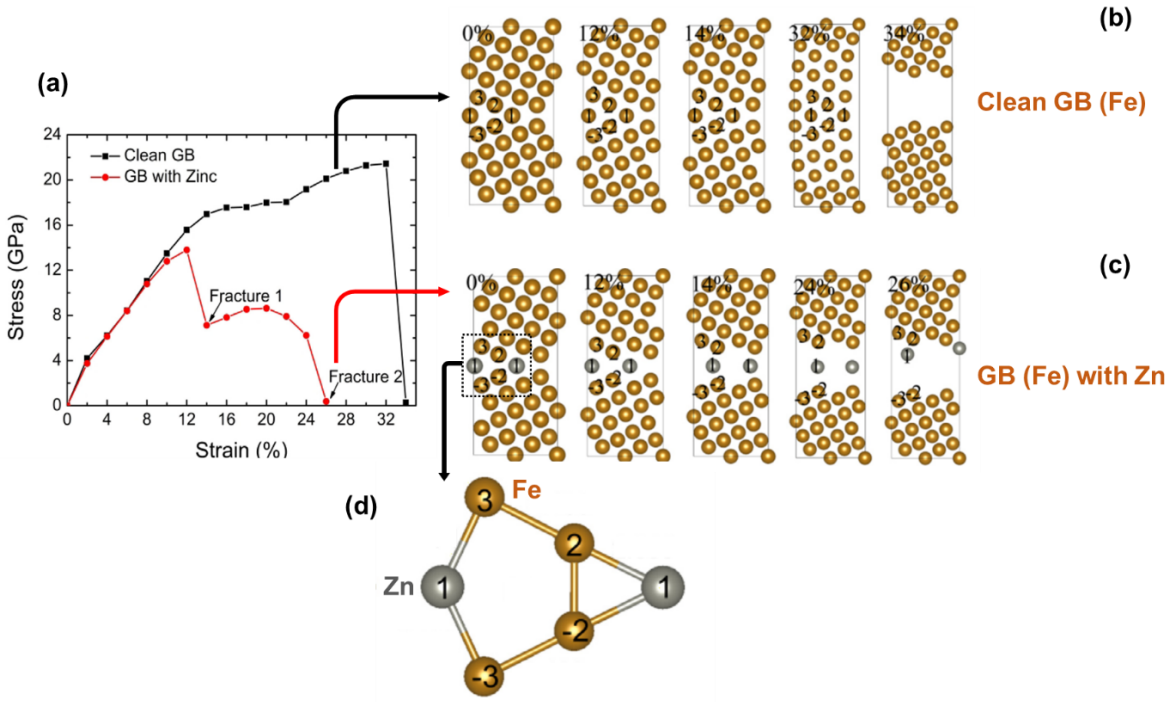

Figure 2.20: (a) The first-principles computational tensile test (FPCTT)-based stress and strain curve of (b) the clean, (c) Zn-doped grain boundaries, and (d) the corresponding configuration of Fe (brown) and Zn (gray) atoms [113].

aries weakens the bonding by drawing charge from neighbor metallic bonds. In a direct comparison of a clean and a Bi-doped grain boundary, it was revealed that Bi-segregation imposed no drastic change in arrangements of grain boundary atomic sites. This is due to the fact that Bi atoms only substitutes Cu in specific atomic sites (the largest space) at grain boundary [116] (Figure 2.21). The absence of drastic bond length modification or lattice distortion questions the viability of the aforementioned embrittlement mechanism. It has been shown that Bi-atoms occupies the middle site of the pentagonal arrangement of Cu-atoms at the grain boundary. Therefore, the s-band of the neighboring Cu-atoms is more than half full (with a closed 3d shell) that detrimentally affects the fracture toughness

of Cu. When the same modeling was carried out using Ag-atoms (as embrittler) located in the same sites with Bi, such behavior was not seen (Figure 2.22). This is consistent with experimental results that show Ag does not embrittle Cu grain boundaries, and in-turn confirms the key role of charge density influence on the grain boundary embrittlement.

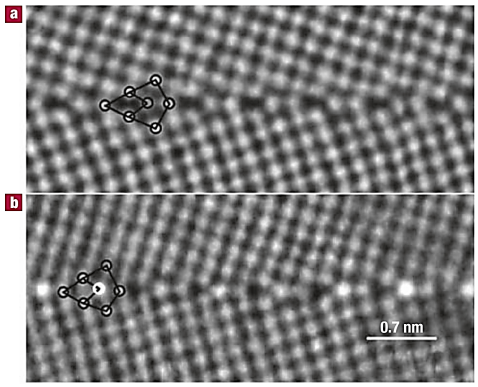

Figure 2.21: Atomic resolution images of (a) clean, and (b) Bi-doped Cu grain boundaries (the brighter atoms: Bi) [116].

The recent study of the Fe-Zn couple also indicated that the charge density plays a key role in bond-strength modification in embrittler-doped grain boundaries. As shown by Peng et al. [113], the primary Fe(2)-Fe(-2) bond strength loss is not only due to the bond length increase but also as a consequence of the charge density change. Peng et al. [113] have observed that in the unstressed state, the charge density of the primary Fe-Fe bond at the Zn-doped grain boundary is considerably lower than the clean grain boundary (Figure 2.23). At 14% of strain, the blue area reaches its maximum and fracture-1 occurs (as shown in Figure 2.20).

Further investigation through differential charge distribution indicated that although there is a metallic bond with the neighboring Fe-atom in the clean grain boundary (as the primary bond of the grain boundary), when Zn is added to the system, the doped-Zn-atom

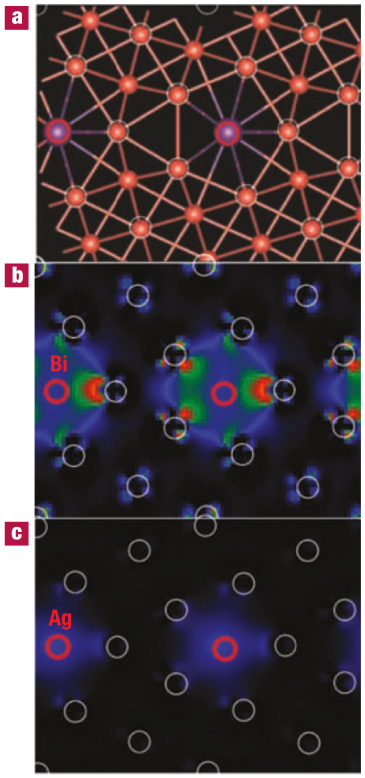

Figure 2.22: The grain boundary structure of Cu (the red-circled atoms represent the embrittler atoms sites, The charge charge density at Cu grain-boundary (b) Bi-doped, and (c) Ag-doped (Note: the brighter regions represent stronger electron charge density) [116].

establishes a directional covalent bonding with the Fe-atom (Figure 2.24). This explains why the directionless charge accumulation (metallic bond) in the clean grain boundary changes to an unequal and directional charge (covalent bond) in the Zn-doped system (Figure 2.24). This led to the transfer of charge between the primary bond of (Fe(2)-Fe(-2)) to the vicinity of the doped Zn-atom at the grain boundary. These findings are consistent with the first-principles study of Ga-doped Al grain boundaries [34]. As Zhang et al. [34] reported, the interatomic distance of Al-atoms at grain boundaries show a minor change after Al-doping, which contradicts the grain boundary expansion hypothesis [12,

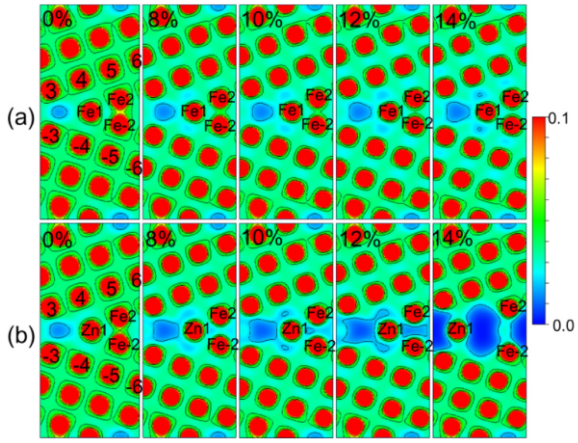

Figure 2.23: Charge distribution map of the primary Fe (2)–Fe (2) bond and the adjacent bonds in the representative (0 0 2) plane of the (a) clean, and (b) Zn-doped grain boundary at different strain values (unit: electrons/ Bohr) [113].

107]. However, the electronic structure of the Ga-doped grain boundary of Al is drastically changed compared to a clean grain boundary [34].

2.5 Effect of Grain Boundary Solute (co-dopant) on LME

Dinda [112] systematically investigated the influence of impurity elements on lead-induced embrittlement of austenite grain boundaries in steels that was used in the earlier hydrogen embrittlement studies [117,118]. This showed that crack propagation follows a path containing impurities such as antimony (Sb), tin, or phosphorus (P). The steel was doped with a considerable level of antimony, tin, and phosphorus, then subjected to various heat-treatments to promote segregation along the prior grain boundaries. Dinda [112] analyzed the material prepared following conditions: (a) unsegregated-not wetted, (b) unsegregated-

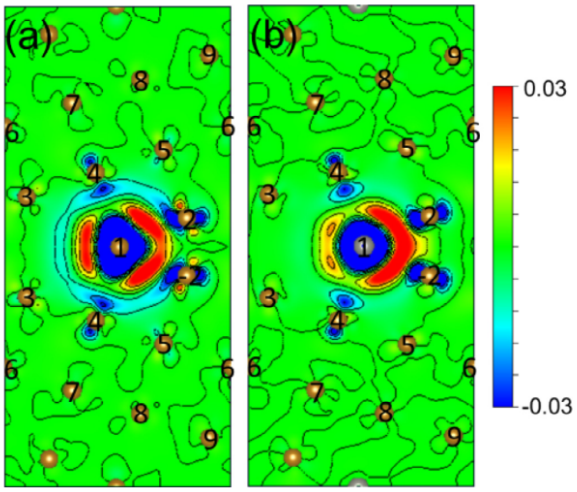

Figure 2.24: Differential charge distribution of (a) Fe (1) atom (brown) in the clean, and (b) Zn (1) atom (gray) in the Zn-doped grain boundary (plane: (0 0 2)). (Note: the red area: charge accumulation, and the blue area: charge loss, unit: electrons/ Bohr) [113]

wetted, (c) segregated-not wetted, (d) segregated-wetted conditions, and (e) an undoped high-purity steel. All the samples were tested in lead and tin environment as embrittler liquids [112]. Interestingly, in the tin- and antimony-doped conditions, LME susceptibility increased (lower ductility). Dinda showed that as phosphorus has a high tendency to segregate to grain boundaries, phosphorus segregation would be unintentionally present. Arsenic (As) also showed similar behavior to phosphorus, where minor segregation could trigger LME. Therefore, the observed inconsistency in phosphorus- and arsenic-segregated conditions shows that these impurities may not be controlled trace elements for investigating the solute-segregation effect on LME.

The effect of grain boundary segregation on LME can be explained based on the brittle bond-breaking approach (the brittle SJWK model [101,102]), where the ratio of the effective strength of bonds at the solid metal surface in the presence of a chemisorbed embrittler atom (σ_e) to that of the shear strength required to overcome barriers to dislocation motion

(τ) should be considered [112]. As this stress ratio (Eq.2.4) falls below a critical value, brittle fracture takes place. However, the critical value of the stress ratio relies on the number of available sites for embrittler atoms to reduce cohesive force of atoms at grain boundary [112]:

$$\frac{\sigma_e}{\tau} = \frac{\sigma_0(1-\beta\theta)}{\tau} < (\frac{\sigma_e}{\tau})_{critical} \tag{2.4}$$

Where σ_0 is the theoretical strength of the surface bonds, β is the embrittlement coefficient, and θ is the fractional coverage of the interface by absorbed embrittler atoms and can be defined as follows (Eq.2.5) [112]:

$$\theta = \frac{N_e}{N_0} = [1 - \exp\frac{\Delta E}{kT}] \tag{2.5}$$

where N_e is the number of available sites adsorbed embrittler atoms and reduce cohesive force at grain boundary, N_0 is the number of possible sites of adsorption. The impurity segregation drastically affects the ability of the embritller atoms to be absorbed at the grain boundary ahead of the crack-tip which is reflected in ΔE (change in free energy as a result of embrittler absorption at grain boundary). The absorbability can be either reduced or increased by segregation, which depends on the size difference of segregated and the matrix atoms [112]. The presence of larger segregated atoms at grain boundary provides more available space for the embrittler atoms. The required lattice expansion to accommodate the embrittler atoms can be significantly increased by the applied tensile stress on the grain boundary [112]. This, in-turn, provides supplementary rationale for the essential role of tensile stresses for LME occurrence. On the other hand, the effects of impurity segregation on solution hardening near the grain boundary and at the tip of propagating crack must be considered. This can increase the shear strength required

for dislocation motion by imposing efficient obstacles against the dislocation at the tip. However, the highly localized obstacles against dislocation motion at the vicinity of LME crack cannot be detected in overall yield strength of the material.

Generally, metallic bonds are ductile due to their spherical and non-directional bond that can easily break and accept inserting atoms by making new bonds and accommodate plasticity through dislocations motions. However, as discussed earlier, the addition of certain embrittler atoms will create covalent bonds along the grain boundary. Covalent bonds are known to be rigid due to orbital overlapping in specific directions, which means they are less ductile than the metallic bonds not exposed to the embrittler [114]. Hence, covalent bonds will have reduced elasticity when exposed to applied deformation, showing brittle characteristics by cleavage fracture. Although it may be speculated that segregation of embrittler atoms into grain boundaries and subsequent formation of covalent bonds are extremely strong, requiring very high applied forces to overcome; the presence of metal-impurity bond reduces the strength of the adjacent metallic (metal-metal) bonds electronically (Figure 2.25a and b). This explains that the fracture path along grain boundaries containing segregated elements is through electronically affected metallic bonds which may frequently cross grain boundaries due to boundary geometrical irregularities [114] (Figure 2.25c).

From another perspective, the presence of impurity segregation at grain boundaries affect the Kc (fracture toughness) [32]. The LME-cracking mechanism includes micro-events, and in particular, a "pure-mechanical" rapid propagation step [32]. Hence, the effects of grain boundary segregation on LME can be interpreted as a toughness reduction of grain boundaries. When K at the crack-tip reaches the segregation-reduced fracture toughness (K_c), rapid and pure mechanical failure takes place [32]. The effects of grain boundary impurities on LME is well evidenced by Meshinchi et al. [119]. In the Ni-Bi

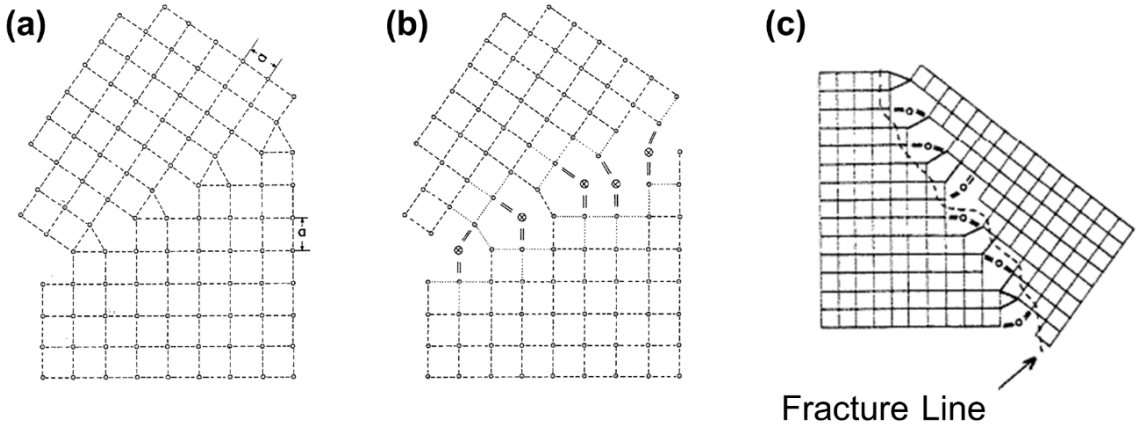

Figure 2.25: Two-dimensional demonstration of (a) clean, (b) impurity-segregated 53 tilt grain boundary where dashed and dotted lines indicate normal M-M metallic bonds and modified M-M bonds due to the impurity segregation, respectively, and (c) the proposed model [114].

couple it has been found that the addition of minor amounts of impurities (co-dopant) in either the solid or embrittler significantly alters embrittler penetration behavior. It was seen that 0.5 at.% of impurity can enhance the penetration depth of liquid metal about six times. The impurity presence also affects the equilibrium dihedral angle in the LME initiation stage. Although the segregation of impurities into grain boundaries reduce their energy, imposing a negative influence on the dihedral angle (increased angle), the presence of impurity can have a larger impact on reducing solid-liquid interface energy. This will lead to an overall decrease in dihedral angle, increasing LME severity. For instance, reduction of dihedral angle from 45 to 10 can increase the penetration depth by 4.7 times [119] (Figure 2.26).

The proposed influence of impurities on dihedral angle by Meshinchi et al. [119] is consistent with the Rice-Wang model [110] of intergranular embrittlement and impurity effect on stress-corrosion-cracking behavior stated by Glickman [105]. As discussed earlier,

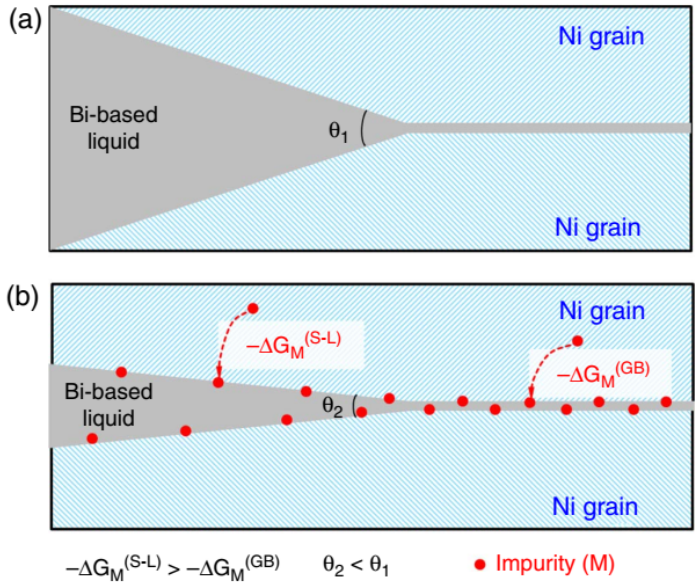

Figure 2.26: Schematic illustration of the effect of impurity on enhancing intergranular embrittler penetration (Note: the red dots represents the impurity) [109].

there is a reduction in grain boundary strength through changes in interface energy, caused by straining due to atomic size difference, and electronic structure modification. Regardless of contribution of each of these concepts in grain boundary decohesion, grain boundary impurity segregation can significantly affect adsorption of embrittler atoms ahead of crack. As a whole, combining the effects of material impurities stated above with the influence of grain boundary-segregation of impurities on mechanical robustness of grain boundary in respect to the "pure-mechanical" stage of crack progression, explains detrimental influence of grain boundary impurity segregation on LME-susceptibility.

Chapter 3

LME-cracking in externally loaded laser welding of AHSS[1]

3.1 Overview

Despite frequent reports of LME during resistance spot welding (RSW), no work has been done to investigate the LME sensitivity in LBW of AHSS. This chapter discusses Zn-induced LME in 3 different AHSS grades: 22MnB5 PHS, medium-Mn TRIP, and TWIP steels. The results show a direct relation between the external load and LME susceptibility, where a threshold tensile stress is necessary to trigger the embrittlement. Electron backscatter diffraction (EBSD) in conjunction with electron probe micro-analyzer (EPMA) results confirmed the intergranular penetration of Zn along the prior austenite grain bound-

[1]This chapter consists of two published Manuscripts: 1-Materials Design, available online: https://www.sciencedirect.com/science/article/pii/S0264127518304507, MH Razmpoosh, A Macwan, E Biro, DL Chen, Y Peng, F Goodwin, Y Zhou, 2018, 2-Materials Characterization, available online: https://www.sciencedirect.com/science/article/pii/S1044580318318515, MH Razmpoosh, E Biro, DL Chen, F Goodwin, Y Zhou, 2018.

aries in upper-critical heat-affected-zone (UCHAZ) of 22MnB5 steel. In 22MnB5 steel, the presence of Zn over the maximum Zn-solubility of austenite promotes α-Fe(Zn) transformation along the LME-crack, which assists ductility loss. In TWIP steel, EPMA results revealed the sequence of LME micro-events: stress-assisted diffusion of Zn into the austenite grain boundaries (ahead of crack-tip), and further liquid-Zn penetration (shown by the peritectic reaction) leading to the decohesion.

3.2 Background

3.2.1 LME in 22MnB5 Press-hardening Steel

In recent years, the production of ultra-high strength components with tailored properties by press hardening of boron steels (e.g. 22MnB5) gained a growing attention for several potential applications such as: A-pillars, B-pillars, bumpers, roof rails, rocker rails, and tunnels [120–126]. Due to issues regarding the Al-Si-coating mixing into the fusion zone and formation of a continuous structure of δ-ferrite, Zn-coating arose as an alternative for the conventional Al-Si-coating for preventing oxidation and decarburization during press-hardening of boron steels [127]. Recently Kang et al. [18] showed the susceptibility of Zn-coated PHS to the intergranular embrittlement through Gleeble high-temperature tensile testing. As claimed by these authors, premature failure occurred in Zn-coated PHS at 850°C due to LME and ductility decreased from 35% to 9%. In addition, Lee et al. [7] reported the occurrence of LME during austenitization/die-quenching of Zn-coated 22MnB5 steel in the outer wall of the press-hardened component.

These results demonstrate that Zn-coated PHS has a potential for Zn-LME when subjected to high-temperature processes under applied tensile stresses, such as laser welding.

Hence, this chapter addresses the influence of process and material parameters on LME phenomenon during LBW of Zn-coated 22MnB5 PHS. The present findings also provide a new insight on LME during the production of tailor welded blanks (TWBs) of Zn-coated AHSSs in automotive structural components.

3.2.2 LME in TWIP and TRIP Steels

Austenite-containing AHSS grades have received significant commercial and research interest because of their exceptional combination of strength and ductility for automotive applications. Among the best known are the classes of TWIP and medium-Mn TRIP steels, in which the austenite phase is stabilized by the addition of high amounts of Mn [129,130]. A high volume fraction of austenite provides a high work-hardening rate through mechanical twinning and deformation-induced martensitic transformation in TWIP and TRIP steels, respectively [131–134]. Zn-based coatings are most commonly used to protect TWIP and MMn-TRIP steels from environmental corrosion; however, the co-presence of a high austenite fraction and Zn-coating has been found to result in severe sensitivity to LME in RSW [135–137].

Based on Gleeble thermomechanical simulation results, Beal et al. [138] reported a drastic reduction in fracture strength and ductility in electrogalvanized (EG) 22Mn-0.6C full austenitic TWIP steel between 700 and 950°C. LME became more severe when Gleeble tests were carried out with reduced holding times at elevated temperatures before the application of tensile stress. At longer holding times, the formation of Fe-Mn-Zn intermetallic compounds at the steel-Zn interface suppressed embrittlement [138]. In other words, by consumption of liquid Zn through the formation of intermetallic compounds, lower amounts of liquid-Zn remained to induce embrittlement. It was also suggested that

the presence of intermetallic phases could act as a barrier between the steel and liquid-Zn [138]. From a practical point of view, during welding, areas of the weld zone are exposed to tensile loading and a temperature range of 700-950°C for short times. RSW and LBW are considered as the main joining methods for thin sheets in the automotive industries. So far, several researchers showed that Zn-coated TWIP steels are prone to Zn-induced embrittlement during RSW. Ashiri et al. [16] showed that, LME could considerably affect the weldable current range of Fe-15Mn-0.5C-2Al TWIP steel. Higher peak temperatures induced by the high electrical resistivity of TWIP steel (rapid nugget growth) and simultaneous presence of liquid Zn resulted in a severe LME cracking. Moreover, it has been shown that the sensitivity of Zn-LME is highly reliant on Zn-coating type. In this regard, GI-coated TWIP steel possesses the highest susceptibility, compared to Galvannealed (GA) and EG-coatings [17].

Based on experimental [7,83,84] and simulation [3,6] research, the tendency to exhibit LME is also governed by the external variables such as composition of the liquid, temperature, and the applied stress. Specifically, it is reported that the penetration depth of liquid layer into the grain boundaries is highly dependent on the applied stress [3,83,139]. According to Nam et al. [3], it is confirmed that liquid-Ga penetrates into the Al grain boundaries much faster by increasing the applied uniaxial tensile stress. More importantly, it has been shown that the effect of the applied stress on Ga penetration depth at the early stage of liquid groove formation is not significant [3]. However, the applied tensile stress over a threshold substantially accelerates grain boundary penetration. Temperature, as the other main external variable, is believed to substantially affect the LME phenomenon [3,140]. Simulation results [3] confirmed that the increase in temperature accelerates nucleation of dislocations along the grain boundaries and overall penetration of the liquid metal.

From a practical point of view, temperature range of 700-950°C and low exposure times could easily come across during welding. In contrast to several studies on LME susceptibility during RSW of TWIP and TRIP steels [15–17,90], there is a lack of knowledge on LME sensitivity during LBW of austenitic TWIP, the new class of austenitic-ferritic MMn-TRIP, and boron press-hardening steels. LME in LBW has only briefly been reported by Favez et al. [139]. This study investigated liquid metal penetration into the austenite grain boundaries in regions adjacent to the weld line during LBW. It is suspected that the presence of liquid-Zn during LBW of AHSS and the stress generated due to clamping could lead to LME crack formation and therefore, affects the structural integrity of the joints and performance of the parts. This chapter studies LME during restrained laser welding of the representative AHSS grades from different generations: 22MnB5 press-hardening, austenitic TWIP, and MMn-TRIP steels.

3.3 Experimental procedure

22MnB5 boron steel sheets with a nominal thickness of 1.2 mm were used in the present study. Table 1 shows the chemical composition of the experimental material. The GA-coating was characterized in detail by means of EPMA and X-Ray Diffraction (XRD). The chemical compositions of the TWIP and MMn-TRIP steels are given in Table 1. The MMn-TRIP steel sheets (1.45 mm thick) were GI-coated (coating weight of 50 g/m^2 per side) and the TWIP steel sheets (1.2 mm thick) were bare. Figure 3.1a shows the experimental setup for applying external loading during LBW. Externally loaded laser bead-on-plate (BoP) trials were performed using an IPG Photonics ytterbium fiber laser system (YLS-6000-S2) mounted to a Panasonic robotic arm. The fiber core diameter, the spot size, and the beam focal length were 0.3, 0.6 and 200 mm, respectively. The experiments were carried out using

Table 3.1: The chemical composition (wt.%) of the experimental 22MnB5, TWIP and MMn-TRIP steels

Steel	C	Mn	Si	P	S	Al	Cr	Ti	B	Fe
22MnB5	0.23	1.2	0.25	0.016	0.002	0.05	0.20	0.031	0.0030	Bal.
TWIP	0.48	14.1	0.04	0.010	0.001	1.95	-	-	-	Bal.
TRIP	0.15	10.4	0.17	0.010	0.010	1.49	-	-	-	Bal.

a laser power range of 4-6 kW and a travel speed range of 8-20 m/min. The machined tensile specimens were used for the laser lap joining of TWIP-TRIP steel and 22MnB5 BoPs are shown in Figure 3.1b and Figure 3.2, respectively. The direction of the applied tensile stresses was parallel to the direction of welding, and the laser bead located at the center of the gauge length. The engineering stress vs. strain curve of the as-received 22MnB5 steel is shown in Figure 3.3 (yield strength of 410 MPa and ultimate tensile strength of 600 MPa). In the 22MnB5 BoP, the normalized tensile stress with respect to the yield strength of the experimental material has been taken into consideration. The engineering stress vs. strain curve of the as-received TWIP and MMn-TRIP steel are shown in Figure 3.4. The results showed yield strength of about 530 and 1100 MPa for TWIP and MMn-TRIP steel, respectively.

In order to investigate the microstructure, sections were cut from the welded material in a plane parallel to the weld line (3mm far from the weld centerline). After mounting, precise grinding (1200 grit) was followed to reach LME-cracks. Afterwards, the prepared samples were polished to a 0.25m diamond finish, and were investigated via scanning electron microscopy (SEM), equipped with energy-dispersive spectroscopy (EDS) and wavelength-dispersive spectroscopy (WDS) for elemental analysis. Detailed analysis of the microstructure and the grain boundaries was carried out by means of EBSD. The EBSD samples were mechanically polished using oxide polishing suspension (OPS) suspension.

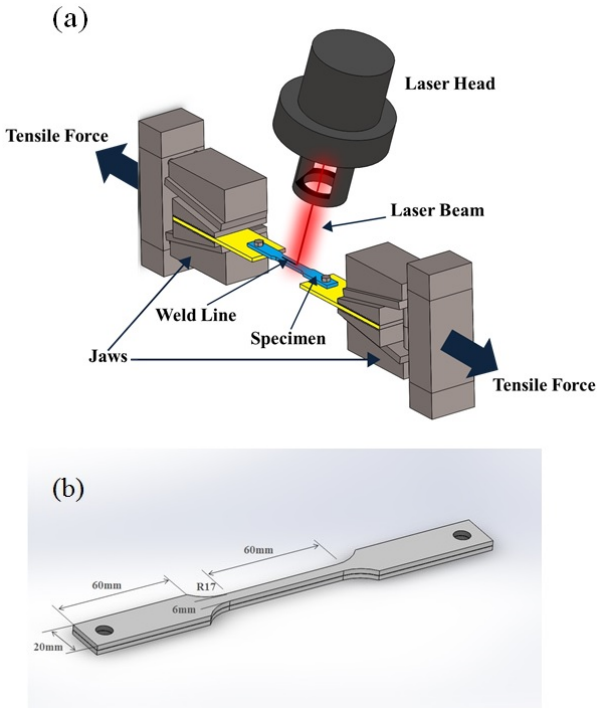

Figure 3.1: (a) The developed setup to apply external loading during laser lap welding, and (b) a schematic illustration of the lap joining specimen geometry and configuration.

The EBSD analysis was carried out by JEOL JSM 7000f field-emission gun SEM equipped with the HKL Technology EBSD system. The acquisition of data was carried out by the Oxford Instruments Aztec software. For EBSD measurements, a step size of 0.25 m, working distance of about 15 mm, and an accelerating voltage of 20 kV were used. The post-processing of the collected data was performed by an HKL Channel5 software. Low-angle boundaries (LABs) and high-angle boundaries (HABs) were defined as grain boundaries with a misorientation of $0.7° < \theta < 15°$ and $\theta > 15°$, respectively.

Various approaches could be used to determine the LME susceptibility: total length of cracks or an overall number of cracks as well as the maximum crack length [141]. As reported by Ashiri et al. [16], the longest cracks could propagate easier under the action

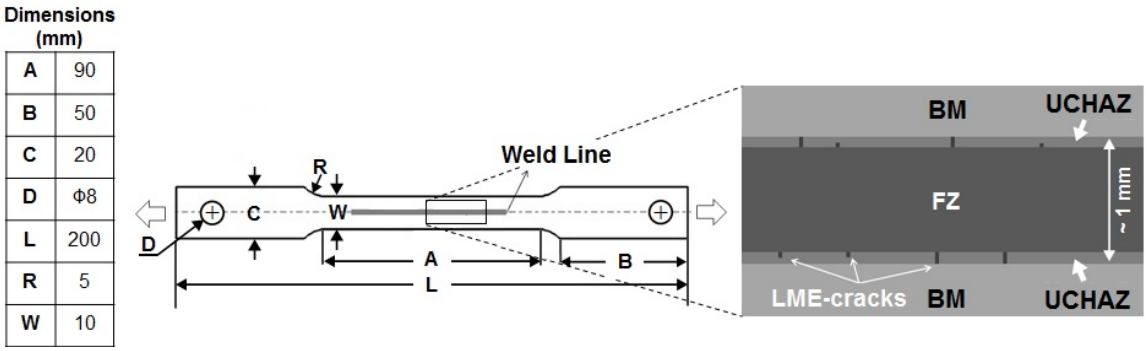

Figure 3.2: Schematic illustration of the specimen, weld line configuration and the observed LME-cracks within the UCHAZ (weld line: 50mm in length) (BM: Base material, FZ: Fusion zone, UCHAZ: Upper-critical heat-affected zone).

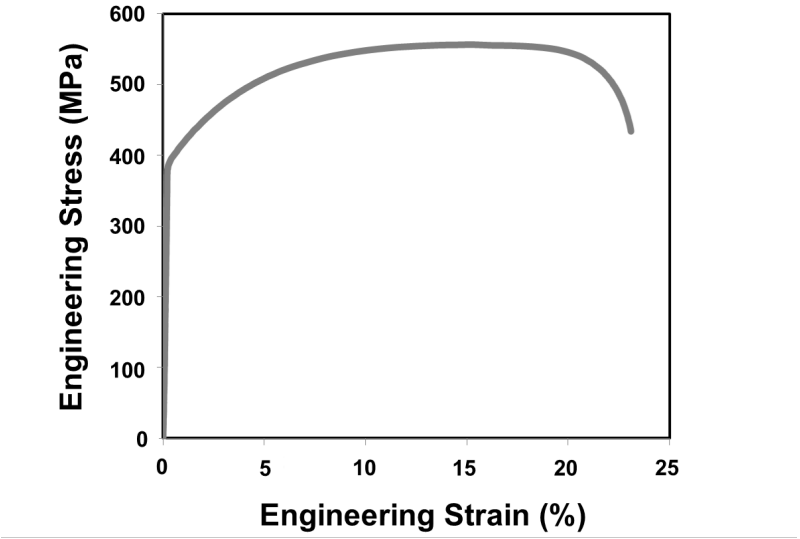

Figure 3.3: Engineering stress-strain curve of the as-received 22MnB5 steel.

of applied stresses because less energy is required. Therefore, the average length of the longest observed micro-cracks in 3 identical welds (100 mm) has been taken into consideration in the present study (Hereafter, the mean crack length is defined as an average of maximum crack length). The term of "micro-crack" refers to LME-cracks with a length

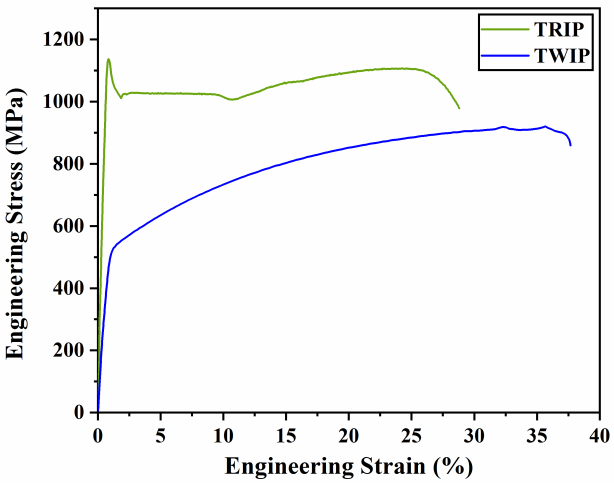

Figure 3.4: Engineering stress-strain curve of the experimental TWIP and TRIP steels.

below $10\mu m$. Any longer crack is referred as "LME crack". It should be noted that according to GM4485M specification for laser welds [142], the joint shall be free of any crack size.

3.4 Results and discussion

3.4.1 LME in 22MnB5 Press-Hardening Steel

Figure 3.5 shows the initial microstructure of the as-received 22MnB5 steel with a ferritic matrix and dispersed colonies of pearlite structure. Moreover, Figure 3.5b-d present the SEM cross-section view of the Zn-coating. The micrograph and EPMA elemental distribution map results illustrate the presence of two main layers inside the coating. In order to provide identification of the phases, XRD analysis was carried out and the results con-

firmed that the coating mainly consisted of Γ-Fe_3Zn_{10}, Γ1-Fe_5Zn_{21} and δ-$FeZn_{10}$ phases (Figure 3.5e). Therefore, the uppermost layer ($\sim 7\mu m$ in thickness) has been identified as δ-phase and Γ/Γ1-phases and were located in the steel-coating interface ($\sim 1-2\mu m$ in thickness). The presence of Γ/Γ1 and δ phases in the coating is in accordance with previous research works, where the (Γ/Γ1) and δ phases are holding about 75 and 90 wt.% of Zn, respectively [143].

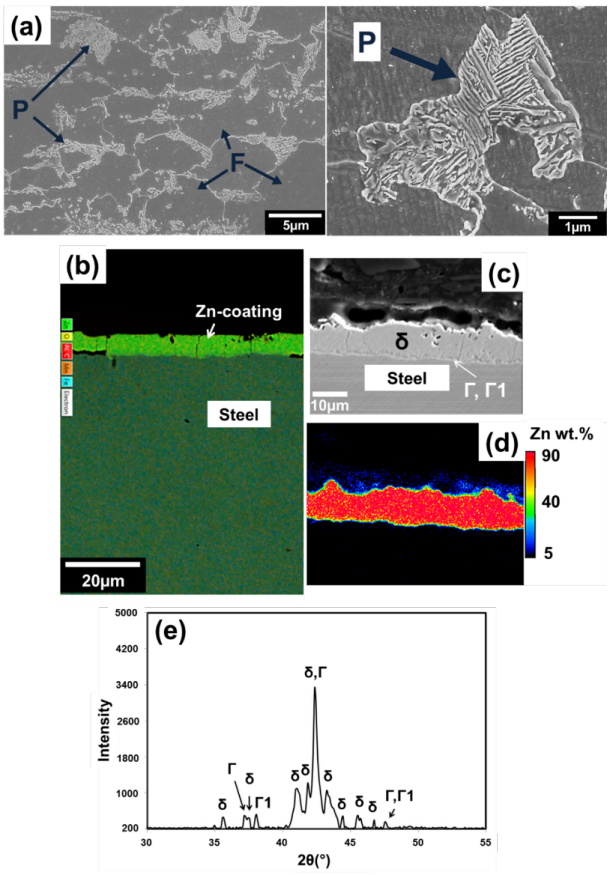

Figure 3.5: (a) Representative microstructure of the as-received 22MnB5 steel, cross sectional (b) EDS elemental distribution map, (c) SEM micrograph, (d) EPMA Zn distribution map, and (e) XRD phase identification of the Zn-coating (where F: Ferrite, P: Pearlite).

It has been observed that laser welding under the applied external load results in the formation of several cracks in the UCHAZ. The influence of the applied external load on mean LME-crack length is shown in Figure 3.6, where the normalized tensile stress to the yield strength (YS) of the experimental material was used. As seen, LME micro-cracking occurs between 80 to 110% of YS. However, LME-free joints can be achieved if the applied tensile stress is less than 80% of YS. Figure 3.7a presents the cross-sectional view of the UCHAZ, where LME micro-cracks appear. Micro-crack initiates from the coating-steel interface and subsequently propagates into the steel substrate. The EDS analysis confirmed the presence of Zn in the vicinity of micro-crack, showing the role of penetrated Zn in weakening at early stages of micro-crack formation (Figure 3.7b).

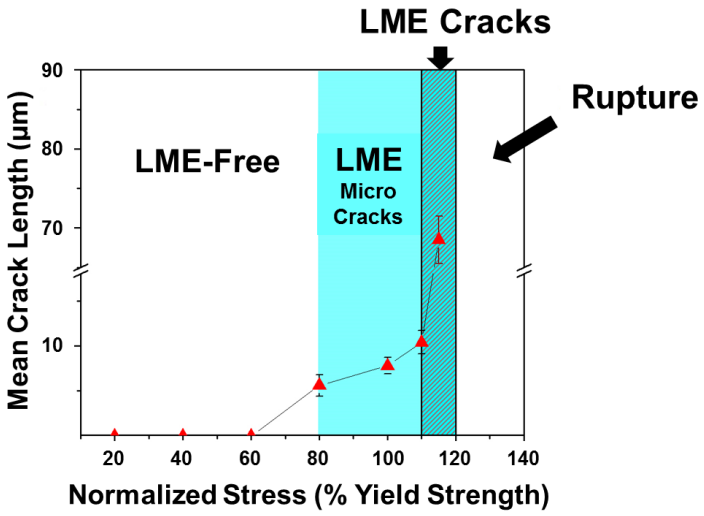

Figure 3.6: Mean crack length vs. the applied tensile stress (under constant heat input per unit thickness of 20 J/mm^2).

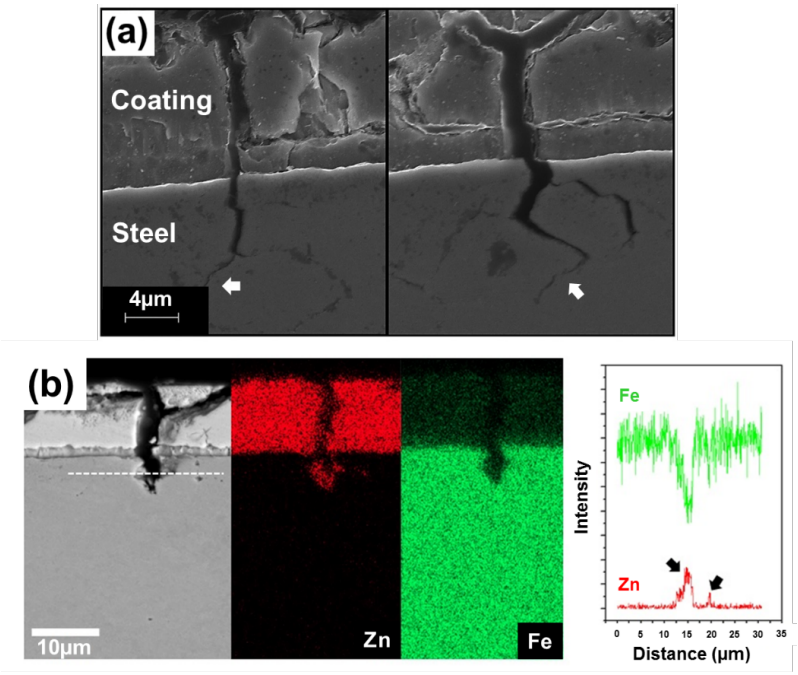

Figure 3.7: (a) Representative LME micro-cracks formed in the UCHAZ under external loading (white arrows), and (b) the corresponding Zn and Fe element map of the LME micro-crack and Zn distribution along the dashed line.

It was observed that at 115% of YS, LME-cracks with an mean length of about 70μm appear in the UCHAZ (Figure 3.8a). Ultimately, by exceeding 120% of YS, abrupt rupture during LBW takes place, which is attributed to a rapid crack propagation into the fusion zone (FZ). Figure 3.8b shows the propagation of LME-cracks from the UCHAZ into the FZ at tensile stresses over 120% YS. In other words, due to a low strength of the molten material in the FZ, any propagation of cracks into the FZ at high stresses result in sudden fracture. Micrograph taken from the fracture surface indicates the presence of 14.9 wt.% of Zn (Figure 3.9b). The observed behavior is in agreement with the LME-failure of Zn-coated 22MnB5 steel under high-temperature tensile testing at 850°C [18].

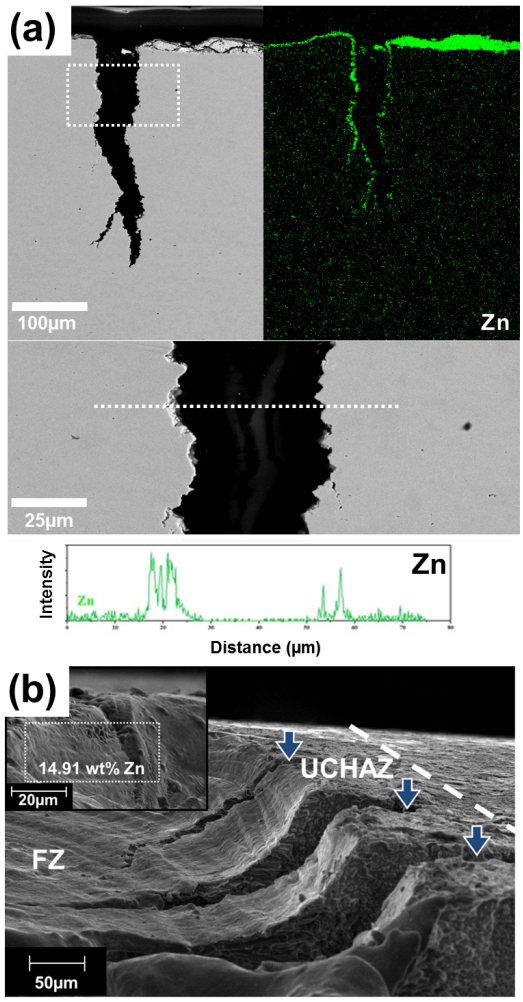

Figure 3.8: (a) SEM micrograph and Zn distribution map of the LME-crack at 115% of the YS, and (b) propagation of LME-cracks formed within the UCHAZ to the FZ during abrupt rupture (arrows) and the presence of Zn on the fracture surface of the specimen.

EBSD results of the LME-crack opening area in the UCHAZ is shown in Figure 3.9. The EBSD phase map (bcc-phase: red), as well as the orientation map, confirms the presence of a fully martensitic structure with a lath martensite morphology in the vicinity of the LME-crack. The presence of negligible retained austenite in the martensitic structure is attributed to the very high hardenability of the material as a consequence of the boron-addition, and is in agreement with previous reports [144,145]. As discussed, the emerged austenite grains in the UCHAZ transforms to martensite during the cooling cycle due to the high hardenability of 22MnB5 steel. To elucidate the role of austenite grain boundaries in penetration of Zn, prior austenite grains (PAGs) should be identified. Based on the literature, there are two main methods for reconstruction of PAGs from EBSD data: complex reconstruction algorithm developed by Nyyssönen et al. [146] and the simpler method described by Hutchinson et al. [144]. The later method is mainly supported by the fact that in a typical martensitic structure boundaries resulting from shear transformation are either LABs or in the range of 50 to 63° [147]. As Ryde [147] suggested, PAGs in EBSD map could be identified by HABs excluding misorientations around $\Sigma 3$, as most of the boundaries resulted from martensitic transformation show $\Sigma 3$ relationship. In contrast, packets of martensite commonly have misorientation over 5° [147]. Based on the comparison by Jarvinen et al. [148], it is indicated that both methods reconstruct almost the same PAG structures. Therefore, in this study PAG structure reconstructed from the EBSD data following the method used by Hutchinson et al. [144]. Figure 3.10a represents the modified EBSD grain map near the LME-crack opening area, revealing prior austenite grain boundaries (PAGBs) (blue lines). The LME-crack propagated intergranularly along prior austenite HABs and it is most likely that the LME-crack did not follow the martensite packet boundaries. This indicates that the LME-crack only propagated before the transformation of martensite during the cooling cycle of the welding. Otherwise, due

to the stress concentration at the tip of the crack after the formation of martensite, the LME-crack tends to follow inter-packets route as well. EPMA Zn-distribution and EBSD maps in Figure 3.10b and c also show how Zn penetrated along PAGBs in side-branches of the main LME-crack. Same color arrows in Figure 3.10b and c illustrate corresponding PAGBs and Zn-penetration.

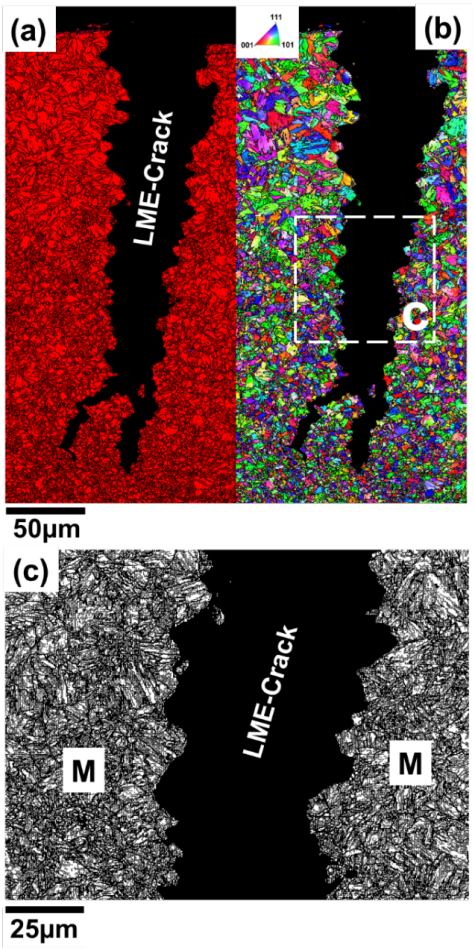

Figure 3.9: The EBSD (a) phase map (red: bcc, blue: fcc), (b) orientation map around the LME-crack opening area, (c) the presence of the martensite lath structure around the LME-crack (M: Martensite).

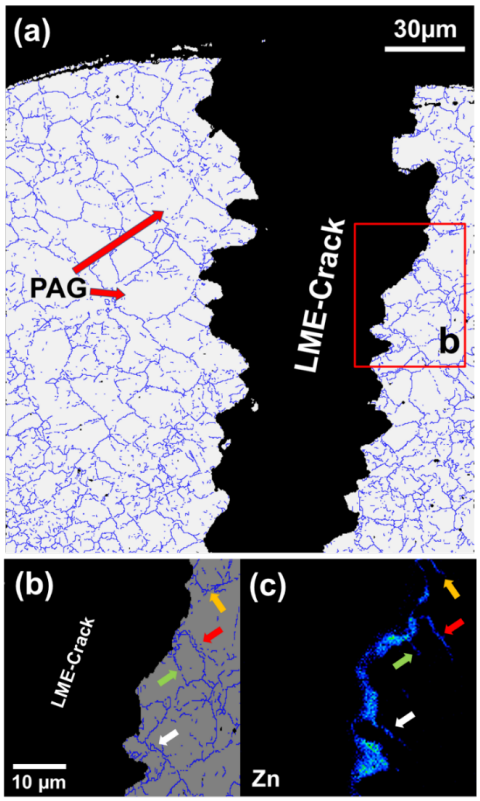

Figure 3.10: (a) and (b) Prior austenite grains boundaries (blue lines) around the LME-crack opening area, and (c) corresponding EMPA Zn distribution map (same color arrows show the diffusion of Zn along the austenite high-angle boundaries) (PAG: Prior austenite grains).

It is noted that due to the limited solubility of Zn in austenite at 900°C, Zn acts as ferrite stabilizer [128]. As claimed by Cho et al. [13], the formation of α-Fe(Zn) at regions surrounding the LME-crack assist the loss of ductility. Figure 3.11a indicates a quantitative distribution of Zn at the LME-crack and side-branches. According to Figure 3.11b, the Zn content in the crack is in the range of 5-42 wt.%. As delineated by Kang et al. [18], the maximum solubility of Zn in austenite and ferrite at the UCHAZ temperature range (>850°C) is about 7 and 40 wt.%, respectively. Therefore, the presence of 42 wt.% Zn in

the vicinity of the LME-crack is in accordance with the solubility range of Zn in ferrite. In other words, as the local Zn-content exceeds the maximum solubility in the austenite (7 wt.%), α-Fe(Zn) becomes stable over the austenite. By the formation of α-Fe(Zn) around the PAGBs, Zn content could reach up to 45 wt.%. It is worth noting that lower Zn-content in the side-branches indicates the diffusional nature of Zn penetration along PAGBs (Figure 3.11b).

So far, different approaches [147,149] have been proposed to discriminate ferrite and martensite as they possess close crystal structure and hence, similar appearance in EBSD phase map. Cho et al. [13] differentiated α-Fe(Zn) grains on either side of LME-crack based on the absence of lath martensite morphology. Other research works [147,149] also pointed out other approaches such as the threshold image quality, the band slope technique and differentiation based on grain size distribution, and morphology. However, the morphology-based technique was used in the present work as the stable α-Fe(Zn) grains did not participate in martensitic transformation during the cooling cycle. Figure 3.11c represents the EBSD orientation map in the vicinity of the LME-crack. As arrows indicate, the penetration of Zn along the austenite HABs at elevated temperatures promoted the formation of fine α-Fe(Zn) grains holding an orientation different from the martensitic matrix. It should be noted that only boundaries in the range of 15-50° have been revealed in Figure 3.11c. This allows nucleated fine α-Fe(Zn) grains (showing HABs) to be differentiated from potential martensite packets or lathes.

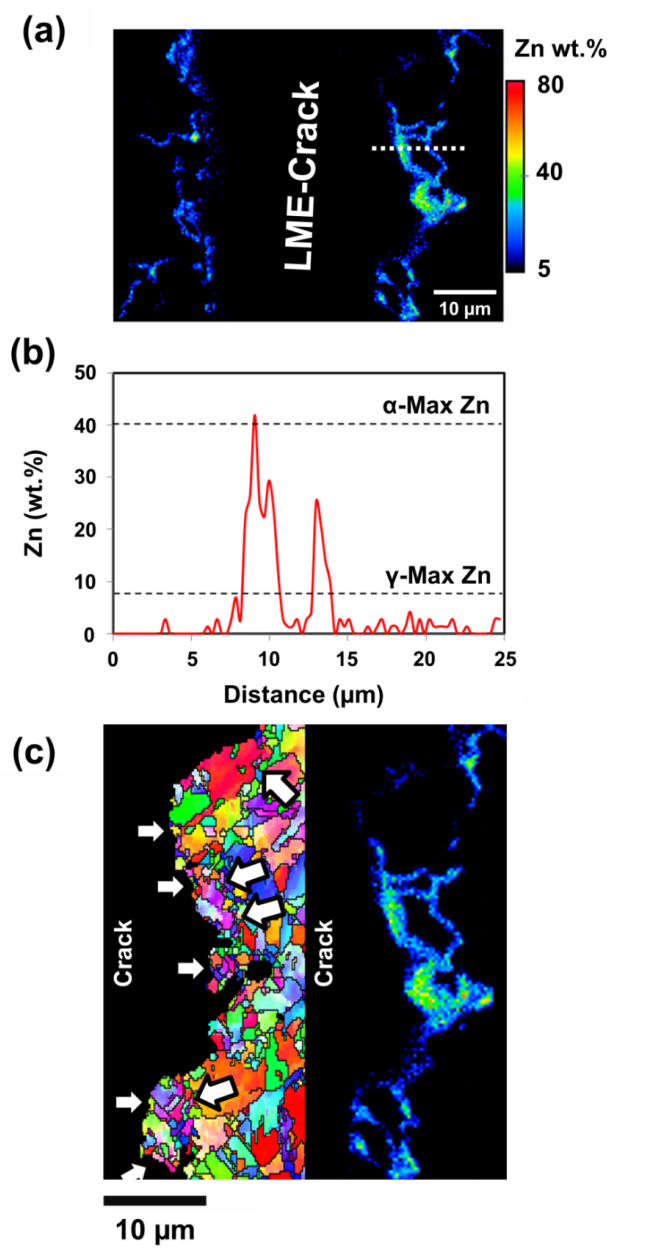

Figure 3.11: (a) EPMA Zn distribution mapping in vicinity of the LME-crack, (b) corresponding EPMA line scan analysis over the white dashed line as well as the maximum solubility of Zn in γ and α, and (c) the formation of fine α-Fe(Zn) grains along the LME-crack opening (white arrows γ: Austenite, α:Ferrite).

To provide a thorough understanding of the underlying LME mechanism in LBW of GA-coated 22MnB5 steel, the schematic of multiple stages of the embrittlement is illustrated in Figure 3.12. In this model, first, the δ and $\Gamma/\Gamma1$ phases within the coating partially melt over the UCHAZ during the heating cycle. As mentioned earlier, $\Gamma/\Gamma1$ and δ phases are holding about 75 and 90 wt.% of Zn, respectively. According to the Fe-Zn binary phase diagram [150] and due to the different Zn-contents, partial melting of Γ and δ phases starts at 782 and 665°C, respectively. It is most likely that the partially melted Zn reaches the steel interface mainly by flowing through the pre-existing cracks in the brittle coating or the cracks created due to the applied tensile stresses (II). As the liquid-Zn reaches the substrate, it starts to penetrate by diffusion through the austenite grain boundaries (III). By penetration of Zn along the austenite HABs and under the effect of the applied tensile stress, a LME-cracks opens. By rapid crack opening, it is expected that more fresh liquid-Zn could flow into the crack and crack opening becomes self-boosted. In this manner, the local propagation path of the crack is governed by the austenite HABs; however, the overall crack propagation path is controlled by the direction of the applied tensile stress. As mentioned, by the accumulation of Zn along austenite HABs and exceeding the maximum Zn-solubility in austenite (7 wt.%), α-Fe(Zn) starts to form locally at the crack opening area as a result of the Zn strong ferrite stabilizing effect. The diffusivity of Zn in γ-Fe and α-Fe at 850°C is 1.11×10^{-17} and 3.53×10^{-15} m^2/s, respectively [18]. Therefore, the formation of α-Fe along the LME-crack promotes Zn penetration due to the higher diffusion distance of Zn. In accordance with the previous reports [13,18,128], the formation of α-Fe(Zn) in Zn-penetrated regions at high temperatures adjacent to austenite could assist the loss of ductility as the ferrite is a soft phase. Finally, during the cooling cycle, austenite transforms into a lath martensitic structure; however, α-Fe(Zn) fine grains adjacent to the LME-crack remain stable due to high Zn-content (stage IV).

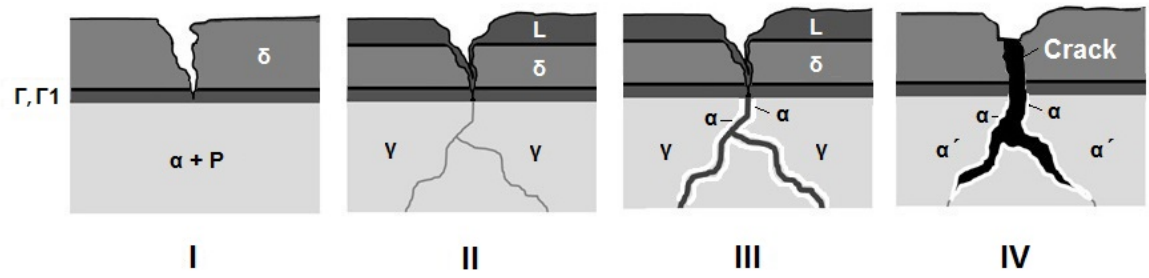

Figure 3.12: The schematic of LME mechanism during FLW of GA-coated 22MnB5 steel (α: Ferrite, P: Pearlite, γ: Austenite, α': Martensite, δ: Fe-Zn delta-phase, L: Liquid, $\Gamma/\Gamma1$: Gamma/Gamma1).

3.4.2 LME in TWIP and MMn-TRIP steels

The initial microstructures of the as-received TWIP and MMn-TRIP steels are shown in Figure 3.13. According to Figure 3.12a, the MMn-TRIP steel microstructure consisted of an ultrafine lamellar austenite in a ferritic matrix. The mean austenite lamella width was approximately 120 nm. By means of image processing, the austenite volume fraction in the initial structure was determined to be about 50%. The lamellar austenite structure agrees with previous research on MMn-TRIP steel [151]. In contrast, the EBSD analysis confirmed a fully austenitic microstructure of TWIP steel with a mean grain size of about 3 μm (Figure 3.13b).

Effect of the external tensile stress on LME susceptibility

As described by several researchers [42,138,152], the simultaneous presence of sufficiently high tensile stresses and a liquid film in a sensitive polycrystalline material leads to grain boundary decohesion. To investigate the role of a tensile load on the LME cracking, LBW trials have been performed under different external loading conditions. The mean length

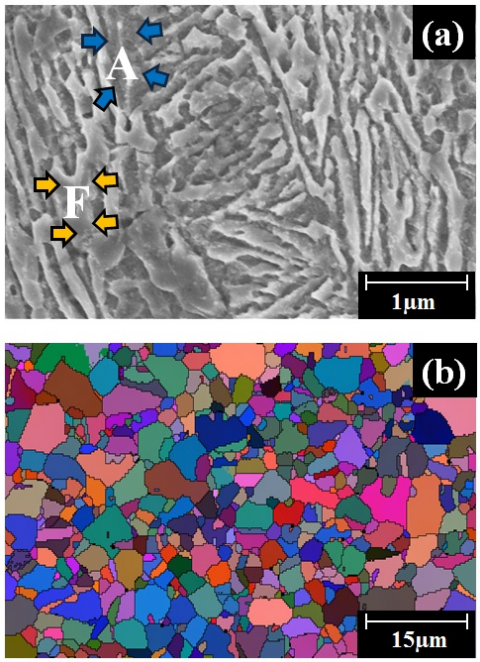

Figure 3.13: The initial microstructure of (a) MMn-TRIP, and (b) TWIP steels (A: austenite and F: ferrite).

of LME-cracks in TWIP and MMn-TRIP steel versus the applied external load is shown in Figure 3.14. The results show that the LME mean crack length increases with increasing applied load, where TWIP steel shows longer cracks compared to TRIP steel (i.e. higher LME susceptibility in the TWIP steel). According to Figure 3.14, the YS of TWIP steel is much lower than that of the TRIP steel. Hence, in addition to higher austenite volume fraction in the TWIP steel, higher LME susceptibility in the TWIP steel can be attributed to lower YS of the material.

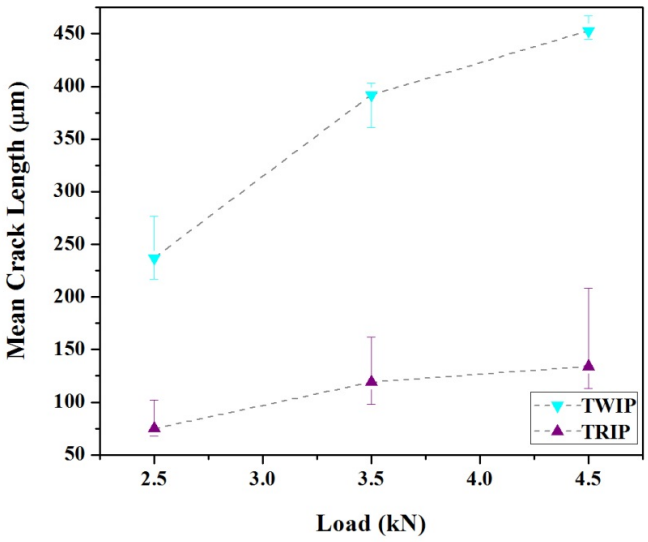

Figure 3.14: Mean crack length versus the applied load in the TWIP and TRIP side of the joint.

LME crack characterization

Figure 3.15 illustrates the occurrence of multiple LME cracks with different lengths after restrained LBW. As described before, sectioning and grinding were carried out parallel to the welding direction to analyze LME crack within the HAZ. The results from various welding conditions indicated that all LME cracks initiated from the TWIP-TRIP interface (Figure 3.15a and b), where Zn-coating from the TRIP side of the joint penetrated into the TWIP side. Even though TWIP steel is not coated, the liquid-Zn from the TRIP side of the joint penetrated along the grain boundaries within the HAZ and created several LME cracks under the applied external stress. The length of the LME cracks are of the order of 100 μm (Figure 3.15c), which is much longer than the acceptable crack length of 10 μm [153]. In addition, as Figure 3.15d shows LME cracking has also occurred in the TRIP side

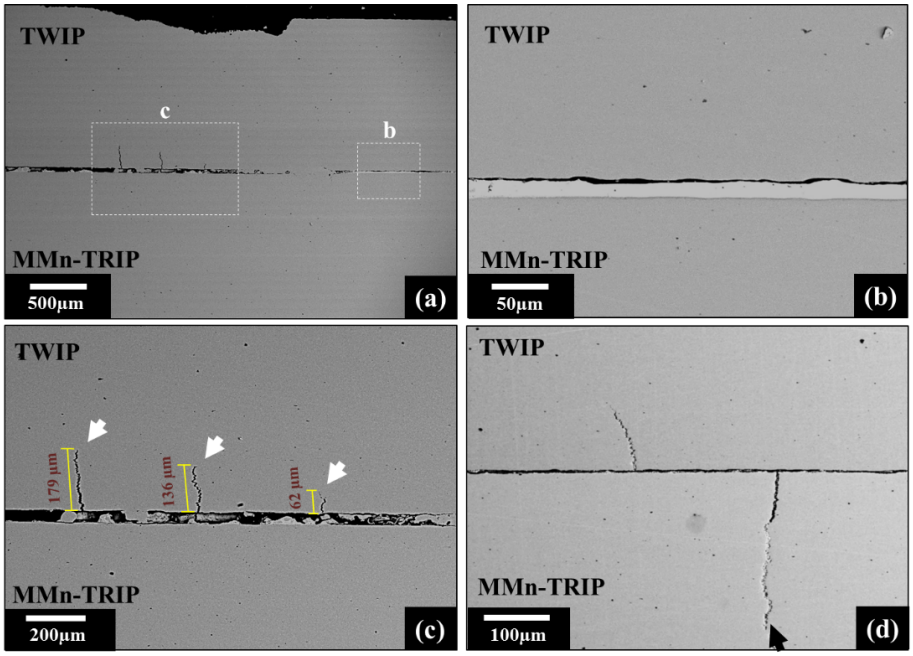

Figure 3.15: SEM micrographs showing (a) overview of LME cracks formed within the HAZ, (b) Zn-coating between two sheets, (c) LME cracks in TWIP side of the joint, and (d) representative LME crack in MMn-TRIP side of the joint (black arrow).

of the joint; however, it has been observed that the total number of LME cracks and the mean crack length are lower than on the TWIP side of the joint.

Figure 3.16a shows EDS Fe and Zn element mapping of a representative LME crack region in the TWIP side of the joint. As seen, a considerable amount of Zn is present inside the crack where it penetrated very deep along the crack. The temperature within the HAZ during LBW of AHSSs exceeds 700°C, falling between the Zn melting and boiling points of 419 and 907°C, respectively [154]. Accordingly, the GI-coating transforms into liquid phase above HAZ and penetrates along the grain boundaries during LBW. Figure 3.16b and c demonstrate the detailed EPMA maps of Zn distribution at the middle and the tip of the LME crack. From Figure 3.16b and c, it may be seen that the Zn-content

at the tip of the crack (I) is less than points II and III. Ashiri et al. [17] and Kang et al. [18] also observed a similar change in Zn concentration along the LME crack length. Lower Zn-content at the crack tip is an indication that grain boundary based diffusion is mainly responsible for the Zn-penetration. The line profiles in Figure 3.16d reveal the Zn content inside the LME crack match the composition of the Γ-$(Fe, Mn)_3Zn_{10}$ phase (72-76.5 wt.% Zn) [18]. The presence of a much lower Zn-content at the tip of the crack is also evidence of a diffusion-based mechanism of Zn penetration. However, the very large penetration depth of Zn (hundreds of micrometers) cannot be justified by only Zn-diffusivity along the austenite grain boundaries. In other words, the observed depth of Zn penetration is orders of magnitude higher than the predicted solid-state diffusion distance of Zn-atoms in the short time period of laser welding. Therefore, the considerable depth of Zn penetration is attributed to the stress-assisted diffusion mechanism [18,105]. As a result of Zn accumulation in the grain boundary, Zn content exceeds the maximum solubility limit in austenite [18]. Over the maximum solubility limit, liquid-Zn starts to form along the austenite grain boundaries. Afterwards, as a consequence of liquid-Zn film presence along grain boundaries, the metallic bond weakening takes place [42], and subsequently, the initial LME crack opens up. It is most likely that by the crack opening, more liquid-Zn from the melted GI-coating flow into the crack through a well-established capillarity effect. More fresh liquid-Zn inside the crack promotes further Zn-penetration and eventually under the applied tensile stresses LME-crack could propagates even more rapidly. During the cooling phase of the weld cycle, after crack propagation ended, the liquid phase inside the crack and the austenite matrix in the vicinity of crack composed of Fe and Mn in addition to Zn due to matrix solid-state diffusion tend to transform into Γ-$(Fe, Mn)_3Zn_{10}$ phase through the following peritectic reaction (Eq.3.1):

$$\gamma(Fe, Mn, Zn) + Liq.Zn(Fe, Mn - saturated) \rightarrow \Gamma - (Fe, Mn)_3Zn_{10} \qquad (3.1)$$

The proposed mechanism is consistent with the Zn alloy inside the crack has a Zn content of 70%, and therefore forms Γ-$(Fe, Mn)_3Zn_{10}$-phase. Even though Zn is a strong ferrite stabilizer, the presence of a significant Mn-content (austenite stabilizer) in the TWIP and MMn-TRIP steels, means that no α-Fe(Zn) phase forms in the vicinity of the LME crack.

The lesser extent to which LME cracking is observed in the TRIP counterpart is attributed to the initial structure. According to Figure 3.13a, initial microstructure of the MMn-TRIP steel is comprised of fine needle-like austenite phase surrounded by a ferrite matrix, and most of the boundaries are inter-phase type. In contrast, the initial structure of the TWIP steel is fully austenitic (Figure 3.13b), and therefore, the occurrence of LME is not dependent on the A_{c3} temperature. The plausible explanation for the occurrence of the LME-cracking in the TRIP counterpart relies on the austenite grain boundaries emerged within the HAZ during the heating cycle of LBW. A fully austenitic structure would appear within the UCHAZ, where the temperature exceeds the A_{c3} temperature of the material (∼780°C). The η-phase as the main phase of GI-coating tends to vaporize at ∼900°C [155]. Therefore, the temperature window (∼750-900°C) for the concurrent presence of liquid Zn and susceptible microstructure (two main prerequisites of LME) is narrow. Figure 3.17a and b shows the EBSD orientation and corresponding Zn penetration map of a representative LME crack in the TWIP side of the joint. According to the IQ-map in Figure 3.17c, the LME crack propagated intergranular (along austenite HABs, black lines). The overall LME crack propagation path is governed by direction of the applied tensile stress; however, the local propagation path is governed by the grain boundaries.

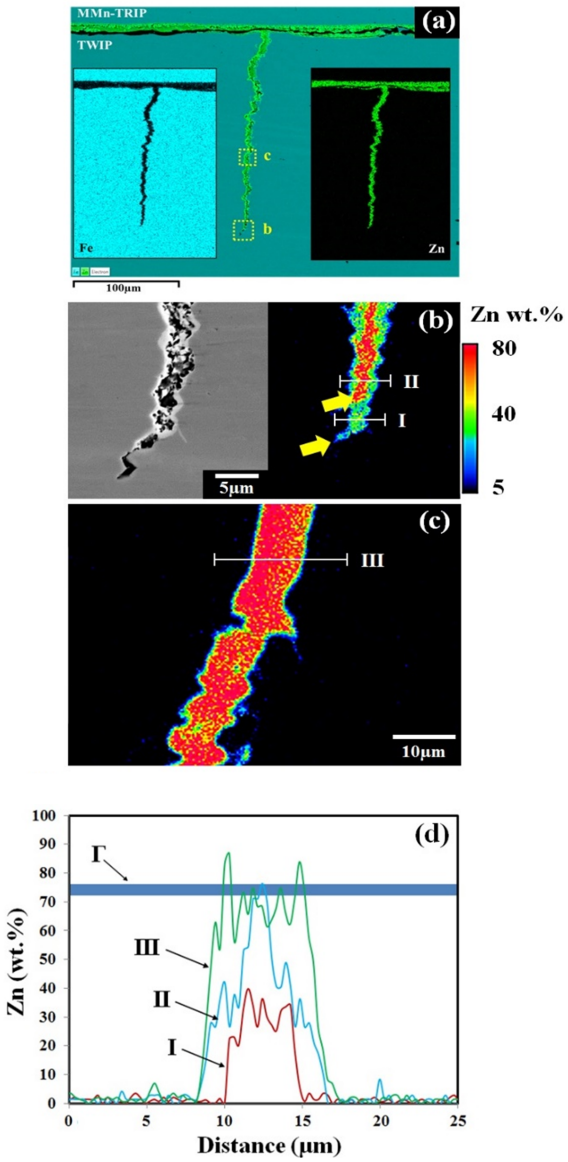

Figure 3.16: (a) EDS elemental map of the LME-crack showing the Zn-penetration, EPMA analysis at (b) tip, (c) middle part of the LME crack, and (d) Zn concentration profile in various regions of the LME crack and Γ-phase Zn-content range.

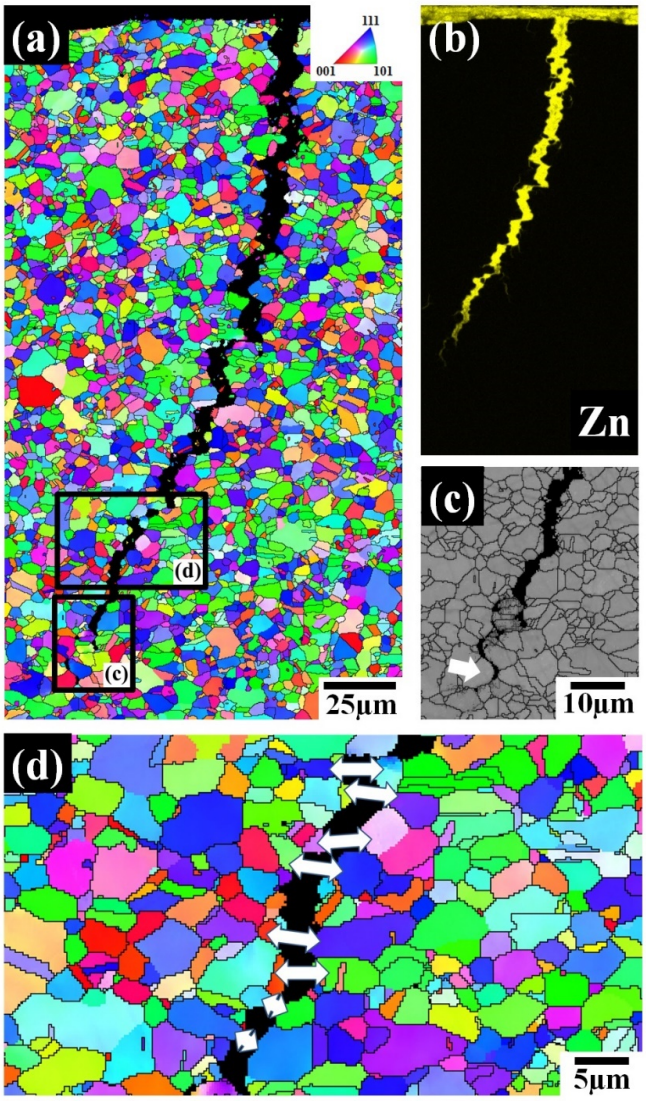

Figure 3.17: The overview of EBSD analysis of a representative LME crack, (b) Zn-penetration along the LME crack, (c) IQ map at the tip of the LME crack showing the propagation along the austenite grain boundaries.

3.5 Summary

The present chapter studied barely reported LME during LBW of Zn-coated 22MnB5 press-hardening, medium-manganese TRIP, and TWIP steels. The following conclusions could be drawn:

(a) Detailed EPMA results indicated the presence of Γ-$(Fe, Mn)_3Zn_{10}$ phase inside the cracks, showing the penetration of liquid-Zn during welding. Based on the crack tip analysis, the stress-assisted diffusion of Zn into the austenite grain boundaries and further liquid-Zn penetration was confirmed by the peritectic reaction.

(b) The results indicated that there exists a direct correlation between the applied external load and LME susceptibility. The threshold tensile stress of about 80%YS is necessary to trigger LME during LBW of 22MnB5 steel. A direct correlation between the applied external load and LME susceptibility was also observed in the TWIP and TRIP steels, however, the TWIP side of the joint showed a higher LME sensitivity compared to the TRIP side.

(c) The accumulation of Zn along the HABs over the maximum solubility in the austenite, promotes α-Fe(Zn) formation in 22MnB5 steel. The formation of α-Fe(Zn) along Zn-penetration area assist the loss of ductility due to the higher Zn diffusivity in α-Fe. The diffusion-based penetration of Zn along austenite HAGs was also confirmed.

Chapter 4

Investigation of Grain Boundaries Role in LME: Geometrical Characteristics[1]

4.1 Overview

Although advances have been made in understanding LME, the role of grain boundary type and characteristics (e.g. grain boundary misorientation angle and grain boundary crystallographic plane) is not fundamentally understood. As shown in the previous chapter, during the welding process, AHSS grades undergo phase transformations due to elevated temperature and extremely high cooling rates. Although PAGBs can be revealed by EBSD

[1]This chapter consists of two Manuscripts 1- Published Manuscript in Materials Letters, available online: https://www.sciencedirect.com/science/article/pii/S0167577X20302160, MH Razmpoosh, A Macwan, F Goodwin, E Biro, Y Zhou, 2020, and 2- Published Manuscript in Metallurgical and Materials Transactions A, available online: https://link.springer.com/article/10.1007/s11661-020-05857-3, MH Razmpoosh, A Macwan, F Goodwin, E Biro, Y Zhou, 2020

analysis, due to severe atomic orientation alterations during non-equilibrium phase transformations, reconstruction of parent grain boundary characteristics is challenging. Hence, Chapters 4 to 6 focus on LME in a fully austenitic stainless steel (grade 304) to avoid this issue, and accurately identify grain boundary characteristics.

This chapter first shows that liquid metal penetration mainly occurs in random-grain boundaries, where its propagation path is a function of misorientation angle (θ) and stress component perpendicular to grain boundary plane. In contrast, low-Σ CSL boundaries: Σ3 (θ=60°) and Σ5-9 ($\sim\theta$=40°) resist LME, even at the maximum stress component. Triple junctions of CSL and random grain boundary block liquid metal penetration through modifying of the random grain boundary misorientation angle. The recently developed trace analysis has been applied to the grain boundaries exhibiting LME cracking. Despite the presence of a diverse range of low- and high-index planes in the entire population of the grain boundaries, liquid metal selectively penetrated high-index random grain boundary planes.

4.2 Background

Grain boundaries act as strong barriers against dislocation motion and can effectively strengthen polycrystalline metals. However, grain boundaries are structural defects with excess free energy, which makes them as the most sensitive sites for atomic decohesion. There are many examples of intergranular degradation such as stress-corrosion-cracking [97,156–158], hydrogen embrittlement [159–161], and LME [3,16,17,19,20,107]. In LME, exposure of stressed ductile metals to certain aggressive liquid metals (known as an LME couple) triggers rapid brittle fracture along grain boundaries [3,107]. The most frequently reported LME couples in the present literature are Al-Ga [6,45,83], Ni-Bi [10,11], Cu-

Bi [5,116], and Fe-Zn [13,18,20]. While LME-crack progression along grain boundaries is well-documented in the literature, little is known about dependence of LME on the grain boundary character distribution (GBCD). To provide a mesoscopic description of a 3-dimentional grain boundary, five independent crystallographic parameters are required: three parameters to determine the misorientation angle, and two parameters for the inclination of the grain boundary plane [162–164].

As discussed in Chapter two, several experimental [5,83–85,116,165] and atomic scale simulation studies [3,6] proposed models to describe the role of grain boundaries in LME. Two models are particularly noteworthy: the SJWK model [166,167] states that chemisorption of liquid metal to crack tip occurs, then the applied tensile stress causes complete debonding and cracking. Conversely, the Krishtal-Gordon-An [96,106] model describes the key role of stress-assisted grain boundary diffusion of embrittler atoms, which precedes the cracking. While the SJWK model emphasizes cohesive strength decrease by the presence of liquid metal at the crack tip, the Krishtal-Gordon-An model states that stress-assisted grain boundary diffusion (solid state) of embrittler atoms along grain boundaries occurs ahead of crack, and then accumulation of embrittler atoms over a sufficient concentration opens the grain boundary [20-23]. The recent studies also indicated the role of interfacial compounds and phase-transformations [13,20,128] along grain boundaries, which accelerate grain boundary decohesion.

The first insights into the influence of grain boundary characteristics on LME have been provided through atomistic modeling [168,169], where grain boundaries with energy lower than 0.55 J/m^2 show lower penetration susceptibility; However, LME susceptibility increases with increasing grain boundary energy to the maximum of 0.65 J/m^2 and then decreases [84]. In the case of CSL boundaries, it was shown that low-Σ CSL boundaries like Σ11 (grain boundary energy of 0.15 J/m^2) show significantly lower LME susceptibility than

those with high Σ-values (Σ >29), and random grain boundaries [84]. Apart from the grain boundary energy role, grain boundary excess volume (per unit area of grain boundary) also corresponds to LME susceptibility. At grain boundary excess volume values over 0.5 Å, LME increases drastically; however, grain boundaries with low values of excess volume (<0.4 Å), with tightly packed structures, show little or no LME. It is believed that grain boundary excess volume for CSL boundaries (such as Σ11 with a grain boundary excess volume of 0.13 Å) is low, and consequently their grain boundary energy is half to one-third as much as those of random grain boundaries [84].

Although atomic-scale modeling introduced as a powerful technique for understanding the embrittlement mechanism in the Al-Ga system, from a practical point of view, it is limited to very low numbers of modeled atoms and extremely short times. Therefore, atomic-level modeling seems unrealistic in prediction of LME in real-life scales. In addition, most of the experimental studies in this field have focused on materials with complex microstructures, which have undergone multifaceted phase transformations during processing; Therefore, detailed examination of the prior grain boundaries after cooling to room temperature is associated with many practical difficulties such as significant change of atomic orientations through low-temperature phase transformations [20]. Hence, the present study uncovers the contribution of random and CSL boundaries in LME of a stable FCC material. This avoids the aforementioned practical difficulties in detailed analysis of grain boundary characteristics. A new qualitative method is presented to map grain boundary misorientation angle-stress component correlation in FCC iron-Zn couple. Moreover, the LME susceptibility of CSL boundaries and the role of random-CSL boundary triple junctions have been investigated.

4.3 Experimental Procedure

304 austenitic stainless (thickness=0.9 mm) and Mn-containing steel grade (thickness=1.45 mm) sheets were used in this chapter. The Mn-containing steel was GI-coated (coating weight of 50 g/m^2 per side) and the 304 steel was bare. LME was induced in the 304 austenitic stainless steel by subjecting it to a thermal cycle from laser processing while under tensile stress. The details of the externally loaded laser processing and the specimens were given in Section 3.3. It must be noted that the present chapter focuses only on the LME behavior of the 304 austenitic steel. After LME cracking was induced, samples were prepared for examination using typical methods. The samples were mechanically ground and polished to a 0.25 μm diamond finish and then a final vibratory polishing in OPS was done for 0.5 hr to remove any undesired surface strains from the samples surface. Detailed analysis of the grain boundaries was carried out by EBSD system attached to a JEOL JSM 7000f field-emission gun SEM (accelerating voltage of 20kV). The step size used for the EBSD analysis ranged 0.05-0.5 μm. Data acquisition and post-processing of the collected EBSD data was performed by Aztec and HKL Channel 5 software, respectively. The low-Σ CSL boundaries were detected by HKL Channel 5 software based on their specific rotation angle and planes: Σ3: 60°-(111), Σ5: 36.9°-(100), Σ7: 38.2°-(111), Σ9: 39°-(110). The method to find misorientation angles and stress component perpendicular to the grain boundary segments is shown in Figure 4.1. The grain boundary misorientation angle (θ) has been measured from the orientation difference between two sides of cracked grain boundaries. The related angle between each grain boundary segment to that of the applied external loading (Φ) has been used for the stress component calculations. The same calculation of stress component and misorientation angle was performed on side-branches of Zn-penetration where no Zn penetration was seen (e.g. the boundary between the grain

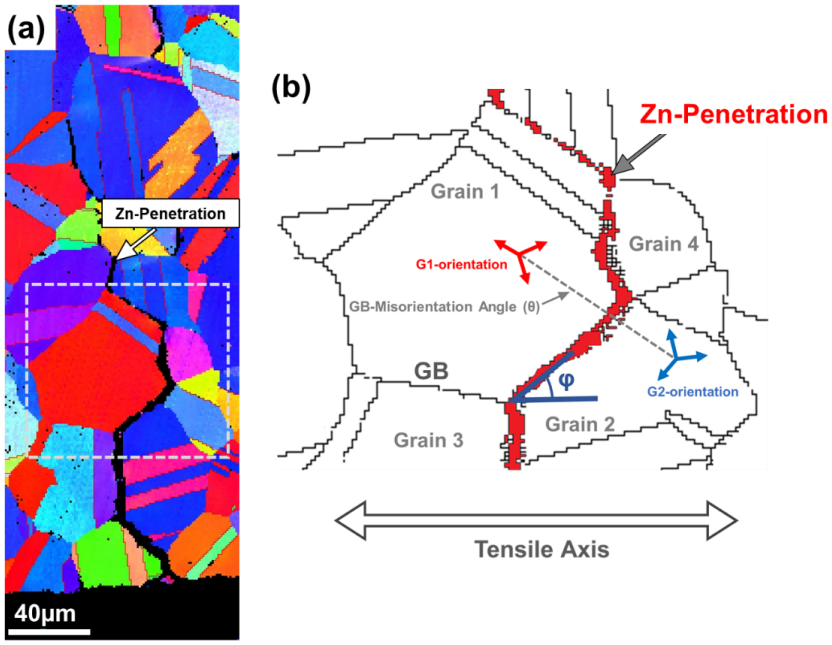

Figure 4.1: (a) Inverse-pole-figure map of a representative Zn-penetration and (b) the details of the method used in to analyze the GB-misorientation angle (θ) of each GB segment, as well as the effective stress component of main penetrated GBs and the side-branches to show the Zn-penetration susceptibility of GB segments (Note: the related angle between each GB segment to that of the applied external loading has been considered in all the measurements).

1 and 3 and grain 2 and 4 in Figure 4.1).

The focused ion beam (FIB) technique was used to lift-out the transmission electron microscopy (TEM) sample from tip of the Zn-penetration. FIB lift-out was performed using a Zeiss NVision 40 FIB-SEM. The area of interest was selected on the polished cross section; afterwards an in-plane slice ($8\times8\mu$m) of the material was lifted out and mounted onto a TEM grid. This was followed by final FIB thinning to prepare a thin foil for further TEM analysis. High-resolution TEM (HRTEM) observation was carried out using a FEI Titan 80-300 HB double aberration-corrected to achieve atomic-resolution imaging. The

HRTEM was operated at voltage of 200 keV. Electron energy-loss spectroscopy (EELS) elemental mapping with 0.3 nm resolution was performed to investigate the distribution of the elements along the grain boundaries.

According to the trace analysis approach [163,170], the collected EBSD data from the grains was used to characterize the grain boundary plane orientations. In this regard, the EBSD data was processed to construct stereographic projections from adjacent grains. Then, the poles from each grain couple were overlaid to find the coinciding plane. It must be noted that for the trace analysis approach, data from more than ∼160 pairs of grains (∼70 liquid metal penetrated, and ∼90 in the initial structure without exhibiting LME) have been examined.

4.4 Results and discussion

4.4.1 Role of grain boundary misorientation angle in LME

The microstructure of the austenitic steel had a mean grain size of about 30 μm and is shown in Figure 4.2a. The grain boundary analysis showed that ∼78% of the high-angle grain boundaries in initial microstructure were random ($\theta > 15^{\circ}$) and ∼22% were CSL boundaries (21% of Σ3, ∼1% of Σ5, Σ7, and Σ9) (Figure 4.2b and c). The Zn-penetration initiated from the grain boundaries exposed to the Zn-coating (Figure 4.3a and b) and rapidly propagated through the material thickness (∼0.9mm) (Figure 4.3c).

The EBSD map of random (R), CSL boundaries and a representative Zn-penetration path is shown in Figure 4.4. The Zn-penetration changes its local propagation path selectively at the grain boundary triple junctions where some of the random-grain boundaries (despite their prefered angle to that of the applied tensile stress) are completely bypassed by

other grain boundaries. Based on the method explained in Figure 4.1, the grain boundary-misorientation angle of each segment of Zn-penetration was correlated to the tensile stress component.

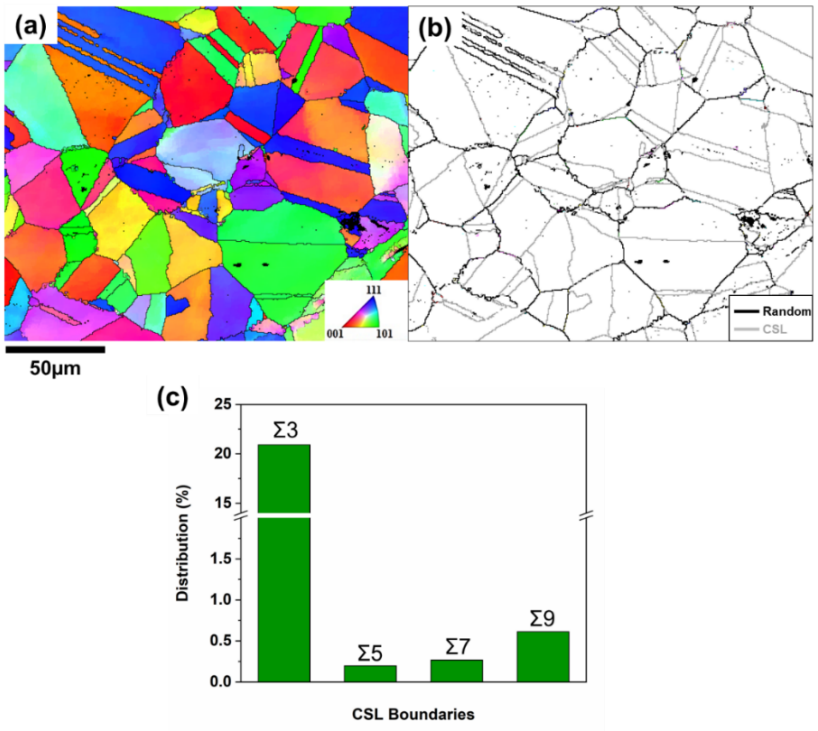

Figure 4.2: Detailed EBSD analysis of (a) the initial austenitic steel showing the overall grain structure with an average grain size of about 30 μm, the (b) corresponding EBSD map of random GBs ($\theta > 15°$) (black lines) and CSL boundaries (gray lines) with a total distribution of various low-Σ boundaries in the initial structure showing the presence of 21% of Σ3 and $\sim$1% of Σ5, Σ7, and Σ9.

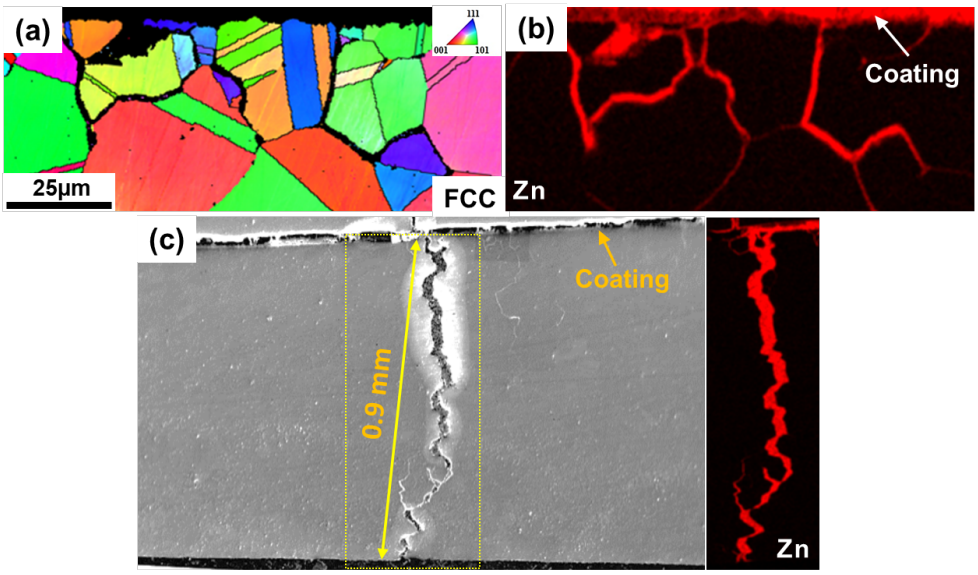

Figure 4.3: (a and b) EBSD inverse-pole-figure and corresponding Zn-map of FCC structure showing the Zn-penetration along FCC grain boundaries, which initiated from the Zn-coating, and (c) the overview of the excessive Zn-penetration through the sheet thickness (0.9 mm).

The same calculation of stress component and misorientation angle was performed on side-branches of Zn-penetration where no Zn penetration was seen. It was observed that high stresses are needed for liquid metal penetration at lower grain boundary misorientation; however, increasing misorientation angle will lower the required stress components to trigger Zn-penetration and subsequent cracking (Figure 4.5). As reported by Ludwig et al. [85], LME is directly linked to grain boundary energy. Therefore, it is logical to conclude that at lower grain boundary energies higher mechanical energy is needed for LME. This explains the clear border between the Zn-penetrated and non-Zn-penetrated grain boundaries in Figure 4.5, where stress component necessary for failure is the highest at θ ~15° (corresponds to the minimum random grain boundary energy). As well, all grain boundaries at θ=60° and some of boundaries at ~40° resist Zn-penetration (Figure 4.5). Recall

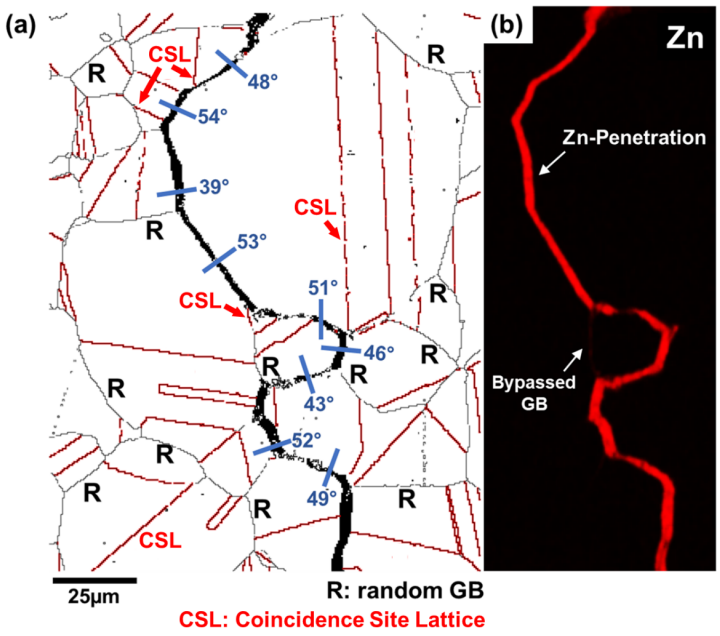

Figure 4.4: (a) EBSD and (b) corresponding Zn-map of representative Zn-penetration path, the propagation path along the random GBs with given misorientation angles (black: random, red: CSL) showing various sharp changes at the triple junctions, and the observation of a random GB that is completely bypassed despite the suitable direction to the applied external load (external loading direction: horizontal).

that the material used in the present study had about 20% of $\Sigma 3$ boundaries (Figure 4.2), explaining the resistance of grain boundaries at θ=60° to Zn-penetration. The resistance of some grain boundaries at $\theta \sim 40°$ despite their large stress component is attributed to $\Sigma 5$-9 boundaries, which all have grain boundary misorientations of about θ=39° (low grain boundary energy). Therefore, Zn-penetration only takes place in high-angle random grain boundaries, where the minimum observed misorientation angle was about 14° (Figure 4.5). This is consistent with the studies [84] of LME in other systems emphasizing minor contribution of low-angle grain boundaries ($\theta < 15°$) in embrittlement.

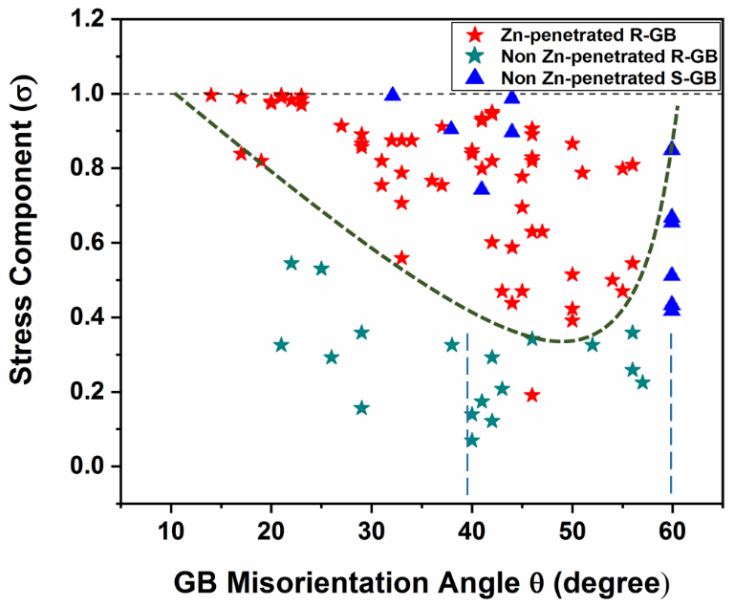

Figure 4.5: The correlation of the GB misorientation angle-stress component (σ=1: Normal to GB, σ=0: parallel with GB) based on the collected information from ∼20 pair of grains showing: 1-The clear boundary between Zn-penetrated and non-Zn-penetrated random (R) GBs where LME takes place only at high-angle random-GBs ($\theta > 15°$), 2- By increasing misorientation angles of random-GBs lower stress components triggers Zn-penetration, and 3- The resistance of GBs at θ=60° and some of boundaries at $\sim 40°$ against Zn-penetration that are attributed to Σ3 at θ=60° and Σ5-9 special (S-GB) occurring at $\sim\theta$=39°.

Despite similar orientation to the applied external load, some LME cracks had a depth between 40-60% of the sheet thickness, showing that the progress of Zn-penetration was arrested (Figure 4.6a and b). The FIB lift-out sample (Figure 4.6c) and further HRTEM observation of the Zn-penetration tip showed that Zn penetrated along the random grain boundary (Figure 4.7a and b); However, the detailed EELS map confirmed that Zn-penetration was blocked at the random-CSL triple junction (Figure 4.7c and d). Atomistic-level analysis of the triple junction in Figure 4.7e revealed that the initial misorientation angle between the G1 and G2 increased to about 71°. This is attributed to the twinned area of G2 (with CSL as its boundary) which changes the initial random-grain boundary

misorientation angle. The increase of the misorientation angle to 71° results in relatively lower energy level [171,172] and consequently further suppresses Zn-penetration (Figure 4.7c).

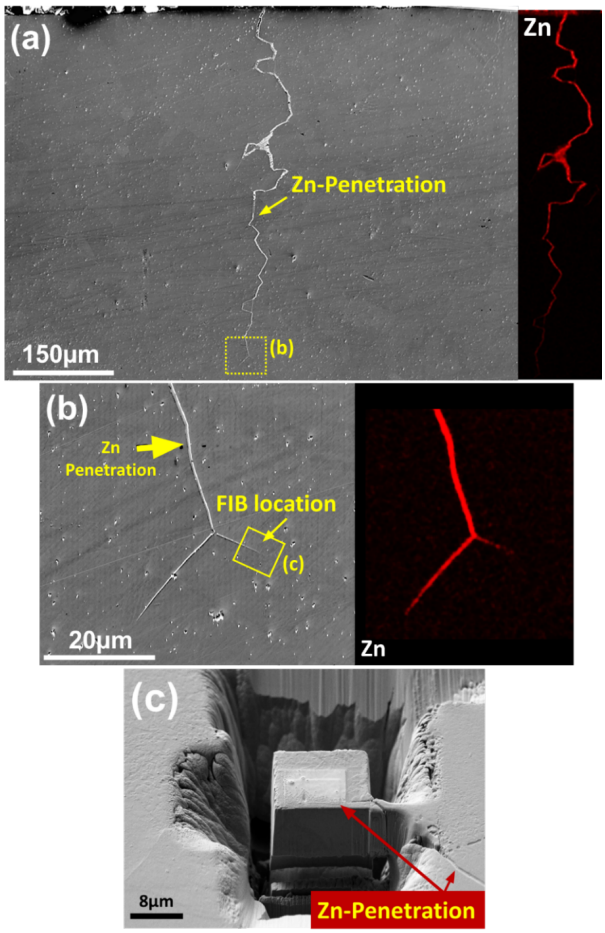

Figure 4.6: (a) Overview of a representative arrested Zn-penetration (only penetrated about 40% of the sheet thickness) with the corresponding Zn-map, and (b) the selected area at the tip of the arrested Zn-penetration for (c) FIB in-plane sample lift-out to analyze the related GB by the atomic-resolution TEM-EELS technique.

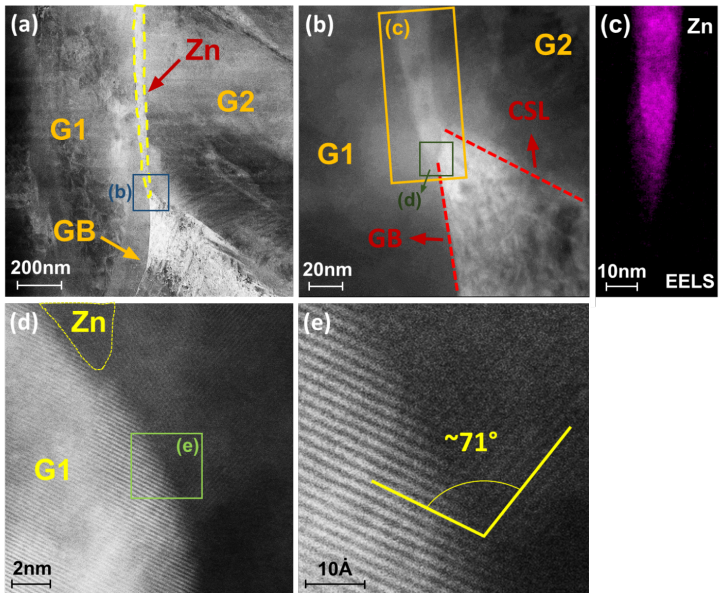

Figure 4.7: The HRTEM observation of the prepared sample by FIB showing (a) the arrested Zn-penetration tip along the random-GB between grains G1 and G2, (b) the complete Zn-penetration block at the random-CSL boundary triple junction, which is confirmed through the (c) atomic-resolution EELS map of Zn at the triple junction. The corresponding EELS Zn-map does not show the presence of GB liquid-metal atomic layers ahead of the Zn-penetration. (d and e) atomic-level resolution of the GB resistant against Zn-penetration in the twinned area of the grain 2 which shows an angle of about 71° to that of the G1.

HRTEM and corresponding EELS element-maps of the Zn-penetrated portion of a random grain boundary (∼40 nm) are shown in Figure 4.8a. Before Zn-penetration along the random-grain boundary (ahead of Zn penetration), segregated-Cr was seen in the grain boundary (Figure 4.8b). After Zn-penetrated and the grain boundary opened, the grain boundary segregated-Cr (Figure 4.8b) was observed to have broken into small particles (Figure 4.8c). Interestingly, the Zn-flow along the broken grain boundary followed a wavy pattern, which shows that the particles of Cr along the grain boundary broke before Zn flow started. This is evidence that the grain boundary opening precedes Zn-flow and is con-

sistent with the Rehbinder and Shchukin [103] and SJWK [166,167] models. The very low dislocation density in the vicinity of the Zn-penetrated grain boundary (Figure 4.8b) and the tip (Figure 4.7a and b) also puts into question the role of dislocations (ductile-nature) in LME. The low dislocation density agrees with the Kang et al. [18] who also showed that there was low dislocation activity at the Zn-penetrated grain boundaries of TWIP steels (with high-alloying element content). Hence, between the two main LME models i.e. ductile (plastic deformation), and brittle-type crack propagation models, the observed low density of dislocation surrounding the liquid metal penetration confirm brittle-fracture-based LME mechanisms (SJWK [166,167] and the Rehbinder and Shchukin [103]) compared to ductile-fracture mechanism. Dislocation density in the vicinity of the Zn-penetrated grain boundary (Figure 4.8b) and the tip (Figure 4.7a and b) also puts into question the role of dislocations (ductile-nature) in LME. The low dislocation density agrees with the Kang et al. [18] who also showed that there was low dislocation activity at the Zn-penetrated grain boundaries of TWIP steels (with high-alloying element content). Hence, between the two main LME models i.e. ductile (plastic deformation), and brittle-type crack propagation models, the observed low density of dislocation surrounding the liquid metal penetration is consistent with the brittle-fracture-based LME mechanisms (SJWK [166,167] and the Rehbinder and Shchukin [103]) compared to ductile-fracture mechanism.

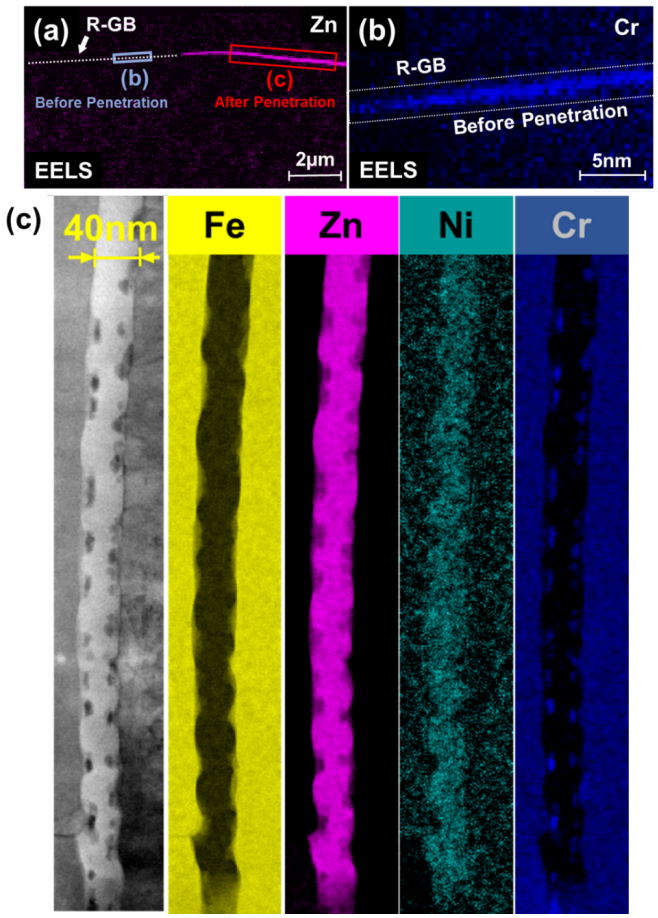

Figure 4.8: (a) The overview of the representative GB showing the Zn-penetrated and non-Zn-penetrated GB-sections, (b) the related side of the GB before Zn-penetration which shows a semi-continuous precipitation of Cr along the GB, and (c) high-resolution TEM and EELS maps of the major alloying elements of the GB after Zn-penetration reveals the precipitated Cr has been broken into small particles and the wavy pattern of Zn-flow along the opened GB shows that the semi-continuous precipitation of Cr along the GB has been broken before the Zn-flow by a brittle-fracture.

4.4.2 Role of Grain Boundary Plane in LME

The previous section described the key role of grain boundary misorientation angle and its relative orientation to the stress direction in the local liquid-metal penetration path; However, it calls for supplementary in-depth analysis of the other grain boundary characteristics to explain why grain boundaries with similar misorientation angles show liquid metal penetration in a wide range of stress-components. Therefore, the other independent GBCD such as grain boundary plane normal distribution must be considered. Sun et al. [173] also showed that LME susceptibility increases with increasing misorientation angle to a saturation plateau in 20-50° of misorientation angle. Figure 4.5 also revealed that the grain boundaries with close misorientation angles showed diverse LME susceptibilities which confirms the role of grain boundary planes. Sun et al. [173] employed laboratory diffraction contrast tomography (LabDCT) in conjunction with attenuation contrast tomography (ACT) methods to obtain grain boundary planes in the Al-Ga LME couple, but their study is mainly limited to a few selected grain boundary planes. Therefore, to fully elucidate the role of grain boundary energy in LME, misorientation angle is not sufficient and all five independent parameters of grain boundary crystallography should be characterized. This requires analysis of plane orientations (or inclination) of liquid metal embrittled grain boundaries. The present work introduces a quick grain boundary-plane-normal analysis method for LME crack-path.

A representative micrograph of the main and side-branch of an LME-crack is shown in Figure 4.9. The Zn-induced LME-crack initiated from the surface of the material, which was in intimate contact with the surface Zn-layer. Then, the main LME-crack propagated through the thickness of the material (∼0.9 mm). As shown, the penetration path follows random grain boundaries and the overall direction follows the closest path that

is perpendicular to the applied external loading direction. Although, the present study presented new insights into the key role of grain boundary misorientation angle, it has been observed that various grain boundaries with similar misorientation angles require a wide range of stress-components to exhibit LME sensitivity. This indicates that the grain boundary misorientation angle cannot fully represent grain boundary energy, and hence, the other independent GBCD such as grain boundary plane orientation must be considered. Hence, the trace analysis approach [163,170] has been used to determine the frequency of plane normal of the LME-cracked grain boundaries as compared to overall grain boundary plane distribution in the initial microstructure. Accordingly, the stereogram of two adjacent grains were collected. It must be noted that the trace analysis approach made it possible to analyze the grain boundary plane distribution even after complete cracking due to liquid metal penetration. In contrast to the LabDCT-ACT method suggested by Sun et al. [173], the trace analysis approach analyzes a considerable population of grain boundaries through a very close estimation based on conventional EBSD characterization, and therefore provides a reliable statistical distribution of the grain boundary planes.

An example of the local orientation relationship of a representative LME-cracked grain boundary is shown in Figure 4.10. According to Figure 4.10a, stereographic projections of low- and high-index planes from grain-1 and 2 were collected. The corresponding grain boundary plane normal (PN) was determined from the EBSD-inverse pole figure map. The same PN direction was used to determine the coincidence grain boundary plane which both grains had in common (overlapped along the PN on the pole figures). It must be noted that (111), (200), (220), (311) and (420), (511), (531), (533) are considered as low- and high-index planes, respectively.

The trace analysis of ∼90 grain boundaries in the initial austenitic microstructure showed that ∼23% of grain boundary plane normals are oriented to (111) (Figure 4.11).

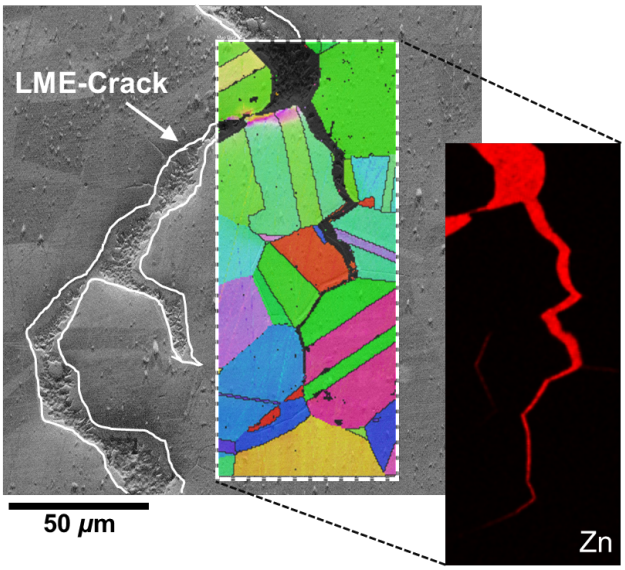

Figure 4.9: EBSD inverse-pole-figure and corresponding Zn-map of a representative LME main crack and a side-branch showing the Zn-penetration along FCC grain boundaries which is initiated from the surface Zn-layer (Note: the external tensile load is applied horizontally).

This is consistent with the previous analysis of the grain boundaries, which showed the presence of ∼20% Σ3 (60°-(111)) CSL boundaries. The other grain boundary planes showed a relatively equal frequency in the initial austenitic microstructure. Interestingly, it has been observed that the LME crack only propagated along high-index grain boundaries, where (531), (511), and (733) plane normals showed the highest frequencies (Figure 4.11). Hugo et al. [84] suggested that only the grain boundaries with energy over 0.6 J/m^2 are LME susceptible. This explains the high frequency of liquid metal penetrated grain boundaries with plane normal of (531) and agrees with the recent studies [173,174] showing the occurrence of LME mainly in random grain boundaries with 30-50° of misorientation angle. The resistance of low-index grain boundary plane normal can be attributed to their relatively low excess volume and energy, where the atomistic modeling of the Al-Ga couple

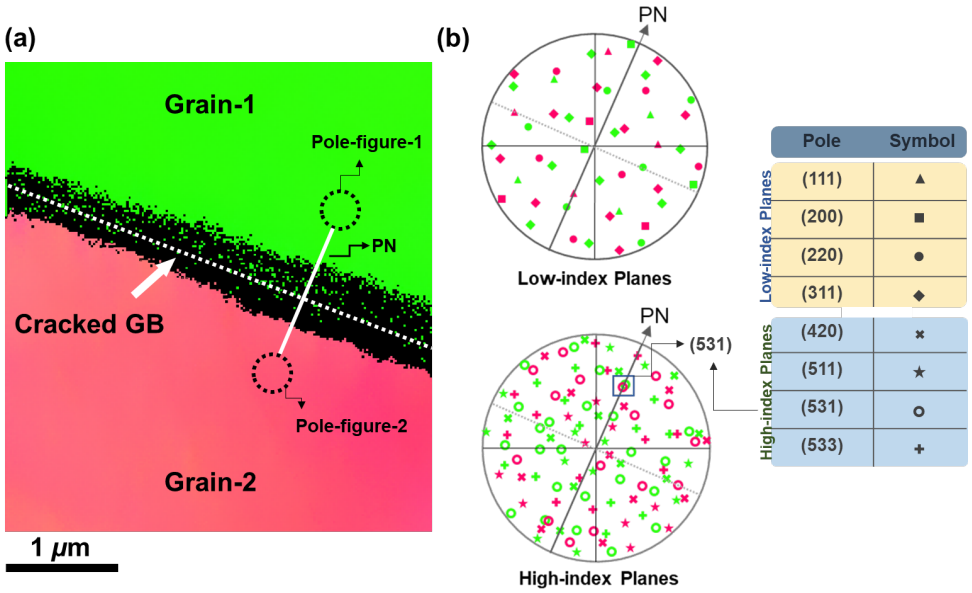

Figure 4.10: The representative (a) EBSD IPF map of a cracked-grain boundary after liquid metal penetration and the plane normal (PN) direction, and (b) the representative trace analysis method by collecting pole figures of low- and high-index crystallography planes from the corresponding regions close to the cracked-grain boundary where the indicated square shows detection of the matching (531) grain boundary plane along the grain boundary PN (Note: the provided table shows the grain crystallography planes and the assigned symbols).

[84] has confirmed that tightly packed random grain boundaries with low excess volume (<0.4 Å) show negligible LME susceptibility. The LME resistance of Σ3-CSL boundaries (oriented to (111) plane [175,176]) was reported previously. However, the grain boundary role in LME may not be completely described through geometrical characteristics and micro-chemistry of grain boundary should be studied.

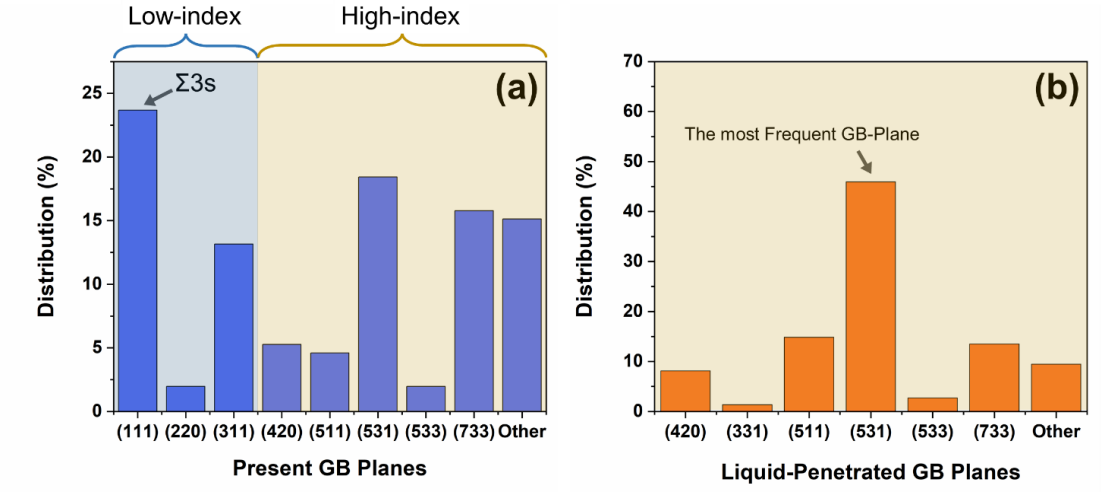

Figure 4.11: (a) The overall distribution of the present low- and high-index grain boundaries in the initial microstructure of the material, and (b) the distribution of the liquid-metal penetrated grain boundary planes showing that only high-index plane grain boundaries are susceptible to LME and the (531) is the most frequently penetrated grain boundary plane.

4.5 Summary

The present chapter investigated the role of grain boundary characteristics in LME of iron(FCC)-Zn couple. The main findings of this chapter are summarized below:

(a) Liquid metal penetration occurs along random grain boundaries ($\theta > 15°$) and the propagation path is governed by grain boundary misorientation angle (grain boundary energy) and applied tensile stress couple. At higher misorientation angles (higher energy), lower stress component triggers liquid metal penetration.

(b) Low-Σ coincidence site lattice boundaries (Σ3-9) resist Zn-penetration even at the maximum applied stress component. The resistance of low-Σ coincidence site lattice boundaries against liquid metal penetration provides new insights toward using grain boundary engineering techniques to manipulate random and CSL grain boundary distribution, and

hence suppress the embrittlement.

(c) Atomic-resolution elemental analysis of the liquid metal penetrated grain boundary shows that grain boundary brittle opening precedes Zn-flow. This evidence together with the minor role of dislocations at the penetration tip supports the brittle-fracture mechanism of LME and stands against the ductile-fracture models of LME.

(d) To describe the LME dependency on the grain boundary characteristics, grain boundary misorientation angle is not sufficient and five independent crystallographic parameters of the grain boundaries must be considered. The present study employed the recently developed trace analysis to investigate the grain boundary character effect in LME of iron(FCC)-Zn couple. It was found that the crystallography of the random grain boundaries is reflected in grain boundary plane orientation significantly governs the LME path.

(e) Despite the presence of low- and high-index grain boundary planes in the microstructure, liquid metal penetrates along the grain boundary with high-index planes. Although grain boundaries with plane normal oriented to (531) was only 18% of the overall grain boundaries, they had the highest LME susceptibility ($\sim$45% of the LME exhibited grain boundaries). This is attributed to their relatively high excess volume and high energy due to the low packing factor.

Chapter 5

Investigation of Grain Boundaries Role in LME: Micro-Chemistry[1]

5.1 Overview

Thus far, LME studies have been limited to micro- and meso-scale grain boundary investigations; however, to fully understand the LME phenomenon, atomic-scale investigation of LME crack-path is required. The present chapter of this study validates the recently proposed hypothesis of embrittler-induced alteration of electronic configuration at grain boundary as a viable atomic-scale LME mechanism. Moreover, the detailed analysis of LME crack-path and molecular dynamics (MD) simulation provide insight to the interrelation between the geometrical configuration and grain boundary chemistry. The present results explain the underlying mechanism of high LME-sensitivity of high-misorientation-angle random (not-ordered) compared to special (ordered) grain boundaries.

[1]This chapter consists of a submitted manuscript in Acta Materialia, MH Razmpoosh, B Langelier, E. Marzbanrad, H.S. Zurob, E Biro, Y Zhou, 2020.

5.2 Background

Most common structural materials are polycrystalline, where grain boundaries play key roles in bulk properties. Although grain boundaries are effective sources of plasticity and strengthening (e.g. in creep, superplasticity, Hall-Petch effect), they can act as preferential sites for intergranular degradations such as LME. Among the various contradicting proposed mechanisms for LME, recent studies have shown that stress-assisted grain boundary embrittler diffusion model best describes LME [96,107]. In this model, the diffusion of embrittler atoms along sensitive grain boundaries (ahead of crack) leads to crack nucleation, grain boundary opening (mass transfer of liquid embrittler to the crack-tip by liquid metal flow), and rapid progression of LME crack.

Considering the stress-assisted grain boundary diffusion model [96,107], it is vital to understand types and geometric configuration of LME-sensitive grain boundaries. A mesoscopic description of 3-dimentional grain boundary requires five independent parameters: misorientation angle (3 parameters), and the inclination of the grain boundary plane (2 parameters) [162–164]. In previous chapter it was revealed that different grain boundary types do not have similar LME-sensitivity; High-angle random (non-ordered) grain boundaries are more LME-sensitive than highly-coherent low-Σ boundaries (ordered). LME crack-path is a function of grain boundary misorientation angle (representative of grain boundary energy) and applied tensile stress, where at higher high misorientation angles, lower tensile stresses trigger the grain boundary decohesion. LME-sensitivity of random boundaries reaches its maximum at misorientation angles of $\sim$40-55°, which agrees with the atomistic modeling of LME in the Al-Ga couple [84]. Although misorientation angle provides a primary insight to understand why liquid metal penetrates non-uniformly into the grain boundary network, complementary analysis of the GBCD and LME-sensitivity

was also required.

The next logical step toward understanding the grain boundary role in LME is the influence of grain boundary chemistry (i.e. segregation of the alloying elements) on its characteristics, and therefore, its LME-sensitivity. Grain boundaries are considered as heterogeneity source, where solute concentration at grain boundaries can be up to several orders of magnitude more than the grain interior [177,178]. At the atomic scale, grain boundary chemistry affects its electronic configuration [179], mobility [180,181], cohesion [182], and local stabilized phases (complexions) [183,184]. The grain boundary chemistry contribution in its LME-sensitivity can be explained from various standpoints: modification of (a) grain boundary energy due to equilibrium segregation, (b) cohesive strength of grain boundary, and (c) atomic site arrangements at grain boundaries. In terms of grain boundary cohesive strength, three different scenarios are possible: grain boundary strengthening (enhancing grain boundary cohesion), weakening (adverse influence on grain boundary cohesion), and bond-strength over a certain value which results in phase transformation at grain boundaries [185]. The vacancy arrangement changes can lead to higher diffusion rate for the embrittler atoms ahead of LME-crack as it affects excess volume of grain boundaries (according to the stress-assisted grain boundary diffusion model [96,107]). This agrees with the observation by Hugo et al. [84], who showed that grain boundary excess volumes (per unit area of grain boundary) greater than 0.5Å result in higher LME-susceptibility.

Therefore, the scope of the present chapter falls within two major unexplored realms of LME. First, it strives to trace the atomistic events at grain boundaries leading to LME-cracking, and validates the recently proposed hypothesis of embrittler-induced alteration of electronic configuration at grain boundary as a viable LME mechanism. Secondly, this study provides knowledge of grain boundary chemistry role in LME, which is still far

from complete. So far, it has been indicated that different chemical compositions show different LME susceptibility [186]; For instance, it has been shown that Si-content can effectively change LME susceptibility of steel. However, without any robust and thorough understanding of the alloying element influence on grain boundaries characteristics, and the interrelation between the geometrical configuration, rationalizing the observed behaviors will be challenging. This calls for an in-depth LME crack-path study from macroscopic, microscopic, and atomic viewpoints. The provided analysis of crack-path paves the road to eliminate, or considerably mitigate LME. More specific, grain-boundary-segregation engineering (as a sub-branch of grain-boundary-engineering approach) can be employed as a microstructure design approach for future LME-resistant materials.

5.3 Experimental Procedure

5.3.1 Experiments

The EBSD observations were used to prepare site-specific-lift-out atom probe tomography (APT) samples. After marking the regions of interest, site-specific APT tips were created using a Zeiss NVision 40 SEM/ FIB and Helios G4 dual-beam plasma-FIB (PFIB) instruments. The APT tips were sharpened by annular ion milling and polishing to the final needle geometry (diameter of ∼250 nm). The APT experiments were carried out on the prepared needle-shaped tips by LEAP^{TM} 4000X HR (Cameca Instruments Inc.). During the APT experiments, the specimen temperature kept at 60K. The collected APT data was analyzed to re-construct the 3D-maps of atomic distributions by the IVAS 3.8 software. Similar APT lift-outs were used for the HRTEM sample preparations, where the unsharpened tips were thinned to 50 nm by FIB. The HRTEM observations were carried out using

an FEI Titan 80-300 HB double aberration-corrected to achieve atomic-resolution imaging at an operating voltage of 200 keV.

5.3.2 Molecular Dynamics Simulation

The MD simulation was performed using a C++ program developed by the authors and visual representation of the results of the simulation was produced using Visual Molecular Dynamics open source software [187] . The embedded atom potential method (EAM) was used for this simulation [188]. In this method, the total energy is defined as follows (Eq.5.1):

$$E_{total} = \sum_{i} F(\rho_i) + \frac{1}{2} \sum_{i,j,i \neq j} \emptyset_{i,j}(r_{ij}) \tag{5.1}$$

where $\emptyset_{ij}$ is the pair potential between two atoms of i and j, and is a function of their distance r_{ij}. $F(\rho_i)$ the energy required to embed atom i into the electronic gas produced by all neighbor atoms, calculated as follows (Eq.5.2):

$$\rho_i = \sum_{i \neq j} f(ij) \tag{5.2}$$

where $f(ij)$ is the electron density contributed by atom j. The interatomic potential parameters of Fe, Cr, and Fe-Cr for EAM have been previously reported [189]. The cut-off radius was set to 15 Å, and the time step used in this research was one femtosecond. The simulations were carried out in a canonical (NVT) ensemble, the temperature was kept constant during the simulation according to the Nose-Hoover thermostat [190,191], and the equations of motion were solved numerically using the Verlet algorithm.

The simulated domain was a square containing 50,000 atoms, however, for visualization purposes only small sections of those are shown in the present chapter. The boundary condition of the model was considered periodic boundary condition at the right and left side of the simulation domain. The atoms arranged in ten grains at the beginning. The temperature set at ∼820°C and the model ran for 20,000 time steps to stabilize the model. Then, two Fe-atoms replaced by Cr-atoms and the model ran for 5,000 time steps. At this stage, a stress equal to 200 MPa applied to the top and bottom boundary of the simulation domain and model run for 100,000 time steps.

5.4 Results and Discussion

A representative micrograph of an intergranular LME-crack is shown in Figure 5.1. The general penetration path was perpendicular to the applied external load direction; however, it followed a specific path through the grain boundary network (GBN). The investigations in the previous chapter revealed that random (non-ordered) grain boundaries with misorientation angle of 30-50° and high-index grain boundary planes are the major LME-susceptible grain boundaries [192]. However, the grain boundary energy state (hence, its LME susceptibility) cannot be described only through geometrical and spatial parameters [173]. The present study first investigates the atomistic events at grain boundaries leading to an LME-crack. With the provided insights, atomic-scale grain boundary chemistry and its inter-connection with grain boundary geometrical configuration is discussed.

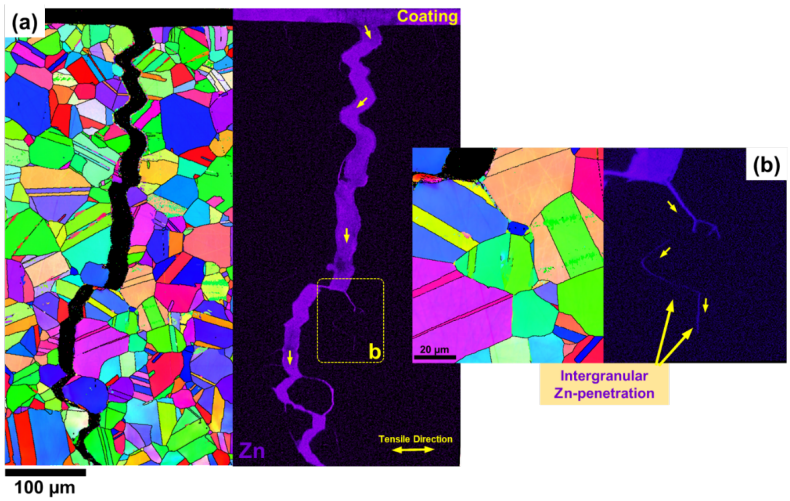

Figure 5.1: (a) EBSD-IPF and the corresponding Zn-maps showing a representative liquid-metal-embrittlement crack and penetration of liquid-Zn from the coating under the external tensile loading; The general crack propagated perpendicular to the external loading direction, and (b) a side-branch of the LME-crack revealing liquid metal penetration along the GBN (Note: the external tensile load is applied horizontally).

5.4.1 APT Analysis of Liquid-Metal-Embrittled Grain Boundary

To analyze the Zn-penetrated grain boundary, the APT needle lift-out (using FIB) was done near the penetrated grain boundary tip (Figure 5.2a). The 3-dimentional reconstruction of the APT analysis is presented in Figure 5.2b, where an ∼40 nm-thick Zn film within the grain boundary has been investigated. The elemental characterization of the Zn film showed the preferential solubility of Ni, Cu, from the matrix into the penetrated liquid-Zn (Figure 5.2c); however, Cr did not dissolve into the Zn film. The 3-dimentional elemental distribution showed that the ∼40 nm-thick Zn film mainly located on one side of the original grain boundary (Figure 5.2c). The detailed composition profiles (measured along the cylinder region of interest) were used to identify the original Zn-diffused grain boundary based on the presence of a region containing 5 at.% of Zn and Cr-segregation (highlighted

in orange, Figure 5.2d) on one side of the Zn-penetration film. A closer inspection of the grain boundary and the liquid-Zn film interface reveals the presence of a ∼5 nm transient region. The distribution of Zn, Ni, and Fe confirms the typical diffusion-driven distribution of the elements. This observation confirms the inter-diffusion of Fe, Zn, Ni between the solid matrix and the liquid-Zn film after fracture of the grain boundary and reveals the sequence of micro-events leading to the LME-crack i.e. fracture path on one side of the grain boundary and the subsequent flow of the fresh liquid Zn and inter-diffusion of Zn, Ni, and Fe.

The presence of the fracture path (due to Zn doping into grain boundary ahead of crack) only on one side of the original grain boundary provides insights to the atomic micro-events leading to an intergranular LME penetration-path. First, the stress-assisted diffusion of the Zn-atoms ahead of the crack affects the adjacent Fe-Fe atomic bonds. Under the applied tensile stress, the weakened Fe-Fe bonds on one side of the boundary fracture, leading to liquid metal flow into the fracture path. The rapid flow of fresh liquid Zn supplies the rapid propagating crack-tip (mass-transfer of Zn) and explains the discrepancy between the grain boundary diffusion rate and LME-crack propagation rate.

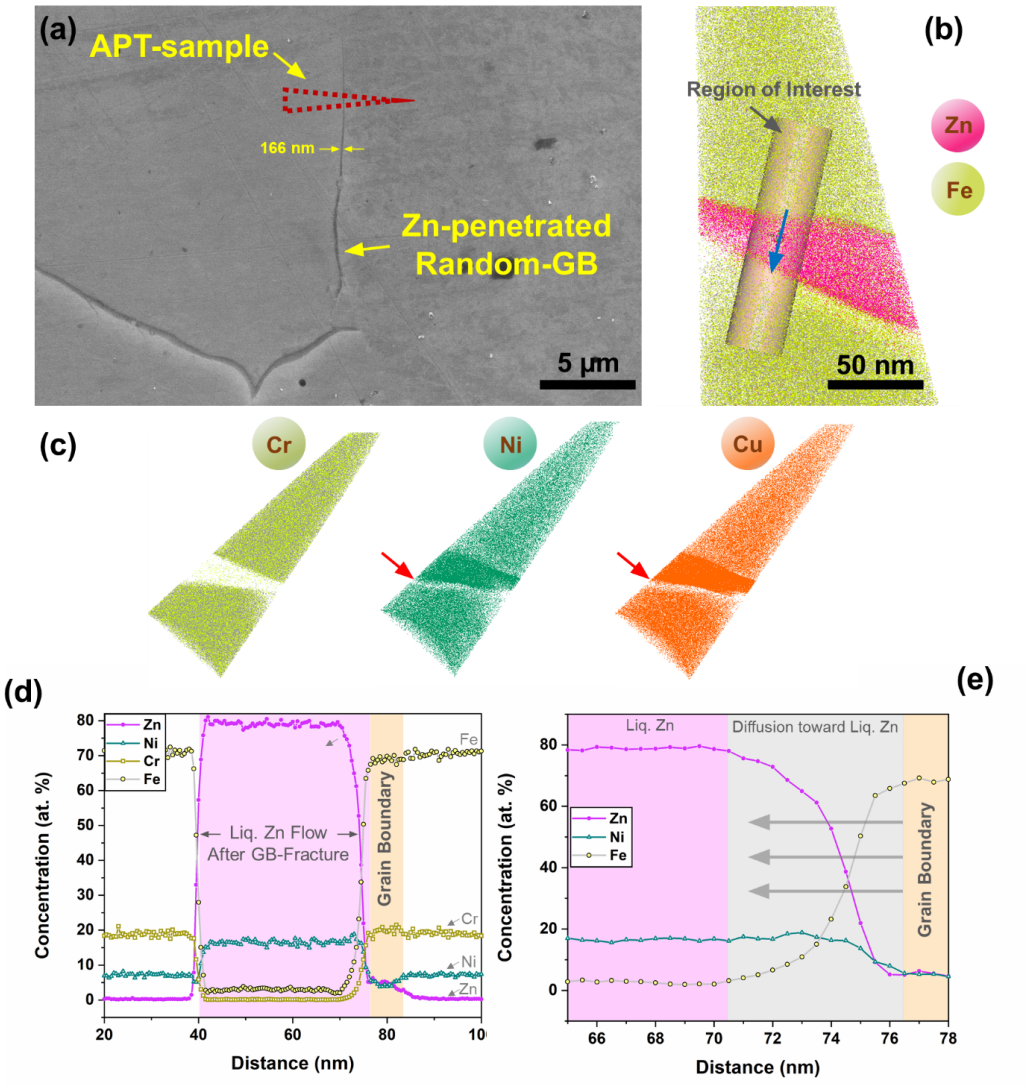

Figure 5.2: (a) The atom probe tomography (APT) needle location from the Zn-penetrated random grain boundary tip with the thickness ∼160 nm, (b) corresponding 3-dimentional reconstruction of the APT analysis of needle (Fe and Zn) containing the Zn-penetrated grain boundary showing the region of interest and direction of analysis, (c) the APT elemental maps of Cr, Ni, Cu, (d) chemical profile obtained from the cylinder region of interest showing the original Zn-diffused grain boundary (highlighted in orange) and the liquid Zn-flow area after fracture of the grain boundary (highlighted in pink), and (e) enlarged view of the interface region between the original Zn-diffused grain boundary and liquid-Zn flow area (highlighted in gray) showing inter-diffusion between of Fe and Zn.

5.4.2 APT Analysis of Random and CSL Grain Boundaries: Solute Effect

To identify the role of inter-relation of grain boundary geometrical characteristics and its chemistry, two representative grain boundary (not exposed to Zn-embrittler) types, i.e. not-ordered and ordered CSL boundaries were investigated. These grain boundaries were chosen in a way that: 1-their location was in a close vicinity of a LME-crack, therefore, the grain boundary experienced similar thermal cycles with the Zn-penetrated grain boundaries, 2-aligned to near perpendicular to the applied stress direction (the external tensile load is applied horizontally) to have similar tensile stress component applied on the grain boundary plane. Figure 5.3a and b show the selected location of the not-ordered grain boundary with a distance of $\sim$100 μm from the LME crack. The detailed high-resolution TEM analysis of the selected grain boundary is shown in Figure 5.3c and d. The HRTEM analysis confirmed the misorientation angle of about 44° and the absence of any observable ordered structure at the grain boundary.

The random grain boundary and the corresponding region of interest is highlighted in the reconstructed atomic map (Figure 5.4a). The APT analysis revealed that Cr as the major solute elements and some of the minor solute elements: B, C, Mo, and Si segregated to the random grain boundary (Figure 5.4b). Although Cr showed a severe segregation along the random boundary, Ni did not show any observable segregation. The analysis showed severe Cr-enrichment of about 12 at.% at the grain boundary (measured within the cylinder region of interest). Minor segregation of C, Si, B, P, Mo, V was observed, however, Cu, Mn, and Co showed no trace of segregation along the random grain boundary. MD simulation of a representative system consisted of random grain boundaries of an FCC-Fe microstructure, and Cr-atoms heated to T$\sim$800°C (the approximate temperature during

the processing) is shown in Figure 5.5.

As shown at time step of 15,000 (before applying the external tensile loading), the Cr-atoms show a random walk behavior due to thermal activation, however, by applying the external tensile loading (time step of 30,000) Cr-atoms show a rapid diffusion toward the random grain boundary (Figure 5.5b). The Cr-atoms show entrapment at the random grain boundary aligned perpendicular to the loading direction (the representative time step of 150,000, Figure 5.5c). The detailed diffusion path of Cr-atom-1 and 2 toward the grain boundary and the entrapment at the grain boundary is presented in Figure 5.5d and e.

With the similar selection criteria for the random grain boundary, a CSL boundary was located a distance of $\sim$25 μm from an LME-crack and aligned nearly perpendicular to the applied stress. To identify the CSL boundary, EBSD IPF-map was used to characterize the boundary misorientation angle of 60° (Figure 5.6a and b). However, the energy of a CSL boundary directly depends on its crystallographic plane. The trace analysis method was used to characterize the crystallography of the selected ordered boundary [163,170]. The stereographic projections of (111) plane from grain-1 and 2 were collected (from two spots close to the boundary) (Figure 5.6c) and the PN direction was determined from the EBSD IPF-map. The trace analysis method showed that (111) poles coinciding along the PN on the pole figures, and hence, confirmed that the selected CSL boundary is a coherent Σ3 boundary. Detailed high-resolution TEM analysis of the selected ordered grain boundary shows high-level of atomic matching at the boundary (Figure 5.6d and e).

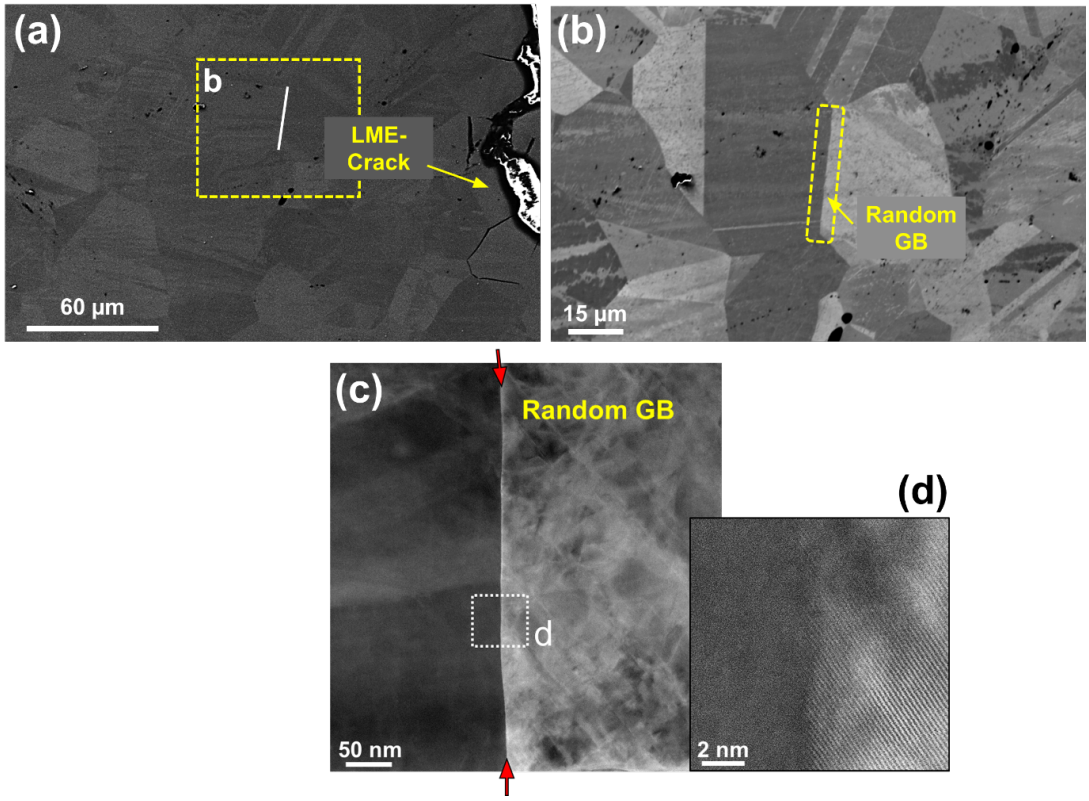

Figure 5.3: (a and b) The selected random grain boundary (not exposed to Zn-embrittler) to study details of elemental distribution, based on two criteria: 1- to be located in a close vicinity of a LME-crack (distance ∼100 μm) which confirms that the grain boundary experienced similar thermal cycles with the LME-crack, 2-to be near perpendicular to the direction of the applied stress (the external tensile load is applied horizontally) which confirms the similar tensile stress component applied on the grain boundary; and (c and d) detailed high-resolution TEM analysis of the selected not-ordered (random) grain boundary with misorientation angle of about 44°.

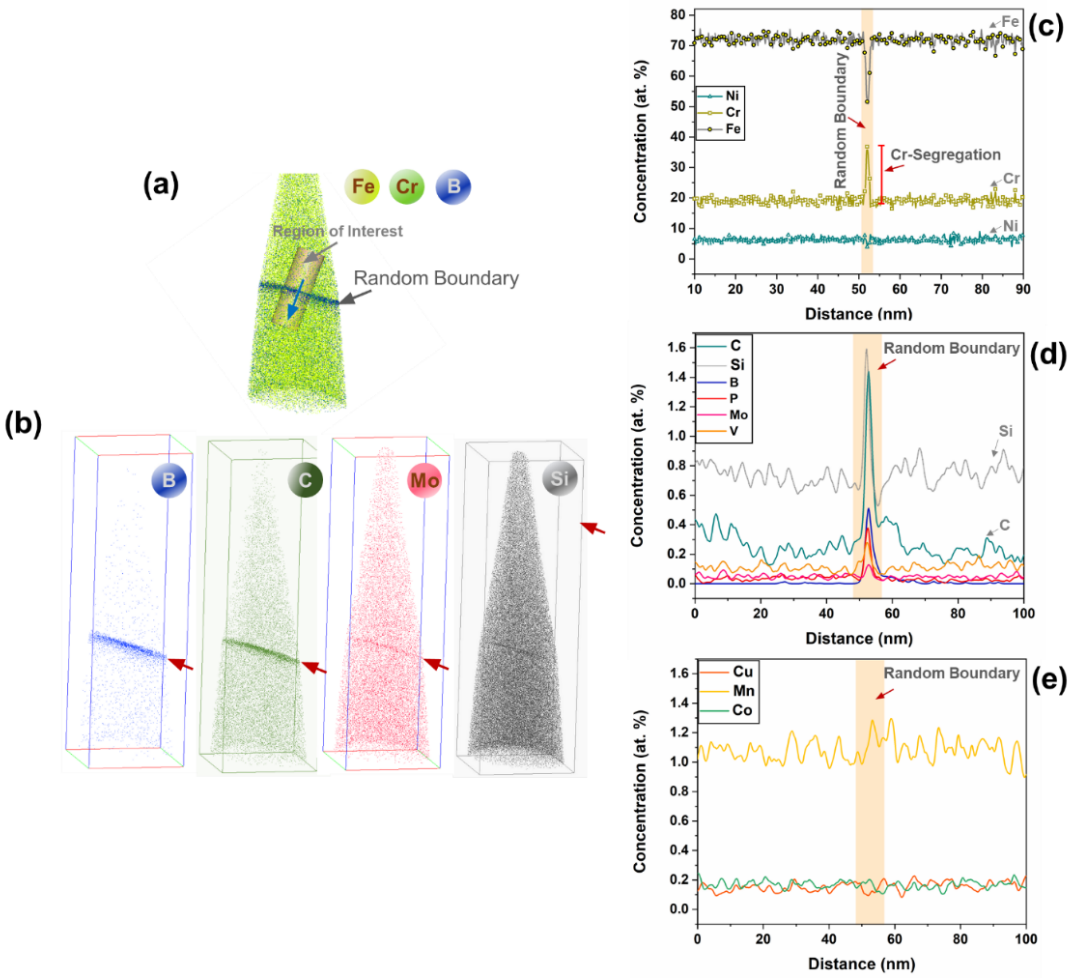

Figure 5.4: (a) Corresponding 3-dimentional reconstruction of the APT analysis of needle containing the selected random grain boundary showing the region of interest and direction of analysis (Fe, Cr, and B are shown to highlight the grain boundary location within the APT needle, (b) APT elemental maps of B, C, Mo, and Si as minor segregating elements into the random grain boundary, chemical profile obtained from the cylinder region of interest showing (c) the severe segregation of Cr along the random grain boundary due to the applied thermal and tensile stress, (d) minor segregation of C, Si, B, P, Mo, V along the random grain boundary, and (e) no trace of segregation for Cu, Mn, and Co along the random grain boundary.

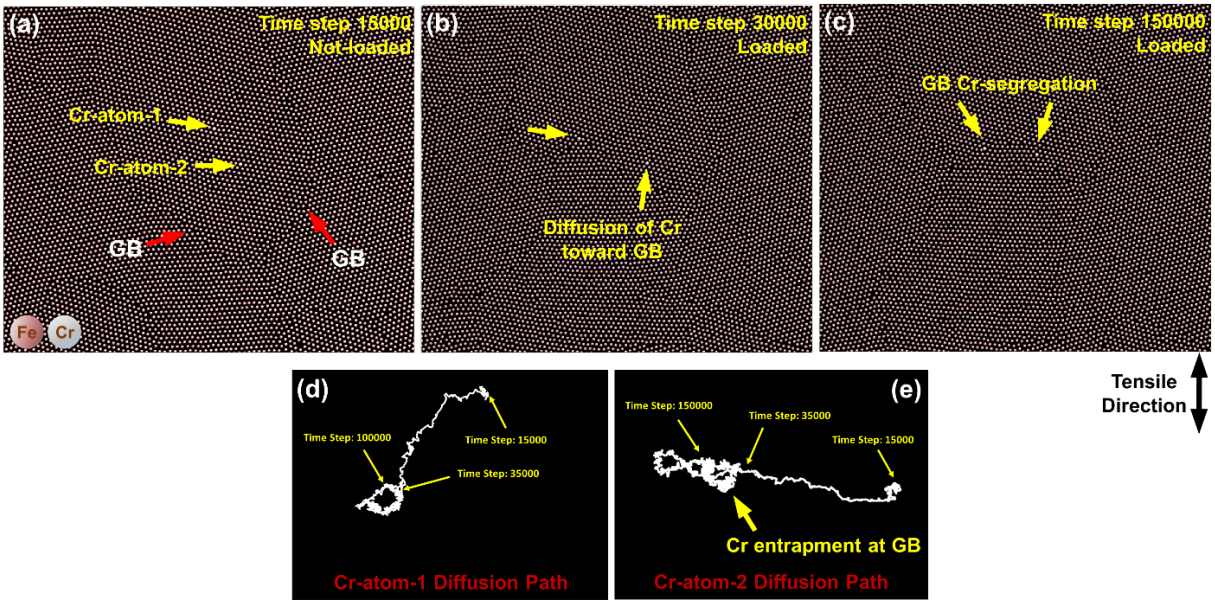

Figure 5.5: Molecular dynamics (MD) simulation of a representative system consisted of FCC-Fe microstructure, the corresponding random grain boundaries (GB), and two Cr-atoms (T∼800°C) (a) at time step of 15,000 before applying the external tensile loading, (b) at time step of 30,000 after applying the external tensile loading showing the diffusion of the Cr-atoms toward the grain boundary, (c) at time step of 150,000 showing that the Cr-atoms were segregated at the grain boundary which is aligned perpendicular to the applied external tensile loading direction, (d and e) detailed diffusion path of Cr-atom-1 and 2, respectively, showing the random-walk behavior of Cr-atoms before applying tensile loading, however, after applying tensile loading the Cr-atoms rapidly diffused toward the grain boundary which was aligned perpendicular to the loading direction and were entrapped at the grain boundary (Note: Pink: Fe atom, Gray: Cr-atom, the external tensile load is applied vertically).

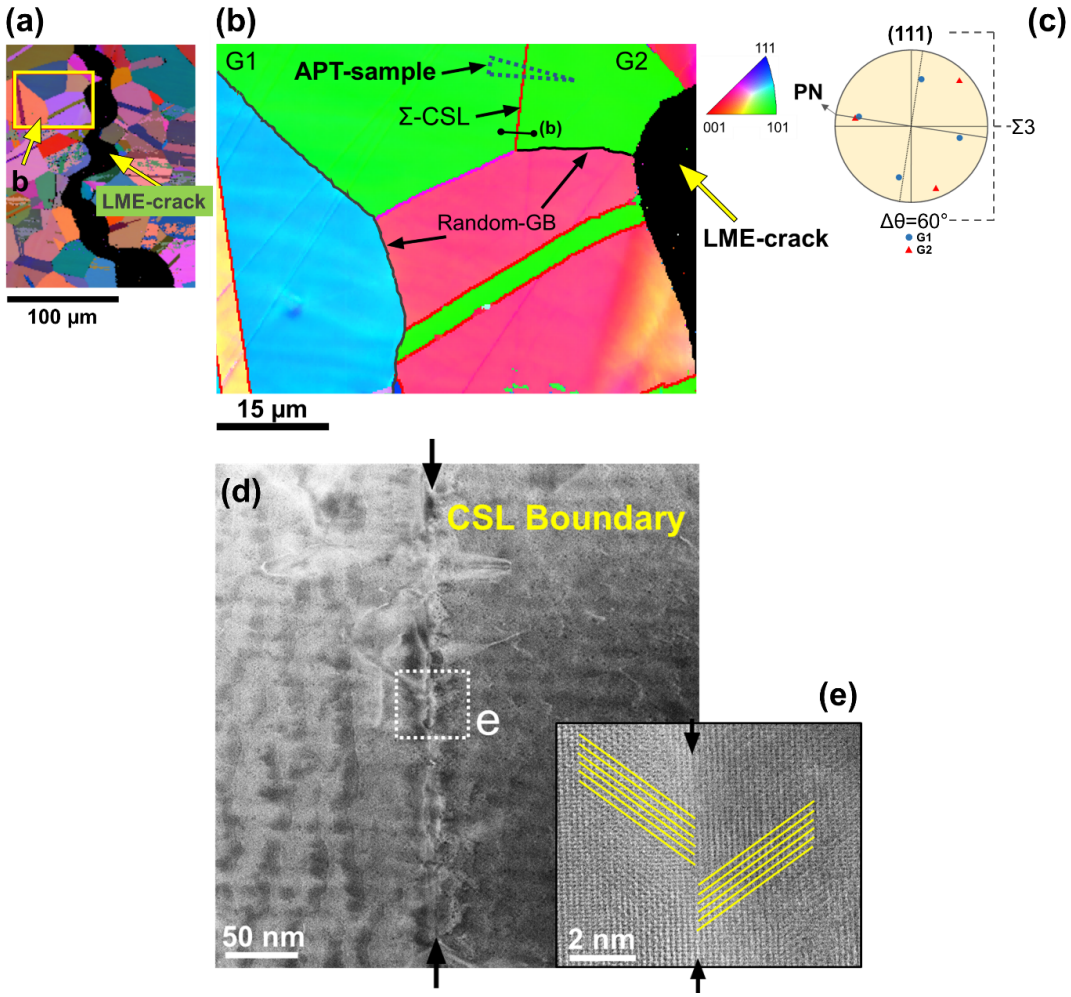

Figure 5.6: (a) The selected ordered (CSL) grain boundary (not exposed to Zn-embrittler) to study details of elemental distribution, based on the same selection criteria of the not-ordered (random) grain boundary (in a close vicinity of a LME-crack (distance 25m) and near perpendicular to the direction of the applied stress which confirms the similar thermal cycles and stress condition experienced by the CSL grain boundary, (b) EBSD IPF map showing the APT needle location from the selected grain boundary, (c) the trace analysis method to characterize the details of the selected ordered boundary which shows collecting pole figures of the crystallographic planes from the regions close to confirm the coinciding planes of grain 1 and 2: G1 and G2 along the plane normal (PN) direction showing the ordered grain boundary (misorientation angle of 60°) is a coherent Σ3 (plane of (111)), (d and e) high-resolution TEM analysis of the selected ordered grain boundary showing high-degree of atomic matching at the selected ordered grain boundary.

Fe atomic density from the APT analysis was used to reveal the CSL boundary in the APT needle sample (Figure 5.7a).The corresponding elemental distribution of Fe, Cr, and Ni along the ordered Σ3 boundary showing the region of interest and direction of analysis (Figure 5.7b and c). The chemical profile obtained from the cylinder region of interest confirmed no trace of major alloying elements (Cr, Ni) segregation along the ordered Σ3 boundary (Figure 5.7d); however, a slight segregation of C was observed. In contrast to the not-ordered boundary, the ordered Σ3 did not show any observable segregation of the minor alloying elements (Si, B, P, Mo, Cu, Mn, V).

The Cr-segregation as the major alloying element, and the co-segregation of the impurity elements makes the high-angle random grain boundaries preferential site for (a) stress-assisted grain boundary short-range diffusion where the Zn-doping induces the embrittlement, and (b) the impurity-segregation facilitates the brittle fracture. In fact, atomic-scale grain boundary chemistry (cohesive strength) connects the GBCD role to the LME-sensitivity of a grain boundary. This, in-turn, explains why liquid metal penetrates non-uniformly into the grain boundary network, and the random (not-ordered) grain boundaries are much more LME-sensitive compared to ordered boundaries.

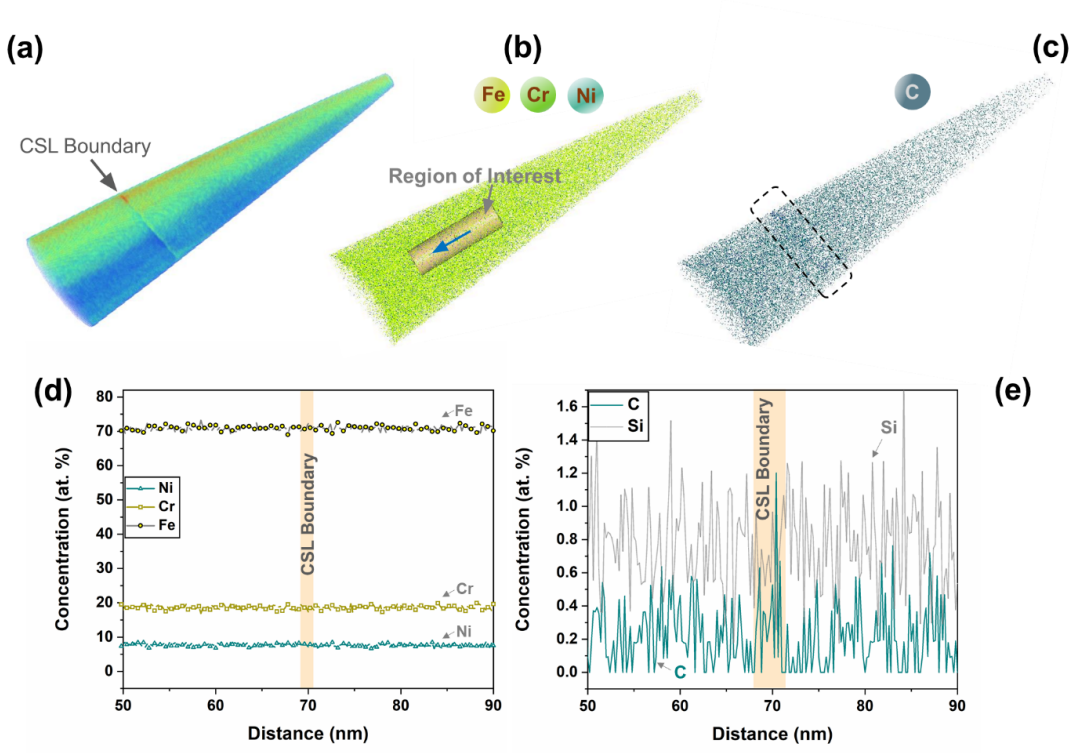

Figure 5.7: 3-dimentional reconstruction of (a) the Fe atomic density of the APT analysis that facilitates revealing the selected ordered Σ3 boundary location in the APT needle, (b) corresponding elemental distribution of Fe, Cr, and Ni along the ordered Σ3 boundary showing the region of interest and direction of analysis, (c) distribution of C shows a slight segregation of C at the representative ordered Σ3 boundary, (d) chemical profile obtained from the cylinder region of interest confirming no trace of major alloying elements segregation along the (Cr, Ni), and (e) in contrast to the not-ordered grain boundary, the ordered CSL boundary did not show segregation of the minor alloying elements (Si, B, P, Mo, Cu, Mn, V), however, a slight segregation of C was observed.

5.5 Summary

This chapter provided new insights to the micro-events leading to intergranular liquid-metal-embrittlement crack-path. The main conclusions of this chapter are summarized below:

(a) The APT analysis presented the first-time experimental support for the recently proposed embrittler-induced alteration of grain boundary electronic configuration model. The results described how the stress-assisted diffusion of the embrittler atoms ahead of progressing LME-crack leads to grain boundary decohesion. The liquid metal flow into the fracture path explained the required micro-mechanism for mass-transfers of fresh liquid embrittler to the further grain boundary, which feeds the rapid propagating crack-tip.

(b) The APT analysis and the MD simulation showed that the thermal cycles and the applied external tensile loading induce a severe Cr-segregation and co-segregation of the impurity elements to high-angle random grain boundaries. This revealed the inter-relation between grain boundary geometrical characteristics and its chemistry, where the grain boundary segregation increased LME-sensitivity. The influence of grain boundary segregation on LME-sensitivity was interpreted from two standpoints. First, the severe segregation facilitates short-range diffusion of the embrittler atoms ahead of a crack-tip due to modified configuration of grain boundary vacant sites. Secondly, the influence on the cohesive strength of grain boundary due to the charge distribution modification at grain boundaries in accordance with the recently proposed electronic structure modification LME mechanism.

Chapter 6

Grain Boundary Engineering: LME-crack Suppression[1]

6.1 Overview

Grain boundary engineering (GBE) has lately been recognized as a viable approach to manipulate grain boundary characteristics to improve resistance against intergranular degradation. As discussed in Chapter four, the CSL boundaries has been shown to be resistant against the embrittlement. The present chapter investigates the feasibility of using a GBE technique to arrest LME in the Fe-Zn couple. Two sets of low-strain-heat-treatment processing routes were used to optimize grain boundary characteristics based on: (a) $\Sigma 3$ and $\Sigma 3^n$ boundaries frequency, and (b) the overall material's texture and grain size evolution. The optimum characteristics resulted in significantly improved resistance against LME. The

[1]This chapter consists of the published manuscript in Materialia, https://www.sciencedirect.com/science/article/pii/S2589152920300855, MH Razmpoosh, A Macwan, F Goodwin, E Biro, Y Zhou, 2020.

mechanism of the embrittlement arrest is discussed based on the random-GBN continuity and the grain boundary triple junction distribution due to the numerous CSL boundaries in the microstructure.

6.2 Background

Recently, the GBE concept has been introduced as a viable method to mitigate the undesirable aspect of grain boundaries [193–197]. The various GBE techniques attempt to eliminate the "weak" high-energy grain boundaries and instead induce the "stable" low-energy grain boundaries [198,199]. Generally, the stable grain boundaries refer to low-Σ (Σ <29) CSL boundaries which contrast to the high-misorientation angle random grain boundaries or higher-Σ (Σ >29) CSL counterparts [198,200,201] (Σ is the density of common sites between grains sharing a boundary). Despite a wide range of proposed thermo-mechanical treatments [202–206], the twin-induced GBE method, which induces a high frequency of low-Σ CSL boundaries is considered the most common GBE approach. This method can be further sub-divided into strain-recrystallization and strain-annealing based approaches [194,196,207–209].

A material's ability to generate numerous CSL boundaries is the main pre-condition of twin-induced GBE, which has been reported in low stacking fault energy (SFE) FCC materials [204] such as nickel-alloys [208,210,211], copper-alloys [209,212], and austenitic steels [194–197,202,205]. GBE mainly relies on the $\Sigma 3$ regeneration micro-mechanism. As a result of thermo-mechanical treatment, generation of low-Σ boundaries during the migration of random boundaries and emission of Σ boundaries from the existing random grain boundaries take place. In this framework, the Σ-boundary regeneration process occur according to ($\Sigma 3^n + \Sigma 3^{n+1} \rightarrow \Sigma 3$) [198,202,207], where, two $\Sigma 3$ boundaries junction generates

a Σ9. When a Σ9 runs into a Σ3 boundary, it would regenerate a new Σ3 in the structure. This example of the Σ-boundary regeneration process explains the efficient process of special grain boundary frequency increase in a microstructure due to thermo-mechanical treatment and fragmentation of random GBN. In other words, boundary-boundary interactions leading to generation of special boundaries in the GBN, creating a discontinuous network of random grain boundaries [198,202,207].

Recent studies have demonstrated examples of successful application of GBE in suppression of grain boundaries-based deterioration phenomena. The study by Shimada et al. [197] has shown that a slight pre-strain and annealing resulted in improved intergranular corrosion of austenitic stainless steel. Kokawa et al. [194] has confirmed that a high frequency of uniform CSL produced by the twin-induced GBE process significantly suppressed intergranular corrosion of type 304 austenitic steel. The optimization of the GBCD generated 82% of CSL boundaries which efficiently disrupted the connection of the random GBN, and hence, arrested grain boundary decay [194]. Bi et al. [199] showed chromium depletion was controlled through the promotion of low-energy special boundaries over the random (high-energy) grain boundaries. Increasing twin-based special boundaries also reduced the intergranular HAZ-liquation-cracking in a nickel-based superalloy [213]. This literature survey shows that GBE improves material performance: (a) directly through the generation of a significant frequency of low-energy grain boundaries (2-3 times more than random boundaries), and (b) indirectly by the special-random grain boundary interactions which creates structural barriers against the degradation of the continuous random GBN.

Atomistic modeling of the Al-Ga couple [85] has shown that the LME-crack progression directly depends on grain boundary energy. LME susceptibility significantly increases with grain boundary energies > 0.65 J/m^2 [85]. The previous chapter showed that only high-energy random grain boundaries are embrittled in the Fe-Zn system, where local

LME progression is governed by the grain boundary misorientation angle (grain boundary energy)-applied tensile stress couple. In contrast, low-energy special grain boundaries at θ=60° (Σ3) and at ∼39° (Σ5-9) completely resisted the liquid penetration and further cracking. The atomic resolution TEM showed that the random and special boundary triple junction effectively arrest LME due to changes the random grain boundary misorientation angle in the twinned area of the grain. The recent observation suggested that by inducing desirable types of triple junctions, such as all special (SSS), special-special-random (SSR), and certain special-random-random (SRR), LME-cracking in the sensitive austenitic (FCC) structure can be mitigated. The present work investigates the feasibility of LME-cracking suppression through materials variables. This includes reducing the material's inherent weak points by inducing a considerable fraction of CSL boundaries into the microstructure, and an efficient increase in entropy of the random GBN.

6.3 Experimental procedure

In this chapter, a commercial 304-type austenitic stainless steel with a nominal thickness of 0.9 mm was used. The as-received samples were solution heat-treated at 1050°C for 0.5 hr under Ar-atmosphere and quenched. The thermo-mechanical treatment to manipulate the GBN started by applying a 5% pre-strain to the material using an Instron universal tensile tester. It has been shown that the combination of low pre-strain values at 5% and subsequent heat-treatment results in the maximum generation of CSL boundaries [197]. The pre-strained specimens were then heat-treated under Ar-atmosphere at various times at 900°C and 1000°C, followed by water-quenching. The annealing temperatures were chosen to avoid considerable grain growth. Any undesired surface oxide layer was removed by a conventional acid-cleaning step. As the acid-cleaning step may cause hydrogen to

be absorbed into the specimens, a low-temperature baking at 190°C for 1 hr was used to diffuse out any hydrogen from the steel structure. The standard metallographic sample preparation procedures were similar to those used in the previous chapters. The grain boundary characteristics and their frequency were investigated by the similar EBSD system attached to a JEOL JSM 7000f field-emission gun SEM (step size 0.05-0.25 μm and accelerating voltage of 20 kV) as discussed in previous chapters. Oxford Instruments Aztec software was used for the EBSD mapping followed by post-processing of the collected maps in the HKL Channel-5 package. The EBSD images were then analyzed in image processing software (ImageJ) to construct distributions of various grain boundary types and the associated triple junctions in each condition.

The LME behavior of the initial and the optimum grain-boundary-engineered samples exposed to the heat source of laser processing under the applied tensile stress were investigated. A Zn surface layer (thickness $\sim$12 μm) was kept in contact with the samples to induce LME. The details of the specimen geometry and the externally loaded laser processing are presented in previous sections. For each optimum GBE condition, 4 specimens were cross-sectioned to measure the LME-crack length and distribution. EDS in SEM and EELS elemental mapping in TEM were used to study the Zn-penetration along the grain boundaries. EELS mapping at the crack tip was performed by a FEI Titan 80-300 HB double aberration-corrected HRTEM on a slice of the material prepared by FIB technique.

6.4 Results and discussion

6.4.1 Special Grain Boundary Frequency

The initial microstructure of the austenitic (FCC) steel contained ∼77% high-angle (θ >15°) random grain boundaries and 23% of special boundaries as shown in Figure 6.1. Most of the special boundaries were Σ3 (22%) whereas only a minor fraction of higher order Σ-boundaries such as Σ5, Σ7, and Σ9 (total ∼2%) was observed. The previous studies [194,197] showed that a thermo-mechanical GBE treatment of 5% tensile deformation followed by annealing at 900°C and 1000°C can effectively modify the initial GBN. It has also been shown that neither the repetition of the strain-annealing treatment nor the application of higher strain levels (>5-6%) further improve the special grain boundaries re-generation process and the resultant CSL frequency [194,197,201,202]. Relatively low strain levels (5%) are insufficient to provoke recrystallization at the moderate annealing temperatures [201]. The EBSD grain boundary maps of the microstructure after the various applied GBE treatments at 900°C and 1000°C are given in Figure 6.2 and Figure 6.3, respectively (Note: the random and special grain boundaries are indicated by black and gray lines, respectively). As seen in the initial structure, the random GBN (black lines) is entirely connected with each other. Whereas, the applied GBE treatment induces a considerable fraction of the special boundaries (gray lines) into the structure. As a result, the initial continuous network of random grain boundaries has been progressively fragmented.

The statistical breakdown of the random and special grain boundary distributions after the various GBE treatments are presented in Figure 6.4. This shows that the GBE treatment successfully increased the fraction of special boundaries in relation to the undesirable random grain boundaries, and agrees with the previous GBE studies of austentic steel

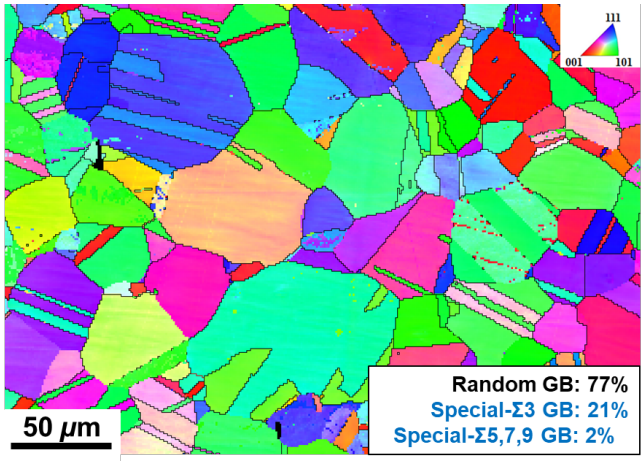

Figure 6.1: EBSD inverse-pole-figure map of the as-received austenitic steel showing the representative general grain microstructure with an average grain size of 28 m and 77% of high-angle (θ >15°) random and 23% of special grain boundaries (21% of Σ3 and 2% of Σ5, Σ7, and Σ9).

[193,202,205]. Special grain boundaries and specifically, Σ3 boundary fraction drastically increased due to the Σ-boundary regeneration mechanism [198,202,207]. At both processing temperatures, the slight applied strain did not trigger any recrystallization. Small random-grain boundary migration takes place during short annealing times at 1000°C (<10min) (Stage-1 of the grain boundary evolution in austenitic structures [201]). However, higher annealing times at 1000°C induce severe random- grain boundary migration (Figure 6.3e and f), which is known as Stage-2 of the grain boundary evolution [201]. Due to the low applied strain, at 900°C no random grain boundary migration was observed up to 1000 min. Through the regeneration mechanism, the higher-order Σ-boundaries produced numerous Σ3 boundaries and changed the random GBN.

Micro-texture analyses were performed on the representative GBE-treated conditions as another GBE optimization criterion (Figure 6.5). Although, the overall materials texture after GBE evolves due to the introduction of a considerable fraction of special grain

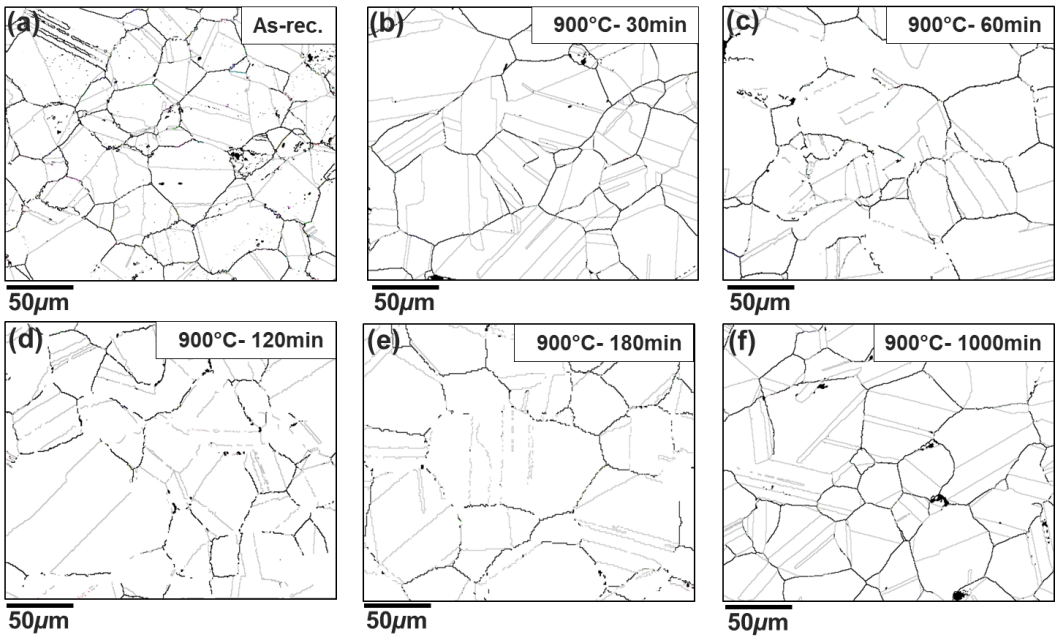

Figure 6.2: EBSD grain boundary character distribution of the representative (a) as-received, and grain boundary engineered material at 900°C (b) 30 min, (c) 60 min, (d) 120 min, (e) 180 min, (f) 1000 min showing increasing total fraction of special boundaries (gray lines) and the progressive fragmentation of the initial random GBN (black lines). The average grain size of the structure is not affected by the various grain boundary engineering treatments.

boundaries in the microstructure, despite the strength of the component, the new texture component at 900°C remains almost unchanged up to 1000 min of treatment. However, over 10 min annealing at 1000°C shifts the material's texture to the initial component. This can be attributed to the severe random-grain boundary migration at higher times of treatment at 1000°C. Based on the special grain boundary distribution (Figure 6.4) and the similar texture component, the optimum GBE treatments are selected as 900°C-180min (GBE-1) and 1000°C-10min (GBE-2).

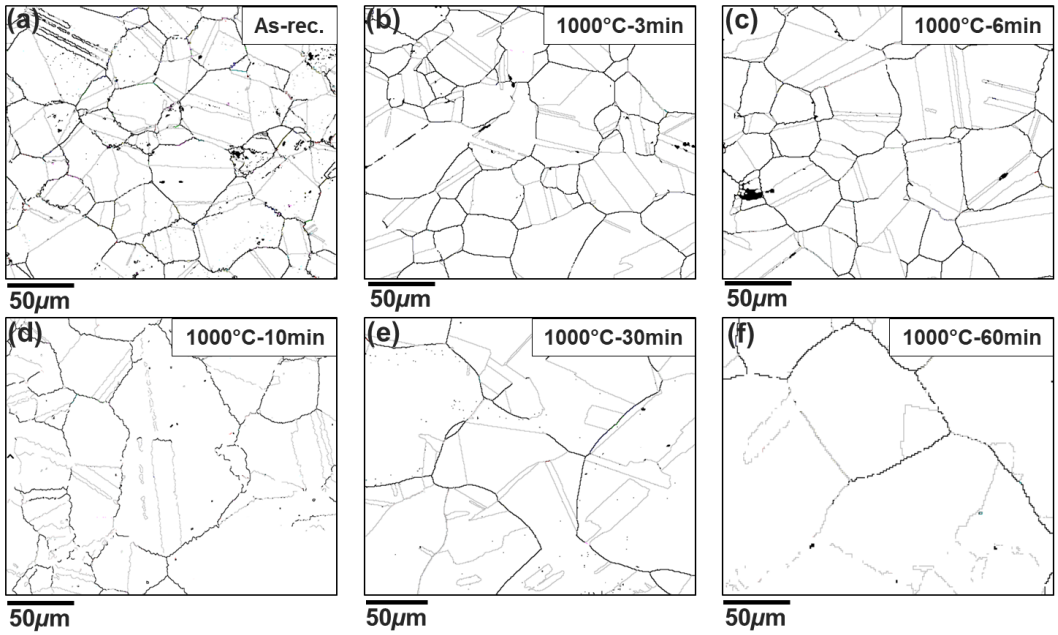

Figure 6.3: EBSD grain boundary character distribution of the representative (a) as-received, and grain boundary engineered material at 1000°C (b) 3 min, (c) 6 min, (d) 10 min, (e) 30 min, (f) 60 min showing increasing total fraction of special boundaries (gray lines) which breaks the initial random GBN (black lines), however, the average grain size of the structure is drastically increased after 10min.

6.4.2 LME Suppression and Triple Junction Distribution

As the vast majority of grain boundary junctions in a material are triple junctions, liquid metal penetration along a GBN depends on the triple junction characteristics. By inducing a high frequency of special boundaries into a GBN, four different type of triple junctions can be considered: all random grain boundaries (RRR), a triple junction with one special boundary (RRS), triple junctions with at least two special boundaries, (RSS), and triple junctions with only special boundaries (SSS). The previous results showed that liquid-Zn only propagates along the random GBN. This means if the stress and misorientation angle couple (as pre-requisite of LME) is sufficient, the liquid metal can pass the RRR type

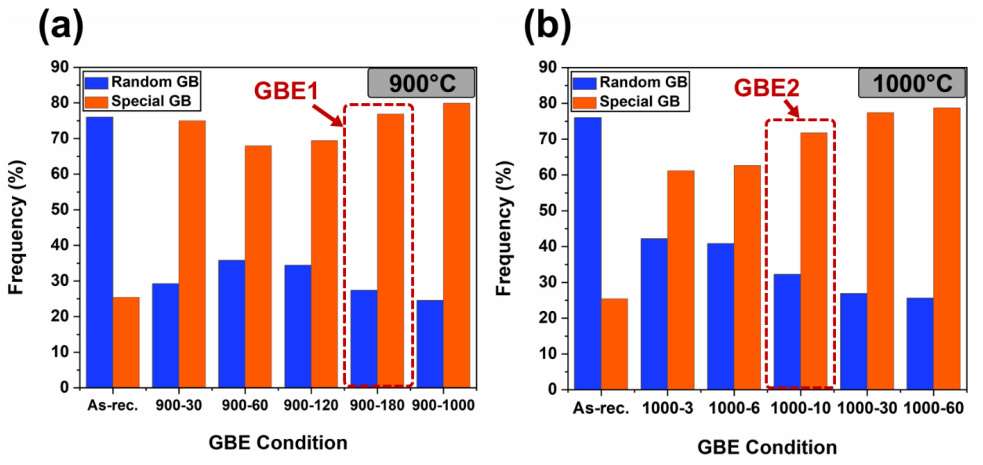

Figure 6.4: Overview of the distribution of random and special grain boundaries in the various grain boundary engineering processed conditions at (a) 900°C, and (b) 1000°C compared to the as-received condition. The optimum GBE conditions of GBE-1 (900°C-180min) and GBE-2 (1000°C-10min) were selected based on the random grain boundary disruption and grain-size and texture evolution criteria.

triple junction. However, the atomistic resolution of RRS triple junction showed that the twinned area of the grain changes the random grain boundary misorientation angle and hence, effectively arrests LME. The recent observations in Fe-Zn couple indicated that special boundaries, and in particular Σ3s, resist liquid penetration at any given stress component, due to their low grain boundary energy. Hence, inducing the desirable SSS, and SSR, and certain SRR type triple junctions can suppress LME progression. On this basis, the SSS, and SSR types can be considered as the desirable triple junctions in the overall GBN.

LME susceptibility of the initial microstructure and the optimum GBE-1 and the GBE-2 conditions is represented in Figure 6.6. The average number of LME-cracks (per sample) and the corresponding total LME-crack length (normalized to the total crack-length of the as-received condition) shows that LME was suppressed through modification of the

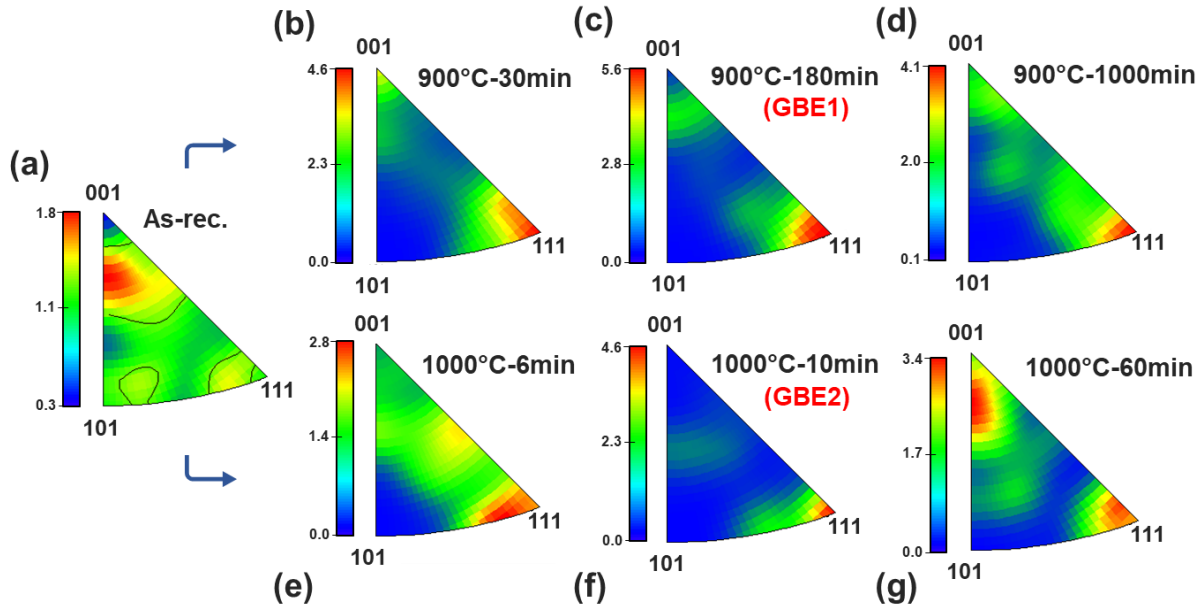

Figure 6.5: Micro-texture analysis of the (a) as-received, and the representative grain boundary engineered material at (b) 900°C-30min, (c) 900°C-180min (GBE-1), (d) 900°C-1000min, and (e) 1000°C-6min, (f) 1000°C-10min (GBE-2), (g) 1000°C-60min, showing the minor evolution of texture at 900°C GBE conditions, however, at 1000°C the overall texture changes drastically after 10min.

initial GBCD. This is attributed to the introduction of (a) high frequency of special Σ-boundaries with high resistivity against LME, (b) RRS, RSS, and SSS type triple junctions that block liquid metal penetration (Figure 6.7a and b), and (c) the loss of the random GBN connectivity.

The corresponding high-resolution EELS map of Zn clearly shows that the RRS junction blocks the Zn penetration pathway (arrest point). The continuation of the random grain boundary did not show liquid metal penetration due to the twin-induced grain orientation. This correlates to the observed triple junction distribution in the initial and the optimum GBE-1 and GBE-2 conditions (Figure 6.8). The proposed grain boundary triple junction

role is also consistent with the RRS and RSS-SSS distributions in the engineered conditions, where longer LME-cracks were observed in the GBE-2. As seen, the LME-resistant triple junctions increase drastically in the engineered samples, leaving only ∼20% of undesired RRR-type triple junctions. The present results agree with the analytical probability study of the distribution of triple junctions in 2-dimentional GBN after introducing CSL [203]. It has been confirmed by Kumar et al. [203] that the RRR-type triple junctions decrease substantially by promotion of special boundaries. The lower frequency of SSS-type triple junctions is consistent with the GBE treatment of Cu (FCC), where processing at lower temperature results in ∼7% higher distribution of SSS-type triple junctions [203]. Although the initial material contained ∼14% of resistive triple junctions, the high fraction of RRR-type triple junctions allows bypass LME-path along the adjacent grain boundaries which has been shown in the previous chapters. This verifies the effect of special-boundary-included triple junctions in arresting LME.

The other factor affecting the LME progression path in the materials GBN is the disruption of the continuous network of random grain boundaries (Figure 6.7b). The ideal case is complete transformation of random grain boundary into a low-energy Σ-boundaries, however, the partial transformation of random grain boundary pathway also is beneficial to LME suppression due to the interruption of random grain boundary connectivity. As shown, the initial random grain boundary with the misorientation angle of 22° transforms into a Σ29-b type special boundary due to the emission of Σ3s from the random grain boundary. This effectively interrupts the continuous network of random grain boundaries as the transformed part of the initial random grain boundary is energetically unfavorable for continuation of Zn-penetration.

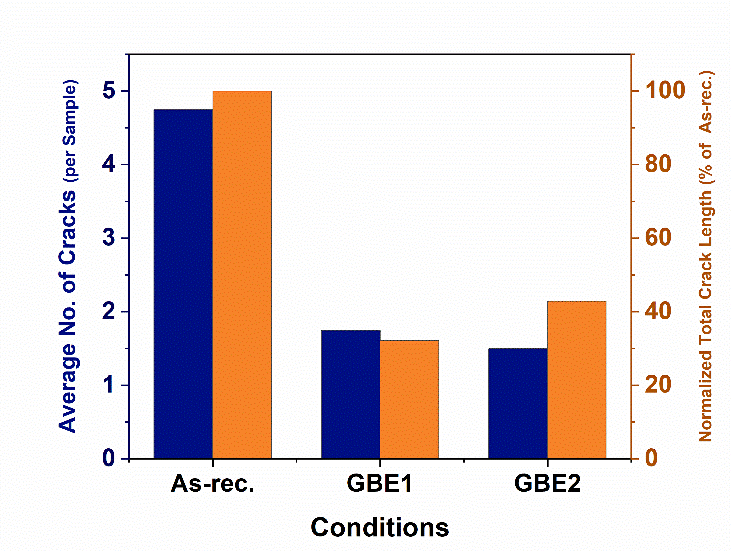

Figure 6.6: The average number of cracks per sample and the corresponding total LME-crack length (normalized to the as-received condition) in the as-received, and the optimum GBE-1 and GBE-2 conditions showing the suppression of LME-cracks by increasing frequency of special boundaries and RSS and SSS type triple junctions and disrupted random GBN.

6.5 Summary

This chapter investigated the feasibility of the twin-based grain-boundary-engineering approach to suppress LME in an austenitic microstructure. The grain boundary character distribution can be modified through the single-step thermo-mechanical grain-boundary-engineering treatment consisted of a slight cold deformation (5%) and subsequent annealing process at 900 and 1000°C. The applied grain-boundary-engineering treatment promotes stable low-Σ special grain boundary frequency from ~20% in the initial state to about 70%. Two optimized grain-boundary-engineered conditions (900°C-180 min and 1000°C-10 min) have been chosen based on overall special grain boundary frequency, grain size, and material texture evolution.

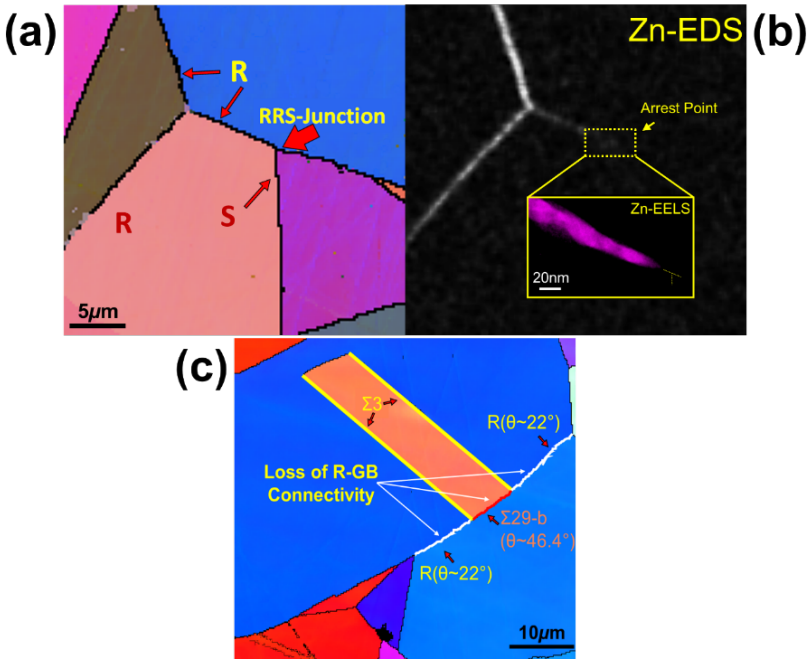

Figure 6.7: A representative EBSD analysis and (b) corresponding SEM-EDS and atomic-resolution-EELS map of the liquid Zn penetration along random grain boundary and Zn penetration arrest point at the RRS triple junction, and (c) an example of connectivity of the random GBN due to the transformation of the random grain boundary to Σ29-b after the emission of Σ3 twin-boundaries from the random grain boundary (R: random GB, S: special GB).

The optimum grain boundary character distribution suppresses liquid metal embrittlement through (a) high frequency of special grain boundaries that are not sensitive to liquid metal embrittlement, (b) inducing special grain boundary-included triple junctions such as random-special-special (RSS), and (c) interruption of continuous network of the remaining random grain boundaries through random to special transformation of the grain boundary pathway due to the emission of Σ3s.

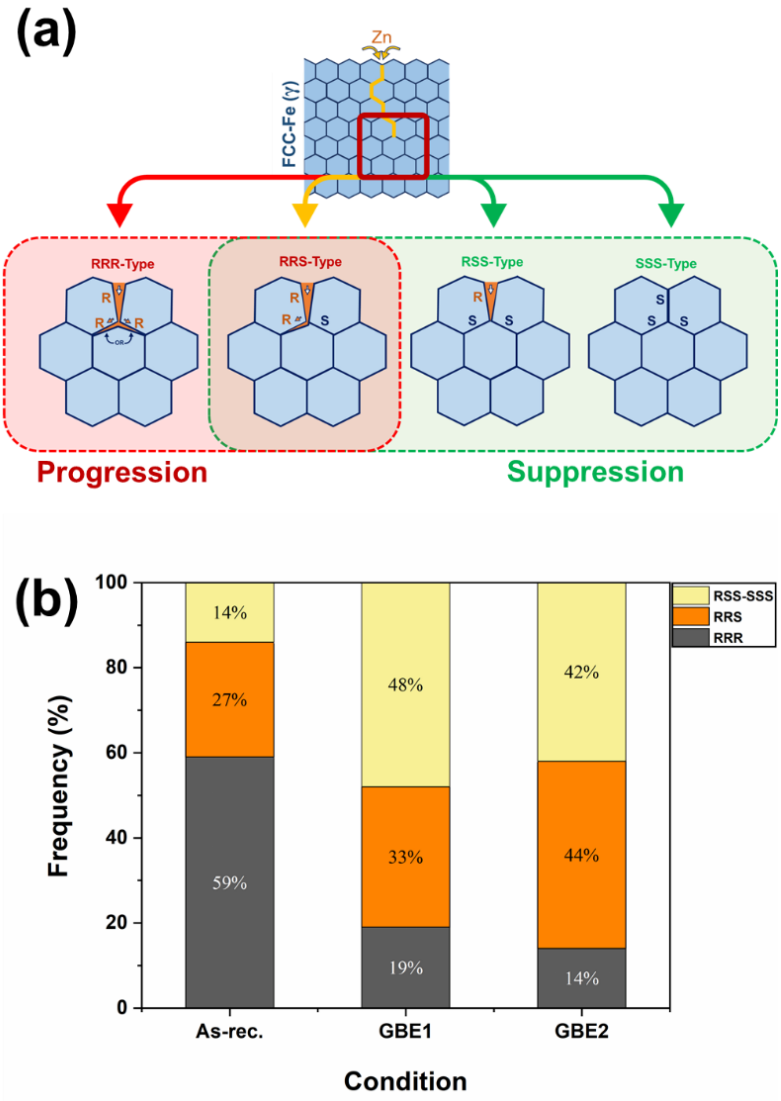

Figure 6.8: A(a) schematic illustration of the different possible triple junctions of random and special grain boundaries where the LME progress continues in all the RRR and some of the RRS type of triple junctions (if the stress-component precondition is satisfied), however, in the RSS and SSS type triple junctions LME-crack suppression occurs, (b) the frequency of the various types of grain boundary triple junctions in as-received, GBE-1, and GBE-2 conditions showing the reduction of undesirable RRR type triple junction to 19 and 14% in GBE-1 and GBE-2 conditions, respectively.

Chapter 7

Comprehensive Discussion on Micro-mechanism of LME and Role of Grain Boundaries

LME occurs in various liquid-solid metal couples, leading to a rapid, uncontrollable crack growth. The literature survey showed that still there is no universal agreement on the LME mechanism, and the role of grain boundaries in this phenomenon is not comprehensively understood. Therefore, this research focused on two major unexplored areas of LME: the micro-mechanism of the embrittler-induced embrittlement, and the role of grain boundary characteristics and distribution in LME behavior.

7.1 Experimental Evidence of Stress-assisted Grain Boundary Diffusion Model

As discussed in Chapter three, detailed EPMA analysis of the Fe-Mn saturated Zn-alloy showed that the liquid embrittler was not present ahead of crack tip, providing an experimental evidence of solid-state grain boundary diffusion of embrittler ahead of progressing crack-tip (Figure 7.1). Moreover, Chapter four presented high-resolution TEM analysis of crack tip confirming the absence of dislocation activity near LME crack-tip (Figure 7.2). These microstructural results along with the tensile stress-sensitivity of LME-cracking in various investigated materials validated the proposed "stress-assisted grain boundary diffusion" model to describe how LME cracks rapidly propagate into a material's grain boundary network. The stress-assisted grain boundary diffusion model also agrees with the observed brittle LME cracking, and explains the role of re-sharpening (grooving) in LME-crack rapid progression. The diffusion of the embrittler atoms into the grain boundary (under the applied tensile stress) creates a diffusion wedge (re-sharpening), otherwise the applied stress causes crack-tip blunting rather than crack opening which would resist rapid LME-crack progression.

7.2 Grain Boundary Characteristics Role in Determination of LME crack-path

By using stress-assisted grain boundary diffusion model to describe LME in polycrystalline metals, it is vital to understand the role of grain boundary energy in LME. It is accepted now that grain boundaries are not just amorphous interfaces, but are structures

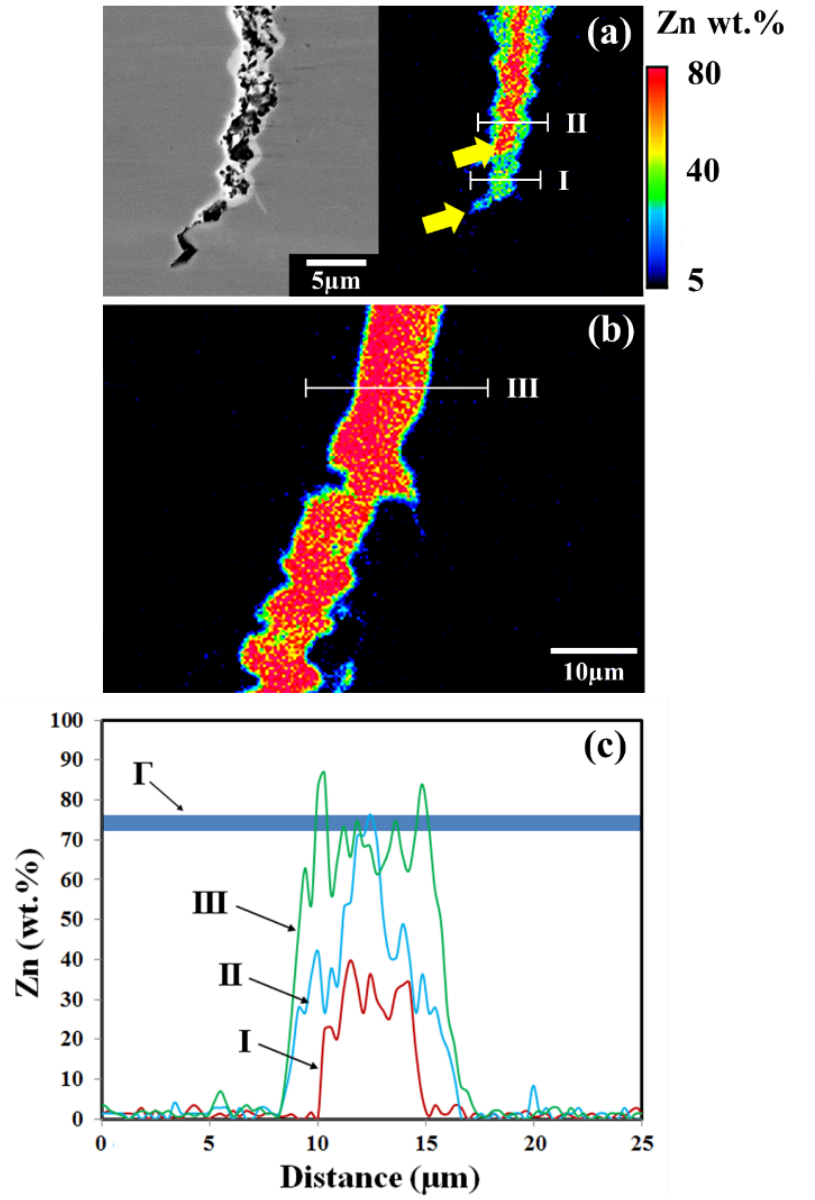

Figure 7.1: Electron probe micro-analysis (EPMA) of the (b) tip, (c) middle part of the LME crack, and (d) corresponding Zn concentration profile in various regions of the LME crack confirming Γ-phase Zn-content range (red regions in (b) and (c)) which represents the liquid Zn during LME-cracking (Copied from Figure 3.16).

with energetic aspects that are relatively ordered [185,214], hence, their energy can be correlated to geometrical characteristics such as misorientation angle and crystallographic plane, as well as grain boundary microchemistry. According to ($2\gamma_{SL}\cos\frac{\theta}{2} = \gamma_{GB}$) [109], liquid metal penetration is governed by the local equilibrium between the energy of the exposed grain boundaries (γ_{GB}) and the solid/liquid interface energy (γ_{SL}), where the necessary condition of grain boundary LME-susceptibility can be defined as $\gamma_{GB} > 2\gamma_{SL}$. Generally, grain boundary Gibbs energy shows a linear negative dependence on temperature, whereas γ_{SL} shows a higher reduction rate [108]. This explains why an elevated temperature (over a transition temperature of T_w) is required for LME, after which the $\gamma_{GB} > 2\gamma_{SL}$ necessary condition can be met.

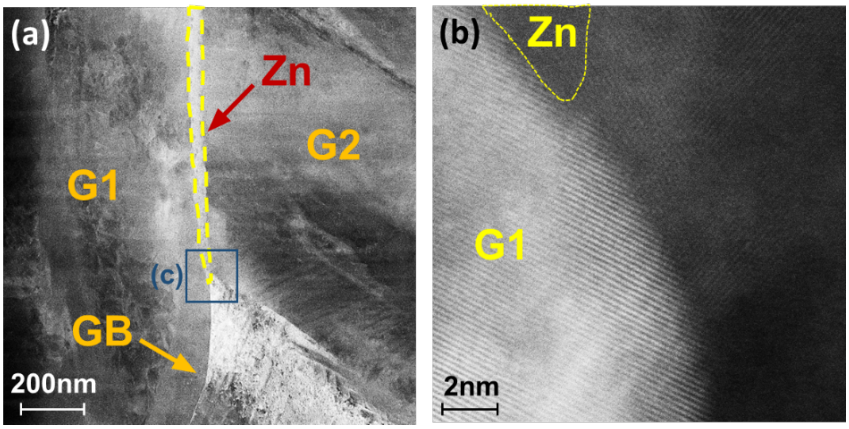

Figure 7.2: TEM micrograph showing the absence of dislocation in the vicinity and crack-tip confirming the minor contribution of dislocation in the Fe-Zn couple LME (copied from Figure 4.7).

In Chapter five, it was shown that general LME-crack path along grain boundaries is governed by a grain boundary misorientation angle (grain boundary energy)-applied tensile stress couple (Figure 7.3). At higher misorientation angles (higher grain boundary energy), lower stress components can trigger liquid metal penetration. This confirmed that lower

grain boundary energies require higher external mechanical energy for the embrittlement. In other words, in grain boundaries with lower energies an external mechanical energy is required to overcome the SL energy barrier. However, in low-Σ ($\Sigma < 29$) and low-angle ($\theta < 15°$) random boundaries even the maximum external mechanical energy will not trigger LME (Figure 7.3).

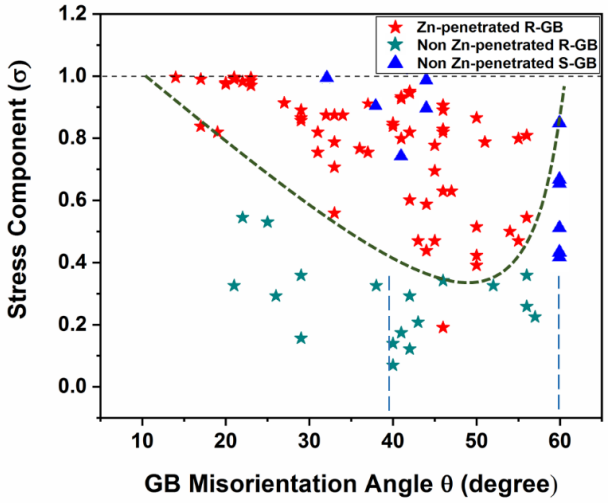

Figure 7.3: The correlation of the GB misorientation angle-stress component (σ=1: Normal to GB, σ=0: parallel with GB) based on the collected information from ~120 pair of grains showing: 1-The clear boundary between Zn-penetrated and non-Zn-penetrated random (R) GBs where LME takes place only at high-angle random-GBs ($\theta > 15°$), 2-By increasing misorientation angles of random-GBs lower stress components triggers Zn-penetration, and 3-The resistance of GBs at θ= 60° and some of boundaries at ~40° against Zn-penetration that are attributed to the Σ3 at θ= 60° and the Σ5-9 CSL (S-GB) occurring at ~ θ= 39° (copied from Figure 4.5).

The modeling study by Hugo et al. [84] first showed that in addition to the role of grain boundary energy, grain boundary excess volume (per unit area of grain boundary) affects LME susceptibility. In this framework, the packing density of atoms at the grain boundary plays a key role in liquid metal penetration rate, where LME sensitivity significantly increases when excess grain boundary volume is greater than 0.5 Å. The results

of the present study (presented in Chapter five) also provided experimental evidence that only high-index-plane random grain boundaries with higher levels of excess volume are LME-sensitive, whereas low-index-plane random grain boundaries and ordered (special) grain boundaries resist grain boundary diffusion of embrittler atoms, and hence, are LME-resistant (Figure 7.4).

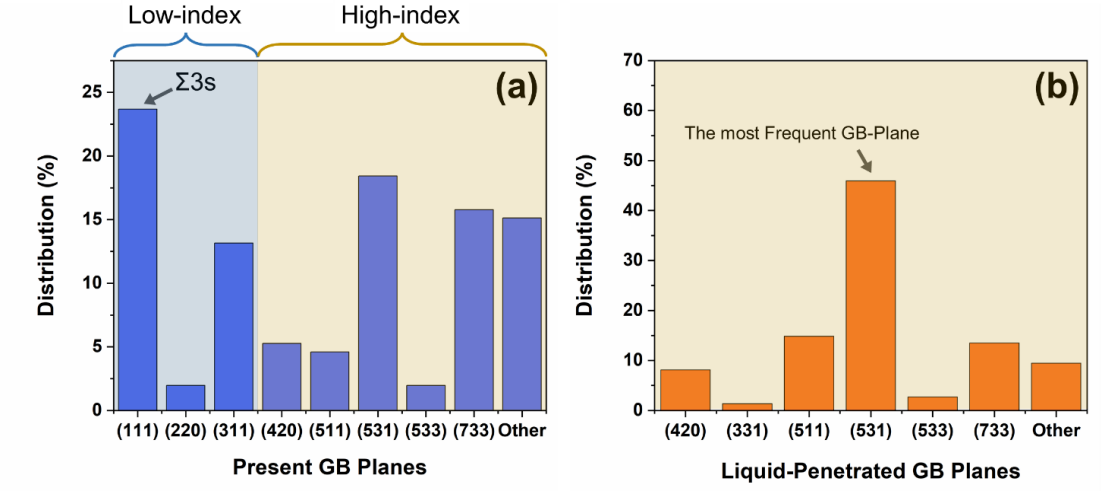

Figure 7.4: (a) The overall distribution of the present low- and high-index grain boundaries in the initial microstructure of the material, and (b) the distribution of the liquid-metal penetrated grain boundary planes showing that only high-index plane grain boundaries are susceptible to LME and the (531) is the most frequently penetrated grain boundary plane (copied from Figure 4.11).

7.3 Grain Boundary Decohesion Mechanism

Although Chapter three and four provided the necessary evidence of grain-boundary-based mechanism of LME and explained rapid propagation of LME-crack, the micro-mechanism leading to the grain boundary decohesion has not been understood. The micro-mechanism leading to grain boundary decohesion ahead of LME crack tip was discussed in Chapter five.

Apart from the earlier proposition [110] identifying the modification of interface energy as the LME grain boundary decohesion mechanism, currently two hypotheses of (a) the matrix and embrittler atomic size difference and the resultant strain at grain boundary [5]; or the most recently proposed (b) embrittler atom induced electronic state modification at grain boundary [111] provide more realistic grain boundary decohesion description. Schweinfest et al. [5] studied the atomic size difference influence on the Cu-Bi LME couple. The first principles quantum mechanical calculations showed the presence of over-sized Bi atoms (embrittler) increased the Cu-Cu bond length at grain boundaries and therefore weakened the atomic bonding. The slightly different Bi- and Pb-induced embrittlement behavior of Cu can be attributed to the atomic size difference hypothesis [5]. This study stands partly against the earlier investigation of tin (Sn) and lead (Pb)-induced embrittlement in steel [112]. Although both Pb and Sn atomic radii are larger than Fe, the size-difference between Pb and Fe is larger than Sn and Fe. Therefore, the higher LME susceptibility of the Fe-Sn couple was attributed to the more difficult accommodation of Pb-atoms in the available atomic sites at the Fe-grain boundary. However, the matrix-embrittler atomic size difference proposition has been challenged by the recent results of the grain boundary modeling study of the Fe-Zn [113] and Cu-Bi couples [116]. Peng et al. [113] have compared a clean grain boundary of the Fe matrix to an Zn-doped grain boundary. Although the original Fe-Fe bond length was expanded due to the Zn-doping (atomic radius of Zn is 0.09 Å larger than Fe). The grain boundary decohesion (strength loss of the primary Fe-Fe bond of grain boundary) is not only due to the bond length increase resulting from the Zn-doping, but mainly because of the charge distribution change [113]. Zn-doping results in a directionless charge density at clean grain boundary changes to a covalent bond with unequal and directional charge distribution. This shifts the weak bonds from the primary Fe bonds to the vicinity of the Zn-doped grain boundary, where the grain boundary failure

occurs. This finding agrees with Zhang et al. [34] who have shown that the Ga-doping has slightly altered the Al bond length, but significantly modified the electronic structure at the grain boundary. This stands against the proposed grain boundary expansion hypothesis [12]. Duscher et al. [116] also have shown that in the Cu grain boundaries, Bi-atoms occupy the middle site of the pentagonal Cu atomic arrangement, which did not impose any considerable Cu bond-length change. However, Bi affects the grain boundary cohesion through drawing charge from the neighbor metallic bonds. Although Ag-atoms (as embrittler) can occupy the same sites at Cu grain boundaries, they do not significantly affect the Cu charge distribution, which is in line with no severe embrittlement behavior in the Cu-Ag system [116].

The observations in Chapter 6 provided experimental evidence for the atomic micro-events leading to an intergranular LME cracking. Schematic illustration of the multi-stage atomic-level LME mechanism is shown along a random grain boundary with a representative tilt angle of 50° (Figure 7.5). As the Gordon-An model [14] described, due to the stress-assisted diffusion of the embrittler atoms, Zn-atoms dope the grain boundary ahead of the progressing LME-crack. Recent atomistic modeling of the Fe-Zn couple [113] showed the electronic structure modification as a results of Zn-atoms occupation of Fe grain boundary sites weakened the adjacent Fe-Fe atomic bonds, leading to the occurrence of fracture on one side of the Zn-doped grain boundary (Figure 7.5b- Stage II). This agrees with the observations in the present study which validates the proposed electronic structure modification of the grain boundary decohesion hypothesis [113]. It is most likely that the preference of the fracture on either side of the grain boundary is governed by orientation of the grains, which needs to be further studied. As the fracture takes place along the grain boundary, liquid-Zn flows into the fracture path that mass-transfer the fresh liquid embrittler to the advancing grain boundary diffusion (III). This partly explains

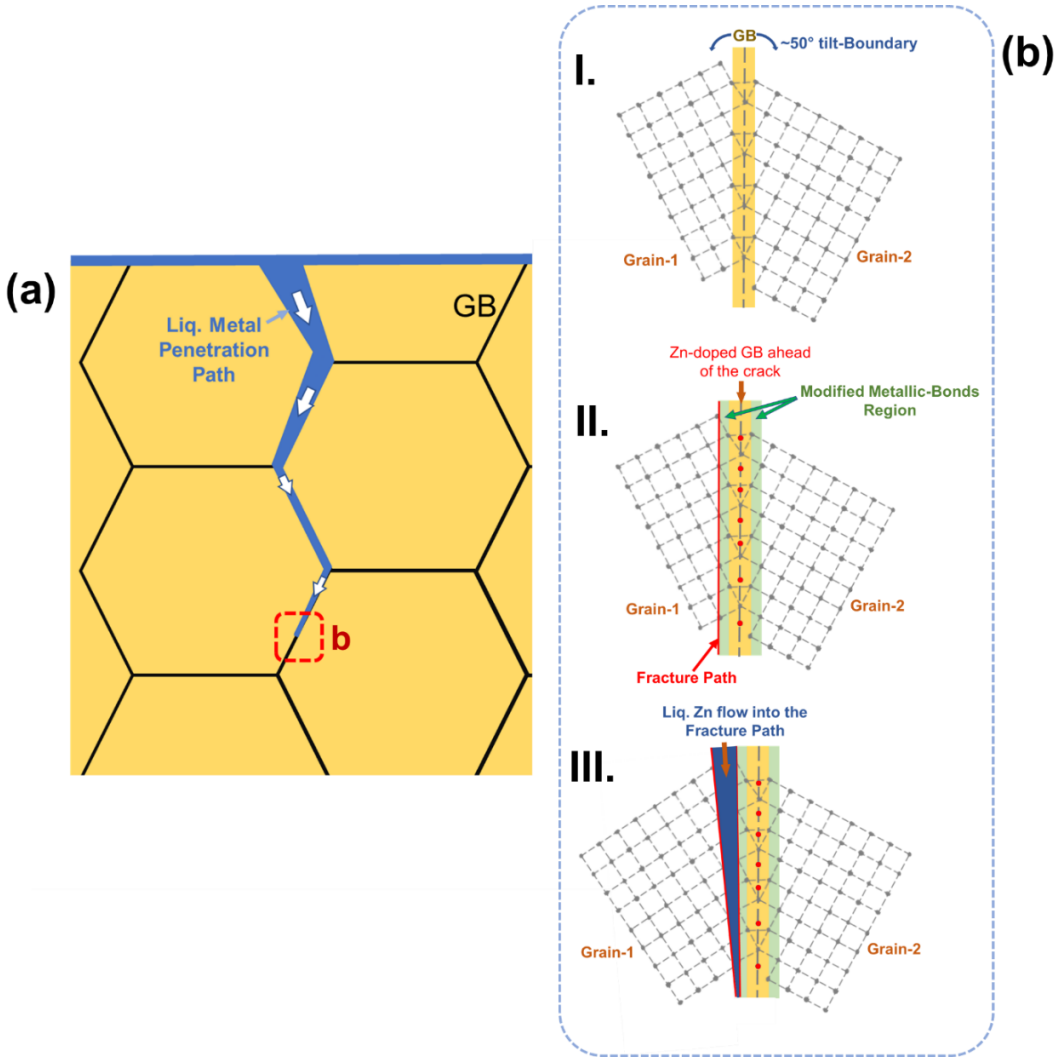

Figure 7.5: (a) Schematic illustration of micro-events leading to an intergranular LME Zn penetration-path, and (b) the multi-stage atomic-level LME mechanism along a random grain boundary with a tilt angle of 50° (I), leading to Zn-doped grain boundary ahead of the progressing LME-crack due to the stress-assisted diffusion of the embrittler atoms (Zn) occupies the sites at Fe grain boundary which results in weakening of the adjacent Fe-Fe atomic bonds and subsequent fracture path on one side of the Zn-doped grain boundary due to the applied tensile stress which agrees with the proposed electronic structure modification of Zn-doped grain boundary (II), and liquid Zn flow into the fracture path which mass-transfer fresh liquid embrittler to the further grain boundary (III).

the existing gap in the proposed stress-assisted diffusion model that requires a mass-transfer micro-mechanism to ensure the embrittler atoms transfer rate can adequately feed the rapid propagating crack-tip. This proposition can be a complementary description of the condensation micro-event of the proposed dissolution-condensation-mechanism (DCM) model (aka RGM) [40-44].

7.4 Grain Boundary Segregation Effect

The environmentally-assisted embrittlement phenomena such as Hydrogen embrittlement (HE) and LME can induce embrittlement independently, or interactively with other grain boundary-based embrittlement, and be more detrimental [215]. Grain boundary embrittlement can be due to (a) precipitation of secondary phase along grain boundaries, or (b) thermal cycles inducing impurity segregation without any phase precipitation. This means that the impurity-induced embrittlement act as preferential fracture-path in LME. The effects of the segregation on grain boundary cohesive strength and its LME-sensitivity are yet to be explored; however, it can be interpreted from 2 major standpoints: (1) considering the matrix and embrittler atomic size difference: the grain boundary segregation affects interfacial energy or atomic site configuration along grain boundary which facilitates the embrittler short-range diffusion ahead of LME crack-tip; (2) considering electronic structure modification proposition [113], where the presence of grain boundary segregation affect the charge distribution, and hence, the cohesive strength of the grain boundary. Schrader et al. [216] showed steel embrittlement as a result of Cr- and Mn-segregation at grain boundary. In contrast, other studies claimed that in the absence of impurities like N, P, S, Sb, As, Sn, or Si, segregation of major alloying elements such as Ni and Cr does not deleteriously impact material's strength [217]. This agrees with the study in which removal of

Ni or Cr from a steel, decreased the embrittlement induced by Sb, Sn, P, or As [218], which highlights the role of major alloying elements e.g. Cr and Ni in provoking co-segregation of the unfavorable impurities to grain boundaries. Based on the above, the interactive effects of alloying elements segregation on the grain boundary strength can be classified as follows: (a) the elements that co-segregate with impurities that known as segregation promoters, (b) segregation promoters without co-segregation effect, i.e. promoters do not segregate themselves, and (c) segregation prohibitors which make bonds with the impurities within the matrix, and hence, prohibit the deleterious grain boundary segregation [215]. Losch [114] has shown that the most of the strong embrittling elements like Sn, Sb, P, S, Si are in the 3-5 period of groups: IV,V, and VI [115], which shows the correlation between the electron configuration in outer shells and the grain boundary embrittling behavior.

LME phenomenon consists of a series of micro-events. As discussed in the previous section, first short-length diffusion of embrittler atoms ahead of the propagating crack-tip takes place. The size difference of the matrix and the segregated atoms at grain boundaries potentially provides more atomic sites for the embrittler diffusion ahead of the crack. Then, the presence of embrittler atoms weakens the grain boundaries (or the grain boundary adjacent region).The present research showed that grain boundary opening precedes liquid-Zn flow, which agrees with brittle bond-breaking LME models (the SJWK [166,167] and the Rehbinder and Shchukin [103]). The brittle fracture occurs in the impurity-decorated-grain-boundaries with drastically reduced fracture toughness (K_c) [32]. In fact, the presence of impurities at grain boundaries can significantly increase the required shear stress for activation of dislocations (i.e. solution hardening near the grain boundary), and as a result, promote brittle fracture [112]. In the investigated austenitic steel, the effects of Cr-segregation can be classified as follows. Firstly, co-segregation of impurity elements embrittles the grain boundary, and causes the grain boundary to be a

preferential path of a brittle fracture after initiation of LME-crack at material's surface. Secondly, the segregated atoms into the grain boundary provides preferential site for embrittler atom diffusion ahead LME crack due to modification of grain boundary packing factor and energy. Here, high-angle random grain boundaries which are aligned normal to the applied tensile stress direction are the most probable LME crack-path.

Chapter 8

Conclusions and Opportunities for Future Research

8.1 Conclusions

In conclusion, the present study focused on the details of liquid-metal-embrittlement (LME) in the Fe-Zn system. Based on the research described herein, the micro-mechanisms responsible for LME phenomenon, from liquid-metal penetration to crack propagation were definitively detailed. Also, the role of grain boundary characteristics and micro-chemistry in LME were clarified. The details of which are described in the conclusions below:

(1) The detailed study of elemental distribution near the LME crack-tip in the austenitic steel confirmed that, within the first micrometers of the crack-tip, liquid phase was not present, however, the LME-crack was filled by a Fe-Mn saturated Zn alloy (showing the presence of liquid-Zn along the propagating LME-crack). This finding confirmed that grain boundary diffusion of embrittler atoms ahead of LME crack, providing a plausible

explanation of LME-cracking sequence in the Fe-Zn couple. Moreover, it was found that LME susceptibility directly depends on the applied external load, where a threshold tensile stress is necessary to trigger LME. This shows that liquid metal penetration is a "stress-assisted" phenomenon which agreed with the microstructural observations. However, no dislocation activity was observed at the crack tip, showing that although LME is stress-assisted but it is not "dislocation-aided".

(2) Considering the stress-assisted grain boundary diffusion mechanism, hence, it was necessary to investigate the grain boundary characteristics effects on LME. It was found that LME crack-path is governed by grain boundary misorientation angle-applied tensile stress couple. At higher misorientation angles (higher grain boundary energy), lower stress components can trigger liquid metal penetration. Lower grain boundary energies require higher external mechanical energy for the embrittlement. However, grain boundary plane also plays a role in grain boundary LME-sensitivity, explaining the different tensile stress levels that results in LME in similar misorientaion angles. This shows that the packing density of atoms at the grain boundary correlates to the liquid metal penetration. It was confirmed that even at maximum applied stress component low energy CSL boundaries (Σ3 and some of Σ5-9) resist LME.

(3) Grain boundary segregation affects grain boundary characteristic in different ways: it decreases grain boundary interfacial energy, modifies the atomic arrangements at grain boundaries, and also affects the cohesive strength of grain boundaries. Hence, to fully understand LME it is vital to identify inter-relation between grain boundary geometrical characteristics and grain boundary chemistry. Atomic study of grain boundaries showed that the thermal cycles and the applied external tensile loading induce a severe enrichment at high-angle random grain boundaries. This facilitates short-range diffusion of the embrittler atoms ahead of a crack-tip due to modified configuration of grain boundary vacant

sites, and affects the cohesive strength of grain boundary. This shows why high-angle random boundaries are the most LME-sensitive sites. This method serves as starting point to understand the correlation between the material chemical composition and its LME susceptibility, and different LME susceptibility in different materials. Moreover, the present study validated the recently proposed embrittler-induced alteration of grain boundary electronic configuration model, and explained how the stress-assisted diffusion of the embrittler atoms ahead of progressing LME-crack leads to grain boundary decohesion.

(4) LME-resistance of special grain boundaries opened a new research area to use grain-boundary-engineering approach to suppress the phenomenon. In this research, grain boundary manipulation technique was examined which showed promising results to suppress LME. The optimized combination of cold deformation and subsequent annealing process promoted stable low-Σ special grain boundary about 3 times. It was revealed that a combination of low frequency of high-energy random grain boundaries, interrupted random grain boundary network within the microstructure, and special boundary-containing triple junctions led to a considerable reduction of the material's LME-susceptibility.

8.2 Recommendations and opportunities for future research

Although the present study provided insights into the role of grain boundary chemistry in LME, the influence of segregation on the grain boundary cohesive strength are yet to be explored. The future studies should quantify the effects of Cr, Mn, Mo, Si, and C segregation and corresponding co-segregation of the impurity elements at grain boundaries on LME sensitivity of various AHSS grades. This analysis will provide a universal map of

alloying element effects on LME susceptibility. HR-TEM (atomic-resolution EELS elemental mapping) and correlative APT analysis of the susceptible grain boundaries will provide a general understanding on beneficial and detrimental effects of the grain boundary segregation on LME. This can be used to recommend guidelines to steel alloying modifications to mitigate/suppress LME.

LME sensitivity as a function of grain boundary geometrical characteristics in stable austenitic structure is investigated in the present work. However, LME sensitivity as a function of grain boundary geometrical characteristics e.g. misorientation angle, grain boundary plane, grain orientation distribution should be investigated in various AHSS grades. As most AHSS grades (especially the recently developed 3rd-generation grades) have a minor fraction of stable austenite in room temperature, various methods to reveal prior austenite grain boundaries (PAGB) should be examined. Although the present research proposed a relatively new method to reveal PAGBs, the validity of this method in identification of misorientation angle, grain boundary plane, grain orientation distribution of prior austenite grains (in which LME-crack takes place) should be studied. This also can clarify the LME-sensitivity of special boundaries at elevated temperature.

As shown in the literature review, there is much debate over LME grain boundary decohesion mechanism. This study validated the recently proposed model of electronic state modification at grain boundary due to the presence of embrittler atoms as a viable grain boundary decohesion mechanism. In the future, it is recommended to validate this model in various LME couples such as Ni-Bi, Cu-Bi, Al-Ga. This provides a general understanding of LME in a wide span of engineering materials, and hence, alleviates the associated safety concerns of LME in various materials and processes. Moreover, the knowledge of the grain boundary decohesion mechanism can be extrapolated to other environmental-assisted failures e.g. hydrogen embrittlement and stress-corrosion-cracking.

Research Contributions

1. M.H. Razmpoosh, A. Macwan, E. Biro, N.Y. Zhou, Effect of Coating Weight on Fiber Laser Welding of Galvanneal-Coated Press Hardening Steel, Surface and Coatings Technology, 337C (2018) pp. 536-543 [126].

2. M.H. Razmpoosh, A. Macwan, E. Biro, D.L. Chen, F. Goodwin, Y. Zhou, Liquid Metal Embrittlement in Laser Beam Welding of Zn-Coated 22MnB5 Steel, Materials and Design, 155 (2018) pp. 375-383 [20].

3. M.H. Razmpoosh E. Biro, F. Goodwin, Y. Zhou, Dynamic Tensile Behavior of Fiber Laser Welds of Medium Manganese Transformation-Induced Plasticity Steel, Metallurgical and Materials Transactions A, 50 (2019) pp. 3578–3588 [219].

4. M.H. Razmpoosh, A. Macwan, E. Biro, D.L. Chen, F. Goodwin, Y. Zhou, Liquid metal embrittlement in laser lap joining of TWIP and medium-manganese TRIP steel: The role of stress and grain boundaries, Materials Characterization, 145 (2018) pp. 627-633 [19].

5. J.J. Guzman Aguilera, C.J. Martinez Gonzalez, V.H. Baltazar Hernandez, M.H. Razmpoosh, A. Gerlich, N.Y.Zhou, Influence of SC-HAZ microstructure on the mechanical behavior of Si-TRIP steel welds, Materials Science and Engineering :A 718 (2018) pp. 216-543 [220].

6. X. Han, M.H. Razmpoosh, A. Macwan, E. Biro, Y. Zhou, Effect of Galvannealed Coating Evolution during Press-Hardening on Resistance Spot Weldability of 22MnB5 Steel, Welding Journal (2019)-article in press [221].

7. M.H. Razmpoosh, A. Macwan, E. Biro, N.Y. Zhou, Microstructure and Dynamic Tensile Characteristic of Zn-coated 22MnB5 dissimilar Laser welds, Materials Science and Engineering :A 773 (2020) pp. 138729 [222].

8. M.H. Razmpoosh, A. Macwan, E. Biro, Y. Zhou, Effect of galvanneal-coating evolution during press-hardening on laser welding of 22MnB5 steel, Science and Technology of Welding and Joining, 25 (2020) pp. 112–118 [223].

9. M.H. Razmpoosh, A. Macwan, F. Goodwin, E. Biro, N.Y. Zhou, Crystallographic Study of Liquid-Metal-Embrittlement Crack Path Using the Five-Parameter Grain Boundary Characterization Approach, Materials Letters, 267 (2020) pp. 127511 [192].

10. A. Ghatei Kalashami, C. DiGiovanni, M.H. Razmpoosh, F. Goodwin, N.Y. Zhou, The role of internal oxides on the liquid metal embrittlement cracking during resistance spot welding of the dual phase steel, Metallurgical and Materials Transactions A, 51A (2020) pp. 2180–2191 [224].

11. M.H. Razmpoosh, A. Macwan, F. Goodwin, E. Biro, N.Y. Zhou, Role of random and coincidence site lattice grain boundaries in liquid metal embrittlement of Iron (FCC)-Zn couple-Metallurgical and Materials Transactions A, 51 (2020) pp. 3938–3944 [225].

12. M. S. Khan, M. H. Razmpoosh, E. Biro, Y. Zhou, A Review on Laser Welding of 22MnB5 Ultra High Strength Press-Hardened Steel, Science and Technology of Welding and Joining, 25 (2020) pp. 447–467 [226].

13. M.H. Razmpoosh, A. Macwan, F. Goodwin, E. Biro, N.Y. Zhou, Suppression of Liquid Metal Embrittlement by Twin-based Grain Boundary Engineering Approach, Materialia, 11 (2020) pp. 100668 [227].

14. M.H. Razmpoosh, A. Macwan, E. Biro, N.Y. Zhou, Fiber Laser Beam Defocusing: A Novel Method to Improve High Strain Rate Tensile Behavior of Zn-coated Press-Hardened 22MnB5 Welds-To be Submitted Manuscript.

15. M.H. Razmpoosh, B. Lanelier, H.S. Zurob, E. Biro, N.Y. Zhou, Revealing Liquid-Metal-Embrittlement Mechanism by Atomic-scale (Atom Prob Tomography) Investigation

of Crack-path- Under Review Manuscript.

16. M.H. Razmpoosh, C. DiGiovanni, F. Goodwin, E. Biro, N.Y. Zhou, Review paper: Pathway to understand Liquid-Metal-Embrittlement: From fundamentals toward applications-Under Review Manuscript.

17. L. H. Shah, W. Hou, M. H. Razmpoosh, S. Walbridge and A. P. Gerlich. Strain rate and microtexture in AA6061 aluminum alloy friction stir welds produced with aligned versus eccentric tools and subjected to rapid quenching, Under Review-Manuscript.

18. A. Ghatei Kalashami, C. DiGiovanni, M.H. Razmpoosh, F. Goodwin, N.Y. Zhou, The effect of silicon content on liquid metal embrittlement cracking in resistance spot welded galvanized dual-phase steel, Journal of Manufacturing Processes, 57 (2020) pp. 370-379.

Chapter 9

References

[1] W.H. Johnson, II. On some remarkable changes produced in iron and steel by the action of hydrogen and acids, Proc. R. Soc. London. 23 (1875) 168–179.

[2] M. Naderi, M. Peterlechner, E. Schafler, S. V Divinski, G. Wilde, Kinetic , volumetric and structural effects induced by liquid Ga penetration into ultrafine grained Al, Acta Mater. 99 (2015) 196–205. https://doi.org/10.1016/j.actamat.2015.07.061.

[3] H. Nam, D.J. Srolovitz, Effect of material properties on liquid metal embrittlement in the Al-Ga system, Acta Mater. 57 (2009) 1546–1553.

[4] A. Kundu, K.M. Asl, J. Luo, M.P. Harmer, Identification of a bilayer grain boundary complexion in Bi-doped Cu, Scr. Mater. 68 (2013) 146–149.

[5] R. Schweinfest, A.T. Paxton, M.W. Finnis, Bismuth embrittlement of copper is an atomic size effect, Nature. 432 (2004) 1008–1011.

[6] M. Rajagopalan, M.A. Bhatia, M.A. Tschopp, D.J. Srolovitz, K.N. Solanki, Atomic-scale analysis of liquid-gallium embrittlement of aluminum grain boundaries, Acta Mater. 73 (2014) 312–325.

[7] E. Perreiro-Lopez, W. Ludwig, D. Bellet, Discontinuous penetration of liquid Ga into grain boundaries of Al polycrystals pez, Acta Mater. 52 (2004) 321–332.

[8] E. Senel, J.C. Walmsley, S. Diplas, K. Nisancioglu, Liquid metal embrittlement of aluminium by segregation of trace element gallium, Corros. Sci. 85 (2014) 167–173. https://doi.org/10.1016/j.corsci.2014.04.012.

[9] J.P. Monchoux, E. Rabkin, Microstucture evolution and interfacial properties in the Fe-Pb system, Acta Mater. 50 (2002) 3161–3176.

[10] N. Marie, K. Wolski, M. Biscondi, Intergranular penetration and embrittlement of solid nickel through bismuth vapour condensation at 700 C, J. Nucl. Mater. 296 (2001) 282–288. [11] N. Marie, K. Wolski, M. Biscondi, Grain boundary penetration of nickel by liquid bismuth as a film of nanometric thickness, Scr. Mater. 10 (2000) 943–949.

[12] C.W. Lee, W.S. Choi, L. Cho, Y.R. Cho, B.C. De Cooman, Liquid-metal-induced embrittlement related microcrack propagation on Zn-coated press hardening steel, ISIJ Int. 55 (2015) 264–271. https://doi.org/10.2355/isijinternational.55.264.

[13] L. Cho, H. Kang, C. Lee, B.C. De Cooman, Microstructure of liquid metal embrittlement cracks on Zn-coated 22MnB5 press-hardened steel, Scr. Mater. 90 (2014) 25–28.

[14] C. Beal, X. Kleber, D. Fabregue, M. Bouzekri, Liquid zinc embrittlement of a high-manganese-content TWIP steel, Philos. Mag. Lett. 91 (2011) 297–303.

[15] C. Beal, X. Kleber, D. Fabregue, M. Bouzekri, Liquid zinc embrittlement of twinning-induced plasticity steel, Scr. Mater. 66 (2012) 1030–1033.

[16] R. Ashiri, M. Shamanian, H.R. Salimijazi, M.A. Haque, J.H. Bae, C.W. Ji, K.G. Chin, Y. Do Park, Liquid metal embrittlement-free welds of Zn-coated twinning induced plasticity steels, Scr. Mater. 114 (2016) 41–47.

[17] R. Ashiri, M.A. Haque, C.W. Ji, M. Shamanian, H.R. Salimijazi, Y. Do Park, Supercritical area and critical nugget diameter for liquid metal embrittlement of Zn-coated twinning induced plasticity steels, Scr. Mater. 109 (2015) 6–10.

[18] H. Kang, L. Cho, C. Lee, B.C. De Cooman, Zn Penetration in Liquid Metal Embrittled TWIP Steel, Metall. Mater. Trans. A. 47 (2016) 2885–2905.

[19] M.H. Razmpoosh, E. Biro, D.L. Chen, F. Goodwin, Y. Zhou, Liquid metal embrittlement in laser lap joining of TWIP and medium- manganese TRIP steel: The role of stress and grain boundaries, Mater. Charact. 145 (2018) 627–633.

[20] M.H. Razmpoosh, A. Macwan, E. Biro, D.L. Chen, Y. Peng, F. Goodwin, Y. Zhou, Liquid metal embrittlement in laser beam welding of Zn-coated 22MnB5 steel, Mater. Des. 155 (2018) 375–383.

[21] J. Barthelmie, A. Schram, V. Wesling, Liquid Metal Embrittlement in Resistance Spot Welding and Hot Tensile Tests of Surface-refined TWIP Steels, IOP Conf. Ser. Mater. Sci. Eng. 118 (2016). https://doi.org/10.1088/1757-899X/118/1/012002.

[22] N. Ding, N. Xu, W. Guo, J. Shi, Q. Zang, C.M.L. Wu, Liquid metal induced embrittlement of a nitrided clutch shell of a motorbike, Eng. Fail. Anal. 61 (2016) 54–61. https://doi.org/10.1016/j.engfailanal.2015.08.008.

[23] J. Frei, M. Rethmeier, Susceptibility of electrolytically galvanized dual-phase steel sheets to liquid metal embrittlement during resistance spot welding, Weld. World. 62 (2018) 1031–1037. https://doi.org/10.1007/s40194-018-0619-1.

[24] G. Jung, I.S. Woo, D.W. Suh, S.J. Kim, Liquid Zn assisted embrittlement of advanced high strength steels with different microstructures, Met. Mater. Int. 22 (2016) 187–195. https://doi.org/10.1007/s12540-016-5579-7.

[25] D. Kim, J.H. Kang, S.J. Kim, Heating rate effect on liquid Zn-assisted embrittlement of high Mn austenitic steel, Surf. Coatings Technol. 347 (2018) 157–163.

[26] J. Mendala, The possibility of the LME phenomenon in elements subjected to metallization in Zn bath with Bi addition, Solid State Phenom. 226 (2015) 167–172.

[27] M. Takahashi, M. Nakata, K. Imai, N. Kojima, N. Otsuka, Liquid metal embrittlement of hot stamped galvannealed boron steel sheet - Effect of heating time on crack formation, ISIJ Int. 57 (2017) 1094–1101. https://doi.org/10.2355/isijinternational.ISIJINT-2016-730.

[28] N. Birbilis, R. Zhang, MLC Lim, RK Gupta. CHJ Davies. SP Lynch, RG Kelly, JR Scully, Corrosion. 69 (2013) 396.

[29] Y. Brechet, M. Veron, S. Peron, A. Deschamps, A. Rodine, Examples of liquid metal embrittlement in industrial aluminium alloys; Exemples de fragilisation par les metaux liquides dans des alliages d'aluminium, (2002).

[30] E. Ferchaud, F. Christien, P. Paillard, V. Barnier, K. Wolski, H. Mourton, P. Azais, C. Rossignol, Gallium distribution in gallium-coated aluminum for brazing application, in: Defect Diffus. Forum, Trans Tech Publ, 2011: pp. 255–260.

[31] E.E. Glickman, Fast penetration of Ga in Al: liquid metal embrittlement near the threshold of grain boundary wetting, Zeitschrift Für Met. 96 (2005) 1204–1210.

[32] E.E. Glickman, Grain Boundary Grooving Accelerated by Local Plasticity as a Possible Mechanism of Liquid Metal Embrittlement, Interface Sci. 11 (2003) 451–459.

[33] Y. Zhang, G.H. Lu, M. Kohyama, T. Wang, Investigating the effects of a Ga layer on an Al grain boundary by a first-principles computational tensile test, Model. Simul. Mater. Sci. Eng. 17 (2009). https://doi.org/10.1088/0965-0393/17/1/015003.

[34] Y. Zhang, G.H. Lu, T. Wang, S. Deng, X. Shu, M. Kohyama, R. Yamamoto, First-principles study of the effects of segregated Ga on an Al grain boundary, J. Phys. Condens. Matter. 18 (2006) 5121–5128. https://doi.org/10.1088/0953-8984/18/22/011.

[35] X. Gu, T. Furuhara, Adv eV iew Pro ofs Adv anc iew Pro ofs, (2015) 1–6.

[36] J.Y. Uan, C.C. Chang, Characterization of gallium-induced intergranular fracture surface and the auger electron spectroscopic analysis for Mg grain boundary segregation in AA6061 T4 Al-Mg-Si alloy, Mater. Trans. 45 (2004) 1925–1932.

[37] J.Y. Uan, C.C. Chang, Gallium-induced magnesium enrichment on grain boundary and the gallium effect on degradation of tensile properties of aluminum alloys, Metall. Mater. Trans. A Phys. Metall. Mater. Sci. 37 (2006) 2133–2145.

[38] S. Schmidt, W. Sigle, W. Gust, M. Rühle, Gallium segregation at grain boundaries in aluminium, Zeitschrift Für Met. 93 (2002) 428–431.

[39] E. Pereiro-López, W. Ludwig, D. Bellet, P. Cloetens, C. Lemaignan, Direct evidence of nanometric invasionlike grain boundary penetration in the Al/Ga system, Phys. Rev. Lett. 95 (2005) 1–4. https://doi.org/10.1103/PhysRevLett.95.215501.

[40] H.S. Nam, D.J. Srolovitz, Molecular dynamics simulation of Ga penetration along 5 symmetric tilt grain boundaries in an Al bicrystal, Phys. Rev. B - Condens. Matter Mater. Phys. 76 (2007) 1–14. https://doi.org/10.1103/PhysRevB.76.184114.

[41] V. V. Maksimenko, V.A. Zagaynov, I.E. Agranovski, Localization of electromagnetic field on the “brouwer-island” and liquid metal embrittlement, Mater. Chem. Phys. 153 (2015) 145–154. https://doi.org/10.1016/j.matchemphys.2014.12.046.

[42] S.P. Lynch, Metal-induced embrittlement of materials, Mater. Charact. 28 (1992) 279–289.

[43] K. Ina, H. Koizumi, Penetration of liquid metals into solid metals and liquid metal embrittlement, Mater. Sci. Eng. A. 387–389 (2004) 390–394.

[44] M. Kobayashi, H. Toda, K. Uesugi, T. Ohgaki, T. Kobayashi, Y. Takayama, B.G. Ahn, Preferential penetration path of gallium into grain boundary in practical aluminium alloy, Philos. Mag. 86 (2006) 4351–4366. https://doi.org/10.1080/14786430600710933.

[45] J. Hagström, O. V. Mishin, B. Hutchinson, Gallium enhanced microscopy for revealing grain boundaries and dislocation subboundaries in aluminium alloys, Scr. Mater. 49 (2003) 1035–1040.

[46] J. Song, Z. Wang, Y. Huang, A. Srinivasan, F. Beckmann, K.U. Kainer, N. Hort, Hot tearing characteristics of Mg–2Ca–xZn alloys, J. Mater. Sci. 51 (2016) 2687–2704. https://doi.org/10.1007/s10853-015-9583-y.

[47] J. Lerner, C.J. McMahon, The effect of precipitation hardening on the Hg-induced embrittlement of a Cu-Be alloy, Mater. Sci. Eng. A. 336 (2002) 72–74.

[48] O. Wouters, J.T.M. De Hosson, Lead induced intergranular fracture in aluminum alloy AA6262, Mater. Sci. Eng. A. 361 (2003) 331–337. https://doi.org/10.1016/S0921-5093(03)00521-5.

[49] J. Van den Bosch, A. Almazouzi, Compatibility of martensitic/austenitic steel welds with liquid lead bismuth eutectic environment, J. Nucl. Mater. 385 (2009) 504–509. https://doi.org/10.1016/j.jnucmat.2008.12.043.

[50] E. Stergar, S.G. Eremin, S. Gavrilov, M. Lambrecht, O. Makarov, V. Iakovlev, Influence of LBE long term exposure and simultaneous fast neutron irradiation on the mechanical properties of T91 and 316L, J. Nucl. Mater. 473 (2016) 28–34.

[51] B. Long, Z. Tong, F. Gröschel, Y. Dai, Liquid Pb-Bi embrittlement effects on the T91 steel after different heat treatments, J. Nucl. Mater. 377 (2008) 219–224.

[52] A. Hojná, F. Di Gabriele, J. Klecka, J. Burda, Behaviour of the steel T91 under uniaxial and multiaxial slow loading in contact with liquid lead, J. Nucl. Mater. 466 (2015) 292–301.

[53] A. Hojna, F. Di Gabriele, J. Klecka, Characteristics and Liquid Metal Embrittlement of the steel T91 in contact with Lead–Bismuth Eutectic, J. Nucl. Mater. 472 (2016) 163–170.

[54] A. Hojna, F. Di Gabriele, On the kinetics of LME for the ferritic–martensitic steel T91 immersed in liquid PbBi eutectic, J. Nucl. Mater. 413 (2011) 21–29.

[55] Z. Hamouche-Hadjem, T. Auger, I. Guillot, D. Gorse, Susceptibility to LME of 316L and T91 steels by LBE: Effect of strain rate, J. Nucl. Mater. 376 (2008) 317–321.

[56] Z. Hadjem-Hamouche, T. Auger, I. Guillot, Temperature effect in the maximum propagation rate of a liquid metal filled crack: The T91 martensitic steel/Lead–Bismuth Eutectic system, Corros. Sci. 51 (2009) 2580–2587.

[57] G. Ilinčev, D. Kárník, M. Paulovič, A. Doubková, The effect of temperature and oxygen content on the flowing liquid metal corrosion of structural steels in the Pb–Bi eutectic, Nucl. Eng. Des. 236 (2006) 1909–1921.

[58] B.W. Baker, L.N. Brewer, Evaluation of liquid metal embrittlement susceptibility of oxide dispersion strengthened steel MA956, J. Nucl. Mater. 453 (2014) 239–246.

[59] F. Gamaoun, M. Dupeux, V. Ghetta, D. Gorse, Cavity formation and accelerated plastic strain in T91 steel in contact with liquid lead, Scr. Mater. 50 (2004) 619–623.

[60] H. Glasbrenner, J. Konys, H.D. Röhrig, K. Stein-Fechner, Z. Voss, Corrosion of ferritic–martensitic steels in the eutectic Pb–17Li, J. Nucl. Mater. 283 (2000) 1332–1335.

[61] J. Klecka, F. Di Gabriele, A. Hojna, Mechanical properties of the steel T91 in contact with lead, Nucl. Eng. Des. 283 (2015) 131–138.

[62] Y.F. Li, M. Kondo, T. Nagasaka, T. Muroga, V. Tsisar, Influence of Exposure to Pb-Li on Microstructure and Mechanical Properties of 9Cr-ODS and CLAM Steels, Fusion Sci. Technol. 60 (2011) 359–363.

[63] J.-B. Vogt, G. Nicaise, A. Legris, F. Foct, The risk of liquid metal embrittlement of the Z10CDNbV 9-1 martensitic steel, in: J. Phys. IV, EDP sciences, 2002: pp. 217–225.

[64] O.. Yas'kiv, V.M. Fedirko, Influence of lead and Pb Bi eutectic melts on the mechanical properties of 20Kh13 ferritic–martensitic steel, Mater. Sci. 48 (2012) 308–315.

[65] O.I. Yaskiv, V.M. Fedirko, Mechanical and fatigue properties of martensitic fe-13cr and austenitic fe-18cr-10ni steels in contact with lead and lead-bismuth melts, probl. At. Sci. Technol. (2013) 109–118.

[66] O.I. Yaskiv, V.M. Fedirko, Mechanical and fatigue properties of martensitic Fe-13Cr steel in contact with lead and lead-bismuth melts, Fusion Eng. Des. 89 (2014) 29–34.

[67] O.I. Yas'kiv, V.M. Fedirko, I.S. Kukhar, Effect of Lead and Lead–Bismuth Eutectic Melts on the Fatigue Life of Steels of the Martensitic and Austenitic Classes, Mater. Sci. 50 (2014) 102–108.

[68] T. Auger, Z. Hamouche, L. Medina-Almazan, D. Gorse, Liquid metal embrittlement of T91 and 316L steels by heavy liquid metals: A fracture mechanics assessment, J. Nucl. Mater. 377 (2008) 253–260.

[69] T. Auger, I. Serre, G. Lorang, Z. Hamouche, D. Gorse, J.-B. Vogt, Role of oxidation on LME of T91 steel studied by small punch test, J. Nucl. Mater. 376 (2008) 336–340.

[70] T. Auger, G. Lorang, Liquid metal embrittlement susceptibility of T91 steel by lead–bismuth, Scr. Mater. 52 (2005) 1323–1328.

[71] M.L. Martin, T. Auger, D.D. Johnson, I.M. Robertson, Liquid–metal-induced fracture mode of martensitic T91 steels, J. Nucl. Mater. 426 (2012) 71–77.

[72] F. Balbaud-Célérier, P. Deloffre, A. Terlain, A. Rusanov, Corrosion of metallic materials in flowing liquid lead-bismuth, in: J. Phys. IV, EDP sciences, 2002: pp. 177–190.

[73] F. Ersoy, S. Gavrilov, K. Verbeken, Investigating liquid-metal embrittlement of T91 steel by fracture toughness tests, J. Nucl. Mater. 472 (2016) 171–177.

[74] X. Gong, P. Marmy, L. Qin, B. Verlinden, M. Wevers, M. Seefeldt, Effect of liquid metal embrittlement on low cycle fatigue properties and fatigue crack propagation behavior of a modified 9Cr–1Mo ferritic–martensitic steel in an oxygen-controlled lead–bismuth eutectic environment at 350 C, Mater. Sci. Eng. A. 618 (2014) 406–415.

[75] X. Gong, P. Marmy, L. Qin, B. Verlinden, M. Wevers, M. Seefeldt, Temperature dependence of liquid metal embrittlement susceptibility of a modified 9Cr–1Mo steel under low cycle fatigue in lead–bismuth eutectic at 160–450 C, J. Nucl. Mater. 468 (2016) 289–298.

[76] X. Gong, P. Marmy, B. Verlinden, M. Wevers, M. Seefeldt, Low cycle fatigue behavior of a modified 9Cr–1Mo ferritic–martensitic steel in lead–bismuth eutectic at 350 C–effects of oxygen concentration in the liquid metal and strain rate, Corros. Sci. 94 (2015) 377–391.

[77] X. Gong, P. Marmy, A. Volodin, B. Amin-Ahmadi, L. Qin, D. Schryvers, S. Gavrilov, E. Stergar, B. Verlinden, M. Wevers, Multiscale investigation of quasi-brittle fracture characteristics in a 9Cr–1Mo ferritic–martensitic steel embrittled by liquid lead–bismuth under low cycle fatigue, Corros. Sci. 102 (2016) 137–152.

[78] D. Gorse, T. Auger, J.-B. Vogt, I. Serre, A. Weisenburger, A. Gessi, P. Agostini, C. Fazio, A. Hojna, F. Di Gabriele, Influence of liquid lead and lead–bismuth eutectic on tensile, fatigue and creep properties of ferritic/martensitic and austenitic steels for transmutation systems, J. Nucl. Mater. 415 (2011) 284–292.

[79] J. Luo, H. Cheng, K.M. Asl, C.J. Kiely, M.P. Harmer, The Role of a Bilayer In-

terfacial Phase on Liquid Metal Embrittlement, Science (80-.). 333 (2011) 1730–1733. https://doi.org/10.1126/science.1208774.

[80] D.G. Kolman, R. Chavarria, Liquid-metal embrittlement of 7075 aluminum and 4340 steel compact tension specimens by gallium, J. Test. Eval. 30 (2002) 452–456.

[81] A. Luithle, M. Pohl, On the influence of cold deformation on liquid metal embrittlement of a steel in a liquid zinc bath, Mater. Corros. 66 (2015) 1491–1497.

[82] D.G. Kolman, A review of recent advances in the understanding of liquid metal embrittlement, Corrosion. 75 (2019) 42–57. https://doi.org/10.5006/2904.

[83] E. Perreiro-Lopez, W. Ludwig, D. Bellet, C. Lemaignan, In situ investigation of Al bicrystal embrittlement by liquid Ga using synchrotron imaging, Acta Mater. 54 (2006) 4307–4316.

[84] R.C. Hugo, R.G. Hoagland, The Kinetics of Gallium Penetration into Aluminum Grain Boundaries-In Situ TEM Observations and atomistic models, Acta Mater. 48 (2000) 1949–1957.

[85] W. Ludwig, D. Bellet, In situ investigation of liquid Ga penetration in Al bicrystal grain boundaries: grain boundary wetting or liquid metal embrittlement?, Acta Mater. 53 (2005) 151–162.

[86] Y. Kikuta, T. Araki, M. Yoneda, K. Uchikawa, Effect of some factors on time-dependence fracture in molten zinc-liquid-metal embrittlement cracking of steel in hot dip galvanizing, in: trans. Iron steel inst. Japan, iron steel inst japan keidanren kaikan 9-4 otemachi 1-chome chiyoda-ku, 1985: pp. B309–b309.

[87] G.W. Austin, The effect of molten solder on some stressed materials, J. Inst. Met. 58 (1936) 173.

[88] R. Genders, The penetration of mild steel by brazing solder and other metals, Institute of Metals, 1927.

[89] Y. Benlatreche, H. Ghassemi-Armaki, M. Duchet, T. Dupuy, G. Cornette, P. Dietsch, Spot-Weld Integrity of Zn-coated 3rd Gen. Advanced High Strength Steel in Presence of LME, in: Int. Automot. Body Congr. (IABC 2017 Dearborn), 2017: pp. 9–18.

[90] Y.G. Kim, I.J. Kim, J.S. Kim, Y. Il Chung, D.Y. Choi, Evaluation of Surface Crack in Resistance Spot Welds of Zn-Coated Steel, Mater. Trans. 55 (2014) 171–175.

[91] R.E. Hargrave, Unusual failures involving copper deposition in boiler tubing, Corrosion. 47 (1991) 555–567.

[92] M.H. Kamdar, M.G. Nicolas, Liquid-metal embrittlement, ASM Handbook. 11 (1986) 225–238.

[93] W.M. Robertson, Embrittlement of titanium by liquid cadmium, Metall. Trans. 1 (1970) 2607–2613.

[94] B. Joseph, M. Picat, F. Barbier, Liquid metal embrittlement: A state-of-the-art appraisal, Eur. Phys. J. Appl. Phys. 5 (1999) 19–31. https://doi.org/10.1051/epjap:1999108.

[95] P.J.L. Fernandes, R.E. Clegg, D.R.H. Jones, Failure by liquid metal induced embrittlement, Eng. Fail. Anal. 1 (1994) 51–63. https://doi.org/10.1016/1350-6307(94)90029-9.

[96] P. Gordon, H.H. An, The mechanisms of crack initiation and crack propagation in metal-induced embrittlement of metals, Metall. Trans. A. 13 (1982) 457–472.

[97] S.P. Lynch, Environmentally assisted cracking: Overview of evidence for an adsorption-induced localised-slip process, Acta Metall. 36 (1988) 2639–2661.

[98] W. Rostoker, J.M. McCaughey, H. Markus, Embrittlement by Liquid Metals, Reinhold Publ, Corp., New York. (1960).

[99] V. V Popovich, Mechanisms of liquid-metal embrittlement, Fiz. Mekhanika Mater. 15 (1979) 11–20.

[100] P.C. Hancock, M.B. Ives, The role of plastic deformation liquid metal embrittlement, Can. Metall. Q. 10 (1971) 207–211. https://doi.org/10.1179/cmq.1971.10.3.207.

[101] N.S. Stoloff, T.L. Johnston, Crack propagation in a liquid metal environment, Acta Metall. 11 (1963) 251–256.

[102] A.R.C. Westwood, M.H. Kamdar, Concerning liquid metal embrittlement, particularly of zinc monocrystals by mercury, Philos. Mag. 8 (1963) 787–804.

[103] P.A. Rehbinder, E.D. Shchukin, Surface phenomena in solids during deformation and fracture processes, Prog. Surf. Sci. 3 (1972). https://doi.org/10.1016/0079-6816(72)90011-1.

[104] W.M. Robertson, Propagation of a crack filled with liquid metal, Trans. AIME. 236 (1966) 1478–1482.

[105] E.E. Glickman, Dissolution Condensation Mechanism of Stress Corrosion Cracking in Liquid Metals: Driving Force and Crack Kinetics, Metall. Mater. Trans. A. 42A (2011) 250–266.

[106] M.A. Krishtal, The Formation of Dislocations in Metals on Diffusion of Surface-Active Substances in Connection with the Effect of Adsorption Embrittlement, in: Sov. Phys. Dokl., 1970: p. 614.

[107] L. Klinger, E. Rabkin, The effect of stress on grain boundary interdiffusion in a semi-infinite bicrystal, Acta Mater. 55 (2007) 4689–4698.

[108] T. Auger, J.-B. Vogt, I.P. Serre, Liquid Metal Embrittlement, in: Mech. Coupling, Elsevier, 2019: pp. 507–534.

[109] J. Luo, A short review of high-temperature wetting and complexion transitions with a critical assessment of their influence on liquid metal embrittlement and corrosion, Corrosion. 72 (2016) 897–910.

[110] J.R. Rice, J.S. Wang, Embrittlement of interfaces by solute segregation, Mater. Sci. Eng. A. 107 (1989) 23–40. https://doi.org/10.1016/0921-5093(89)90372-9.

[111] H.K. Masatake Yamaguchi, Motoyuki Shiga, Grain Boundary Decohesion by Impurity Segregation in a Nickel-Sulfur System, Science (80-.). 307 (2005) 393–398.

[112] S. Dinda, The Effect of Grain Boundary Segregation on Liquid Metal Induced Embrittlement of Steel, Mater. Sci. Eng. 24 (1976) 199–208.

[113] W. Peng, H. Peng, G. Wu, J. Zhang, Effect of zinc-doping on tensile strength of 5 bcc Fe symmetric tilt grain boundary, Comput. Mater. Sci. 171 (2020) 109204. https://doi.org/10.1016/j.commatsci.2019.109204.

[114] W. Losch, A new model of grain boundary failure in temper embrittled steel, Acta Metall. 27 (1979) 1885–1892. https://doi.org/10.1016/0001-6160(79)90079-8.

[115] C.J. McMahon Jr, L. Marchut, Solute segregation in iron-based alloys, J. Vac. Sci. Technol. 15 (1978) 450–466.

[116] G. Duscher, M.F. Chisholm, U. Alber, M. Rühle, Bismuth-induced embrittlement of copper grain boundaries, Nat. Mater. 3 (2004) 621–626.

[117] K. Yoshino, C.J. McMahon, The cooperative relation between temper embrittlement and hydrogen embrittlement in a high strength steel, Metall. Trans. 5 (1974) 363–370.

[118] U.Q. Cabral, A. Hache, A. Constant, Determination of annealing brittleness by corrosion tests under tension in the presence of hydrogen, CR Acad. Sci. Paris, Fr. 260 (1965) 6887–6890.

[119] K.M. Asl, J. Luo, Impurity effects on the intergranular liquid bismuth penetration in polycrystalline nickel, Acta Mater. 60 (2012) 149–165.

[120] J. Zhou, B. Wang, M. Huang, Two constitutive descriptions of boron steel 22MnB5 at high temperature, J. Mater. 63 (2014) 738–748. https://doi.org/10.1016/j.matdes.2014.07.008.

[121] M. Nikravesh, M. Naderi, G.H. Akbari, W. Bleck, Phase transformations in a simulated hot stamping process of the boron bearing steel, Mater. Des. 84 (2015) 18–24.

[122] J. Kaars, P. Mayr, K. Koppe, Generalized dynamic transition resistance in spot welding of aluminized 22MnB5, Mater. Des. 106 (2016) 139–145.

[123] Z. xiang Gui, W. kang Liang, Y. Liu, Y. sheng Zhang, Thermo-mechanical behavior of the Al-Si alloy coated hot stamping boron steel, Mater. Des. 60 (2014) 26–33.

[124] M. Abbasi, M. Naderi, A. Saeed-Akbari, Isothermal versus non-isothermal hot compression process: A comparative study on phase transformations and structure-property relationships, Mater. Des. 45 (2013) 1–5.

[125] H. Karbasian, A.E. Tekkaya, A review on hot stamping, J. Mater. Process. Technol. 210 (2010) 2103–2118.

[126] M.H. Razmpoosh, A. Macwan, E. Biro, Y. Zhou, Effect of coating weight on fiber laser welding of Galvanneal-coated 22MnB5 press hardening steel, Surf. Coat. Technol. 337 (2018) 536–543.

[127] X. Wang, X. Chen, Q. Sun, H. Di, L. Sun, Formation mechanism of detla-ferrite and metallurgy reaction in molten pool during press-hardened steel laser welding, Mater. Lett. 206 (2017) 143–145.

[128] C.W. Lee, W.S. Choi, L. Cho, Y.R. Cho, B.C. De Cooman, Liquid-Metal-Induced Embrittlement Related Microcrack Propagation on Zn-coated Press Hardening Steel, ISIJ Int. 55 (2015) 264–271.

[129] P. Lan, J. Zhang, Tensile property and microstructure of Fe-22Mn-0 . 5C TWIP steel, Mater. Sci. Eng. A. 707 (2017) 373–382.

[130] H. Liu, J. Liu, B. Wu, Y. Shen, Y. He, H. Ding, X. Su, Effect of Mn and Al contents on hot ductility of high alloy Fe-xMn-C-yAl austenite TWIP steels, Mater. Sci. Eng. A. 708 (2017) 360–374.

[131] R. Ueji, N. Tsuchida, D. Terada, N. Tsuji, Y. Tanaka, A. Takemura, K. Kunishige, Tensile properties and twinning behavior of high manganese austenitic steel with fine-grained structure, Scr. Mater. 59 (2008) 963–966.

[132] J.E. Jin, Y.K. Lee, Effects of Al on microstructure and tensile properties of C-bearing high Mn TWIP steel, Acta Mater. 60 (2012) 1680–1688.

[133] M.H. Razmpoosh, A. Zarei-hanzaki, N. Haghdadi, J. Cho, W. Jae, S. Heshmati-manesh, Thermal stability of an ultra fi ne-grained dual phase TWIP steel, Mater. Sci. Eng. A. 638 (2015) 5–14.

[134] M.H. Razmpoosh, M. Shamanian, M. Esmailzadeh, The microstructural evolution and mechanical properties of resistance spot welded Fe–31Mn–3Al–3Si TWIP steel, Mater. Des. 67 (2015) 571–576.

[135] Z.H. Cai, H. Ding, R.D.K. Misra, Z.Y. Ying, Austenite stability and deformation behavior in a cold-rolled transformation-induced plasticity steel with medium manganese content, Acta Mater. 84 (2015) 229–236.

[136] S. Lee, S.J. Lee, B.C. De Cooman, Austenite stability of ultrafine-grained transformation-induced plasticity steel with Mn partitioning, Scr. Mater. 66 (2012) 832–833.

[137] J. Han, Y.K. Lee, The effects of the heating rate on the reverse transformation mechanism and the phase stability of reverted austenite in medium Mn steels, Acta Mater. 67 (2014) 354–361.

[138] C. Beal, X. Kleber, D. Fabregue, M. Bouzekri, Embrittlement of a zinc coated high manganese TWIP steel, Mater. Sci. Eng. A. 543 (2012) 76–83.

[139] D. Favez, L. Deillon, J. Wagnie, M. Rappaz, Intergranular penetration of liquid gold into stainless steel, Acta Mater. 59 (2011) 6530–6537.

[140] B. Joseph, F. Barbier, M. Aucouturier, Grain boundary penetration of liquid Bi in Cu polycrystals, in: Mater. Sci. Forum, Trans Tech Publ, 1999: pp. 735–738.

[141] T. Böllinghaus, H. Herold, C.E. Cross, J.C. Lippold, Hot cracking phenomena in welds II, Springer Science Business Media, 2008.

[142] GM4485M Weld Specification For Lasers Welds - Butt Joints, (2002) 1–6.

[143] A.R. Marder, Metallurgy of zinc-coated steel, Prog. Mater. Sci. 45 (2000) 191–271.

[144] B. Hutchinson, J. Hagstro, Microstructures and hardness of as-quenched martensites (0.1–0.5%C), Acta Mater. 59 (2011) 5845–5858.

[145] A. Bardelcik, C.P. Salisbury, S. Winkler, M.A. Wells, M.J. Worswick, Effect of cooling rate on the high strain rate properties of boron steel, Int. J. Impact Eng. 37 (2010) 694–702. https://doi.org/10.1016/j.ijimpeng.2009.05.009.

[146] M. Isakov, T. Nyysso, Iterative Determination of the Orientation Relationship Between Austenite and Martensite from a Large Amount of Grain Pair Misorientations, Metall. Mater. Trans. A. 47 (2016) 2587–2590. https://doi.org/10.1007/s11661-016-3462-2.

[147] L. Ryde, Application of EBSD to analysis of microstructures in commercial steels, Mater. Sci. Technol. 22 (2006) 1297–1306.

[148] H. Järvinen, M. Isakov, T. Nyyssönen, M. Järvenpää, P. Peura, The effect of initial microstructure on the final properties of press hardened 22MnB5 steels, Mater. Sci. Eng. A. 676 (2016) 109–120. https://doi.org/10.1016/j.msea.2016.08.096.

[149] N. Haghdadi, A. Zarei-Hanzaki, E. Farabi, P. Cizek, H. Beladi, P.D. Hodgson, Strain rate dependence of ferrite dynamic restoration mechanism in a duplex low-density steel, Mater. Des. 132 (2017) 360–366.

[150] P.N. P. Pokorny, J. Kolisko, L. Balik, Description of Structure of Fe-Zn Intermetalic Compounds Present in Hot-Dip Galvanized Coatings on Steel, Metalurgica. 54 (2015) 707–710.

[151] N. Lun, D.C. Saha, A. Macwan, H. Pan, L. Wang, F. Goodwin, Y. Zhou, Microstructure and mechanical properties of fibre laser welded medium manganese TRIP steel, Mater. Des. 131 (2017) 450–459. https://doi.org/10.1016/j.matdes.2017.06.037.

[152] P.J.L. Fernandes, D.R.H. Jones, Specificity in liquid metal induced embrittlement, Eng. Fail. Anal. 3 (1996) 299–302.

[153] Global Welding Standard, Test procedures resistance spot welding of steel, Glob. Weld. Stand. Test Proced. Resist. Spot Weld. Steel, GWS-5A Stand. (2011).

[154] D.C. Saha, E. Biro, A.P. Gerlich, Y. Zhou, Effects of tempering mode on the structural changes of martensite, Mater. Sci. Eng. A. 673 (2016) 467–475.

[155] D.W. Fan, B.C. De Cooman, State-of-the-knowledge on coating systems for hot stamped parts, Steel Res. Int. 83 (2012) 412–433.

[156] M. Bobby Kannan, R.K. Singh Raman, Evaluating the stress corrosion cracking susceptibility of Mg-Al-Zn alloy in modified-simulated body fluid for orthopaedic implant application, Scr. Mater. 59 (2008) 175–178.

[157] B. Alexandreanu, G.S. Was, The role of stress in the efficacy of coincident site lattice boundaries in improving creep and stress corrosion cracking, Scr. Mater. 54 (2006) 1047–1052.

[158] V.Y. Gertsman, S.M. Bruemmer, Study of Grain Boundary Character Along Intergranular Stress Corrosion Crack Paths in Austenitic Alloys, Acta Mater. 49 (2001) 1589–1598.

[159] M. Koyama, E. Akiyama, T. Sawaguchi, D. Raabe, K. Tsuzaki, Hydrogen-induced cracking at grain and twin boundaries in an Fe-Mn-C austenitic steel, Scr. Mater. 66 (2012) 459–462.

[160] A. Oudriss, J. Creus, J. Bouhattate, C. Savall, B. Peraudeau, X. Feaugas, The diffusion and trapping of hydrogen along the grain boundaries in polycrystalline nickel, Scr. Mater. 66 (2012) 37–40.

[161] R. Kirchheim, Revisiting hydrogen embrittlement models and hydrogen-induced homogeneous nucleation of dislocations, Scr. Mater. 62 (2010) 67–70.

[162] N. Haghdadi, P. Cizek, P.D. Hodgson, V. Tari, G.S. Rohrer, H. Beladi, Effect of ferrite-to-austenite phase transformation path on the interface crystallographic character distributions in a duplex stainless steel, Acta Mater. 145 (2018) 196–209.

[163] N. Haghdadi, D. Abou-Ras, P. Cizek, P.D. Hodgson, A.D. Rollett, H. Beladi, Austenite-ferrite interface crystallography dependence of sigma phase precipitation using the five-parameter characterization approach, Mater. Lett. 196 (2017) 264–268.

[164] E. Farabi, P.D. Hodgson, G.S. Rohrer, H. Beladi, Five-parameter intervariant boundary characterization of martensite in commercially pure titanium, Acta Mater. 154 (2018) 147–160.

[165] J. Luo, H. Cheng, K. Meshinchi Asl, C.J. Kiely, M.P. Harmer, The Role of a Bilayer Interfacial Phase, Science (80-.). 1730 (2011) 1730–1734.

[166] A.R.C. Westwood, M.H. Kamdar, Concerning liquid metal embrittlement, particularly of zinc monocrystals by mercury, Philos. Mag. 8 (1963) 787–804.

[167] N.S. Stoloff, T.L. Johnston, Crack propagation inStoloff, N. S., Johnston, T. L. (1963). Crack propagation in a liquid metal environment. Acta Metallurgica, 11(4), 251–256. a liquid metal environment, Acta Metall. 11 (1963) 251–256.

[168] S. Namilae, B. Radhakrishnan, J.R. Morris, Atomistic simulation of the effect of Ga on crack tip opening in Al bicrystals, Model. Simul. Mater. Sci. Eng. 16 (2008).

[169] H.S. Nam, D.J. Srolovitz, Molecular dynamics simulation of Ga penetration along grain boundaries in Al: A dislocation climb mechanism, Phys. Rev. Lett. 99 (2007) 1–4.

[170] X. Liu, N.T. Nuhfer, A.D. Rollett, S. Sinha, S.B. Lee, J.S. Carpenter, J.E. Ledonne, A. Darbal, K. Barmak, Interfacial orientation and misorientation relationships in nanolamellar Cu/Nb composites using transmission-electron-microscope-based orientation and phase mapping, Acta Mater. 64 (2014) 333–344.

[171] A. Jaatinen, C. V Achim, K.R. Elder, T. Ala-Nissila, Phase field crystal study of symmetric tilt grain boundaries of iron, ArXiv Prepr. ArXiv1006.5405. (2010).

[172] Q. Zhu, A. Samanta, B. Li, R.E. Rudd, T. Frolov, Predicting phase behavior of grain boundaries with evolutionary search and machine learning, Nat. Commun. 9 (2018). https://doi.org/10.1038/s41467-018-02937-2.

[173] J. Sun, Y. Zhang, A. Lyckegaard, F. Bachmann, E.M. Lauridsen, D. Juul Jensen, Grain boundary wetting correlated to the grain boundary properties: A laboratory-based multimodal X-ray tomography investigation, Scr. Mater. 163 (2019) 77–81.

[174] M.H. Razmpoosh, E. Biro, N.Y. Zhou, Liquid metal embrittlement during laser welding of Zn-coated steel: role of random and coincidence site lattice grain boundaries, in: IIW, Bratislava, 2019.

[175] D.L. Olmsted, S.M. Foiles, E.A. Holm, Survey of computed grain boundary properties in face-centered cubic metals: I. Grain boundary energy, Acta Mater. 57 (2009) 3694–3703.

[176] D.L. Olmsted, A new class of metrics for the macroscopic crystallographic space of grain boundaries, Acta Mater. 57 (2009) 2793–2799.

[177] P. Lejcek, S. Hofmann, Thermodynamics of grain boundary segregation and applications to anisotropy, compensation effect and prediction, Crit. Rev. Solid State Mater. Sci. 33 (2008) 133–163. https://doi.org/10.1080/10408430801907649.

[178] S. Hofmann, P. Lejcek, Solute segregation at grain boundaries, Interface Sci. 3 (1996) 241–267. https://doi.org/10.1007/BF00194704.

[179] L. Lu, Y. Shen, X. Chen, L. Qian, K. Lu, Ultrahigh Strength and High Electrical Conductivity in Copper, Science (80-.). 304 (2004) 422–426.

[180] J.W. Cahn, The impurity-drag effect in grain boundary motion, Acta Metall. 10 (1962) 789–798. https://doi.org/10.1016/0001-6160(62)90092-5.

[181] M. Winning, G. Gottstein, L.S. Shvindlerman, On the mechanisms of grain boundary migration, Acta Mater. 50 (2002) 353–363. https://doi.org/10.1016/S1359-6454(01)00343-3.

[182] P. Lejček, S. Hofmann, V. Paidar, Solute segregation and classification of [100] tilt grain boundaries in -iron: Consequences for grain boundary engineering, Acta Mater. 51 (2003) 3951–3963. https://doi.org/10.1016/S1359-6454(03)00219-2.

[183] M. Baram, D. Chatain, W.D. Kaplan, Nanometer-thick equilibrium films: The interface between thermodynamics and atomistics, Science (80-.). 332 (2011) 206–209. https://doi.org/10.1126/science.1201596.

[184] S.J. Dillon, M.P. Harmer, Multiple grain boundary transitions in ceramics: A case study of alumina, Acta Mater. 55 (2007) 5247–5254.

[185] D. Raabe, M. Herbig, S. Sandlöbes, Y. Li, D. Tytko, M. Kuzmina, D. Ponge, P.P. Choi, Grain boundary segregation engineering in metallic alloys: A pathway to

the design of interfaces, Curr. Opin. Solid State Mater. Sci. 18 (2014) 253–261. https://doi.org/10.1016/j.cossms.2014.06.002.

[186] M. Tumuluru, Effect of Silicon and Retained Austenite on the Liquid Metal Embrittlement Cracking Behavior of GEN3 and High-Strength Automotive Steels, Weld. J. 98 (2019) 351S-364S.

[187] K.S. W. Humphrey, A. Dalke, VMD: Visual Molecular Dynamics.Pdf, J. Mol. Graph. 14 (1996) 33–38.

[188] M.S. Daw, M.I. Baskes, Embedded-atom method: Derivation and application to impurities, surfaces, and other defects in metals, Phys. Rev. B. 29 (1984) 6443–6453. https://doi.org/10.1103/PhysRevB.29.6443.

[189] S.M. Eich, D. Beinke, G. Schmitz, Embedded-atom potential for an accurate thermodynamic description of the iron-chromium system, Comput. Mater. Sci. 104 (2015) 185–192. https://doi.org/10.1016/j.commatsci.2015.03.047.

[190] W.G. Hoover, Canonical dynamics: Equilibrium phase-space distributions, Phys. Rev. A. 31 (1985) 1695.

[191] J.M. Haile, I. Johnston, A.J. Mallinckrodt, S. McKay, Molecular dynamics simulation: elementary methods, Comput. Phys. 7 (1993) 625.

[192] M.H. Razmpoosh, A. Macwan, F. Goodwin, E. Biro, Y. Zhou, Crystallographic study of liquid-metal-embrittlement crack path, Mater. Lett. 267 (2020) 127511.

[193] C. Hu, S. Xia, H. Li, T. Liu, B. Zhou, W. Chen, N. Wang, Improving the intergranular corrosion resistance of 304 stainless steel by grain boundary network control, Corros. Sci. 53 (2011) 1880–1886. https://doi.org/10.1016/j.corsci.2011.02.005.

[194] H. Kokawa, M. Shimada, M. Michiuchi, Z.J. Wang, Y.S. Sato, Arrest of weld-decay

in 304 austenitic stainless steel by twin-induced grain boundary engineering, Acta Mater. 55 (2007) 5401–5407. https://doi.org/10.1016/j.actamat.2007.06.005.

[195] S. Rahimi, D.L. Engelberg, J.A. Duff, T.J. Marrow, In situ observation of intergranular crack nucleation in a grain boundary controlled austenitic stainless steel, J. OfMicroscopy. 233 (2009) 423–431.

[196] H. Kokawa, Weld decay-resistant austenitic stainless steel by grain boundary engineering, J. Mater. Sci. 40 (2005) 927–932.

[197] M. Shimada, H. Kokawa, Z.J. Wang, Y.S. Sato, I. Karibe, Optimization of grain boundary character distribution for intergranular corrosion resistant 304 stainless steel by twin- induced grain boundary engineering, Acta Mater. 50 (2002) 2331–2341.

[198] V. Randle, V. Randle, Grain boundary engineering: an overview after 25 years, Mater. Sci. Technol. 26 (2010) 253–261. https://doi.org/10.1179/026708309X12601952777747.

[199] H.Y. Bi, H. Kokawa, Z.J. Wang, M. Shimada, Y.S. Sato, Suppression of chromium depletion by grain boundary structural change during twin-induced grain boundary engineering of 304 stainless steel, 49 (2003) 219–223. https://doi.org/10.1016/S1359-6462(03)00261-6.

[200] H. Grimmer, W. Bollmann, D.H. Warrington, Coincidence-ste lattices and complete patter-shift lattices in cubic crystals, Acta Crystallogr A. 30 (1974) 197–207.

[201] D.L. Engelberg, F.J. Humphreys, T.J. Marrow, The influence of low-strain thermomechanical processing on grain boundary network characteristics in type 304 austenitic stainless steel, J. of Microscopy. 230 (2008) 435–444.

[202] X. Fang, K. Zhang, H. Guo, Twin-induced grain boundary engineering in 304 stainless steel, 487 (2008) 7–13. https://doi.org/10.1016/j.msea.2007.09.075.

[203] M. Kumar, W.E. King, A.J. Schwartz, Modifications to the microstructural topology in f.c.c. materials through thermomechanical processing, Acta Mater. 48 (2000) 2081–2091. https://doi.org/10.1016/S1359-6454(00)00045-8.

[204] M. Kumar, A.J. Schwartz, W.E. King, Microstructural evolution during grain boundary engineering of low to medium stacking fault energy fcc materials, Acta Mater. 50 (2002) 2599–2612. https://doi.org/10.1016/S1359-6454(02)00090-3.

[205] S. Yang, Æ.Z. Jie, W.Æ. Hiroyuki, Y.S. Sato, Grain boundary engineering of 304 austenitic stainless steel by laser surface melting and annealing, (2007) 847–853. https://doi.org/10.1007/s10853-006-0063-2.

[206] S.Y. Lee, Y.B. Chun, J.W. Han, S.K. Hwang, Effect of thermomechanical processing on grain boundary characteristics in two-phase brass, Mater. Sci. Eng. A. 363 (2003) 307–315. https://doi.org/10.1016/S0921-5093(03)00668-3.

[207] V. Randle, Twinning-related grain boundary engineering, 52 (2004) 4067–4081.

[208] C.B. Thomson, V. Randle, "Fine tuning" at 3n boundaries in nickel, Acta Mater. 45 (1997) 4909–4916. https://doi.org/10.1016/S1359-6454(97)00192-4.

[209] A.J. Schwartz, W.E. King, M. Kumar, Influence of processing method on the network of grain boundaries, Scr. Mater. 54 (2006) 963–968.

[210] E.M. Lehockey, G. Palumbo, P. Lin, Improving the Weldability and Service Performance of Nickeland Iron-Based Superalloys by Grain Boundary Engineering, Metall. Mater. Trans. A Phys. Metall. Mater. Sci. 29 (1998) 3069–3079. https://doi.org/10.1007/s11661-998-0214-y.

[211] G. Palumbo, E.M. Lehockey, P. Lin, Applications for grain boundary engineered materials, Jom. 50 (1998) 40–43. https://www.overleaf.com/project/5ea5d713ba83f9000112dd67

[212] M. Coleman, V. Randle, Changes in interface parameters and tensile properties in copper as a consequence of iterative processing, Metall. Mater. Trans. A Phys. Metall. Mater. Sci. 39 (2008) 2175–2183. https://doi.org/10.1007/s11661-008-9574-6.

[213] M. Qian, J.C. Lippold, The effect of annealing twin-generated special grain boundaries on HAZ liquation cracking of nickel-base superalloys, Acta Mater. 51 (2003) 3351–3361. https://doi.org/10.1016/S1359-6454(03)00090-9.

[214] G.S. Rohrer, Grain boundary energy anisotropy: A review, J. Mater. Sci. 46 (2011) 5881–5895. https://doi.org/10.1007/s10853-011-5677-3.

[215] C.L. Briant, S.K. Banerji, Intergranular failure in steel: The role of grain-boundary composition, Int. Met. Rev. 23 (1978) 164–199. https://doi.org/10.1179/imtr.1978.23.1.164.

[216] H. Schrader, H. Wiester, H. Siepmann, Embrittlement of Heat Treated Steels When Tempered at 250 to 400 C, Arch. Eisenhuettenwes. 21 (1950) 21.

[217] J.M. Capus, G. Mayer, The mechanical properties of some tempered alloy martensites, J. Iron Steel Institute, London. 196 (1960) 149–158.

[218] J.R. Low Jr, D.F. Stein, A.M. Turkalo, R.P. LaForce, Transactions of the Metallurgical society of the AIME, MTGTBM. 242 (1968) 14.

[219] M.H. Razmpoosh, A. Macwan, F. Goodwin, E. Biro, Y. Zhou, Dynamic Tensile Behavior of Fiber Laser Welded Medium Manganese TRIP Steel, Metall. Mater. Trans. A. 50 (2019) 3578–3588.

[220] J.J. Guzman-aguilera, C.J. Martinez-gonzalez, V.H. Baltazar-hernandez, S. Basak, In fl uence of SC-HAZ microstructure on the mechanical behavior of Si-TRIP steel welds, Mater. Sci. Eng. A. 718 (2018) 216–227.

[221] X. Han, M.H. Razmpoosh, A. Macwan, E. Biro, Y. Zhou, Effect of Galvannealed

Coating Evolution during Press-Hardening on RSW Weldability, Weld. Journal- In-Press. (2020).

[222] M.H. Razmpoosh, A. Macwan, E. Biro, Y. Zhou, Microstructure and dynamic tensile characteristics of dissimilar fiber laser welded advanced high strength steels, Mater. Sci. Eng. A. 773 (2020) 138729.

[223] M.H. Razmpoosh, A. Macwan, E. Biro, Y. Zhou, Effect of galvanneal-coating evolution during press-hardening on laser welding of 22MnB5 steel, Sci. Technol. Weld. Join. 25 (2020) 112–118.

[224] A.G. Kalashami, C. DiGiovanni, M.H. Razmpoosh, F. Goodwin, N.Y. Zhou, The Role of Internal Oxides on the Liquid Metal Embrittlement Cracking During Resistance Spot Welding of the Dual Phase Steel, Metall. Mater. Trans. A. 51A (2020) 2180–2191.

[225] M.H. Razmpoosh, A. Macwan, F. Goodwin, E. Biro, Y. Zhou, Role of Random and Coincidence Site Lattice Grain Boundaries in Liquid Metal Embrittlement of Iron (FCC)-Zn Couple, Metall. Mater. Trans. A. 51 (2020) 3938–3944.

[226] M.S. Khan, M.H. Razmpoosh, E. Biro, Y. Zhou, A review on the laser welding of coated 22MnB5 press-hardened steel and its impact on the production of tailor-welded blanks, Sci. Technol. Weld. Join. 25 (2020) 447–467.

[227] M.H. Razmpoosh, A. Macwan, F. Goodwin, E. Biro, Y. Zhou, Suppression of Liquid-Metal-Embrittlement by Twin-Induced Grain Boundary Engineering Approach, Materialia. 11 (2020) 100668.

APPENDICES

Appendix A

Letters of Copyright permission

ELSEVIER LICENSE
TERMS AND CONDITIONS

Jul 19, 2020

This Agreement between 200 University Ave, University of Waterloo, E3-3110A ("You") and Elsevier ("Elsevier") consists of your license details and the terms and conditions provided by Elsevier and Copyright Clearance Center.

License Number	4872560225094
License date	Jul 19, 2020
Licensed Content Publisher	Elsevier
Licensed Content Publication	Acta Metallurgica
Licensed Content Title	Environmentally assisted cracking: Overview of evidence for an adsorption-induced localised-slip process
Licensed Content Author	S.P. Lynch

Licensed Content Date	Oct 1, 1988
Licensed Content Volume	36
Licensed Content Issue	10
Licensed Content Pages	23
Start Page	2639
End Page	2661
Type of Use	reuse in a thesis/dissertation
Portion	figures/tables/illustrations
Number of figures/tables/illustrations	2
Format	electronic
Are you the author of this Elsevier article?	No
Will you be translating?	No
Title	Investigation of Liquid-Metal-Embrittlement Crack-path: Role of Grain Boundaries and Responsible Mechanism

	200 University Ave, University of Waterloo, E3-3110A 200 University Ave, University of Waterl
Requestor Location	waterloo, ON n2l3g1 Canada Attn: 200 University Ave, University of Waterloo, E3-3110A
Publisher Tax ID	GB 494 6272 12
Total	0.00 CAD

Terms and Conditions

INTRODUCTION

1. The publisher for this copyrighted material is Elsevier. By clicking "accept" in connection with completing this licensing transaction, you agree that the following terms and conditions apply to this transaction (along with the Billing and Payment terms and conditions established by Copyright Clearance Center, Inc. ("CCC"), at the time that you opened your Rightslink account and that are available at any time at http://myaccount.copyright.com).

GENERAL TERMS

2. Elsevier hereby grants you permission to reproduce the aforementioned material subject to the terms and conditions indicated.

3. Acknowledgement: If any part of the material to be used (for example, figures) has appeared in our publication with credit or acknowledgement to another source, permission must also be sought from that source. If such permission is not obtained then that material may not be included in your publication/copies. Suitable acknowledgement to the source must be made, either as a footnote or in a reference list at the end of your publication, as follows:

"Reprinted from Publication title, Vol /edition number, Author(s), Title of article / title of chapter, Pages No., Copyright (Year), with permission from Elsevier [OR APPLICABLE SOCIETY COPYRIGHT OWNER]." Also Lancet special credit - "Reprinted from The Lancet, Vol. number, Author(s), Title of article, Pages No., Copyright (Year), with permission from Elsevier."

4. Reproduction of this material is confined to the purpose and/or media for which permission is hereby given.

5. Altering/Modifying Material: Not Permitted. However figures and illustrations may be altered/adapted minimally to serve your work. Any other abbreviations, additions, deletions and/or any other alterations shall be made only with prior written authorization of Elsevier Ltd. (Please contact Elsevier at permissions@elsevier.com). No modifications can be made to any Lancet figures/tables and they must be reproduced in full.

6. If the permission fee for the requested use of our material is waived in this instance, please be advised that your future requests for Elsevier materials may attract a fee.

7. Reservation of Rights: Publisher reserves all rights not specifically granted in the combination of (i) the license details provided by you and accepted in the course of this licensing transaction, (ii) these terms and conditions and (iii) CCC's Billing and Payment terms and conditions.

8. License Contingent Upon Payment: While you may exercise the rights licensed immediately upon issuance of the license at the end of the licensing process for the transaction, provided that you have disclosed complete and accurate details of your proposed use, no license is finally effective unless and until full payment is received from you (either by publisher or by CCC) as provided in CCC's Billing and Payment terms and conditions. If full payment is not received on a timely basis, then any license preliminarily granted shall be deemed automatically revoked and shall be void as if never granted. Further, in the event that you breach any of these terms and conditions or any of CCC's Billing and Payment terms and conditions, the license is automatically revoked and shall be void as if never granted. Use of materials as described in a revoked license, as well as any use of the materials beyond the scope of an unrevoked license, may constitute copyright infringement and publisher reserves the right to take any and all action to protect its copyright in the materials.

9. Warranties: Publisher makes no representations or warranties with respect to the licensed material.

10. Indemnity: You hereby indemnify and agree to hold harmless publisher and CCC, and their respective officers, directors, employees and agents, from and against any and all claims arising out of your use of the licensed material other than as specifically authorized pursuant to this license.

11. No Transfer of License: This license is personal to you and may not be sublicensed, assigned, or transferred by you to any other person without publisher's written permission.

12. No Amendment Except in Writing: This license may not be amended except in a writing signed by both parties (or, in the case of publisher, by CCC on publisher's behalf).

13. Objection to Contrary Terms: Publisher hereby objects to any terms contained in any purchase order, acknowledgment, check endorsement or other writing prepared by you, which terms are inconsistent with these terms and conditions or CCC's Billing and Payment terms and conditions. These terms and conditions, together with CCC's Billing and Payment terms and conditions (which are incorporated herein), comprise the entire agreement between you and publisher (and CCC) concerning this licensing transaction. In the event of any conflict between your obligations established by these terms and conditions and those established by CCC's Billing and Payment terms and conditions, these terms and conditions shall control.

14. Revocation: Elsevier or Copyright Clearance Center may deny the permissions described in this License at their sole discretion, for any reason or no reason, with a full refund payable to you. Notice of such denial will be made using the contact information provided by you. Failure to receive such notice will not alter or invalidate the denial. In no event will Elsevier or Copyright Clearance Center be responsible or liable for any costs, expenses or damage incurred by you as a result of a denial of your permission request, other than a refund of the amount(s) paid by you to Elsevier and/or Copyright Clearance Center for denied permissions.

9. Warranties: Publisher makes no representations or warranties with respect to the licensed material.

10. Indemnity: You hereby indemnify and agree to hold harmless publisher and CCC, and their respective officers, directors, employees and agents, from and against any and all claims arising out of your use of the licensed material other than as specifically authorized pursuant to this license.

11. No Transfer of License: This license is personal to you and may not be sublicensed, assigned, or transferred by you to any other person without publisher's written permission.

12. No Amendment Except in Writing: This license may not be amended except in a writing signed by both parties (or, in the case of publisher, by CCC on publisher's behalf).

13. Objection to Contrary Terms: Publisher hereby objects to any terms contained in any purchase order, acknowledgment, check endorsement or other writing prepared by you, which terms are inconsistent with these terms and conditions or CCC's Billing and Payment terms and conditions. These terms and conditions, together with CCC's Billing and Payment terms and conditions (which are incorporated herein), comprise the entire agreement between you and publisher (and CCC) concerning this licensing transaction. In the event of any conflict between your obligations established by these terms and conditions and those established by CCC's Billing and Payment terms and conditions, these terms and conditions shall control.

14. Revocation: Elsevier or Copyright Clearance Center may deny the permissions described in this License at their sole discretion, for any reason or no reason, with a full refund payable to you. Notice of such denial will be made using the contact information provided by you. Failure to receive such notice will not alter or invalidate the denial. In no event will Elsevier or Copyright Clearance Center be responsible or liable for any costs, expenses or damage incurred by you as a result of a denial of your permission request, other than a refund of the amount(s) paid by you to Elsevier and/or Copyright Clearance Center for denied permissions.

LIMITED LICENSE

The following terms and conditions apply only to specific license types:

15. **Translation**: This permission is granted for non-exclusive world **English** rights only unless your license was granted for translation rights. If you licensed translation rights you may only translate this content into the languages you requested. A professional translator must perform all translations and reproduce the content word for word preserving the integrity of the article.

16. **Posting licensed content on any Website**: The following terms and conditions apply as follows: Licensing material from an Elsevier journal: All content posted to the web site must maintain the copyright information line on the bottom of each image; A hyper-text must be included to the Homepage of the journal from which you are licensing at http://www.sciencedirect.com/science/journal/xxxxx or the Elsevier homepage for books at http://www.elsevier.com; Central Storage: This license does not include permission for a scanned version of the material to be stored in a central repository such as that provided by Heron/XanEdu.

Licensing material from an Elsevier book: A hyper-text link must be included to the Elsevier homepage at http://www.elsevier.com . All content posted to the web site must maintain the copyright information line on the bottom of each image.

Posting licensed content on Electronic reserve: In addition to the above the following clauses are applicable: The web site must be password-protected and made available only to bona fide students registered on a relevant course. This permission is granted for 1 year only. You may obtain a new license for future website posting.

17. **For journal authors:** the following clauses are applicable in addition to the above:

Preprints:

A preprint is an author's own write-up of research results and analysis, it has not been peer-reviewed, nor has it had any other value added to it by a publisher (such as formatting, copyright, technical enhancement etc.).

Authors can share their preprints anywhere at any time. Preprints should not be added to or enhanced in any way in order to appear more like, or to substitute for, the final versions of articles however authors can update their preprints on arXiv or RePEc with their Accepted Author Manuscript (see below).

If accepted for publication, we encourage authors to link from the preprint to their formal publication via its DOI. Millions of researchers have access to the formal publications on ScienceDirect, and so links will help users to find, access, cite and use the best available version. Please note that Cell Press, The Lancet and some society-owned have different preprint policies. Information on these policies is available on the journal homepage.

Accepted Author Manuscripts: An accepted author manuscript is the manuscript of an article that has been accepted for publication and which typically includes author-incorporated changes suggested during submission, peer review and editor-author communications.

Authors can share their accepted author manuscript:

- immediately
  - via their non-commercial person homepage or blog
  - by updating a preprint in arXiv or RePEc with the accepted manuscript
  - via their research institute or institutional repository for internal institutional uses or as part of an invitation-only research collaboration work-group
  - directly by providing copies to their students or to research collaborators for their personal use
  - for private scholarly sharing as part of an invitation-only work group on commercial sites with which Elsevier has an agreement
- After the embargo period
  - via non-commercial hosting platforms such as their institutional repository
  - via commercial sites with which Elsevier has an agreement

In all cases accepted manuscripts should:

- link to the formal publication via its DOI
- bear a CC-BY-NC-ND license - this is easy to do
- if aggregated with other manuscripts, for example in a repository or other site, be shared in alignment with our hosting policy not be added to or enhanced in any way to appear more like, or to substitute for, the published journal article.

Published journal article (JPA): A published journal article (PJA) is the definitive final record of published research that appears or will appear in the journal and embodies all

value-adding publishing activities including peer review co-ordination, copy-editing, formatting, (if relevant) pagination and online enrichment.

Policies for sharing publishing journal articles differ for subscription and gold open access articles:

Subscription Articles: If you are an author, please share a link to your article rather than the full-text. Millions of researchers have access to the formal publications on ScienceDirect, and so links will help your users to find, access, cite, and use the best available version.

Theses and dissertations which contain embedded PJAs as part of the formal submission can be posted publicly by the awarding institution with DOI links back to the formal publications on ScienceDirect.

If you are affiliated with a library that subscribes to ScienceDirect you have additional private sharing rights for others' research accessed under that agreement. This includes use for classroom teaching and internal training at the institution (including use in course packs and courseware programs), and inclusion of the article for grant funding purposes.

Gold Open Access Articles: May be shared according to the author-selected end-user license and should contain a CrossMark logo, the end user license, and a DOI link to the formal publication on ScienceDirect.

Please refer to Elsevier's posting policy for further information.

18. **For book authors** the following clauses are applicable in addition to the above: Authors are permitted to place a brief summary of their work online only. You are not allowed to download and post the published electronic version of your chapter, nor may you scan the printed edition to create an electronic version. **Posting to a repository:** Authors are permitted to post a summary of their chapter only in their institution's repository.

19. **Thesis/Dissertation**: If your license is for use in a thesis/dissertation your thesis may be submitted to your institution in either print or electronic form. Should your thesis be published commercially, please reapply for permission. These requirements include permission for the Library and Archives of Canada to supply single copies, on demand, of the complete thesis and include permission for Proquest/UMI to supply single copies, on demand, of the complete thesis. Should your thesis be published commercially, please reapply for permission. Theses and dissertations which contain embedded PJAs as part of the formal submission can be posted publicly by the awarding institution with DOI links back to the formal publications on ScienceDirect.

Elsevier Open Access Terms and Conditions

You can publish open access with Elsevier in hundreds of open access journals or in nearly 2000 established subscription journals that support open access publishing. Permitted third party re-use of these open access articles is defined by the author's choice of Creative Commons user license. See our open access license policy for more information.

Terms & Conditions applicable to all Open Access articles published with Elsevier:

Any reuse of the article must not represent the author as endorsing the adaptation of the article nor should the article be modified in such a way as to damage the author's honour or reputation. If any changes have been made, such changes must be clearly indicated.

SPRINGER NATURE LICENSE
TERMS AND CONDITIONS

Jul 19, 2020

This Agreement between 200 University Ave, University of Waterloo, E3-3110A ("You") and Springer Nature ("Springer Nature") consists of your license details and the terms and conditions provided by Springer Nature and Copyright Clearance Center.

License Number	4872690472869
License date	Jul 19, 2020
Licensed Content Publisher	Springer Nature
Licensed Content Publication	Metallurgical and Materials Transactions A
Licensed Content Title	Dissolution Condensation Mechanism of Stress Corrosion Cracking in Liquid Metals: Driving Force and Crack Kinetics
Licensed Content Author	Evgeny E. Glickman
Licensed Content Date	Dec 1, 2010
Type of Use	Thesis/Dissertation
Requestor type	academic/university or research institute
Format	electronic
Portion	figures/tables/illustrations
Number of figures/tables/illustrations	2

Will you be translating?	no
Circulation/distribution	1 - 29
Author of this Springer Nature content	no
Title	Investigation of Liquid-Metal-Embrittlement Crack-path: Role of Grain Boundaries and Responsible Mechanism
Institution name	University of Waterloo
Expected presentation date	Jul 2020
Portions	Figures 5 and 9
Requestor Location	200 University Ave, University of Waterloo, E3-3110A 200 University Ave, University of Waterl waterloo, ON n2l3g1 Canada Attn: 200 University Ave, University of Waterloo, E3-3110A
Total	0.00 CAD

Terms and Conditions

Springer Nature Customer Service Centre GmbH
Terms and Conditions

This agreement sets out the terms and conditions of the licence (the **Licence**) between you and **Springer Nature Customer Service Centre GmbH** (the **Licensor**). By clicking 'accept' and completing the transaction for the material (**Licensed Material**), you also confirm your acceptance of these terms and conditions.

1. Grant of License

1. 1. The Licensor grants you a personal, non-exclusive, non-transferable, world-wide licence to reproduce the Licensed Material for the purpose specified in your order only. Licences are granted for the specific use requested in the order and for no other

use, subject to the conditions below.

1. 2. The Licensor warrants that it has, to the best of its knowledge, the rights to license reuse of the Licensed Material. However, you should ensure that the material you are requesting is original to the Licensor and does not carry the copyright of another entity (as credited in the published version).

1. 3. If the credit line on any part of the material you have requested indicates that it was reprinted or adapted with permission from another source, then you should also seek permission from that source to reuse the material.

2. Scope of Licence

2. 1. You may only use the Licensed Content in the manner and to the extent permitted by these Ts&Cs and any applicable laws.

2. 2. A separate licence may be required for any additional use of the Licensed Material, e.g. where a licence has been purchased for print only use, separate permission must be obtained for electronic re-use. Similarly, a licence is only valid in the language selected and does not apply for editions in other languages unless additional translation rights have been granted separately in the licence. Any content owned by third parties are expressly excluded from the licence.

2. 3. Similarly, rights for additional components such as custom editions and derivatives require additional permission and may be subject to an additional fee. Please apply to Journalpermissions@springernature.com/bookpermissions@springernature.com for these rights.

2. 4. Where permission has been granted **free of charge** for material in print, permission may also be granted for any electronic version of that work, provided that the material is incidental to your work as a whole and that the electronic version is essentially equivalent to, or substitutes for, the print version.

2. 5. An alternative scope of licence may apply to signatories of the STM Permissions Guidelines, as amended from time to time.

3. Duration of Licence

3. 1. A licence for is valid from the date of purchase ('Licence Date') at the end of the relevant period in the below table:

Scope of Licence	Duration of Licence
Post on a website	12 months
Presentations	12 months
Books and journals	Lifetime of the edition in the language purchased

4. Acknowledgement

4. 1. The Licensor's permission must be acknowledged next to the Licenced Material in print. In electronic form, this acknowledgement must be visible at the same time as the figures/tables/illustrations or abstract, and must be hyperlinked to the journal/book's homepage. Our required acknowledgement format is in the Appendix below.

5. Restrictions on use

5. 1. Use of the Licensed Material may be permitted for incidental promotional use and minor editing privileges e.g. minor adaptations of single figures, changes of format, colour and/or style where the adaptation is credited as set out in Appendix 1 below. Any other changes including but not limited to, cropping, adapting, omitting material that affect the meaning, intention or moral rights of the author are strictly prohibited.

5. 2. You must not use any Licensed Material as part of any design or trademark.

5. 3. Licensed Material may be used in Open Access Publications (OAP) before publication by Springer Nature, but any Licensed Material must be removed from OAP sites prior to final publication.

6. Ownership of Rights

6. 1. Licensed Material remains the property of either Licensor or the relevant third party and any rights not explicitly granted herein are expressly reserved.

7. Warranty

IN NO EVENT SHALL LICENSOR BE LIABLE TO YOU OR ANY OTHER PARTY OR ANY OTHER PERSON OR FOR ANY SPECIAL, CONSEQUENTIAL, INCIDENTAL OR INDIRECT DAMAGES, HOWEVER CAUSED, ARISING OUT OF OR IN CONNECTION WITH THE DOWNLOADING, VIEWING OR USE OF THE MATERIALS REGARDLESS OF THE FORM OF ACTION, WHETHER FOR BREACH OF CONTRACT, BREACH OF WARRANTY, TORT, NEGLIGENCE, INFRINGEMENT OR OTHERWISE (INCLUDING, WITHOUT LIMITATION, DAMAGES BASED ON LOSS OF PROFITS, DATA, FILES, USE, BUSINESS OPPORTUNITY OR CLAIMS OF THIRD PARTIES), AND
WHETHER OR NOT THE PARTY HAS BEEN ADVISED OF THE POSSIBILITY OF SUCH DAMAGES. THIS LIMITATION SHALL APPLY NOTWITHSTANDING ANY FAILURE OF ESSENTIAL PURPOSE OF ANY LIMITED REMEDY PROVIDED HEREIN.

8. Limitations

8. 1. ***BOOKS ONLY:*** Where **'reuse in a dissertation/thesis'** has been selected the following terms apply: Print rights of the final author's accepted manuscript (for clarity, NOT the published version) for up to 100 copies, electronic rights for use only on a personal website or institutional repository as defined by the Sherpa guideline

(www.sherpa.ac.uk/romeo/).

9. Termination and Cancellation

9. 1. Licences will expire after the period shown in Clause 3 (above).

9. 2. Licensee reserves the right to terminate the Licence in the event that payment is not received in full or if there has been a breach of this agreement by you.

Appendix 1 — Acknowledgements:

For Journal Content:
Reprinted by permission from [**the Licensor**]: [**Journal Publisher** (e.g. Nature/Springer/Palgrave)] [**JOURNAL NAME**] [**REFERENCE CITATION** (Article name, Author(s) Name), [**COPYRIGHT**] (year of publication)

For **Advance Online Publication papers:**
Reprinted by permission from [**the Licensor**]: [**Journal Publisher** (e.g. Nature/Springer/Palgrave)] [**JOURNAL NAME**] [**REFERENCE CITATION** (Article name, Author(s) Name), [**COPYRIGHT**] (year of publication), advance online publication, day month year (doi: 10.1038/sj.[JOURNAL ACRONYM].)

For Adaptations/Translations:
Adapted/Translated by permission from [**the Licensor**]: [**Journal Publisher** (e.g. Nature/Springer/Palgrave)] [**JOURNAL NAME**] [**REFERENCE CITATION** (Article name, Author(s) Name), [**COPYRIGHT**] (year of publication)

Note: For any republication from the British Journal of Cancer, the following credit line style applies:

Reprinted/adapted/translated by permission from [**the Licensor**]: on behalf of Cancer Research UK: : [**Journal Publisher** (e.g. Nature/Springer/Palgrave)] [**JOURNAL NAME**] [**REFERENCE CITATION** (Article name, Author(s) Name), [**COPYRIGHT**] (year of publication)

For **Advance Online Publication** papers:
Reprinted by permission from The [**the Licensor**]: on behalf of Cancer Research UK: [**Journal Publisher** (e.g. Nature/Springer/Palgrave)] [**JOURNAL NAME**] [**REFERENCE CITATION** (Article name, Author(s) Name), [**COPYRIGHT**] (year of publication), advance online publication, day month year (doi: 10.1038/sj.[JOURNAL ACRONYM])

For Book content:
Reprinted/adapted by permission from [**the Licensor**]: [**Book Publisher** (e.g. Palgrave Macmillan, Springer etc) [**Book Title**] by [**Book author**(s)] [**COPYRIGHT**] (year of publication)

Other Conditions:

SPRINGER NATURE LICENSE
TERMS AND CONDITIONS

Jul 19, 2020

This Agreement between 200 University Ave, University of Waterloo, E3-3110A ("You") and Springer Nature ("Springer Nature") consists of your license details and the terms and conditions provided by Springer Nature and Copyright Clearance Center.

License Number	4872690677366
License date	Jul 19, 2020
Licensed Content Publisher	Springer Nature
Licensed Content Publication	Metallurgical and Materials Transactions A
Licensed Content Title	Zn Penetration in Liquid Metal Embrittled TWIP Steel
Licensed Content Author	Heeseung Kang et al
Licensed Content Date	Apr 11, 2016
Type of Use	Thesis/Dissertation
Requestor type	academic/university or research institute
Format	electronic
Portion	figures/tables/illustrations
Number of figures/tables/illustrations	1

Will you be translating?	no
Circulation/distribution	1 - 29
Author of this Springer Nature content	no
Title	Investigation of Liquid-Metal-Embrittlement Crack-path: Role of Grain Boundaries and Responsible Mechanism
Institution name	University of Waterloo
Expected presentation date	Jul 2020
Portions	Figure 10
Requestor Location	200 University Ave, University of Waterloo, E3-3110A 200 University Ave, University of Waterl waterloo, ON n2l3g1 Canada Attn: 200 University Ave, University of Waterloo, E3-3110A
Total	0.00 CAD

Terms and Conditions

Springer Nature Customer Service Centre GmbH
Terms and Conditions

This agreement sets out the terms and conditions of the licence (the **Licence**) between you and **Springer Nature Customer Service Centre GmbH** (the **Licensor**). By clicking 'accept' and completing the transaction for the material (**Licensed Material**), you also confirm your acceptance of these terms and conditions.

1. Grant of License

1. 1. The Licensor grants you a personal, non-exclusive, non-transferable, world-wide licence to reproduce the Licensed Material for the purpose specified in your order only. Licences are granted for the specific use requested in the order and for no other use, subject to the conditions below.

1. 2. The Licensor warrants that it has, to the best of its knowledge, the rights to license reuse of the Licensed Material. However, you should ensure that the material you are requesting is original to the Licensor and does not carry the copyright of another entity (as credited in the published version).

1. 3. If the credit line on any part of the material you have requested indicates that it was reprinted or adapted with permission from another source, then you should also seek permission from that source to reuse the material.

2. Scope of Licence

2. 1. You may only use the Licensed Content in the manner and to the extent permitted by these Ts&Cs and any applicable laws.

2. 2. A separate licence may be required for any additional use of the Licensed Material, e.g. where a licence has been purchased for print only use, separate permission must be obtained for electronic re-use. Similarly, a licence is only valid in the language selected and does not apply for editions in other languages unless additional translation rights have been granted separately in the licence. Any content owned by third parties are expressly excluded from the licence.

2. 3. Similarly, rights for additional components such as custom editions and derivatives require additional permission and may be subject to an additional fee. Please apply to Journalpermissions@springernature.com/bookpermissions@springernature.com for these rights.

2. 4. Where permission has been granted **free of charge** for material in print, permission may also be granted for any electronic version of that work, provided that the material is incidental to your work as a whole and that the electronic version is essentially equivalent to, or substitutes for, the print version.

2. 5. An alternative scope of licence may apply to signatories of the STM Permissions Guidelines, as amended from time to time.

3. Duration of Licence

3. 1. A licence for is valid from the date of purchase ('Licence Date') at the end of the relevant period in the below table:

Scope of Licence	Duration of Licence
Post on a website	12 months
Presentations	12 months
Books and journals	Lifetime of the edition in the language purchased

4. Acknowledgement

4. 1. The Licensor's permission must be acknowledged next to the Licenced Material in print. In electronic form, this acknowledgement must be visible at the same time as the figures/tables/illustrations or abstract, and must be hyperlinked to the journal/book's

homepage. Our required acknowledgement format is in the Appendix below.

5. Restrictions on use

5. 1. Use of the Licensed Material may be permitted for incidental promotional use and minor editing privileges e.g. minor adaptations of single figures, changes of format, colour and/or style where the adaptation is credited as set out in Appendix 1 below. Any other changes including but not limited to, cropping, adapting, omitting material that affect the meaning, intention or moral rights of the author are strictly prohibited.

5. 2. You must not use any Licensed Material as part of any design or trademark.

5. 3. Licensed Material may be used in Open Access Publications (OAP) before publication by Springer Nature, but any Licensed Material must be removed from OAP sites prior to final publication.

6. Ownership of Rights

6. 1. Licensed Material remains the property of either Licensor or the relevant third party and any rights not explicitly granted herein are expressly reserved.

7. Warranty

IN NO EVENT SHALL LICENSOR BE LIABLE TO YOU OR ANY OTHER PARTY OR ANY OTHER PERSON OR FOR ANY SPECIAL, CONSEQUENTIAL, INCIDENTAL OR INDIRECT DAMAGES, HOWEVER CAUSED, ARISING OUT OF OR IN CONNECTION WITH THE DOWNLOADING, VIEWING OR USE OF THE MATERIALS REGARDLESS OF THE FORM OF ACTION, WHETHER FOR BREACH OF CONTRACT, BREACH OF WARRANTY, TORT, NEGLIGENCE, INFRINGEMENT OR OTHERWISE (INCLUDING, WITHOUT LIMITATION, DAMAGES BASED ON LOSS OF PROFITS, DATA, FILES, USE, BUSINESS OPPORTUNITY OR CLAIMS OF THIRD PARTIES), AND
WHETHER OR NOT THE PARTY HAS BEEN ADVISED OF THE POSSIBILITY OF SUCH DAMAGES. THIS LIMITATION SHALL APPLY NOTWITHSTANDING ANY FAILURE OF ESSENTIAL PURPOSE OF ANY LIMITED REMEDY PROVIDED HEREIN.

8. Limitations

8. 1. ***BOOKS ONLY:*** Where **'reuse in a dissertation/thesis'** has been selected the following terms apply: Print rights of the final author's accepted manuscript (for clarity, NOT the published version) for up to 100 copies, electronic rights for use only on a personal website or institutional repository as defined by the Sherpa guideline (www.sherpa.ac.uk/romeo/).

9. Termination and Cancellation

9. 1. Licences will expire after the period shown in Clause 3 (above).

9. 2. Licensee reserves the right to terminate the Licence in the event that payment is not received in full or if there has been a breach of this agreement by you.

Appendix 1 — Acknowledgements:

For Journal Content:
Reprinted by permission from [**the Licensor**]: [**Journal Publisher** (e.g. Nature/Springer/Palgrave)] [**JOURNAL NAME**] [**REFERENCE CITATION** (Article name, Author(s) Name), [**COPYRIGHT**] (year of publication)

For **Advance Online Publication papers:**
Reprinted by permission from [**the Licensor**]: [**Journal Publisher** (e.g. Nature/Springer/Palgrave)] [**JOURNAL NAME**] [**REFERENCE CITATION** (Article name, Author(s) Name), [**COPYRIGHT**] (year of publication), advance online publication, day month year (doi: 10.1038/sj.[JOURNAL ACRONYM].)

For Adaptations/Translations:
Adapted/Translated by permission from [**the Licensor**]: [**Journal Publisher** (e.g. Nature/Springer/Palgrave)] [**JOURNAL NAME**] [**REFERENCE CITATION** (Article name, Author(s) Name), [**COPYRIGHT**] (year of publication)

Note: For any republication from the British Journal of Cancer, the following credit line style applies:

Reprinted/adapted/translated by permission from [**the Licensor**]: on behalf of Cancer Research UK: : [**Journal Publisher** (e.g. Nature/Springer/Palgrave)] [**JOURNAL NAME**] [**REFERENCE CITATION** (Article name, Author(s) Name), [**COPYRIGHT**] (year of publication)

For **Advance Online Publication** papers:
Reprinted by permission from The [**the Licensor**]: on behalf of Cancer Research UK: [**Journal Publisher** (e.g. Nature/Springer/Palgrave)] [**JOURNAL NAME**] [**REFERENCE CITATION** (Article name, Author(s) Name), [**COPYRIGHT**] (year of publication), advance online publication, day month year (doi: 10.1038/sj.[JOURNAL ACRONYM])

For Book content:
Reprinted/adapted by permission from [**the Licensor**]: [**Book Publisher** (e.g. Palgrave Macmillan, Springer etc) [**Book Title**] by [**Book author**(s)] [**COPYRIGHT**] (year of publication)

Other Conditions:

Version 1.2

Copyright Clearance Center Marketplace™

Order Confirmation

Thank you, your order has been placed. An email confirmation has been sent to you. Your order license details and printable licenses will be available within 24 hours. Please access Manage Account for final order details.

This is not an invoice. Please go to manage account to access your order history and invoices.

CUSTOMER INFORMATION

Payment by invoice: You can cancel your order until the invoice is generated by contacting customer service.

Billing Address

Mr. Mohammad Hadi Razmpoosh
200 University Ave, University of Waterl
Waterloo, ON n2l3g1
Canada

+1 (226) 978-3045
mhrazmpoosh@uwaterloo.ca

Customer Location

Mr. Mohammad Hadi Razmpoosh
200 University Ave, University of Waterl
Waterloo, ON n2l3g1
Canada

PO Number (optional)

N/A

Payment options

Invoice

PENDING ORDER CONFIRMATION

Confirmation Number: Pending

Order Date: 19-Jul-2020

1. Corrosion

0.00 CAD

Order license ID	Pending	Publisher	N A C E INTERNATIONAL
ISSN	0010-9312		
Type of Use	Republish in a thesis/dissertation	Portion	Chart/graph/table/figure

LICENSED CONTENT

Publication Title	Corrosion	Country	United States of America
Author/Editor	NATIONAL ASSOCIATION OF CORROSION ENGINEERS.	Rightsholder	NACE International - Corrosion Society
		Publication Type	Journal
Date	01/01/1945		
Language	English		

REQUEST DETAILS

Portion Type	Chart/graph/table/figure	Distribution	Worldwide
Number of charts / graphs / tables / figures requested	4	Translation	Original language of publication
		Copies for the disabled?	No
Format (select all that apply)	Electronic	Minor editing privileges?	No
Who will republish the content?	Academic institution	Incidental promotional use?	No
Duration of Use	Life of current edition	Currency	CAD
Lifetime Unit Quantity	Up to 499		
Rights Requested	Main product		

NEW WORK DETAILS

Title	A Short Review of High-Temperature a Critical Assessment of Their Influence on Wetting and Complexion Transitions with Liquid Metal Embrittlement and Corrosion	Institution name	University of Waterloo
		Expected presentation date	2020-07-19
Instructor name	Mohammad Hadi Razmpoosh		

ADDITIONAL DETAILS

Order reference number	N/A	The requesting person / organization to appear on the license	University of Waterloo

REUSE CONTENT DETAILS

Title, description or numeric reference of the portion(s)	Figures	Title of the article/chapter the portion is from	A Short Review of High-Temperature a Critical Assessment of Their Influence on Wetting and Complexion Transitions with Liquid Metal Embrittlement and Corrosion
Editor of portion(s)	Jian Luo		
Volume of serial or monograph	72		
Page or page range of portion	897-910		

Author of portion(s)	NATIONAL ASSOCIATION OF CORROSION ENGINEERS.
Issue, if republishing an article from a serial	N/A
Publication date of portion	2020-07-19

2. Corrosion

0.00 CAD

Order license ID	Pending	Publisher	N A C E INTERNATIONAL
ISSN	0010-9312		
Type of Use	Republish in a thesis/dissertation	Portion	Chart/graph/table/figure

LICENSED CONTENT

Publication Title	Corrosion	Country	United States of America
Author/Editor	NATIONAL ASSOCIATION OF CORROSION ENGINEERS.	Rightsholder	NACE International - Corrosion Society
		Publication Type	Journal
Date	01/01/1945		
Language	English		

REQUEST DETAILS

Portion Type	Chart/graph/table/figure	Distribution	Worldwide
Number of charts / graphs / tables / figures requested	4	Translation	Original language of publication
		Copies for the disabled?	No
Format (select all that apply)	Electronic	Minor editing privileges?	No
Who will republish the content?	Academic institution	Incidental promotional use?	No
Duration of Use	Life of current edition	Currency	CAD
Lifetime Unit Quantity	Up to 499		
Rights Requested	Main product		

NEW WORK DETAILS

Title	Investigation of Liquid-Metal-Embrittlement Crack-path: Role of Grain Boundaries and Responsible Mechanism	Institution name	University of Waterloo
		Expected presentation date	2020-07-19
Instructor name	Mohammad Hadi Razmpoosh		

ADDITIONAL DETAILS

Order reference number	N/A	The requesting person / organization to appear on the license	University of Waterloo

REUSE CONTENT DETAILS

Title, description or numeric reference of the portion(s)	Investigation of Liquid-Metal-Embrittlement Crack-path: Role of Grain Boundaries and Responsible Mechanism	Title of the article/chapter the portion is from	A Short Review of High-Temperature a Critical Assessment of Their Influence on Wetting and Complexion Transitions with Liquid Metal Embrittlement and Corrosion
Editor of portion(s)	Mohammad Hadi Razmpoosh	Author of portion(s)	NATIONAL ASSOCIATION OF CORROSION ENGINEERS.
Volume of serial or monograph	72	Issue, if republishing an article from a serial	N/A
Page or page range of portion	897-910	Publication date of portion	2020-07-19

Total Items: 2 **Total Due: 0.00 CAD**

Accepted: All Publisher and CCC Terms and Conditions

ELSEVIER LICENSE
TERMS AND CONDITIONS

Jul 19, 2020

This Agreement between 200 University Ave, University of Waterloo, E3-3110A ("You") and Elsevier ("Elsevier") consists of your license details and the terms and conditions provided by Elsevier and Copyright Clearance Center.

License Number	4872590062007
License date	Jul 19, 2020
Licensed Content Publisher	Elsevier
Licensed Content Publication	Elsevier Books
Licensed Content Title	Mechanics - Microstructure - Corrosion Coupling
Licensed Content Author	Thierry Auger,Jean-Bernard Vogt,Ingrid Proriol Serre
Licensed Content Date	Jan 1, 2019
Licensed Content Pages	28
Start Page	507
End Page	534
Type of Use	reuse in a thesis/dissertation
Portion	figures/tables/illustrations

Number of figures/tables/illustrations	2
Format	electronic
Are you the author of this Elsevier chapter?	No
Will you be translating?	No
Title	Investigation of Liquid-Metal-Embrittlement Crack-path: Role of Grain Boundaries and Responsible Mechanism
Institution name	University of Waterloo
Expected presentation date	Jul 2020
Portions	Figure 22.13 and 22.14
Requestor Location	200 University Ave, University of Waterloo, E3-3110A 200 University Ave, University of Waterl waterloo, ON n2l3g1 Canada Attn: 200 University Ave, University of Waterloo, E3-3110A
Publisher Tax ID	GB 494 6272 12
Total	0.00 CAD
Terms and Conditions	

INTRODUCTION

1. The publisher for this copyrighted material is Elsevier. By clicking "accept" in connection with completing this licensing transaction, you agree that the following terms and conditions apply to this transaction (along with the Billing and Payment terms and conditions established by Copyright Clearance Center, Inc. ("CCC"), at the time that you opened your Rightslink account and that are available at any time at http://myaccount.copyright.com).

GENERAL TERMS

2. Elsevier hereby grants you permission to reproduce the aforementioned material subject to the terms and conditions indicated.

3. Acknowledgement: If any part of the material to be used (for example, figures) has appeared in our publication with credit or acknowledgement to another source, permission must also be sought from that source. If such permission is not obtained then that material may not be included in your publication/copies. Suitable acknowledgement to the source must be made, either as a footnote or in a reference list at the end of your publication, as follows:

"Reprinted from Publication title, Vol /edition number, Author(s), Title of article / title of chapter, Pages No., Copyright (Year), with permission from Elsevier [OR APPLICABLE SOCIETY COPYRIGHT OWNER]." Also Lancet special credit - "Reprinted from The Lancet, Vol. number, Author(s), Title of article, Pages No., Copyright (Year), with permission from Elsevier."

4. Reproduction of this material is confined to the purpose and/or media for which permission is hereby given.

5. Altering/Modifying Material: Not Permitted. However figures and illustrations may be altered/adapted minimally to serve your work. Any other abbreviations, additions, deletions and/or any other alterations shall be made only with prior written authorization of Elsevier Ltd. (Please contact Elsevier at permissions@elsevier.com). No modifications can be made to any Lancet figures/tables and they must be reproduced in full.

6. If the permission fee for the requested use of our material is waived in this instance, please be advised that your future requests for Elsevier materials may attract a fee.

7. Reservation of Rights: Publisher reserves all rights not specifically granted in the combination of (i) the license details provided by you and accepted in the course of this licensing transaction, (ii) these terms and conditions and (iii) CCC's Billing and Payment terms and conditions.

8. License Contingent Upon Payment: While you may exercise the rights licensed immediately upon issuance of the license at the end of the licensing process for the transaction, provided that you have disclosed complete and accurate details of your proposed use, no license is finally effective unless and until full payment is received from you (either by publisher or by CCC) as provided in CCC's Billing and Payment terms and conditions. If full payment is not received on a timely basis, then any license preliminarily granted shall be deemed automatically revoked and shall be void as if never granted. Further, in the event that you breach any of these terms and conditions or any of CCC's Billing and Payment terms and conditions, the license is automatically revoked and shall be void as if never granted. Use of materials as described in a revoked license, as well as any use of the materials beyond the scope of an unrevoked license, may constitute copyright infringement and publisher reserves the right to take any and all action to protect its copyright in the materials.

9. Warranties: Publisher makes no representations or warranties with respect to the licensed material.

10. Indemnity: You hereby indemnify and agree to hold harmless publisher and CCC, and their respective officers, directors, employees and agents, from and against any and all

claims arising out of your use of the licensed material other than as specifically authorized pursuant to this license.

11. No Transfer of License: This license is personal to you and may not be sublicensed, assigned, or transferred by you to any other person without publisher's written permission.

12. No Amendment Except in Writing: This license may not be amended except in a writing signed by both parties (or, in the case of publisher, by CCC on publisher's behalf).

13. Objection to Contrary Terms: Publisher hereby objects to any terms contained in any purchase order, acknowledgment, check endorsement or other writing prepared by you, which terms are inconsistent with these terms and conditions or CCC's Billing and Payment terms and conditions. These terms and conditions, together with CCC's Billing and Payment terms and conditions (which are incorporated herein), comprise the entire agreement between you and publisher (and CCC) concerning this licensing transaction. In the event of any conflict between your obligations established by these terms and conditions and those established by CCC's Billing and Payment terms and conditions, these terms and conditions shall control.

14. Revocation: Elsevier or Copyright Clearance Center may deny the permissions described in this License at their sole discretion, for any reason or no reason, with a full refund payable to you. Notice of such denial will be made using the contact information provided by you. Failure to receive such notice will not alter or invalidate the denial. In no event will Elsevier or Copyright Clearance Center be responsible or liable for any costs, expenses or damage incurred by you as a result of a denial of your permission request, other than a refund of the amount(s) paid by you to Elsevier and/or Copyright Clearance Center for denied permissions.

LIMITED LICENSE

The following terms and conditions apply only to specific license types:

15. **Translation**: This permission is granted for non-exclusive world **English** rights only unless your license was granted for translation rights. If you licensed translation rights you may only translate this content into the languages you requested. A professional translator must perform all translations and reproduce the content word for word preserving the integrity of the article.

16. **Posting licensed content on any Website**: The following terms and conditions apply as follows: Licensing material from an Elsevier journal: All content posted to the web site must maintain the copyright information line on the bottom of each image; A hyper-text must be included to the Homepage of the journal from which you are licensing at http://www.sciencedirect.com/science/journal/xxxxx or the Elsevier homepage for books at http://www.elsevier.com; Central Storage: This license does not include permission for a scanned version of the material to be stored in a central repository such as that provided by Heron/XanEdu.

Licensing material from an Elsevier book: A hyper-text link must be included to the Elsevier homepage at http://www.elsevier.com . All content posted to the web site must maintain the copyright information line on the bottom of each image.

Posting licensed content on Electronic reserve: In addition to the above the following clauses are applicable: The web site must be password-protected and made available only to

bona fide students registered on a relevant course. This permission is granted for 1 year only. You may obtain a new license for future website posting.

17. **For journal authors:** the following clauses are applicable in addition to the above:

Preprints:

A preprint is an author's own write-up of research results and analysis, it has not been peer-reviewed, nor has it had any other value added to it by a publisher (such as formatting, copyright, technical enhancement etc.).

Authors can share their preprints anywhere at any time. Preprints should not be added to or enhanced in any way in order to appear more like, or to substitute for, the final versions of articles however authors can update their preprints on arXiv or RePEc with their Accepted Author Manuscript (see below).

If accepted for publication, we encourage authors to link from the preprint to their formal publication via its DOI. Millions of researchers have access to the formal publications on ScienceDirect, and so links will help users to find, access, cite and use the best available version. Please note that Cell Press, The Lancet and some society-owned have different preprint policies. Information on these policies is available on the journal homepage.

Accepted Author Manuscripts: An accepted author manuscript is the manuscript of an article that has been accepted for publication and which typically includes author-incorporated changes suggested during submission, peer review and editor-author communications.

Authors can share their accepted author manuscript:

- immediately
  - via their non-commercial person homepage or blog
  - by updating a preprint in arXiv or RePEc with the accepted manuscript
  - via their research institute or institutional repository for internal institutional uses or as part of an invitation-only research collaboration work-group
  - directly by providing copies to their students or to research collaborators for their personal use
  - for private scholarly sharing as part of an invitation-only work group on commercial sites with which Elsevier has an agreement
- After the embargo period
  - via non-commercial hosting platforms such as their institutional repository
  - via commercial sites with which Elsevier has an agreement

In all cases accepted manuscripts should:

- link to the formal publication via its DOI
- bear a CC-BY-NC-ND license - this is easy to do
- if aggregated with other manuscripts, for example in a repository or other site, be shared in alignment with our hosting policy not be added to or enhanced in any way to appear more like, or to substitute for, the published journal article.

Published journal article (JPA): A published journal article (PJA) is the definitive final record of published research that appears or will appear in the journal and embodies all value-adding publishing activities including peer review co-ordination, copy-editing, formatting, (if relevant) pagination and online enrichment.

Policies for sharing publishing journal articles differ for subscription and gold open access articles:

Subscription Articles: If you are an author, please share a link to your article rather than the full-text. Millions of researchers have access to the formal publications on ScienceDirect, and so links will help your users to find, access, cite, and use the best available version.

Theses and dissertations which contain embedded PJAs as part of the formal submission can be posted publicly by the awarding institution with DOI links back to the formal publications on ScienceDirect.

If you are affiliated with a library that subscribes to ScienceDirect you have additional private sharing rights for others' research accessed under that agreement. This includes use for classroom teaching and internal training at the institution (including use in course packs and courseware programs), and inclusion of the article for grant funding purposes.

Gold Open Access Articles: May be shared according to the author-selected end-user license and should contain a CrossMark logo, the end user license, and a DOI link to the formal publication on ScienceDirect.

Please refer to Elsevier's posting policy for further information.

18. **For book authors** the following clauses are applicable in addition to the above: Authors are permitted to place a brief summary of their work online only. You are not allowed to download and post the published electronic version of your chapter, nor may you scan the printed edition to create an electronic version. **Posting to a repository:** Authors are permitted to post a summary of their chapter only in their institution's repository.

19. **Thesis/Dissertation**: If your license is for use in a thesis/dissertation your thesis may be submitted to your institution in either print or electronic form. Should your thesis be published commercially, please reapply for permission. These requirements include permission for the Library and Archives of Canada to supply single copies, on demand, of the complete thesis and include permission for Proquest/UMI to supply single copies, on demand, of the complete thesis. Should your thesis be published commercially, please reapply for permission. Theses and dissertations which contain embedded PJAs as part of the formal submission can be posted publicly by the awarding institution with DOI links back to the formal publications on ScienceDirect.

Elsevier Open Access Terms and Conditions

You can publish open access with Elsevier in hundreds of open access journals or in nearly 2000 established subscription journals that support open access publishing. Permitted third party re-use of these open access articles is defined by the author's choice of Creative Commons user license. See our open access license policy for more information.

Terms & Conditions applicable to all Open Access articles published with Elsevier:

Any reuse of the article must not represent the author as endorsing the adaptation of the article nor should the article be modified in such a way as to damage the author's honour or reputation. If any changes have been made, such changes must be clearly indicated.

The author(s) must be appropriately credited and we ask that you include the end user license and a DOI link to the formal publication on ScienceDirect.

SPRINGER NATURE LICENSE
TERMS AND CONDITIONS

Jul 19, 2020

This Agreement between 200 University Ave, University of Waterloo, E3-3110A ("You") and Springer Nature ("Springer Nature") consists of your license details and the terms and conditions provided by Springer Nature and Copyright Clearance Center.

License Number	4872650067255
License date	Jul 19, 2020
Licensed Content Publisher	Springer Nature
Licensed Content Publication	Interface Science
Licensed Content Title	Grain Boundary Grooving Accelerated by Local Plasticity as a Possible Mechanism of Liquid Metal Embrittlement
Licensed Content Author	E.E. Glickman
Licensed Content Date	Oct 1, 2003
Type of Use	Thesis/Dissertation
Requestor type	academic/university or research institute
Format	electronic
Portion	figures/tables/illustrations
Number of figures/tables/illustrations	1

Will you be translating?	no
Circulation/distribution	1 - 29
Author of this Springer Nature content	no
Title	Investigation of Liquid-Metal-Embrittlement Crack-path: Role of Grain Boundaries and Responsible Mechanism
Institution name	University of Waterloo
Expected presentation date	Jul 2020
Portions	Figure 4
Requestor Location	200 University Ave, University of Waterloo, E3-3110A 200 University Ave, University of Waterl waterloo, ON n2l3g1 Canada Attn: 200 University Ave, University of Waterloo, E3-3110A
Total	0.00 CAD

Terms and Conditions

Springer Nature Customer Service Centre GmbH
Terms and Conditions

This agreement sets out the terms and conditions of the licence (the **Licence**) between you and **Springer Nature Customer Service Centre GmbH** (the **Licensor**). By clicking 'accept' and completing the transaction for the material (**Licensed Material**), you also confirm your acceptance of these terms and conditions.

1. Grant of License

1. 1. The Licensor grants you a personal, non-exclusive, non-transferable, world-wide licence to reproduce the Licensed Material for the purpose specified in your order only. Licences are granted for the specific use requested in the order and for no other

use, subject to the conditions below.

1. 2. The Licensor warrants that it has, to the best of its knowledge, the rights to license reuse of the Licensed Material. However, you should ensure that the material you are requesting is original to the Licensor and does not carry the copyright of another entity (as credited in the published version).

1. 3. If the credit line on any part of the material you have requested indicates that it was reprinted or adapted with permission from another source, then you should also seek permission from that source to reuse the material.

2. Scope of Licence

2. 1. You may only use the Licensed Content in the manner and to the extent permitted by these Ts&Cs and any applicable laws.

2. 2. A separate licence may be required for any additional use of the Licensed Material, e.g. where a licence has been purchased for print only use, separate permission must be obtained for electronic re-use. Similarly, a licence is only valid in the language selected and does not apply for editions in other languages unless additional translation rights have been granted separately in the licence. Any content owned by third parties are expressly excluded from the licence.

2. 3. Similarly, rights for additional components such as custom editions and derivatives require additional permission and may be subject to an additional fee. Please apply to Journalpermissions@springernature.com/bookpermissions@springernature.com for these rights.

2. 4. Where permission has been granted **free of charge** for material in print, permission may also be granted for any electronic version of that work, provided that the material is incidental to your work as a whole and that the electronic version is essentially equivalent to, or substitutes for, the print version.

2. 5. An alternative scope of licence may apply to signatories of the STM Permissions Guidelines, as amended from time to time.

3. Duration of Licence

3. 1. A licence for is valid from the date of purchase ('Licence Date') at the end of the relevant period in the below table:

Scope of Licence	Duration of Licence
Post on a website	12 months
Presentations	12 months
Books and journals	Lifetime of the edition in the language purchased

4. Acknowledgement

4. 1. The Licensor's permission must be acknowledged next to the Licenced Material in print. In electronic form, this acknowledgement must be visible at the same time as the figures/tables/illustrations or abstract, and must be hyperlinked to the journal/book's homepage. Our required acknowledgement format is in the Appendix below.

5. Restrictions on use

5. 1. Use of the Licensed Material may be permitted for incidental promotional use and minor editing privileges e.g. minor adaptations of single figures, changes of format, colour and/or style where the adaptation is credited as set out in Appendix 1 below. Any other changes including but not limited to, cropping, adapting, omitting material that affect the meaning, intention or moral rights of the author are strictly prohibited.

5. 2. You must not use any Licensed Material as part of any design or trademark.

5. 3. Licensed Material may be used in Open Access Publications (OAP) before publication by Springer Nature, but any Licensed Material must be removed from OAP sites prior to final publication.

6. Ownership of Rights

6. 1. Licensed Material remains the property of either Licensor or the relevant third party and any rights not explicitly granted herein are expressly reserved.

7. Warranty

IN NO EVENT SHALL LICENSOR BE LIABLE TO YOU OR ANY OTHER PARTY OR ANY OTHER PERSON OR FOR ANY SPECIAL, CONSEQUENTIAL, INCIDENTAL OR INDIRECT DAMAGES, HOWEVER CAUSED, ARISING OUT OF OR IN CONNECTION WITH THE DOWNLOADING, VIEWING OR USE OF THE MATERIALS REGARDLESS OF THE FORM OF ACTION, WHETHER FOR BREACH OF CONTRACT, BREACH OF WARRANTY, TORT, NEGLIGENCE, INFRINGEMENT OR OTHERWISE (INCLUDING, WITHOUT LIMITATION, DAMAGES BASED ON LOSS OF PROFITS, DATA, FILES, USE, BUSINESS OPPORTUNITY OR CLAIMS OF THIRD PARTIES), AND
WHETHER OR NOT THE PARTY HAS BEEN ADVISED OF THE POSSIBILITY OF SUCH DAMAGES. THIS LIMITATION SHALL APPLY NOTWITHSTANDING ANY FAILURE OF ESSENTIAL PURPOSE OF ANY LIMITED REMEDY PROVIDED HEREIN.

8. Limitations

8. 1. ***BOOKS ONLY:*** Where **'reuse in a dissertation/thesis'** has been selected the following terms apply: Print rights of the final author's accepted manuscript (for clarity, NOT the published version) for up to 100 copies, electronic rights for use only on a personal website or institutional repository as defined by the Sherpa guideline

(www.sherpa.ac.uk/romeo/).

9. Termination and Cancellation

9. 1. Licences will expire after the period shown in Clause 3 (above).

9. 2. Licensee reserves the right to terminate the Licence in the event that payment is not received in full or if there has been a breach of this agreement by you.

Appendix 1 — Acknowledgements:

For Journal Content:
Reprinted by permission from [**the Licensor**]: [**Journal Publisher** (e.g. Nature/Springer/Palgrave)] [**JOURNAL NAME**] [**REFERENCE CITATION** (Article name, Author(s) Name), [**COPYRIGHT**] (year of publication)

For **Advance Online Publication papers:**
Reprinted by permission from [**the Licensor**]: [**Journal Publisher** (e.g. Nature/Springer/Palgrave)] [**JOURNAL NAME**] [**REFERENCE CITATION** (Article name, Author(s) Name), [**COPYRIGHT**] (year of publication), advance online publication, day month year (doi: 10.1038/sj.[JOURNAL ACRONYM].)

For Adaptations/Translations:
Adapted/Translated by permission from [**the Licensor**]: [**Journal Publisher** (e.g. Nature/Springer/Palgrave)] [**JOURNAL NAME**] [**REFERENCE CITATION** (Article name, Author(s) Name), [**COPYRIGHT**] (year of publication)

Note: For any republication from the British Journal of Cancer, the following credit line style applies:

Reprinted/adapted/translated by permission from [**the Licensor**]: on behalf of Cancer Research UK: : [**Journal Publisher** (e.g. Nature/Springer/Palgrave)] [**JOURNAL NAME**] [**REFERENCE CITATION** (Article name, Author(s) Name), [**COPYRIGHT**] (year of publication)

For **Advance Online Publication** papers:
Reprinted by permission from The [**the Licensor**]: on behalf of Cancer Research UK: [**Journal Publisher** (e.g. Nature/Springer/Palgrave)] [**JOURNAL NAME**] [**REFERENCE CITATION** (Article name, Author(s) Name), [**COPYRIGHT**] (year of publication), advance online publication, day month year (doi: 10.1038/sj.[JOURNAL ACRONYM])

For Book content:
Reprinted/adapted by permission from [**the Licensor**]: [**Book Publisher** (e.g. Palgrave Macmillan, Springer etc) [**Book Title**] by [**Book author**(s)] [**COPYRIGHT**] (year of publication)

Other Conditions:

ELSEVIER LICENSE
TERMS AND CONDITIONS

Jul 19, 2020

This Agreement between 200 University Ave, University of Waterloo, E3-3110A ("You") and Elsevier ("Elsevier") consists of your license details and the terms and conditions provided by Elsevier and Copyright Clearance Center.

License Number	4872641324633
License date	Jul 19, 2020
Licensed Content Publisher	Elsevier
Licensed Content Publication	Acta Materialia
Licensed Content Title	The effect of stress on grain boundary interdiffusion in a semi-infinite bicrystal
Licensed Content Author	L. Klinger,E. Rabkin
Licensed Content Date	Aug 1, 2007
Licensed Content Volume	55
Licensed Content Issue	14
Licensed Content Pages	10
Start Page	4689
End Page	4698

Type of Use	reuse in a thesis/dissertation
Portion	figures/tables/illustrations
Number of figures/tables/illustrations	3
Format	electronic
Are you the author of this Elsevier article?	No
Will you be translating?	No
Title	Investigation of Liquid-Metal-Embrittlement Crack-path: Role of Grain Boundaries and Responsible Mechanism
Institution name	University of Waterloo
Expected presentation date	Jul 2020
Portions	Figures 1, 4, 5
Requestor Location	200 University Ave, University of Waterloo, E3-3110A 200 University Ave, University of Waterl waterloo, ON n2l3g1 Canada Attn: 200 University Ave, University of Waterloo, E3-3110A
Publisher Tax ID	GB 494 6272 12
Total	0.00 CAD
Terms and Conditions	

INTRODUCTION

1. The publisher for this copyrighted material is Elsevier. By clicking "accept" in connection with completing this licensing transaction, you agree that the following terms and conditions apply to this transaction (along with the Billing and Payment terms and conditions established by Copyright Clearance Center, Inc. ("CCC"), at the time that you opened your Rightslink account and that are available at any time at http://myaccount.copyright.com).

GENERAL TERMS

2. Elsevier hereby grants you permission to reproduce the aforementioned material subject to the terms and conditions indicated.

3. Acknowledgement: If any part of the material to be used (for example, figures) has appeared in our publication with credit or acknowledgement to another source, permission must also be sought from that source. If such permission is not obtained then that material may not be included in your publication/copies. Suitable acknowledgement to the source must be made, either as a footnote or in a reference list at the end of your publication, as follows:

"Reprinted from Publication title, Vol /edition number, Author(s), Title of article / title of chapter, Pages No., Copyright (Year), with permission from Elsevier [OR APPLICABLE SOCIETY COPYRIGHT OWNER]." Also Lancet special credit - "Reprinted from The Lancet, Vol. number, Author(s), Title of article, Pages No., Copyright (Year), with permission from Elsevier."

4. Reproduction of this material is confined to the purpose and/or media for which permission is hereby given.

5. Altering/Modifying Material: Not Permitted. However figures and illustrations may be altered/adapted minimally to serve your work. Any other abbreviations, additions, deletions and/or any other alterations shall be made only with prior written authorization of Elsevier Ltd. (Please contact Elsevier at permissions@elsevier.com). No modifications can be made to any Lancet figures/tables and they must be reproduced in full.

6. If the permission fee for the requested use of our material is waived in this instance, please be advised that your future requests for Elsevier materials may attract a fee.

7. Reservation of Rights: Publisher reserves all rights not specifically granted in the combination of (i) the license details provided by you and accepted in the course of this licensing transaction, (ii) these terms and conditions and (iii) CCC's Billing and Payment terms and conditions.

8. License Contingent Upon Payment: While you may exercise the rights licensed immediately upon issuance of the license at the end of the licensing process for the transaction, provided that you have disclosed complete and accurate details of your proposed use, no license is finally effective unless and until full payment is received from you (either by publisher or by CCC) as provided in CCC's Billing and Payment terms and conditions. If full payment is not received on a timely basis, then any license preliminarily granted shall be deemed automatically revoked and shall be void as if never granted. Further, in the event that you breach any of these terms and conditions or any of CCC's Billing and Payment terms and conditions, the license is automatically revoked and shall be void as if never granted. Use of materials as described in a revoked license, as well as any use of the materials beyond the scope of an unrevoked license, may constitute copyright infringement and publisher reserves the right to take any and all action to protect its copyright in the materials.

9. Warranties: Publisher makes no representations or warranties with respect to the licensed material.

10. Indemnity: You hereby indemnify and agree to hold harmless publisher and CCC, and their respective officers, directors, employees and agents, from and against any and all claims arising out of your use of the licensed material other than as specifically authorized pursuant to this license.

11. No Transfer of License: This license is personal to you and may not be sublicensed, assigned, or transferred by you to any other person without publisher's written permission.

12. No Amendment Except in Writing: This license may not be amended except in a writing signed by both parties (or, in the case of publisher, by CCC on publisher's behalf).

13. Objection to Contrary Terms: Publisher hereby objects to any terms contained in any purchase order, acknowledgment, check endorsement or other writing prepared by you, which terms are inconsistent with these terms and conditions or CCC's Billing and Payment terms and conditions. These terms and conditions, together with CCC's Billing and Payment terms and conditions (which are incorporated herein), comprise the entire agreement between you and publisher (and CCC) concerning this licensing transaction. In the event of any conflict between your obligations established by these terms and conditions and those established by CCC's Billing and Payment terms and conditions, these terms and conditions shall control.

14. Revocation: Elsevier or Copyright Clearance Center may deny the permissions described in this License at their sole discretion, for any reason or no reason, with a full refund payable to you. Notice of such denial will be made using the contact information provided by you. Failure to receive such notice will not alter or invalidate the denial. In no event will Elsevier or Copyright Clearance Center be responsible or liable for any costs, expenses or damage incurred by you as a result of a denial of your permission request, other than a refund of the amount(s) paid by you to Elsevier and/or Copyright Clearance Center for denied permissions.

LIMITED LICENSE

The following terms and conditions apply only to specific license types:

15. **Translation**: This permission is granted for non-exclusive world **English** rights only unless your license was granted for translation rights. If you licensed translation rights you may only translate this content into the languages you requested. A professional translator must perform all translations and reproduce the content word for word preserving the integrity of the article.

16. **Posting licensed content on any Website**: The following terms and conditions apply as follows: Licensing material from an Elsevier journal: All content posted to the web site must maintain the copyright information line on the bottom of each image; A hyper-text must be included to the Homepage of the journal from which you are licensing at http://www.sciencedirect.com/science/journal/xxxxx or the Elsevier homepage for books at http://www.elsevier.com; Central Storage: This license does not include permission for a scanned version of the material to be stored in a central repository such as that provided by Heron/XanEdu.

Licensing material from an Elsevier book: A hyper-text link must be included to the Elsevier homepage at http://www.elsevier.com . All content posted to the web site must maintain the copyright information line on the bottom of each image.

Posting licensed content on Electronic reserve: In addition to the above the following clauses are applicable: The web site must be password-protected and made available only to bona fide students registered on a relevant course. This permission is granted for 1 year only. You may obtain a new license for future website posting.

17. **For journal authors:** the following clauses are applicable in addition to the above:

Preprints:

A preprint is an author's own write-up of research results and analysis, it has not been peer-reviewed, nor has it had any other value added to it by a publisher (such as formatting, copyright, technical enhancement etc.).

Authors can share their preprints anywhere at any time. Preprints should not be added to or enhanced in any way in order to appear more like, or to substitute for, the final versions of articles however authors can update their preprints on arXiv or RePEc with their Accepted Author Manuscript (see below).

If accepted for publication, we encourage authors to link from the preprint to their formal publication via its DOI. Millions of researchers have access to the formal publications on ScienceDirect, and so links will help users to find, access, cite and use the best available version. Please note that Cell Press, The Lancet and some society-owned have different preprint policies. Information on these policies is available on the journal homepage.

Accepted Author Manuscripts: An accepted author manuscript is the manuscript of an article that has been accepted for publication and which typically includes author-incorporated changes suggested during submission, peer review and editor-author communications.

Authors can share their accepted author manuscript:

- immediately
    - via their non-commercial person homepage or blog
    - by updating a preprint in arXiv or RePEc with the accepted manuscript
    - via their research institute or institutional repository for internal institutional uses or as part of an invitation-only research collaboration work-group
    - directly by providing copies to their students or to research collaborators for their personal use
    - for private scholarly sharing as part of an invitation-only work group on commercial sites with which Elsevier has an agreement
- After the embargo period
    - via non-commercial hosting platforms such as their institutional repository
    - via commercial sites with which Elsevier has an agreement

In all cases accepted manuscripts should:

- link to the formal publication via its DOI
- bear a CC-BY-NC-ND license - this is easy to do
- if aggregated with other manuscripts, for example in a repository or other site, be shared in alignment with our hosting policy not be added to or enhanced in any way to appear more like, or to substitute for, the published journal article.

Published journal article (JPA): A published journal article (PJA) is the definitive final record of published research that appears or will appear in the journal and embodies all

value-adding publishing activities including peer review co-ordination, copy-editing, formatting, (if relevant) pagination and online enrichment.

Policies for sharing publishing journal articles differ for subscription and gold open access articles:

Subscription Articles: If you are an author, please share a link to your article rather than the full-text. Millions of researchers have access to the formal publications on ScienceDirect, and so links will help your users to find, access, cite, and use the best available version.

Theses and dissertations which contain embedded PJAs as part of the formal submission can be posted publicly by the awarding institution with DOI links back to the formal publications on ScienceDirect.

If you are affiliated with a library that subscribes to ScienceDirect you have additional private sharing rights for others' research accessed under that agreement. This includes use for classroom teaching and internal training at the institution (including use in course packs and courseware programs), and inclusion of the article for grant funding purposes.

Gold Open Access Articles: May be shared according to the author-selected end-user license and should contain a CrossMark logo, the end user license, and a DOI link to the formal publication on ScienceDirect.

Please refer to Elsevier's posting policy for further information.

18. **For book authors** the following clauses are applicable in addition to the above: Authors are permitted to place a brief summary of their work online only. You are not allowed to download and post the published electronic version of your chapter, nor may you scan the printed edition to create an electronic version. **Posting to a repository:** Authors are permitted to post a summary of their chapter only in their institution's repository.

19. **Thesis/Dissertation**: If your license is for use in a thesis/dissertation your thesis may be submitted to your institution in either print or electronic form. Should your thesis be published commercially, please reapply for permission. These requirements include permission for the Library and Archives of Canada to supply single copies, on demand, of the complete thesis and include permission for Proquest/UMI to supply single copies, on demand, of the complete thesis. Should your thesis be published commercially, please reapply for permission. Theses and dissertations which contain embedded PJAs as part of the formal submission can be posted publicly by the awarding institution with DOI links back to the formal publications on ScienceDirect.

Elsevier Open Access Terms and Conditions

You can publish open access with Elsevier in hundreds of open access journals or in nearly 2000 established subscription journals that support open access publishing. Permitted third party re-use of these open access articles is defined by the author's choice of Creative Commons user license. See our open access license policy for more information.

Terms & Conditions applicable to all Open Access articles published with Elsevier:

Any reuse of the article must not represent the author as endorsing the adaptation of the article nor should the article be modified in such a way as to damage the author's honour or reputation. If any changes have been made, such changes must be clearly indicated.

The author(s) must be appropriately credited and we ask that you include the end user license and a DOI link to the formal publication on ScienceDirect.

If any part of the material to be used (for example, figures) has appeared in our publication with credit or acknowledgement to another source it is the responsibility of the user to ensure their reuse complies with the terms and conditions determined by the rights holder.

Additional Terms & Conditions applicable to each Creative Commons user license:

CC BY: The CC-BY license allows users to copy, to create extracts, abstracts and new works from the Article, to alter and revise the Article and to make commercial use of the Article (including reuse and/or resale of the Article by commercial entities), provided the user gives appropriate credit (with a link to the formal publication through the relevant DOI), provides a link to the license, indicates if changes were made and the licensor is not represented as endorsing the use made of the work. The full details of the license are available at http://creativecommons.org/licenses/by/4.0.

CC BY NC SA: The CC BY-NC-SA license allows users to copy, to create extracts, abstracts and new works from the Article, to alter and revise the Article, provided this is not done for commercial purposes, and that the user gives appropriate credit (with a link to the formal publication through the relevant DOI), provides a link to the license, indicates if changes were made and the licensor is not represented as endorsing the use made of the work. Further, any new works must be made available on the same conditions. The full details of the license are available at http://creativecommons.org/licenses/by-nc-sa/4.0.

CC BY NC ND: The CC BY-NC-ND license allows users to copy and distribute the Article, provided this is not done for commercial purposes and further does not permit distribution of the Article if it is changed or edited in any way, and provided the user gives appropriate credit (with a link to the formal publication through the relevant DOI), provides a link to the license, and that the licensor is not represented as endorsing the use made of the work. The full details of the license are available at http://creativecommons.org/licenses/by-nc-nd/4.0. Any commercial reuse of Open Access articles published with a CC BY NC SA or CC BY NC ND license requires permission from Elsevier and will be subject to a fee.

Commercial reuse includes:

- Associating advertising with the full text of the Article
- Charging fees for document delivery or access
- Article aggregation
- Systematic distribution via e-mail lists or share buttons

Posting or linking by commercial companies for use by customers of those companies.

20. **Other Conditions**:

v1.9

Questions? customercare@copyright.com or +1-855-239-3415 (toll free in the US) or +1-978-646-2777.

THE AMERICAN ASSOCIATION FOR THE ADVANCEMENT OF SCIENCE LICENSE TERMS AND CONDITIONS

Jul 19, 2020

This Agreement between 200 University Ave, University of Waterloo, E3-3110A ("You") and The American Association for the Advancement of Science ("The American Association for the Advancement of Science") consists of your license details and the terms and conditions provided by The American Association for the Advancement of Science and Copyright Clearance Center.

License Number	4872660237437
License date	Jul 19, 2020
Licensed Content Publisher	The American Association for the Advancement of Science
Licensed Content Publication	Science
Licensed Content Title	The Role of a Bilayer Interfacial Phase on Liquid Metal Embrittlement
Licensed Content Author	Jian Luo,Huikai Cheng,Kaveh Meshinchi Asl,Christopher J. Kiely,Martin P. Harmer
Licensed Content Date	Sep 23, 2011
Licensed Content Volume	333
Licensed Content Issue	6050
Volume number	333

Issue number	6050
Type of Use	Thesis / Dissertation
Requestor type	Scientist/individual at a research institution
Format	Electronic
Portion	Text Excerpt
Number of pages requested	3
Title	Investigation of Liquid-Metal-Embrittlement Crack-path: Role of Grain Boundaries and Responsible Mechanism
Institution name	University of Waterloo
Expected presentation date	Jul 2020
Portions	Figures 1, 2, 4
Requestor Location	200 University Ave, University of Waterloo, E3-3110A 200 University Ave, University of Waterl waterloo, ON n2l3g1 Canada Attn: 200 University Ave, University of Waterloo, E3-3110A
Total	0.00 CAD

Terms and Conditions

American Association for the Advancement of Science TERMS AND CONDITIONS

Regarding your request, we are pleased to grant you non-exclusive, non-transferable permission, to republish the AAAS material identified above in your work identified above, subject to the terms and conditions herein. We must be contacted for permission for any uses other than those specifically identified in your request above.

The following credit line must be printed along with the AAAS material: "From [Full Reference Citation]. Reprinted with permission from AAAS."

All required credit lines and notices must be visible any time a user accesses any part of the AAAS material and must appear on any printed copies and authorized user might make.

This permission does not apply to figures / photos / artwork or any other content or materials included in your work that are credited to non-AAAS sources. If the requested material is sourced to or references non-AAAS sources, you must obtain authorization from that source as well before using that material. You agree to hold harmless and indemnify AAAS against any claims arising from your use of any content in your work that is credited to non-AAAS sources.

If the AAAS material covered by this permission was published in Science during the years 1974 - 1994, you must also obtain permission from the author, who may grant or withhold permission, and who may or may not charge a fee if permission is granted. See original article for author's address. This condition does not apply to news articles.

The AAAS material may not be modified or altered except that figures and tables may be modified with permission from the author. Author permission for any such changes must be secured prior to your use.

Whenever possible, we ask that electronic uses of the AAAS material permitted herein include a hyperlink to the original work on AAAS's website (hyperlink may be embedded in the reference citation).

AAAS material reproduced in your work identified herein must not account for more than 30% of the total contents of that work.

AAAS must publish the full paper prior to use of any text.

AAAS material must not imply any endorsement by the American Association for the Advancement of Science.

This permission is not valid for the use of the AAAS and/or Science logos.

AAAS makes no representations or warranties as to the accuracy of any information contained in the AAAS material covered by this permission, including any warranties of

merchantability or fitness for a particular purpose.

If permission fees for this use are waived, please note that AAAS reserves the right to charge for reproduction of this material in the future.

Permission is not valid unless payment is received within sixty (60) days of the issuance of this permission. If payment is not received within this time period then all rights granted herein shall be revoked and this permission will be considered null and void.

In the event of breach of any of the terms and conditions herein or any of CCC's Billing and Payment terms and conditions, all rights granted herein shall be revoked and this permission will be considered null and void.

AAAS reserves the right to terminate this permission and all rights granted herein at its discretion, for any purpose, at any time. In the event that AAAS elects to terminate this permission, you will have no further right to publish, publicly perform, publicly display, distribute or otherwise use any matter in which the AAAS content had been included, and all

fees paid hereunder shall be fully refunded to you. Notification of termination will be sent to the contact information as supplied by you during the request process and termination shall be immediate upon sending the notice. Neither AAAS nor CCC shall be liable for any costs, expenses, or damages you may incur as a result of the termination of this permission, beyond the refund noted above.

This Permission may not be amended except by written document signed by both parties.

The terms above are applicable to all permissions granted for the use of AAAS material. Below you will find additional conditions that apply to your particular type of use.

FOR A THESIS OR DISSERTATION
If you are using figure(s)/table(s), permission is granted for use in print and electronic versions of your dissertation or thesis. A full text article may be used in print versions only of a dissertation or thesis.

Permission covers the distribution of your dissertation or thesis on demand by ProQuest / UMI, provided the AAAS material covered by this permission remains in situ.

If you are an Original Author on the AAAS article being reproduced, please refer to your License to Publish for rules on reproducing your paper in a dissertation or thesis.

FOR JOURNALS:
Permission covers both print and electronic versions of your journal article, however the AAAS material may not be used in any manner other than within the context of your article.

FOR BOOKS/TEXTBOOKS:
If this license is to reuse figures/tables, then permission is granted for non-exclusive world rights in all languages in both print and electronic formats (electronic formats are defined below).

If this license is to reuse a text excerpt or a full text article, then permission is granted for non-exclusive world rights in English only. You have the option of securing either print or electronic rights or both, but electronic rights are not automatically granted and do garner additional fees. Permission for translations of text excerpts or full text articles into other languages must be obtained separately.

Licenses granted for use of AAAS material in electronic format books/textbooks are valid only in cases where the electronic version is equivalent to or substitutes for the print version of the book/textbook. The AAAS material reproduced as permitted herein must remain in situ and must not be exploited separately (for example, if permission covers the use of a full text article, the article may not be offered for access or for purchase as a stand-alone unit), except in the case of permitted textbook companions as noted below.

You must include the following notice in any electronic versions, either adjacent to the reprinted AAAS material or in the terms and conditions for use of your electronic products: "Readers may view, browse, and/or download material for temporary copying purposes only, provided these uses are for noncommercial personal purposes. Except as provided by law, this material may not be further reproduced, distributed, transmitted, modified, adapted, performed, displayed, published, or sold in whole or in part, without prior written permission from the publisher."

If your book is an academic textbook, permission covers the following companions to your textbook, provided such companions are distributed only in conjunction with your textbook at no additional cost to the user:

- Password-protected website
- Instructor's image CD/DVD and/or PowerPoint resource
- Student CD/DVD

All companions must contain instructions to users that the AAAS material may be used for non-commercial, classroom purposes only. Any other uses require the prior written permission from AAAS.

If your license is for the use of AAAS Figures/Tables, then the electronic rights granted herein permit use of the Licensed Material in any Custom Databases that you distribute the electronic versions of your textbook through, so long as the Licensed Material remains within the context of a chapter of the title identified in your request and cannot be downloaded by a user as an independent image file.

Rights also extend to copies/files of your Work (as described above) that you are required to provide for use by the visually and/or print disabled in compliance with state and federal laws.

This permission only covers a single edition of your work as identified in your request.

FOR NEWSLETTERS:
Permission covers print and/or electronic versions, provided the AAAS material reproduced as permitted herein remains in situ and is not exploited separately (for example, if permission covers the use of a full text article, the article may not be offered for access or for purchase as a stand-alone unit)

FOR ANNUAL REPORTS:
Permission covers print and electronic versions provided the AAAS material reproduced as permitted herein remains in situ and is not exploited separately (for example, if permission covers the use of a full text article, the article may not be offered for access or for purchase as a stand-alone unit)

FOR PROMOTIONAL/MARKETING USES:
Permission covers the use of AAAS material in promotional or marketing pieces such as information packets, media kits, product slide kits, brochures, or flyers limited to a single print run. The AAAS Material may not be used in any manner which implies endorsement or promotion by the American Association for the Advancement of Science (AAAS) or Science of any product or service. AAAS does not permit the reproduction of its name, logo or text on promotional literature.

If permission to use a full text article is permitted, The Science article covered by this permission must not be altered in any way. No additional printing may be set onto an article copy other than the copyright credit line required above. Any alterations must be approved in advance and in writing by AAAS. This includes, but is not limited to, the placement of sponsorship identifiers, trademarks, logos, rubber stamping or self-adhesive stickers onto the article copies.

Additionally, article copies must be a freestanding part of any information package (i.e. media kit) into which they are inserted. They may not be physically attached to anything, such as an advertising insert, or have anything attached to them, such as a sample product. Article copies must be easily removable from any kits or informational packages in which they are used. The only exception is that article copies may be inserted into three-ring binders.

the material is to be distributed online, access must be restricted to students and instructors enrolled in that particular course by some means of password or access control.

FOR WEBSITES:
You must include the following notice in any electronic versions, either adjacent to the reprinted AAAS material or in the terms and conditions for use of your electronic products: "Readers may view, browse, and/or download material for temporary copying purposes only, provided these uses are for noncommercial personal purposes. Except as provided by law, this material may not be further reproduced, distributed, transmitted, modified, adapted, performed, displayed, published, or sold in whole or in part, without prior written permission from the publisher."

Permissions for the use of Full Text articles on third party websites are granted on a case by case basis and only in cases where access to the AAAS Material is restricted by some means of password or access control. Alternately, an E-Print may be purchased through our reprints department (brocheleau@rockwaterinc.com).

REGARDING FULL TEXT ARTICLE USE ON THE WORLD WIDE WEB IF YOU ARE AN 'ORIGINAL AUTHOR' OF A SCIENCE PAPER

If you chose "Original Author" as the Requestor Type, you are warranting that you are one of authors listed on the License Agreement as a "Licensed content author" or that you are acting on that author's behalf to use the Licensed content in a new work that one of the authors listed on the License Agreement as a "Licensed content author" has written.

Original Authors may post the 'Accepted Version' of their full text article on their personal or on their University website and not on any other website. The 'Accepted Version' is the version of the paper accepted for publication by AAAS including changes resulting from peer review but prior to AAAS's copy editing and production (in other words not the AAAS published version).

FOR MOVIES / FILM / TELEVISION:
Permission is granted to use, record, film, photograph, and/or tape the AAAS material in connection with your program/film and in any medium your program/film may be shown or heard, including but not limited to broadcast and cable television, radio, print, world wide web, and videocassette.

The required credit line should run in the program/film's end credits.

FOR MUSEUM EXHIBITIONS:
Permission is granted to use the AAAS material as part of a single exhibition for the duration of that exhibit. Permission for use of the material in promotional materials for the exhibit must be cleared separately with AAAS (please contact us at permissions@aaas.org).

FOR TRANSLATIONS:
Translation rights apply only to the language identified in your request summary above.

The following disclaimer must appear with your translation, on the first page of the article, after the credit line: "This translation is not an official translation by AAAS staff, nor is it endorsed by AAAS as accurate. In crucial matters, please refer to the official English-language version originally published by AAAS."

FOR USE ON A COVER:
Permission is granted to use the AAAS material on the cover of a journal issue, newsletter

SPRINGER NATURE LICENSE
TERMS AND CONDITIONS

Jul 19, 2020

This Agreement between 200 University Ave, University of Waterloo, E3-3110A ("You") and Springer Nature ("Springer Nature") consists of your license details and the terms and conditions provided by Springer Nature and Copyright Clearance Center.

License Number	4872660408220
License date	Jul 19, 2020
Licensed Content Publisher	Springer Nature
Licensed Content Publication	Nature
Licensed Content Title	Bismuth embrittlement of copper is an atomic size effect
Licensed Content Author	Rainer Schweinfest et al
Licensed Content Date	Dec 23, 2004
Type of Use	Thesis/Dissertation
Requestor type	academic/university or research institute
Format	electronic
Portion	figures/tables/illustrations
Number of figures/tables/illustrations	1

High-res required	no
Will you be translating?	no
Circulation/distribution	1 - 29
Author of this Springer Nature content	no
Title	Investigation of Liquid-Metal-Embrittlement Crack-path: Role of Grain Boundaries and Responsible Mechanism
Institution name	University of Waterloo
Expected presentation date	Jul 2020
Portions	Figure 1
Requestor Location	200 University Ave, University of Waterloo, E3-3110A 200 University Ave, University of Waterl waterloo, ON n2l3g1 Canada Attn: 200 University Ave, University of Waterloo, E3-3110A
Total	0.00 CAD

Terms and Conditions

Springer Nature Customer Service Centre GmbH
Terms and Conditions

This agreement sets out the terms and conditions of the licence (the **Licence**) between you and **Springer Nature Customer Service Centre GmbH** (the **Licensor**). By clicking 'accept' and completing the transaction for the material (**Licensed Material**), you also confirm your acceptance of these terms and conditions.

1. Grant of License

1. 1. The Licensor grants you a personal, non-exclusive, non-transferable, world-wide licence to reproduce the Licensed Material for the purpose specified in your order

only. Licences are granted for the specific use requested in the order and for no other use, subject to the conditions below.

1. 2. The Licensor warrants that it has, to the best of its knowledge, the rights to license reuse of the Licensed Material. However, you should ensure that the material you are requesting is original to the Licensor and does not carry the copyright of another entity (as credited in the published version).

1. 3. If the credit line on any part of the material you have requested indicates that it was reprinted or adapted with permission from another source, then you should also seek permission from that source to reuse the material.

2. Scope of Licence

2. 1. You may only use the Licensed Content in the manner and to the extent permitted by these Ts&Cs and any applicable laws.

2. 2. A separate licence may be required for any additional use of the Licensed Material, e.g. where a licence has been purchased for print only use, separate permission must be obtained for electronic re-use. Similarly, a licence is only valid in the language selected and does not apply for editions in other languages unless additional translation rights have been granted separately in the licence. Any content owned by third parties are expressly excluded from the licence.

2. 3. Similarly, rights for additional components such as custom editions and derivatives require additional permission and may be subject to an additional fee. Please apply to Journalpermissions@springernature.com/bookpermissions@springernature.com for these rights.

2. 4. Where permission has been granted **free of charge** for material in print, permission may also be granted for any electronic version of that work, provided that the material is incidental to your work as a whole and that the electronic version is essentially equivalent to, or substitutes for, the print version.

2. 5. An alternative scope of licence may apply to signatories of the STM Permissions Guidelines, as amended from time to time.

3. Duration of Licence

3. 1. A licence for is valid from the date of purchase ('Licence Date') at the end of the relevant period in the below table:

Scope of Licence	Duration of Licence
Post on a website	12 months
Presentations	12 months
Books and journals	Lifetime of the edition in the language purchased

4. Acknowledgement

4. 1. The Licensor's permission must be acknowledged next to the Licenced Material in print. In electronic form, this acknowledgement must be visible at the same time as the figures/tables/illustrations or abstract, and must be hyperlinked to the journal/book's homepage. Our required acknowledgement format is in the Appendix below.

5. Restrictions on use

5. 1. Use of the Licensed Material may be permitted for incidental promotional use and minor editing privileges e.g. minor adaptations of single figures, changes of format, colour and/or style where the adaptation is credited as set out in Appendix 1 below. Any other changes including but not limited to, cropping, adapting, omitting material that affect the meaning, intention or moral rights of the author are strictly prohibited.

5. 2. You must not use any Licensed Material as part of any design or trademark.

5. 3. Licensed Material may be used in Open Access Publications (OAP) before publication by Springer Nature, but any Licensed Material must be removed from OAP sites prior to final publication.

6. Ownership of Rights

6. 1. Licensed Material remains the property of either Licensor or the relevant third party and any rights not explicitly granted herein are expressly reserved.

7. Warranty

IN NO EVENT SHALL LICENSOR BE LIABLE TO YOU OR ANY OTHER PARTY OR ANY OTHER PERSON OR FOR ANY SPECIAL, CONSEQUENTIAL, INCIDENTAL OR INDIRECT DAMAGES, HOWEVER CAUSED, ARISING OUT OF OR IN CONNECTION WITH THE DOWNLOADING, VIEWING OR USE OF THE MATERIALS REGARDLESS OF THE FORM OF ACTION, WHETHER FOR BREACH OF CONTRACT, BREACH OF WARRANTY, TORT, NEGLIGENCE, INFRINGEMENT OR OTHERWISE (INCLUDING, WITHOUT LIMITATION, DAMAGES BASED ON LOSS OF PROFITS, DATA, FILES, USE, BUSINESS OPPORTUNITY OR CLAIMS OF THIRD PARTIES), AND
WHETHER OR NOT THE PARTY HAS BEEN ADVISED OF THE POSSIBILITY OF SUCH DAMAGES. THIS LIMITATION SHALL APPLY NOTWITHSTANDING ANY FAILURE OF ESSENTIAL PURPOSE OF ANY LIMITED REMEDY PROVIDED HEREIN.

8. Limitations

8. 1. ***BOOKS ONLY:*** Where **'reuse in a dissertation/thesis'** has been selected the following terms apply: Print rights of the final author's accepted manuscript (for clarity, NOT the published version) for up to 100 copies, electronic rights for use only on a personal website or institutional repository as defined by the Sherpa guideline

(www.sherpa.ac.uk/romeo/).

9. Termination and Cancellation

9. 1. Licences will expire after the period shown in Clause 3 (above).

9. 2. Licensee reserves the right to terminate the Licence in the event that payment is not received in full or if there has been a breach of this agreement by you.

Appendix 1 — Acknowledgements:

For Journal Content:
Reprinted by permission from [**the Licensor**]: [**Journal Publisher** (e.g. Nature/Springer/Palgrave)] [**JOURNAL NAME**] [**REFERENCE CITATION** (Article name, Author(s) Name), [**COPYRIGHT**] (year of publication)

For **Advance Online Publication papers:**
Reprinted by permission from [**the Licensor**]: [**Journal Publisher** (e.g. Nature/Springer/Palgrave)] [**JOURNAL NAME**] [**REFERENCE CITATION** (Article name, Author(s) Name), [**COPYRIGHT**] (year of publication), advance online publication, day month year (doi: 10.1038/sj.[JOURNAL ACRONYM].)

For Adaptations/Translations:
Adapted/Translated by permission from [**the Licensor**]: [**Journal Publisher** (e.g. Nature/Springer/Palgrave)] [**JOURNAL NAME**] [**REFERENCE CITATION** (Article name, Author(s) Name), [**COPYRIGHT**] (year of publication)

Note: For any republication from the British Journal of Cancer, the following credit line style applies:

Reprinted/adapted/translated by permission from [**the Licensor**]: on behalf of Cancer Research UK: : [**Journal Publisher** (e.g. Nature/Springer/Palgrave)] [**JOURNAL NAME**] [**REFERENCE CITATION** (Article name, Author(s) Name), [**COPYRIGHT**] (year of publication)

For **Advance Online Publication** papers:
Reprinted by permission from The [**the Licensor**]: on behalf of Cancer Research UK: [**Journal Publisher** (e.g. Nature/Springer/Palgrave)] [**JOURNAL NAME**] [**REFERENCE CITATION** (Article name, Author(s) Name), [**COPYRIGHT**] (year of publication), advance online publication, day month year (doi: 10.1038/sj.[JOURNAL ACRONYM])

For Book content:
Reprinted/adapted by permission from [**the Licensor**]: [**Book Publisher** (e.g. Palgrave Macmillan, Springer etc) [**Book Title**] by [**Book author**(s)] [**COPYRIGHT**] (year of publication)

Other Conditions:

ELSEVIER LICENSE
TERMS AND CONDITIONS

Jul 19, 2020

This Agreement between 200 University Ave, University of Waterloo, E3-3110A ("You") and Elsevier ("Elsevier") consists of your license details and the terms and conditions provided by Elsevier and Copyright Clearance Center.

License Number	4872660623341
License date	Jul 19, 2020
Licensed Content Publisher	Elsevier
Licensed Content Publication	Computational Materials Science
Licensed Content Title	Effect of zinc-doping on tensile strength of Σ5 bcc Fe symmetric tilt grain boundary
Licensed Content Author	Wangjun Peng,Hao Peng,Guangxin Wu,Jieyu Zhang
Licensed Content Date	Jan 1, 2020
Licensed Content Volume	171
Licensed Content Issue	n/a
Licensed Content Pages	1
Start Page	109204
End Page	0

Type of Use	reuse in a thesis/dissertation
Portion	figures/tables/illustrations
Number of figures/tables/illustrations	6
Format	electronic
Are you the author of this Elsevier article?	No
Will you be translating?	No
Title	Investigation of Liquid-Metal-Embrittlement Crack-path: Role of Grain Boundaries and Responsible Mechanism
Institution name	University of Waterloo
Expected presentation date	Jul 2020
Portions	Figures 3, 4, 5, 7, 8, 10
Requestor Location	200 University Ave, University of Waterloo, E3-3110A 200 University Ave, University of Waterl waterloo, ON n2l3g1 Canada Attn: 200 University Ave, University of Waterloo, E3-3110A
Publisher Tax ID	GB 494 6272 12
Total	0.00 CAD
Terms and Conditions	

INTRODUCTION

1. The publisher for this copyrighted material is Elsevier. By clicking "accept" in connection with completing this licensing transaction, you agree that the following terms and conditions apply to this transaction (along with the Billing and Payment terms and conditions established by Copyright Clearance Center, Inc. ("CCC"), at the time that you opened your Rightslink account and that are available at any time at http://myaccount.copyright.com).

GENERAL TERMS

2. Elsevier hereby grants you permission to reproduce the aforementioned material subject to the terms and conditions indicated.

3. Acknowledgement: If any part of the material to be used (for example, figures) has appeared in our publication with credit or acknowledgement to another source, permission must also be sought from that source. If such permission is not obtained then that material may not be included in your publication/copies. Suitable acknowledgement to the source must be made, either as a footnote or in a reference list at the end of your publication, as follows:

"Reprinted from Publication title, Vol /edition number, Author(s), Title of article / title of chapter, Pages No., Copyright (Year), with permission from Elsevier [OR APPLICABLE SOCIETY COPYRIGHT OWNER]." Also Lancet special credit - "Reprinted from The Lancet, Vol. number, Author(s), Title of article, Pages No., Copyright (Year), with permission from Elsevier."

4. Reproduction of this material is confined to the purpose and/or media for which permission is hereby given.

5. Altering/Modifying Material: Not Permitted. However figures and illustrations may be altered/adapted minimally to serve your work. Any other abbreviations, additions, deletions and/or any other alterations shall be made only with prior written authorization of Elsevier Ltd. (Please contact Elsevier at permissions@elsevier.com). No modifications can be made to any Lancet figures/tables and they must be reproduced in full.

6. If the permission fee for the requested use of our material is waived in this instance, please be advised that your future requests for Elsevier materials may attract a fee.

7. Reservation of Rights: Publisher reserves all rights not specifically granted in the combination of (i) the license details provided by you and accepted in the course of this licensing transaction, (ii) these terms and conditions and (iii) CCC's Billing and Payment terms and conditions.

8. License Contingent Upon Payment: While you may exercise the rights licensed immediately upon issuance of the license at the end of the licensing process for the transaction, provided that you have disclosed complete and accurate details of your proposed use, no license is finally effective unless and until full payment is received from you (either by publisher or by CCC) as provided in CCC's Billing and Payment terms and conditions. If full payment is not received on a timely basis, then any license preliminarily granted shall be deemed automatically revoked and shall be void as if never granted. Further, in the event that you breach any of these terms and conditions or any of CCC's Billing and Payment terms and conditions, the license is automatically revoked and shall be void as if never granted. Use of materials as described in a revoked license, as well as any use of the materials beyond the scope of an unrevoked license, may constitute copyright infringement and publisher reserves the right to take any and all action to protect its copyright in the materials.

9. Warranties: Publisher makes no representations or warranties with respect to the licensed material.

10. Indemnity: You hereby indemnify and agree to hold harmless publisher and CCC, and their respective officers, directors, employees and agents, from and against any and all claims arising out of your use of the licensed material other than as specifically authorized pursuant to this license.

11. No Transfer of License: This license is personal to you and may not be sublicensed, assigned, or transferred by you to any other person without publisher's written permission.

12. No Amendment Except in Writing: This license may not be amended except in a writing signed by both parties (or, in the case of publisher, by CCC on publisher's behalf).

13. Objection to Contrary Terms: Publisher hereby objects to any terms contained in any purchase order, acknowledgment, check endorsement or other writing prepared by you, which terms are inconsistent with these terms and conditions or CCC's Billing and Payment terms and conditions. These terms and conditions, together with CCC's Billing and Payment terms and conditions (which are incorporated herein), comprise the entire agreement between you and publisher (and CCC) concerning this licensing transaction. In the event of any conflict between your obligations established by these terms and conditions and those established by CCC's Billing and Payment terms and conditions, these terms and conditions shall control.

14. Revocation: Elsevier or Copyright Clearance Center may deny the permissions described in this License at their sole discretion, for any reason or no reason, with a full refund payable to you. Notice of such denial will be made using the contact information provided by you. Failure to receive such notice will not alter or invalidate the denial. In no event will Elsevier or Copyright Clearance Center be responsible or liable for any costs, expenses or damage incurred by you as a result of a denial of your permission request, other than a refund of the amount(s) paid by you to Elsevier and/or Copyright Clearance Center for denied permissions.

LIMITED LICENSE

The following terms and conditions apply only to specific license types:

15. **Translation**: This permission is granted for non-exclusive world **English** rights only unless your license was granted for translation rights. If you licensed translation rights you may only translate this content into the languages you requested. A professional translator must perform all translations and reproduce the content word for word preserving the integrity of the article.

16. **Posting licensed content on any Website**: The following terms and conditions apply as follows: Licensing material from an Elsevier journal: All content posted to the web site must maintain the copyright information line on the bottom of each image; A hyper-text must be included to the Homepage of the journal from which you are licensing at http://www.sciencedirect.com/science/journal/xxxxx or the Elsevier homepage for books at http://www.elsevier.com; Central Storage: This license does not include permission for a scanned version of the material to be stored in a central repository such as that provided by Heron/XanEdu.

Licensing material from an Elsevier book: A hyper-text link must be included to the Elsevier homepage at http://www.elsevier.com . All content posted to the web site must maintain the copyright information line on the bottom of each image.

Posting licensed content on Electronic reserve: In addition to the above the following clauses are applicable: The web site must be password-protected and made available only to bona fide students registered on a relevant course. This permission is granted for 1 year only. You may obtain a new license for future website posting.

17. **For journal authors:** the following clauses are applicable in addition to the above:

Preprints:

A preprint is an author's own write-up of research results and analysis, it has not been peer-reviewed, nor has it had any other value added to it by a publisher (such as formatting, copyright, technical enhancement etc.).

Authors can share their preprints anywhere at any time. Preprints should not be added to or enhanced in any way in order to appear more like, or to substitute for, the final versions of articles however authors can update their preprints on arXiv or RePEc with their Accepted Author Manuscript (see below).

If accepted for publication, we encourage authors to link from the preprint to their formal publication via its DOI. Millions of researchers have access to the formal publications on ScienceDirect, and so links will help users to find, access, cite and use the best available version. Please note that Cell Press, The Lancet and some society-owned have different preprint policies. Information on these policies is available on the journal homepage.

Accepted Author Manuscripts: An accepted author manuscript is the manuscript of an article that has been accepted for publication and which typically includes author-incorporated changes suggested during submission, peer review and editor-author communications.

Authors can share their accepted author manuscript:

- immediately
    - via their non-commercial person homepage or blog
    - by updating a preprint in arXiv or RePEc with the accepted manuscript
    - via their research institute or institutional repository for internal institutional uses or as part of an invitation-only research collaboration work-group
    - directly by providing copies to their students or to research collaborators for their personal use
    - for private scholarly sharing as part of an invitation-only work group on commercial sites with which Elsevier has an agreement
- After the embargo period
    - via non-commercial hosting platforms such as their institutional repository
    - via commercial sites with which Elsevier has an agreement

In all cases accepted manuscripts should:

- link to the formal publication via its DOI
- bear a CC-BY-NC-ND license - this is easy to do
- if aggregated with other manuscripts, for example in a repository or other site, be shared in alignment with our hosting policy not be added to or enhanced in any way to appear more like, or to substitute for, the published journal article.

Published journal article (JPA): A published journal article (PJA) is the definitive final record of published research that appears or will appear in the journal and embodies all

value-adding publishing activities including peer review co-ordination, copy-editing, formatting, (if relevant) pagination and online enrichment.

Policies for sharing publishing journal articles differ for subscription and gold open access articles:

Subscription Articles: If you are an author, please share a link to your article rather than the full-text. Millions of researchers have access to the formal publications on ScienceDirect, and so links will help your users to find, access, cite, and use the best available version.

Theses and dissertations which contain embedded PJAs as part of the formal submission can be posted publicly by the awarding institution with DOI links back to the formal publications on ScienceDirect.

If you are affiliated with a library that subscribes to ScienceDirect you have additional private sharing rights for others' research accessed under that agreement. This includes use for classroom teaching and internal training at the institution (including use in course packs and courseware programs), and inclusion of the article for grant funding purposes.

Gold Open Access Articles: May be shared according to the author-selected end-user license and should contain a CrossMark logo, the end user license, and a DOI link to the formal publication on ScienceDirect.

Please refer to Elsevier's posting policy for further information.

18. **For book authors** the following clauses are applicable in addition to the above: Authors are permitted to place a brief summary of their work online only. You are not allowed to download and post the published electronic version of your chapter, nor may you scan the printed edition to create an electronic version. **Posting to a repository:** Authors are permitted to post a summary of their chapter only in their institution's repository.

19. **Thesis/Dissertation**: If your license is for use in a thesis/dissertation your thesis may be submitted to your institution in either print or electronic form. Should your thesis be published commercially, please reapply for permission. These requirements include permission for the Library and Archives of Canada to supply single copies, on demand, of the complete thesis and include permission for Proquest/UMI to supply single copies, on demand, of the complete thesis. Should your thesis be published commercially, please reapply for permission. Theses and dissertations which contain embedded PJAs as part of the formal submission can be posted publicly by the awarding institution with DOI links back to the formal publications on ScienceDirect.

Elsevier Open Access Terms and Conditions

You can publish open access with Elsevier in hundreds of open access journals or in nearly 2000 established subscription journals that support open access publishing. Permitted third party re-use of these open access articles is defined by the author's choice of Creative Commons user license. See our open access license policy for more information.

Terms & Conditions applicable to all Open Access articles published with Elsevier:

Any reuse of the article must not represent the author as endorsing the adaptation of the article nor should the article be modified in such a way as to damage the author's honour or reputation. If any changes have been made, such changes must be clearly indicated.

The author(s) must be appropriately credited and we ask that you include the end user license and a DOI link to the formal publication on ScienceDirect.

If any part of the material to be used (for example, figures) has appeared in our publication with credit or acknowledgement to another source it is the responsibility of the user to ensure their reuse complies with the terms and conditions determined by the rights holder.

Additional Terms & Conditions applicable to each Creative Commons user license:

CC BY: The CC-BY license allows users to copy, to create extracts, abstracts and new works from the Article, to alter and revise the Article and to make commercial use of the Article (including reuse and/or resale of the Article by commercial entities), provided the user gives appropriate credit (with a link to the formal publication through the relevant DOI), provides a link to the license, indicates if changes were made and the licensor is not represented as endorsing the use made of the work. The full details of the license are available at http://creativecommons.org/licenses/by/4.0.

CC BY NC SA: The CC BY-NC-SA license allows users to copy, to create extracts, abstracts and new works from the Article, to alter and revise the Article, provided this is not done for commercial purposes, and that the user gives appropriate credit (with a link to the formal publication through the relevant DOI), provides a link to the license, indicates if changes were made and the licensor is not represented as endorsing the use made of the work. Further, any new works must be made available on the same conditions. The full details of the license are available at http://creativecommons.org/licenses/by-nc-sa/4.0.

CC BY NC ND: The CC BY-NC-ND license allows users to copy and distribute the Article, provided this is not done for commercial purposes and further does not permit distribution of the Article if it is changed or edited in any way, and provided the user gives appropriate credit (with a link to the formal publication through the relevant DOI), provides a link to the license, and that the licensor is not represented as endorsing the use made of the work. The full details of the license are available at http://creativecommons.org/licenses/by-nc-nd/4.0. Any commercial reuse of Open Access articles published with a CC BY NC SA or CC BY NC ND license requires permission from Elsevier and will be subject to a fee.

Commercial reuse includes:

- Associating advertising with the full text of the Article
- Charging fees for document delivery or access
- Article aggregation
- Systematic distribution via e-mail lists or share buttons

Posting or linking by commercial companies for use by customers of those companies.

20. **Other Conditions**:

v1.9

Questions? customercare@copyright.com or +1-855-239-3415 (toll free in the US) or +1-978-646-2777.

SPRINGER NATURE LICENSE
TERMS AND CONDITIONS

Jul 19, 2020

This Agreement between 200 University Ave, University of Waterloo, E3-3110A ("You") and Springer Nature ("Springer Nature") consists of your license details and the terms and conditions provided by Springer Nature and Copyright Clearance Center.

License Number	4872680857820
License date	Jul 19, 2020
Licensed Content Publisher	Springer Nature
Licensed Content Publication	Nature Materials
Licensed Content Title	Bismuth-induced embrittlement of copper grain boundaries
Licensed Content Author	Gerd Duscher et al
Licensed Content Date	Aug 22, 2004
Type of Use	Thesis/Dissertation
Requestor type	academic/university or research institute
Format	electronic
Portion	figures/tables/illustrations
Number of figures/tables/illustrations	2

High-res required	no
Will you be translating?	no
Circulation/distribution	1 - 29
Author of this Springer Nature content	no
Title	Investigation of Liquid-Metal-Embrittlement Crack-path: Role of Grain Boundaries and Responsible Mechanism
Institution name	University of Waterloo
Expected presentation date	Jul 2020
Portions	Figures 1 and 5
Requestor Location	200 University Ave, University of Waterloo, E3-3110A 200 University Ave, University of Waterl waterloo, ON n2l3g1 Canada Attn: 200 University Ave, University of Waterloo, E3-3110A
Total	0.00 CAD

Terms and Conditions

Springer Nature Customer Service Centre GmbH
Terms and Conditions

This agreement sets out the terms and conditions of the licence (the **Licence**) between you and **Springer Nature Customer Service Centre GmbH** (the **Licensor**). By clicking 'accept' and completing the transaction for the material (**Licensed Material**), you also confirm your acceptance of these terms and conditions.

1. Grant of License

1. 1. The Licensor grants you a personal, non-exclusive, non-transferable, world-wide licence to reproduce the Licensed Material for the purpose specified in your order

only. Licences are granted for the specific use requested in the order and for no other use, subject to the conditions below.

1. 2. The Licensor warrants that it has, to the best of its knowledge, the rights to license reuse of the Licensed Material. However, you should ensure that the material you are requesting is original to the Licensor and does not carry the copyright of another entity (as credited in the published version).

1. 3. If the credit line on any part of the material you have requested indicates that it was reprinted or adapted with permission from another source, then you should also seek permission from that source to reuse the material.

2. Scope of Licence

2. 1. You may only use the Licensed Content in the manner and to the extent permitted by these Ts&Cs and any applicable laws.

2. 2. A separate licence may be required for any additional use of the Licensed Material, e.g. where a licence has been purchased for print only use, separate permission must be obtained for electronic re-use. Similarly, a licence is only valid in the language selected and does not apply for editions in other languages unless additional translation rights have been granted separately in the licence. Any content owned by third parties are expressly excluded from the licence.

2. 3. Similarly, rights for additional components such as custom editions and derivatives require additional permission and may be subject to an additional fee. Please apply to Journalpermissions@springernature.com/bookpermissions@springernature.com for these rights.

2. 4. Where permission has been granted **free of charge** for material in print, permission may also be granted for any electronic version of that work, provided that the material is incidental to your work as a whole and that the electronic version is essentially equivalent to, or substitutes for, the print version.

2. 5. An alternative scope of licence may apply to signatories of the STM Permissions Guidelines, as amended from time to time.

3. Duration of Licence

3. 1. A licence for is valid from the date of purchase ('Licence Date') at the end of the relevant period in the below table:

Scope of Licence	Duration of Licence
Post on a website	12 months
Presentations	12 months
Books and journals	Lifetime of the edition in the language purchased

4. Acknowledgement

4. 1. The Licensor's permission must be acknowledged next to the Licenced Material in print. In electronic form, this acknowledgement must be visible at the same time as the figures/tables/illustrations or abstract, and must be hyperlinked to the journal/book's homepage. Our required acknowledgement format is in the Appendix below.

5. Restrictions on use

5. 1. Use of the Licensed Material may be permitted for incidental promotional use and minor editing privileges e.g. minor adaptations of single figures, changes of format, colour and/or style where the adaptation is credited as set out in Appendix 1 below. Any other changes including but not limited to, cropping, adapting, omitting material that affect the meaning, intention or moral rights of the author are strictly prohibited.

5. 2. You must not use any Licensed Material as part of any design or trademark.

5. 3. Licensed Material may be used in Open Access Publications (OAP) before publication by Springer Nature, but any Licensed Material must be removed from OAP sites prior to final publication.

6. Ownership of Rights

6. 1. Licensed Material remains the property of either Licensor or the relevant third party and any rights not explicitly granted herein are expressly reserved.

7. Warranty

IN NO EVENT SHALL LICENSOR BE LIABLE TO YOU OR ANY OTHER PARTY OR ANY OTHER PERSON OR FOR ANY SPECIAL, CONSEQUENTIAL, INCIDENTAL OR INDIRECT DAMAGES, HOWEVER CAUSED, ARISING OUT OF OR IN CONNECTION WITH THE DOWNLOADING, VIEWING OR USE OF THE MATERIALS REGARDLESS OF THE FORM OF ACTION, WHETHER FOR BREACH OF CONTRACT, BREACH OF WARRANTY, TORT, NEGLIGENCE, INFRINGEMENT OR OTHERWISE (INCLUDING, WITHOUT LIMITATION, DAMAGES BASED ON LOSS OF PROFITS, DATA, FILES, USE, BUSINESS OPPORTUNITY OR CLAIMS OF THIRD PARTIES), AND
WHETHER OR NOT THE PARTY HAS BEEN ADVISED OF THE POSSIBILITY OF SUCH DAMAGES. THIS LIMITATION SHALL APPLY NOTWITHSTANDING ANY FAILURE OF ESSENTIAL PURPOSE OF ANY LIMITED REMEDY PROVIDED HEREIN.

8. Limitations

8. 1. ***BOOKS ONLY:*** Where **'reuse in a dissertation/thesis'** has been selected the following terms apply: Print rights of the final author's accepted manuscript (for clarity, NOT the published version) for up to 100 copies, electronic rights for use only on a personal website or institutional repository as defined by the Sherpa guideline

(www.sherpa.ac.uk/romeo/).

9. Termination and Cancellation

9. 1. Licences will expire after the period shown in Clause 3 (above).

9. 2. Licensee reserves the right to terminate the Licence in the event that payment is not received in full or if there has been a breach of this agreement by you.

Appendix 1 — Acknowledgements:

For Journal Content:
Reprinted by permission from [**the Licensor**]: [**Journal Publisher** (e.g. Nature/Springer/Palgrave)] [**JOURNAL NAME**] [**REFERENCE CITATION** (Article name, Author(s) Name), [**COPYRIGHT**] (year of publication)

For **Advance Online Publication papers:**
Reprinted by permission from [**the Licensor**]: [**Journal Publisher** (e.g. Nature/Springer/Palgrave)] [**JOURNAL NAME**] [**REFERENCE CITATION** (Article name, Author(s) Name), [**COPYRIGHT**] (year of publication), advance online publication, day month year (doi: 10.1038/sj.[JOURNAL ACRONYM].)

For Adaptations/Translations:
Adapted/Translated by permission from [**the Licensor**]: [**Journal Publisher** (e.g. Nature/Springer/Palgrave)] [**JOURNAL NAME**] [**REFERENCE CITATION** (Article name, Author(s) Name), [**COPYRIGHT**] (year of publication)

Note: For any republication from the British Journal of Cancer, the following credit line style applies:

Reprinted/adapted/translated by permission from [**the Licensor**]: on behalf of Cancer Research UK: : [**Journal Publisher** (e.g. Nature/Springer/Palgrave)] [**JOURNAL NAME**] [**REFERENCE CITATION** (Article name, Author(s) Name), [**COPYRIGHT**] (year of publication)

For **Advance Online Publication** papers:
Reprinted by permission from The [**the Licensor**]: on behalf of Cancer Research UK: [**Journal Publisher** (e.g. Nature/Springer/Palgrave)] [**JOURNAL NAME**] [**REFERENCE CITATION** (Article name, Author(s) Name), [**COPYRIGHT**] (year of publication), advance online publication, day month year (doi: 10.1038/sj.[JOURNAL ACRONYM])

For Book content:
Reprinted/adapted by permission from [**the Licensor**]: [**Book Publisher** (e.g. Palgrave Macmillan, Springer etc) [**Book Title**] by [**Book author**(s)] [**COPYRIGHT**] (year of publication)

Other Conditions:

ELSEVIER LICENSE
TERMS AND CONDITIONS

Jul 19, 2020

This Agreement between 200 University Ave, University of Waterloo, E3-3110A ("You") and Elsevier ("Elsevier") consists of your license details and the terms and conditions provided by Elsevier and Copyright Clearance Center.

License Number	4872681041715
License date	Jul 19, 2020
Licensed Content Publisher	Elsevier
Licensed Content Publication	Acta Metallurgica
Licensed Content Title	A new model of grain boundary failure in temper embrittled steel
Licensed Content Author	Wolfgang Losch
Licensed Content Date	Dec 1, 1979
Licensed Content Volume	27
Licensed Content Issue	12
Licensed Content Pages	8
Start Page	1885
End Page	1892

Type of Use	reuse in a thesis/dissertation
Portion	figures/tables/illustrations
Number of figures/tables/illustrations	3
Format	electronic
Are you the author of this Elsevier article?	No
Will you be translating?	No
Title	Investigation of Liquid-Metal-Embrittlement Crack-path: Role of Grain Boundaries and Responsible Mechanism
Institution name	University of Waterloo
Expected presentation date	Jul 2020
Portions	Figures 3, 4, 5
Requestor Location	200 University Ave, University of Waterloo, E3-3110A 200 University Ave, University of Waterl waterloo, ON n2l3g1 Canada Attn: 200 University Ave, University of Waterloo, E3-3110A
Publisher Tax ID	GB 494 6272 12
Total	0.00 CAD
Terms and Conditions	

INTRODUCTION

1. The publisher for this copyrighted material is Elsevier. By clicking "accept" in connection with completing this licensing transaction, you agree that the following terms and conditions apply to this transaction (along with the Billing and Payment terms and conditions established by Copyright Clearance Center, Inc. ("CCC"), at the time that you opened your Rightslink account and that are available at any time at http://myaccount.copyright.com).

GENERAL TERMS

2. Elsevier hereby grants you permission to reproduce the aforementioned material subject to the terms and conditions indicated.

3. Acknowledgement: If any part of the material to be used (for example, figures) has appeared in our publication with credit or acknowledgement to another source, permission must also be sought from that source. If such permission is not obtained then that material may not be included in your publication/copies. Suitable acknowledgement to the source must be made, either as a footnote or in a reference list at the end of your publication, as follows:

"Reprinted from Publication title, Vol /edition number, Author(s), Title of article / title of chapter, Pages No., Copyright (Year), with permission from Elsevier [OR APPLICABLE SOCIETY COPYRIGHT OWNER]." Also Lancet special credit - "Reprinted from The Lancet, Vol. number, Author(s), Title of article, Pages No., Copyright (Year), with permission from Elsevier."

4. Reproduction of this material is confined to the purpose and/or media for which permission is hereby given.

5. Altering/Modifying Material: Not Permitted. However figures and illustrations may be altered/adapted minimally to serve your work. Any other abbreviations, additions, deletions and/or any other alterations shall be made only with prior written authorization of Elsevier Ltd. (Please contact Elsevier at permissions@elsevier.com). No modifications can be made to any Lancet figures/tables and they must be reproduced in full.

6. If the permission fee for the requested use of our material is waived in this instance, please be advised that your future requests for Elsevier materials may attract a fee.

7. Reservation of Rights: Publisher reserves all rights not specifically granted in the combination of (i) the license details provided by you and accepted in the course of this licensing transaction, (ii) these terms and conditions and (iii) CCC's Billing and Payment terms and conditions.

8. License Contingent Upon Payment: While you may exercise the rights licensed immediately upon issuance of the license at the end of the licensing process for the transaction, provided that you have disclosed complete and accurate details of your proposed use, no license is finally effective unless and until full payment is received from you (either by publisher or by CCC) as provided in CCC's Billing and Payment terms and conditions. If full payment is not received on a timely basis, then any license preliminarily granted shall be deemed automatically revoked and shall be void as if never granted. Further, in the event that you breach any of these terms and conditions or any of CCC's Billing and Payment terms and conditions, the license is automatically revoked and shall be void as if never granted. Use of materials as described in a revoked license, as well as any use of the materials beyond the scope of an unrevoked license, may constitute copyright infringement and publisher reserves the right to take any and all action to protect its copyright in the materials.

9. Warranties: Publisher makes no representations or warranties with respect to the licensed material.

10. Indemnity: You hereby indemnify and agree to hold harmless publisher and CCC, and their respective officers, directors, employees and agents, from and against any and all claims arising out of your use of the licensed material other than as specifically authorized pursuant to this license.

11. No Transfer of License: This license is personal to you and may not be sublicensed, assigned, or transferred by you to any other person without publisher's written permission.

12. No Amendment Except in Writing: This license may not be amended except in a writing signed by both parties (or, in the case of publisher, by CCC on publisher's behalf).

13. Objection to Contrary Terms: Publisher hereby objects to any terms contained in any purchase order, acknowledgment, check endorsement or other writing prepared by you, which terms are inconsistent with these terms and conditions or CCC's Billing and Payment terms and conditions. These terms and conditions, together with CCC's Billing and Payment terms and conditions (which are incorporated herein), comprise the entire agreement between you and publisher (and CCC) concerning this licensing transaction. In the event of any conflict between your obligations established by these terms and conditions and those established by CCC's Billing and Payment terms and conditions, these terms and conditions shall control.

14. Revocation: Elsevier or Copyright Clearance Center may deny the permissions described in this License at their sole discretion, for any reason or no reason, with a full refund payable to you. Notice of such denial will be made using the contact information provided by you. Failure to receive such notice will not alter or invalidate the denial. In no event will Elsevier or Copyright Clearance Center be responsible or liable for any costs, expenses or damage incurred by you as a result of a denial of your permission request, other than a refund of the amount(s) paid by you to Elsevier and/or Copyright Clearance Center for denied permissions.

LIMITED LICENSE

The following terms and conditions apply only to specific license types:

15. **Translation**: This permission is granted for non-exclusive world **English** rights only unless your license was granted for translation rights. If you licensed translation rights you may only translate this content into the languages you requested. A professional translator must perform all translations and reproduce the content word for word preserving the integrity of the article.

16. **Posting licensed content on any Website**: The following terms and conditions apply as follows: Licensing material from an Elsevier journal: All content posted to the web site must maintain the copyright information line on the bottom of each image; A hyper-text must be included to the Homepage of the journal from which you are licensing at http://www.sciencedirect.com/science/journal/xxxxx or the Elsevier homepage for books at http://www.elsevier.com; Central Storage: This license does not include permission for a scanned version of the material to be stored in a central repository such as that provided by Heron/XanEdu.

Licensing material from an Elsevier book: A hyper-text link must be included to the Elsevier homepage at http://www.elsevier.com . All content posted to the web site must maintain the copyright information line on the bottom of each image.

Posting licensed content on Electronic reserve: In addition to the above the following clauses are applicable: The web site must be password-protected and made available only to bona fide students registered on a relevant course. This permission is granted for 1 year only. You may obtain a new license for future website posting.

17. **For journal authors:** the following clauses are applicable in addition to the above:

Preprints:

A preprint is an author's own write-up of research results and analysis, it has not been peer-reviewed, nor has it had any other value added to it by a publisher (such as formatting, copyright, technical enhancement etc.).

Authors can share their preprints anywhere at any time. Preprints should not be added to or enhanced in any way in order to appear more like, or to substitute for, the final versions of articles however authors can update their preprints on arXiv or RePEc with their Accepted Author Manuscript (see below).

If accepted for publication, we encourage authors to link from the preprint to their formal publication via its DOI. Millions of researchers have access to the formal publications on ScienceDirect, and so links will help users to find, access, cite and use the best available version. Please note that Cell Press, The Lancet and some society-owned have different preprint policies. Information on these policies is available on the journal homepage.

Accepted Author Manuscripts: An accepted author manuscript is the manuscript of an article that has been accepted for publication and which typically includes author-incorporated changes suggested during submission, peer review and editor-author communications.

Authors can share their accepted author manuscript:

- immediately
    - via their non-commercial person homepage or blog
    - by updating a preprint in arXiv or RePEc with the accepted manuscript
    - via their research institute or institutional repository for internal institutional uses or as part of an invitation-only research collaboration work-group
    - directly by providing copies to their students or to research collaborators for their personal use
    - for private scholarly sharing as part of an invitation-only work group on commercial sites with which Elsevier has an agreement
- After the embargo period
    - via non-commercial hosting platforms such as their institutional repository
    - via commercial sites with which Elsevier has an agreement

In all cases accepted manuscripts should:

- link to the formal publication via its DOI
- bear a CC-BY-NC-ND license - this is easy to do
- if aggregated with other manuscripts, for example in a repository or other site, be shared in alignment with our hosting policy not be added to or enhanced in any way to appear more like, or to substitute for, the published journal article.

Published journal article (JPA): A published journal article (PJA) is the definitive final record of published research that appears or will appear in the journal and embodies all

value-adding publishing activities including peer review co-ordination, copy-editing, formatting, (if relevant) pagination and online enrichment.

Policies for sharing publishing journal articles differ for subscription and gold open access articles:

Subscription Articles: If you are an author, please share a link to your article rather than the full-text. Millions of researchers have access to the formal publications on ScienceDirect, and so links will help your users to find, access, cite, and use the best available version.

Theses and dissertations which contain embedded PJAs as part of the formal submission can be posted publicly by the awarding institution with DOI links back to the formal publications on ScienceDirect.

If you are affiliated with a library that subscribes to ScienceDirect you have additional private sharing rights for others' research accessed under that agreement. This includes use for classroom teaching and internal training at the institution (including use in course packs and courseware programs), and inclusion of the article for grant funding purposes.

Gold Open Access Articles: May be shared according to the author-selected end-user license and should contain a CrossMark logo, the end user license, and a DOI link to the formal publication on ScienceDirect.

Please refer to Elsevier's posting policy for further information.

18. **For book authors** the following clauses are applicable in addition to the above: Authors are permitted to place a brief summary of their work online only. You are not allowed to download and post the published electronic version of your chapter, nor may you scan the printed edition to create an electronic version. **Posting to a repository:** Authors are permitted to post a summary of their chapter only in their institution's repository.

19. **Thesis/Dissertation**: If your license is for use in a thesis/dissertation your thesis may be submitted to your institution in either print or electronic form. Should your thesis be published commercially, please reapply for permission. These requirements include permission for the Library and Archives of Canada to supply single copies, on demand, of the complete thesis and include permission for Proquest/UMI to supply single copies, on demand, of the complete thesis. Should your thesis be published commercially, please reapply for permission. Theses and dissertations which contain embedded PJAs as part of the formal submission can be posted publicly by the awarding institution with DOI links back to the formal publications on ScienceDirect.

Elsevier Open Access Terms and Conditions

You can publish open access with Elsevier in hundreds of open access journals or in nearly 2000 established subscription journals that support open access publishing. Permitted third party re-use of these open access articles is defined by the author's choice of Creative Commons user license. See our open access license policy for more information.

Terms & Conditions applicable to all Open Access articles published with Elsevier:

Any reuse of the article must not represent the author as endorsing the adaptation of the article nor should the article be modified in such a way as to damage the author's honour or reputation. If any changes have been made, such changes must be clearly indicated.

SPRINGER NATURE LICENSE
TERMS AND CONDITIONS

Jul 19, 2020

This Agreement between 200 University Ave, University of Waterloo, E3-3110A ("You") and Springer Nature ("Springer Nature") consists of your license details and the terms and conditions provided by Springer Nature and Copyright Clearance Center.

License Number	4872690058964
License date	Jul 19, 2020
Licensed Content Publisher	Springer Nature
Licensed Content Publication	Metallurgical and Materials Transactions A
Licensed Content Title	Role of Random and Coincidence Site Lattice Grain Boundaries in Liquid Metal Embrittlement of Iron (FCC)-Zn Couple
Licensed Content Author	M. H. Razmpoosh et al
Licensed Content Date	Jun 14, 2020
Type of Use	Thesis/Dissertation
Requestor type	academic/university or research institute
Format	electronic
Portion	full article/chapter
Will you be	no

translating?	
Circulation/distribution	100 - 199
Author of this Springer Nature content	yes
Title	Investigation of Liquid-Metal-Embrittlement Crack-path: Role of Grain Boundaries and Responsible Mechanism
Institution name	University of Waterloo
Expected presentation date	Jul 2020
Requestor Location	200 University Ave, University of Waterloo, E3-3110A 200 University Ave, University of Waterl waterloo, ON n2l3g1 Canada Attn: 200 University Ave, University of Waterloo, E3-3110A
Total	0.00 CAD

Terms and Conditions

Springer Nature Customer Service Centre GmbH
Terms and Conditions

This agreement sets out the terms and conditions of the licence (the **Licence**) between you and **Springer Nature Customer Service Centre GmbH** (the **Licensor**). By clicking 'accept' and completing the transaction for the material (**Licensed Material**), you also confirm your acceptance of these terms and conditions.

1. Grant of License

1. 1. The Licensor grants you a personal, non-exclusive, non-transferable, world-wide licence to reproduce the Licensed Material for the purpose specified in your order only. Licences are granted for the specific use requested in the order and for no other use, subject to the conditions below.

1. 2. The Licensor warrants that it has, to the best of its knowledge, the rights to license reuse of the Licensed Material. However, you should ensure that the material you are requesting is original to the Licensor and does not carry the copyright of

another entity (as credited in the published version).

1. 3. If the credit line on any part of the material you have requested indicates that it was reprinted or adapted with permission from another source, then you should also seek permission from that source to reuse the material.

2. Scope of Licence

2. 1. You may only use the Licensed Content in the manner and to the extent permitted by these Ts&Cs and any applicable laws.

2. 2. A separate licence may be required for any additional use of the Licensed Material, e.g. where a licence has been purchased for print only use, separate permission must be obtained for electronic re-use. Similarly, a licence is only valid in the language selected and does not apply for editions in other languages unless additional translation rights have been granted separately in the licence. Any content owned by third parties are expressly excluded from the licence.

2. 3. Similarly, rights for additional components such as custom editions and derivatives require additional permission and may be subject to an additional fee. Please apply to Journalpermissions@springernature.com/bookpermissions@springernature.com for these rights.

2. 4. Where permission has been granted **free of charge** for material in print, permission may also be granted for any electronic version of that work, provided that the material is incidental to your work as a whole and that the electronic version is essentially equivalent to, or substitutes for, the print version.

2. 5. An alternative scope of licence may apply to signatories of the STM Permissions Guidelines, as amended from time to time.

3. Duration of Licence

3. 1. A licence for is valid from the date of purchase ('Licence Date') at the end of the relevant period in the below table:

Scope of Licence	Duration of Licence
Post on a website	12 months
Presentations	12 months
Books and journals	Lifetime of the edition in the language purchased

4. Acknowledgement

4. 1. The Licensor's permission must be acknowledged next to the Licenced Material in print. In electronic form, this acknowledgement must be visible at the same time as the figures/tables/illustrations or abstract, and must be hyperlinked to the journal/book's homepage. Our required acknowledgement format is in the Appendix below.

5. Restrictions on use

5. 1. Use of the Licensed Material may be permitted for incidental promotional use and minor editing privileges e.g. minor adaptations of single figures, changes of format, colour and/or style where the adaptation is credited as set out in Appendix 1 below. Any other changes including but not limited to, cropping, adapting, omitting material that affect the meaning, intention or moral rights of the author are strictly prohibited.

5. 2. You must not use any Licensed Material as part of any design or trademark.

5. 3. Licensed Material may be used in Open Access Publications (OAP) before publication by Springer Nature, but any Licensed Material must be removed from OAP sites prior to final publication.

6. Ownership of Rights

6. 1. Licensed Material remains the property of either Licensor or the relevant third party and any rights not explicitly granted herein are expressly reserved.

7. Warranty

IN NO EVENT SHALL LICENSOR BE LIABLE TO YOU OR ANY OTHER PARTY OR ANY OTHER PERSON OR FOR ANY SPECIAL, CONSEQUENTIAL, INCIDENTAL OR INDIRECT DAMAGES, HOWEVER CAUSED, ARISING OUT OF OR IN CONNECTION WITH THE DOWNLOADING, VIEWING OR USE OF THE MATERIALS REGARDLESS OF THE FORM OF ACTION, WHETHER FOR BREACH OF CONTRACT, BREACH OF WARRANTY, TORT, NEGLIGENCE, INFRINGEMENT OR OTHERWISE (INCLUDING, WITHOUT LIMITATION, DAMAGES BASED ON LOSS OF PROFITS, DATA, FILES, USE, BUSINESS OPPORTUNITY OR CLAIMS OF THIRD PARTIES), AND
WHETHER OR NOT THE PARTY HAS BEEN ADVISED OF THE POSSIBILITY OF SUCH DAMAGES. THIS LIMITATION SHALL APPLY NOTWITHSTANDING ANY FAILURE OF ESSENTIAL PURPOSE OF ANY LIMITED REMEDY PROVIDED HEREIN.

8. Limitations

8. 1. ***BOOKS ONLY:*** Where **'reuse in a dissertation/thesis'** has been selected the following terms apply: Print rights of the final author's accepted manuscript (for clarity, NOT the published version) for up to 100 copies, electronic rights for use only on a personal website or institutional repository as defined by the Sherpa guideline (www.sherpa.ac.uk/romeo/).

9. Termination and Cancellation

9. 1. Licences will expire after the period shown in Clause 3 (above).

9. 2. Licensee reserves the right to terminate the Licence in the event that payment is not received in full or if there has been a breach of this agreement by you.

Appendix 1 — Acknowledgements:

For Journal Content:
Reprinted by permission from [**the Licensor**]: [**Journal Publisher** (e.g. Nature/Springer/Palgrave)] [**JOURNAL NAME**] [**REFERENCE CITATION** (Article name, Author(s) Name), [**COPYRIGHT**] (year of publication)

For **Advance Online Publication papers:**
Reprinted by permission from [**the Licensor**]: [**Journal Publisher** (e.g. Nature/Springer/Palgrave)] [**JOURNAL NAME**] [**REFERENCE CITATION** (Article name, Author(s) Name), [**COPYRIGHT**] (year of publication), advance online publication, day month year (doi: 10.1038/sj.[JOURNAL ACRONYM].)

For Adaptations/Translations:
Adapted/Translated by permission from [**the Licensor**]: [**Journal Publisher** (e.g. Nature/Springer/Palgrave)] [**JOURNAL NAME**] [**REFERENCE CITATION** (Article name, Author(s) Name), [**COPYRIGHT**] (year of publication)

Note: For any republication from the British Journal of Cancer, the following credit line style applies:

Reprinted/adapted/translated by permission from [**the Licensor**]: on behalf of Cancer Research UK: : [**Journal Publisher** (e.g. Nature/Springer/Palgrave)] [**JOURNAL NAME**] [**REFERENCE CITATION** (Article name, Author(s) Name), [**COPYRIGHT**] (year of publication)

For **Advance Online Publication** papers:
Reprinted by permission from The [**the Licensor**]: on behalf of Cancer Research UK: [**Journal Publisher** (e.g. Nature/Springer/Palgrave)] [**JOURNAL NAME**] [**REFERENCE CITATION** (Article name, Author(s) Name), [**COPYRIGHT**] (year of publication), advance online publication, day month year (doi: 10.1038/sj.[JOURNAL ACRONYM])

For Book content:
Reprinted/adapted by permission from [**the Licensor**]: [**Book Publisher** (e.g. Palgrave Macmillan, Springer etc) [**Book Title**] by [**Book author**(s)] [**COPYRIGHT**] (year of publication)

Other Conditions:

Version 1.2

Questions? customercare@copyright.com or +1-855-239-3415 (toll free in the US) or +1-978-646-2777.